



University
of Glasgow

Brzezinska, Elspeth Anne (2015) *The role of β -catenin in prostate cancer tumourigenesis and treatment resistance*. PhD thesis.

<http://theses.gla.ac.uk/7019/>

Copyright and moral rights for this work are retained by the author

A copy can be downloaded for personal non-commercial research or study, without prior permission or charge

This work cannot be reproduced or quoted extensively from without first obtaining permission in writing from the author

The content must not be changed in any way or sold commercially in any format or medium without the formal permission of the author

When referring to this work, full bibliographic details including the author, title, awarding institution and date of the thesis must be given

Glasgow Theses Service

<http://theses.gla.ac.uk/>

theses@gla.ac.uk

The Role of β -catenin in Prostate Cancer Tumourigenesis and Treatment Resistance

Elsbeth Anne Brzezinska

BSc (Hons)

Submitted to the University of Glasgow in fulfilment of the requirements for the degree of Doctor of Philosophy

Beatson Institute for Cancer Research
Garscube Estate
Switchback Road
Glasgow, G61 1BD

Institute of Cancer Sciences
College of Medicine, Veterinary and
Life Sciences
University of Glasgow



Abstract

Prostate cancer is a significant health problem for men in the western world. Of particular concern are patients who present with aggressive, invasive and metastatic disease, and develop lethal castration-resistant prostate cancer (CRPC) following androgen deprivation therapy. The activation of Wnt/ β -catenin signalling is a common event in patients with the poorest prognosis, and frequently associated with the loss of PTEN and activation of the PI3K/Akt signalling pathway. However, the molecular basis for the significant impact of these aberrations in prostate cancer remains unclear.

By using pre-clinical transgenic *in vivo* models, we have demonstrated that β -catenin is a potent proto-oncogene that drives prostate cancer tumourigenesis. Concurrent heterozygous loss of *Pten* exacerbates β -catenin-driven tumour progression and decreases host survival, while tumours are most aggressive when *Pten* is deleted.

We have contributed to the field by identifying an important mechanism for the progression of β -catenin-driven tumourigenesis, through β -catenin/ROS-mediated modulation of *Pten* localisation, required to overcome *Pten*-mediated tumour suppression during cancer initiation. Subsequently, *Pten* expression is downregulated in advanced adenocarcinoma, associated with upregulation of miRNAs and emergence of *Pten* haploinsufficiency. When *Pten* is already haploinsufficient, β -catenin activation drives prostate cancer evolution through *Pten* loss of heterozygosity.

By investigating differential gene and protein expression, we have characterised further co-operation between β -catenin activation and *Pten* loss through a complex network of intrinsic and extrinsic molecular events. These drive survival, growth and proliferation signals, and modulate tumour-immune response interactions to evade anti-tumourigenic processes, resulting in aggressive prostate cancer.

Furthermore, by examining novel *in vivo* models of β -catenin-driven CRPC, we have indicated that β -catenin may promote treatment-resistance through androgen receptor (AR) reprogramming. We propose a mechanism for β -catenin-

driven CRPC that is independent of classical AR signalling, and mediated through significant upregulation of canonical and non-canonical Wnt pathway components, which may be effectively targeted by Wnt inhibition.

In summary, this thesis highlights a number of potential biomarkers and molecular targets that may be exploited to develop new strategies to manage patients with aggressive prostate cancer, to improve prognosis and avoid progression to lethal castration-resistant disease.

2.1.5	Cell lines	62
2.1.6	Solutions and buffers.....	63
2.2	<i>Methods</i>	65
2.2.1	Animal studies.....	65
2.2.1.1	Transgenic models.....	65
2.2.1.2	Haematological analysis of whole blood from mice.....	66
2.2.1.3	N-acetyl-cysteine treatment.....	66
2.2.1.4	Tamoxifen induction	66
2.2.1.5	RFP fluorescence imaging	67
2.2.1.6	Bilateral orchiectomy (castration).....	67
2.2.1.7	Prostate regeneration.....	67
2.2.1.8	LGK-974 (Porcupine inhibitor) treatment.....	67
2.2.2	Histology and immunohistochemistry	67
2.2.2.1	Haematoxylin and eosin image analysis.....	69
2.2.2.2	Ki67 scoring.....	69
2.2.3	Zeptosens' reverse-phase protein array	69
2.2.4	Immunoblotting	70
2.2.5	RT-PCR.....	71
2.2.5.1	mRNA analysis.....	71
2.2.5.2	miRNA analysis	72
2.2.6	Transcriptomic analysis.....	72
2.2.6.1	RNA-sequencing.....	72
2.2.6.2	Data analysis.....	73
2.2.6.3	Pathway enrichment analysis.....	74
2.2.7	Cytokine array.....	74
2.2.8	Laser-capture microdissection.....	75
2.2.8.1	<i>Pten</i> RNA expression analysis	76
2.2.8.2	<i>Pten</i> copy number analysis.....	77
2.2.9	Primary cell line derivation and culture	77
2.2.9.1	CP1 ICG-001 treatment	78
2.2.10	RNAscope®	79
2.2.11	Immunoprecipitation	79
2.2.12	Chromatin immunoprecipitation assay	80
2.2.12.1	Chromatin preparation.....	80
2.2.12.2	Chromatin-immunoprecipitation (ChIP).....	81
2.2.12.3	Quantitative PCR analysis	82
2.2.13	Statistics	83

Chapter 3 - β-catenin activation drives prostate tumourigenesis and co-operates with Pten loss to advance cancer progression.....	84
3.1 <i>Introduction</i>	85
3.2 <i>Wnt/β-catenin pathway activation and Pten loss co-operate to drive aggressive prostate cancer</i>	87
3.2.1 <i>Characterisation of an <i>in vivo</i> prostate cancer model with β-catenin activation and concurrent Pten loss.....</i>	88
3.2.2 <i>ROS-driven proliferation and Pten-modulation overcome tumour suppression in β-catenin-driven prostate cancer</i>	100
3.2.3 <i>Progressive loss of Pten correlates with advanced cancer stage in β-catenin-driven prostate cancer</i>	110
3.3 <i>Tumour intrinsic events that facilitate co-operation between β-catenin activation and Pten loss in prostate cancer</i>	121
3.4 <i>Tumour extrinsic events that facilitate co-operation between β-catenin activation and Pten loss in prostate cancer</i>	129
3.5 <i>Discussion</i>	142
Chapter 4 - Activation of β-catenin promotes treatment-resistant prostate cancer	151
4.1 <i>Introduction</i>	152
4.2 <i>Manipulating the $Nkx3.1^{CreERT2}$ transgenic mouse model to study treatment resistant prostate cancer</i>	154
4.2.1 <i>Optimisation of the tamoxifen induction protocol</i>	154
4.2.2 <i>$Nkx3.1$ expression is retained in a sub-population of cells in regressed and regenerated prostate</i>	161
4.3 <i>Tumours with β-catenin activation are resistant to androgen deprivation therapy - a novel pre-clinical model for castration resistant prostate cancer.....</i>	165
4.3.1 <i>Investigating the effect of castration in $Nkx3.1^{CreERT2} Pten^{fl/+} Ctnnb1^{(ex3)\Delta/+}$ genetically engineered mouse model</i>	165
4.3.2 <i>The $Nkx3.1^{CreERT2} Pten^{fl/fl} Ctnnb1^{(ex3)\Delta/+}$ mouse model develops aggressive castration-resistant prostate cancer.....</i>	171
4.3.3 <i>Transcriptomic analysis of gene expression changes associated with castration-resistant tumours highlighted increased expression of Wnts ...</i>	174
4.3.4 <i>Investigating the effect of Wnt inhibition and androgen deprivation combination therapy in $Nkx3.1^{CreERT2} Pten^{fl/+} Ctnnb1^{\Delta(ex3)/+}$ mice.....</i>	182
4.4 <i>Evidence for androgen receptor reprogramming in tumours with β-catenin activation</i>	184
4.4.1 <i>Identification of a pseudo-castrate gene expression signature in β-catenin-driven prostate cancer</i>	184
4.4.2 <i>Optimisation of ChIP protocol in tissue samples.....</i>	192
4.4.3 <i>Enrichment of AR binding at target genes is altered in β-catenin-driven prostate cancer</i>	197
4.5 <i>Discussion</i>	200

Chapter 5 - Final Summary and Concluding Remarks	206
5.1 <i>Final Summary</i>	207
5.2 <i>Concluding Remarks</i>	214
References	215
Appendix I - Publication	227

List of Tables

Table 1.1-1 Mechanisms for the continuation or reactivation of the AR signalling pathway in CRPC [84]	32
Table 2.1-1 General reagents	56
Table 2.1-2 Antibodies used for immunohistochemistry.....	59
Table 2.1-3 Reverse Phase Protein Array antibodies.....	59
Table 2.1-4 Immunoblotting antibodies	60
Table 2.1-5 Immunoprecipitation antibodies.....	60
Table 2.1-6 TaqMan qPCR primers	61
Table 2.1-7 TaqMan MicroRNA assays (Applied Biosystems)	62
Table 2.1-8 CHIP-qPCR primers	62
Table 3.2-1 Transnetyx genotyping results for CP cell lines, tumour tissue and tail tips	117
Table 4.4-1 Androgen responsive genes downregulated in HNPC with aberrant β -catenin activation	186
Table 4.4-2 Androgen responsive genes downregulated in HNPC are not significantly altered in CRPC.....	186

List of Figures

Figure 1.1.1 Human prostate cancer carcinogenesis	24
Figure 1.1.2 Androgen receptor signalling	26
Figure 1.3.1 Mechanisms of PTEN tumour suppression	38
Figure 1.3.2 Canonical Wnt signalling pathway	42
Figure 1.3.3 PTEN/PI3K and Wnt/ β -catenin pathway deregulation in aggressive prostate cancer (MSKCC prostate adenocarcinoma study data set [41] analysed in cBio Portal for Cancer Genomics)	45
Figure 1.4.1 Human and mouse prostate anatomy	48
Figure 1.4.2 Pathology of normal mouse prostate	49
Figure 1.4.3 Murine prostate carcinogenesis	50
Figure 3.1.1 Clinical relevance of studying Wnt/ β -catenin and PTEN in prostate cancer	86
Figure 3.2.1 Increased circulating Wnt co-operates with Pten loss to drive aggressive prostate cancer	87
Figure 3.2.2 Co-operation between β -catenin activation and Pten loss results in poor survival outcome <i>in vivo</i>	89
Figure 3.2.3 β -catenin activation alone drives prostate tumourigenesis	90
Figure 3.2.4 Co-operation between β -catenin activation and Pten loss drives prostate tumour growth	92
Figure 3.2.5 Histopathological characterisation of <i>Pb-Cre Pten^{fl/+} Ctnnb1^{(ex3)Δ/+}</i> mouse model	93
Figure 3.2.6 Analysis of haematoxylin and eosin staining to measure tumour burden	94
Figure 3.2.7 Analysis of PIN number and tumour area in <i>Pb-Cre Ctnnb1^{(ex3)Δ/+}</i> and <i>Pb-Cre Pten^{fl/+} Ctnnb1^{(ex3)Δ/+}</i> prostates	95
Figure 3.2.8 Ki67 scoring to quantify levels of proliferation in <i>Pb-Cre Pten^{fl/+} Ctnnb1^{(ex3)Δ/+}</i> and control prostate tissue	96
Figure 3.2.9 Reverse-Phase Protein Array screen to identify changes in protein levels associated with β -catenin activation and Pten loss in prostate cancer	97
Figure 3.2.10 Pten and Akt pathway analysis	98
Figure 3.2.11 Nuclear Pten observed in <i>Pb-Cre Ctnnb1^{(ex3)Δ/+}</i> PIN lesions corresponds with elevated levels of ROS and p21	100
Figure 3.2.12 N-acetyl cysteine (NAC) treatment decreased tumour burden in <i>Pb-Cre Ctnnb1^{(ex3)Δ/+}</i> mice	101
Figure 3.2.13 NAC treatment had a pro-proliferative effect on <i>Pb-Cre Pten^{fl/+}</i> prostate cells but was chemopreventive in <i>Pb-Cre Ctnnb1^{(ex3)Δ/+}</i> mice	102
Figure 3.2.14 Effects of NAC treatment on Pten, ROS and p21 in <i>Pb-Cre Pten^{fl/+}</i> and <i>Pb-Cre Ctnnb1^{(ex3)Δ/+}</i> prostate tissue	103
Figure 3.2.15 NAC treatment had little effect on prostate cancer progression in <i>Pb-Cre Pten^{fl/+} Ctnnb1^{(ex3)Δ/+}</i> mice	104

Figure 3.2.16 Effects of NAC treatment on Pten, ROS and p21 in <i>Pb-Cre Pten^{fl/+} Ctnnb1^{(ex3)Δ/+}</i> prostate tissue.....	105
Figure 3.2.17 Differential effects of NAC treatment on phospho-Akt expression in <i>Pb-Cre Pten^{fl/+}</i> , <i>Pb-Cre Ctnnb1^{(ex3)Δ/+}</i> and <i>Pb-Cre Pten^{fl/+} Ctnnb1^{(ex3)Δ/+}</i> prostate tissue.....	106
Figure 3.2.18 High levels of ROS positively correlate with Rac1 activity in <i>Pb-Cre Ctnnb1^{(ex3)Δ/+}</i> PIN lesions.....	107
Figure 3.2.19 Rac-GEFs, <i>Tiam1</i> and <i>Vav3</i> , are not significantly altered in prostate tissue with β-catenin activation at 6 months	108
Figure 3.2.20 <i>Tiam1</i> and <i>Vav3</i> are significantly upregulated in <i>Pb-Cre Ctnnb1^{(ex3)Δ/+}</i> prostate tissue at 3 months	109
Figure 3.2.21 Levels of <i>Tiam1</i> and <i>Vav3</i> expression do not vary significantly between 3, 6 and 12 month time points in <i>wildtype</i> prostate tissue	109
Figure 3.2.22 Progressive loss of Pten in tumours driven by β-catenin activation	110
Figure 3.2.23 Pten expression is heterogeneous in epithelial and stromal regions of prostate tumour	111
Figure 3.2.24 <i>Pten</i> expression significantly decreases in <i>Pb-Cre Ctnnb1^{(ex3)Δ/+}</i> tumour epithelial tissue between 6 and 12 months.....	113
Figure 3.2.25 <i>Pten</i> copy number in <i>Pten^{fl/+} Ctnnb1^{(ex3)Δ/+}</i> prostate tumour epithelia tissue is comparable to homozygous Pten loss	114
Figure 3.2.26 <i>Pten</i> copy number is significantly higher in the stroma compared to epithelia of <i>Ctnnb1^{(ex3)Δ/+}</i> prostate tissue	115
Figure 3.2.27 Primary cell lines derived from <i>Pb-Cre Pten^{fl/+} Ctnnb1^{(ex3)Δ/+}</i> prostate tumours.....	116
Figure 3.2.28 Pten is completely lost in CP cell lines 1-3 but present in CP4 cells	116
Figure 3.2.29 Upregulation of <i>miRNA-17</i> , <i>-18</i> , <i>19b</i> and <i>-21</i> expression is associated with aberrant β-catenin activation	119
Figure 3.2.30 Western blot analysis of CP1 and CP2 cells treated with ICG-001 inhibitor	120
Figure 3.2.31 Preliminary data suggests that blocking β-catenin transcriptional activity decreases expression of <i>miRNA-17</i>	120
Figure 3.3.1 mTOR pathway analysis	122
Figure 3.3.2 AMPK and PKA pathway analysis	123
Figure 3.3.3 <i>Pb-Cre Ctnnb1^{(ex3)Δ/+}</i> and <i>Pb-Cre Pten^{fl/+} Ctnnb1^{(ex3)Δ/+}</i> tumours have similar gene expression patterns.....	124
Figure 3.3.4 Validation of expression changes observed in genes associated with innate immune response, cAMP biosynthesis, lipid metabolism and glycolysis.	126
Figure 3.3.5 MetaCore pathway analysis of gene expression changes in <i>Pb-Cre Ctnnb1^{(ex3)Δ/+}</i> tumour tissue compared to <i>wildtype</i>	127
Figure 3.3.6 MetaCore pathway analysis of gene expression changes in <i>Pb-Cre Pten^{fl/+} Ctnnb1^{(ex3)Δ/+}</i> tumour tissue compared to <i>wildtype</i>	128

Figure 3.4.1 Characterisation of macrophage infiltration in prostate tissue with β -catenin activation and <i>Pten</i> haploinsufficiency	131
Figure 3.4.2 Characterisation of neutrophil infiltration in prostate tissue with β -catenin activation and <i>Pten</i> haploinsufficiency.....	132
Figure 3.4.3 Analysis of circulating red blood cells and platelets in mice harbouring β -catenin-driven prostate tumours with heterozygous <i>Pten</i> loss ...	134
Figure 3.4.4 Analysis of circulating white blood cells in mice harbouring β -catenin-driven prostate tumours with heterozygous <i>Pten</i> loss.....	135
Figure 3.4.5 Analysis of circulating red blood cells and platelets in mice harbouring β -catenin-driven prostate tumours with homozygous <i>Pten</i> loss.....	136
Figure 3.4.6 Analysis of circulating white blood cells in mice harbouring β -catenin-driven prostate tumours with homozygous <i>Pten</i> loss	137
Figure 3.4.7 Endpoint prostate tumour weights and quantity of tumour infiltrate do not vary significantly between tumour genotypes.....	138
Figure 3.4.8 Protein array showing differential expression of cytokines associated with β -catenin activation and <i>Pten</i> loss in prostate tumour tissue .	139
Figure 3.4.9 Cytokines BLC/CXCL13, TREM-1, IL-16, MIP-2 and IL-1ra differ significantly between <i>Pten</i> loss- and β -catenin-driven prostate tumours	140
Figure 3.5.1 β -catenin activation modulates <i>Pten</i> localisation to overcome tumour suppression.....	144
Figure 3.5.2 <i>Pten</i> status determines the latency of β -catenin-driven prostate cancer	145
Figure 3.5.3 <i>Pten</i> is lost during the evolution of β -catenin-driven prostate cancer	146
Figure 4.2.1 Schematic of the tamoxifen-inducible <i>Nkx3.1</i> ^{CreERT2} <i>Cre-loxP</i> system	154
Figure 4.2.2 Detection of RFP expression in <i>Nkx3.1</i> ^{CreERT2} <i>RFP</i> ^{+/-} prostate tissue following tamoxifen induction.....	156
Figure 4.2.3 Detection of β -catenin exon 3 deletion in <i>Nkx3.1</i> ^{CreERT2} <i>Ctnnb1</i> ^{(ex3)Δ/+} prostate tissue following tamoxifen induction.....	157
Figure 4.2.4 Detection of β -catenin activation in <i>Nkx3.1</i> ^{CreERT2} <i>Ctnnb1</i> ^{(ex3)Δ/+} prostate tissue following tamoxifen induction.....	158
Figure 4.2.5 Using the inducible <i>Nkx3.1</i> ^{CreERT2} <i>loxP</i> system to manipulate <i>Pten</i> (<i>Pten</i> ^{fl/+}) and β -catenin (<i>Ctnnb1</i> ^{(ex3)Δ/+}) and investigate effects of castration <i>in vivo</i>	160
Figure 4.2.6 The effect of castration on wildtype mouse prostate	161
Figure 4.2.7 Manipulating androgen levels to study regression and regeneration of the mouse prostate	162
Figure 4.2.8 Detection of castration-resistant <i>Nkx3.1</i> -expressing cells (CARNs) in regressed and regenerated prostate.....	164
Figure 4.3.1 <i>Nkx3.1</i> ^{CreERT2} <i>Pten</i> ^{fl/+} <i>Ctnnb1</i> ^{(ex3)Δ/+} tumours develop resistance to ADT.....	166
Figure 4.3.2 The effect of ADT on body weight of <i>Nkx3.1</i> ^{CreERT2} <i>Pten</i> ^{fl/+} <i>Ctnnb1</i> ^{(ex3)Δ/+} mice compared to controls.....	167

Figure 4.3.3 Treatment of <i>Nkx3.1^{CreERT2} Pten^{fl/+} Ctnnb1^{(ex3)Δ/+}</i> mice with ADT provides no survival benefit.....	167
Figure 4.3.4 <i>Nkx3.1^{CreERT2} Pten^{fl/+} Ctnnb1^{(ex3)Δ/+}</i> mice develop aggressive adenocarcinoma and maintain high levels of proliferation following ADT	169
Figure 4.3.5 Growth of <i>Nkx3.1^{CreERT2} Pten^{fl/+} Ctnnb1^{(ex3)Δ/+}</i> castration-resistant tumours is not dependent on PI3K/Akt or classical androgen receptor signalling	170
Figure 4.3.6 ADT increases survival in <i>Nkx3.1^{CreERT2} Pten^{fl/fl} Ctnnb1^{(ex3)Δ/+}</i> mice but tumour burden is comparable at endpoint	172
Figure 4.3.7 Castration-resistant <i>Nkx3.1^{CreERT2} Pten^{fl/fl} Ctnnb1^{(ex3)Δ/+}</i> tumours have increased stroma area, high levels of proliferation and maintain high levels of nuclear β-catenin.....	173
Figure 4.3.8 Pathways significantly altered in <i>Nkx3.1^{CreERT2} Pten^{fl/+} Ctnnb1^{(ex3)Δ/+}</i> castration-resistant tumours compared to hormone naïve controls.....	175
Figure 4.3.9 Increased Wnt signalling pathway activity in <i>Nkx3.1^{CreERT2} Pten^{fl/+} Ctnnb1^{(ex3)Δ/+}</i> castration-resistant tumours	176
Figure 4.3.10 The classical androgen receptor signalling pathway is not reactivated in <i>Nkx3.1^{CreERT2} Pten^{fl/+} Ctnnb1^{(ex3)Δ/+}</i> castration-resistant tumours	177
Figure 4.3.11 Expression of <i>Tcf3</i> and <i>Adcy8</i> , but not <i>Ccnd1</i> or <i>Myc</i> , is significantly upregulated in prostate tissue with β-catenin activation	178
Figure 4.3.12 Upregulation of Wnt pathway genes in castration-resistant compared to hormone-naïve tumours	179
Figure 4.3.13 <i>Myc</i> expression is elevated in <i>Nkx3.1^{CreERT2} Pten^{fl/+} Ctnnb1^{(ex3)Δ/+}</i> castration-resistant tumours.....	180
Figure 4.3.14 Wnt5a expression is elevated in castration-resistant prostate tumour tissue	181
Figure 4.3.15 The effect of ADT and Wnt inhibition on regression of prostate tumours in <i>Nkx3.1^{CreERT2} Pten^{fl/+} Ctnnb1^{(ex3)Δ/+}</i> mice	182
Figure 4.3.16 Histology of <i>Nkx3.1^{CreERT2} Pten^{fl/+} Ctnnb1^{(ex3)Δ/+}</i> tumours following treatment with ADT and Wnt inhibitor	183
Figure 4.4.1 Co-immunoprecipitation experiments show AR and β-catenin interaction	184
Figure 4.4.2 Prostate cancer driven by aberrant β-catenin activation has a pseudo-castrate gene expression signature	185
Figure 4.4.3 Expression of androgen responsive genes is reprogrammed in HNPC and maintained in CRPC	187
Figure 4.4.4 <i>Fkbp5</i> and <i>ApoF</i> transcript expression is downregulated in hormone-naïve prostate tissue with β-catenin activation	188
Figure 4.4.5 <i>AR</i> , <i>Fkbp5</i> and <i>ApoF</i> expression is similar in hormone-naïve and castration-resistant tumours with β-catenin activation and Pten loss.....	189
Figure 4.4.6 <i>Fkbp5</i> and <i>ApoF</i> are not downregulated at early stages of tumorigenesis	191
Figure 4.4.7 LNCaP chromatin sonication optimisation.....	192
Figure 4.4.8 ChIP protocol validation using CTCF ChIP in LNCaPs	193

Figure 4.4.9 Optimisation of cross-linking and sonication in tissue chromatin	194
Figure 4.4.10 AR ChIP antibody selection	195
Figure 4.4.11 AR enrichment at <i>Fkbp5</i> in fresh and frozen tissue	196
Figure 4.4.12 Hormone-naïve <i>Nkx3.1^{CreERT2} Pten^{fl/+} Ctnnb1^{(ex3)Δ/+}</i> tumours have decreased enrichment of AR binding at <i>Fkbp5</i> compared to <i>wildtype</i>	197
Figure 4.4.13 Hormone-naïve <i>Nkx3.1^{CreERT2} Pten^{fl/+} Ctnnb1^{(ex3)Δ/+}</i> tumours have decreased enrichment of AR binding at <i>ApoF</i> compared to <i>wildtype</i>	198
Figure 4.4.14 No enrichment of AR binding is observed at non-target negative control	199
Figure 5.1.1 Summary of the role of β-catenin in prostate cancer tumourigenesis and treatment resistance.....	213

Acknowledgements

It has been a privilege to carry out my PhD at the Beatson Institute under the supervision of Professor Hing Leung. Hing has been a fantastic mentor and I am indebted to him for the opportunity to work in his lab and for his continuous guidance, support and patience. My advisor, Professor Owen Sansom, initiated the β -catenin project in collaboration with Hing, and I would like to thank Owen for his support and many helpful discussions during my PhD.

I would like to thank all members of R08, past and present: Rachana, Janis, Carolyn, Meiling, Eugenia, Imran, Prabs, Ernest, Yan, Jacqui, Sarah, Lisa, Mark, Paul, Yashmin and Ee Hong, for making the last four years so enjoyable and for all their help in the lab. I am particularly grateful to Rachana for her guidance and input into my project, for teaching me so much and helping me to persevere through those 'character building' challenges. Also, thank you to Janis and Carolyn for their patience in teaching me many experimental techniques and imparting their help and advice throughout my PhD.

This work would not have been possible without Colin Nixon and his team in Histology Services, all staff in the Biological Services Unit, our collaborator Dr Neil Carragher who carried out the Reverse Phase Protein Array, Gabriela Kalna and Ann Hedley for all their help with Bioinformatics analysis, the Beatson Advanced Imaging Resource team, all staff in Central Services, and many other great colleagues at the Beatson Institute and University of Glasgow.

Thank you to the wonderful friends I have met during my time at the Beatson and a big thank you to Mateusz, my parents and family for their endless love and support.

Cancer Research UK funded this PhD at the Beatson Institute for Cancer Research and I would like to thank all the fundraisers and donors who make this work possible.

Author's Declaration

I hereby declare that all of the work presented in this thesis is the result of my own independent investigation unless otherwise stated.

No part of this work has been submitted for consideration as part of any other degree or award.

Elspeth Anne Brzezinska

Abbreviations

18S	18S ribosomal RNA
ADCY8	Adenylate cyclase 8
ADT	Androgen deprivation therapy
Akt	Protein kinase B
AMPK	AMP-activated protein kinase
APC	Adenomatous polyposis coli
APOC4	Apolipoprotein C-IV
APOF	Apolipoprotein F
AR	Androgen receptor
ARE	Androgen response element
BLC	B lymphocyte chemoattractant
BPH	Benign prostatic hyperplasia
CARNs	Castration-resistant Nkx3.1-expressing cells
CCL	Chemokine ligand
CCND1	Cyclin D1
CK1	Casein kinase 1
CNA	Copy number alteration
<i>Cre</i>	Cre recombinase mouse transgene
CRPC	Castrate resistant prostate cancer
CTNNB1	β -catenin
<i>Ctnnb1</i> ^{(ex3)Δ/+}	Mouse heterozygous for deletion of <i>B-catenin</i> exon3
CXCL	Chemokine (C-X-C motif) ligand
DEFA20	Defensin 20
dH ₂ O	Distilled water
DHT	5 α -dihydrotestosterone
DNA	Deoxyribonucleic acid
E2F	E2F transcription factor
EGFR	Epidermal growth factor receptor
EMT	Epithelial mesenchymal transition
ERG	v-ets avian erythroblastosis virus E26 oncogene homolog
ERK	Extracellular signal-regulated protein kinase
ESC	Embryonic stem cell
ETS	E26 transformation-specific transcription factor
F4/80	Adhesion G protein-coupled receptor E1
FBP1	Fructose-1,6-bisphosphatase 1
FFPE	Formalin-fixed paraffin-embedded
FISH	Fluorescence <i>in situ</i> hybridisation
FKBP5	FK506 binding protein 5
FZD	Frizzled receptor
GAPDH	Glyceraldehyde-3-phosphate dehydrogenase
GSK3	Glycogen synthase kinase 3
HNPC	Hormone naïve prostate cancer
HRP	Horseradish peroxidase
HSP	Heat shock protein
IHC	Immunohistochemistry
IL-16	Interleukin-16
IL-1ra	Interleukin-1 receptor antagonist
JNK	Mitogen activated protein kinase 8
Ki67	Marker of proliferation Ki67

KLK3	Kallikrein-related peptidase 3 (PSA)
LBD	Ligand binding domain
LCM	Laser-capture microdissection
Lcor	Ligand dependent nuclear receptor corepressor
LEF	Lymphoid enhancer factor
LHRH	Luteinising hormone-releasing hormone
LOH	Loss of heterozygosity
LoxP	Locus of X-over P1
LRP	Low density lipoprotein receptor-related protein
MAPK	Mitogen-activated protein kinase
MIP2	Macrophage inflammatory protein 2
MMP	Matrix metalloproteinase
MSKCC	Memorial Slone Kettering Cancer Center
mTORC1/2	Mammalian target of rapamycin complex 1/2
MYC	v-myc avian myelocytomatosis viral oncogene homolog
NAC	N-acetyl cysteine
NADPH	Nicotinamide adenine dinucleotide phosphate
NGS	Next generation sequencing
NIMP	Reticulon 4 interacting protein 1
NKX3.1	NK3 homeobox 1
<i>Nkx3.1^{CreERT2}</i>	Mouse heterozygous for tamoxifen-inducible, <i>Nkx3.1</i> promoter-driven <i>Cre</i> expression
NOX	NADPH oxidase
p21	Cyclin-dependent kinase inhibitor 1A
p53/TP53	Tumour protein p53
p63	Tumour protein p63
PI3K	Phosphatidylinositol-3-kinase
<i>Pb-Cre</i>	Mouse heterozygous for <i>ARR₂PB probasin</i> promoter derivative-driven <i>Cre</i> expression
PIA	Proliferative inflammatory atrophy
PIK3CA	Phosphatidylinositol-4,5-bisphosphate 3-kinase catalytic subunit α
PIK3R1/2	Phosphatidylinositide-3-kinase, regulatory subunit 1(α)/2(β)
PIN	Prostatic intraepithelial neoplasia
PIP2	Phosphatidylinositol-4,5-bisphosphate
PIP3	Phosphatidylinositol-3,4,5-trisphosphate
PKA	Protein kinase A
PORCN	Porcupine homolog (<i>Drosophila</i>)
PNLIPRP2	Pancreatic lipase-related protein 2
PSA	Prostate-specific antigen
PTEN	Phosphatase and tensin homolog
<i>Pten^{fl/+}</i>	Mouse heterozygous for <i>Pten</i> deletion
<i>Pten^{fl/fl}</i>	Mouse homozygous for <i>Pten</i> deletion
RAC1	Ras-related C3 botulinum substrate 1
RBC	Red blood cell
RB	Retinoblastoma protein
RFP	Red fluorescent protein
<i>RFP+/-</i>	Mouse heterozygous <i>RFP</i> transgene expression
RNA	Ribonucleic acid
RNF43	Ring finger protein 43 E3 ubiquitin-protein ligase
ROS	Reactive oxygen species
RPPA	Reverse phase protein array

RT-(q)PCR	Reverse transcription-(quantitative) polymerase chain reaction
RTK	Receptor tyrosine kinase
S6	Ribosomal protein S6
S6K	Ribosomal protein S6 kinase, polypeptide 1
SD/SEM	Standard deviation/Standard error of the mean
SV40	Simian virus 40
snoRNA202	Small nucleolar RNA 202
SRC	SRC proto-oncogene non-receptor tyrosine kinase
STAT	Signal transducer and activator of transcription
TCF	T-cell factor
TIAM1	T-cell lymphoma invasion and metastasis 1
TIMP4	Tissue inhibitor of metalloproteinase 4
TMA	Tissue microarray
TMEM97	Transmembrane protein 97
TMPRSS2	Transmembrane protease, serine 2
TrCP	β -transducin repeat containing E3 ubiquitin-protein ligase
TREM1	Triggering receptor expressed on myeloid cells 1
TSC1/2	Tuberous sclerosis 1/2
VAV3	Vav 3 guanine nucleotide exchange factor
WBC	White blood cell
Wnt	Wingless-type MMTV integration site family member
ZNRF3	Zinc and ring finger 3 E3 ubiquitin-protein ligase

Chapter 1 – Introduction

Introduction

Prostate cancer affects one in every eight men in the UK, and is the most common cancer diagnosed in males in the developed world. The majority of patients present with indolent disease and can be monitored by active surveillance. However, at least 20% of patients progress to locally advanced and metastatic disease. For this reason, prostate cancer remains the second leading cause of cancer death in UK males, with 10,837 men dying from prostate cancer in 2012 [1].

In 1941, Huggins and Hodges revolutionised the understanding of prostate cancer by demonstrating the androgen dependence of prostate cell growth and tumourigenesis, when regression of prostate cancer was observed following orchiectomy or oestrogenic injections [2]. This led to the use of endocrine therapy, currently known as androgen deprivation therapy (ADT), in the treatment of locally advanced and metastatic prostate cancer. Unfortunately, most patients that initially respond favourably to ADT become castration-resistant and relapse with incurable disease within 3 years of receiving treatment [3]. Therefore, much focus is still required on elucidating the molecular mechanisms involved in prostate cancer tumourigenesis and treatment resistance. This is fundamental for the development of new diagnostic and therapeutic strategies to manage aggressive and treatment-resistant disease.

1.1 Prostate cancer

1.1.1 Initiation and development of human prostate cancer

Prostate development occurs during embryogenesis, through interactions between epithelial and mesenchymal tissues, which require androgen signalling for prostate induction and growth [4, 5]. All stages of prostate growth and development, thereafter, remain dependent on androgen signalling and interactions between epithelial and stromal compartments [6]. Disruption of epithelial-stromal interactions is, therefore, likely to contribute to cancer initiation and progression.

The human prostate duct consists of blood vessels, stromal tissue, comprising fibroblasts, smooth muscle cells and infiltrating immune cells, and epithelium, characterised by at least three different epithelial cell types: secretory luminal cells, basal cells and a few neuroendocrine cells [7, 8]. The majority of the epithelium is composed of androgen-dependent, terminally differentiated luminal cells, distinguished by their expression of androgen receptor (AR) and cytokeratin 8 and 18. The functional role of the adult prostate gland is the contribution of secretory proteins, produced by the luminal cells, to seminal fluid.

The second most prevalent epithelial cell type, basal cells, forms a continuous layer between luminal cells and the basement membrane, which encapsulates the prostate gland. Basal cells are characterised by expression of cytokeratin 5 and 14, p63 and CD44. The expression of AR in basal cells has been subject to contention but, if expressed, is present at very low levels [9, 10]. The basal cell compartment contains a subset of progenitor stem cells and a larger number of proliferative transit-amplifying cells involved in self-renewal of the epithelium. These intermediate transit-amplifying cells harbour both luminal and basal cell markers and have been shown to give rise to both cell types [11, 12]. Basal cells play an important role in converting testosterone to 5- α -dihydrotestosterone (DHT), which diffuses to luminal cells and contributes to the activation of androgen receptor signalling [13].

Neuroendocrine cells are androgen-independent and, therefore, do not express AR. They are scattered among the epithelium and thought to support luminal cell growth in a paracrine manner [14]. While neuroendocrine cells constitute a small part of the normal prostate epithelium, neuroendocrine differentiation and expansion of the neuroendocrine cell population are associated with aggressive prostate cancer [15-17].

The cell of origin for prostate cancer has been widely debated and continues to be researched. The cancer stem cell (CSC) model proposes that tumour-initiating cells originate from a rare population of stem cells, which have an indefinite ability to self-renew and can accumulate mutations overtime, leading to oncogenic transformation and differentiation into cancer cells. In this model, therapeutic efficacy may be achieved by directly targeting the CSCs, which drive

malignant proliferation, disease recurrence and treatment resistance [18]. An alternative model suggests that cancer initiates and progresses by clonal evolution, whereby most cancer cells are highly tumourigenic, and clones harbouring genetic and epigenetic events, which provide selective advantages for survival, growth and treatment resistance, drive tumour evolution and progression. In this model, eradication of almost all tumour cells would be required to prevent cancer recurrence [18]. These models are not necessarily mutually exclusive; it is feasible that more than one tumour-initiating cell may drive malignancy in prostate epithelium and their clonal progeny then be subjected to selection during cancer progression.

Luminal epithelial cells are the predominant cell type present in prostate cancer, but intermediate cell types harbouring basal and luminal markers have also been observed [19]. Recent investigations have shown that prostate cancer can potentially arise from multipotent basal or luminal stem cells (reviewed by Wang et al. [18], Goldstein et al. [20] and Xin [21]). Goldstein et al. [22] demonstrated the tumour-initiating capability of basal cells, but not luminal cells, when transduced with activated Akt and ERG, and transplanted into immunosuppressed mice. These basal cells gave rise to prostatic intraepithelial neoplasia (PIN), cancer precursor lesions, with luminal features. Additional transduction of AR co-operated with Akt and ERG activation in basal cells to drive the development of adenocarcinoma, characterised by loss of basal cells and expansion of luminal cells, mimicking human disease. Basal cells are androgen-independent and, therefore, survive ADT, implicating the potential involvement of basal CSCs in the emergence of treatment-resistant disease [22].

Conversely, Wang et al [23] identified a rare androgen-independent luminal epithelial stem cell population as a cell of origin for prostate cancer, characterised by expression of the prostate epithelial differentiation marker *Nkx3.1*. These castration-resistant *Nkx3.1*-expressing cells (CARNs) were present in the regressed mouse prostate following ablation of testicular androgens, and targeted *Pten* deletion in CARNs resulted in prostate tumourigenesis following androgen-mediated prostate regeneration. However, it is unclear whether CARNs are also a cell of origin in the hormone-naïve prostate. Recent work by Wang et al [24] used lineage marking of basal or luminal cells to trace the origin of PIN and adenocarcinoma lesions in a number of prostate cancer mouse

models, including *Nkx3.1^{+/-} Pten^{+/-}*, *Pten^{+/-}*, *Hi-Myc* and *TRAMP* mice, and consistently demonstrated luminal cells as the favoured cell of origin for prostate cancer. Renal grafting of basal cells from these mice did generate tumours, corroborating evidence for the tumour-initiating capability of basal cells, but indicating these were not the preferred cell of origin in the native prostate microenvironment.

In addition, partially or terminally differentiated luminal cells have also been proposed as potential tumour-initiating cells in prostate cancer [25]. Partially differentiated luminal cells may arise due to a differentiation block induced in intermediate cells, which reprograms an embryonic stem cell (ESC)-like phenotype, facilitating self-renewal of these cells [26]. Alternatively, terminally differentiated cells may undergo *de novo* reprogramming to induced pluripotent stem cells following stimulation by factors such as MYC, KLF4, Oct4 and SOX2 [26]. Overall, it is possible that prostate cancer can arise from either multipotent stem cells or (de)differentiated progenitor cells in a context-dependent manner, resulting in different subtypes of prostate cancer. In this way, the cell of origin is likely to have implications for prostate cancer prognosis and therapeutic strategies.

Although prostate cancer is a multifocal and phenotypically heterogeneous disease, common features have been identified that are broadly characteristic of prostate cancer initiation and progression (Figure 1.1.1). It has been suggested that sites of proliferative inflammatory atrophy (PIA) within the prostate epithelium are precursor lesions to PIN and adenocarcinoma [27]. PIA has been observed in aging men and is associated with prostatic inflammation [28]. It should be noted that benign prostatic hyperplasia (BPH) is another abnormality of the prostate gland, associated with age and characterised by overproliferation of the basal layer and stroma, but this is not thought to be a precursor for prostate cancer. There is strong evidence to suggest that PIN is a precursor lesion of prostatic adenocarcinoma [27], and it is characterised by hyperplasia of luminal epithelia, a reduction in basal epithelia and enlarged, atypical nuclei [29]. Oxidative stress [30] and telomere shortening [31, 32] have been linked to prostate cancer initiation, and both contribute to DNA damage. The emergence of PIN is associated with specific genomic changes, including downregulation of *NKX3.1*, often due to loss of heterozygosity of the 8p21 chromosome region that

codes for the *NKX3.1* homeobox gene [33] or otherwise as a result of epigenetic silencing [34]. The up-regulation of *MYC* expression has also been correlated with cancer initiation [35], although not as a direct result of gene amplification.

As PIN lesions develop into localised adenocarcinoma, *TMPRSS2-ERG* fusions are frequently observed: present in approximately 15% of high-grade PIN lesions and 50% of localised adenocarcinoma [36-38]. Disease progression correlates with further genomic alterations, including copy number loss of the *phosphatase and tensin homolog (PTEN)* tumour suppressor gene [39-41]. Conversely, an increase in senescence markers has also been associated with prostate cancer progression [42]. However, these may be markers of latent disease, with cellular senescence preventing carcinogenesis and clinical progression. Alternatively, senescence may later be overcome by other oncogenic events leading to invasive adenocarcinoma. Invasive carcinoma can be generally characterised by loss of basal lamina as a single-cell lining, which distinguishes it from high-grade PIN. There is consequential loss of the basal cell markers, p63 and cytokeratin 5 and 14, as well as increased expression of the luminal cell marker α -methylacyl-CoA (AMACR) [43]. Progression to invasive adenocarcinoma has been further associated with the re-activation of developmental signalling pathways, such as canonical Wnt signalling [44, 45] and ERK/MAPK pathway activation [41].

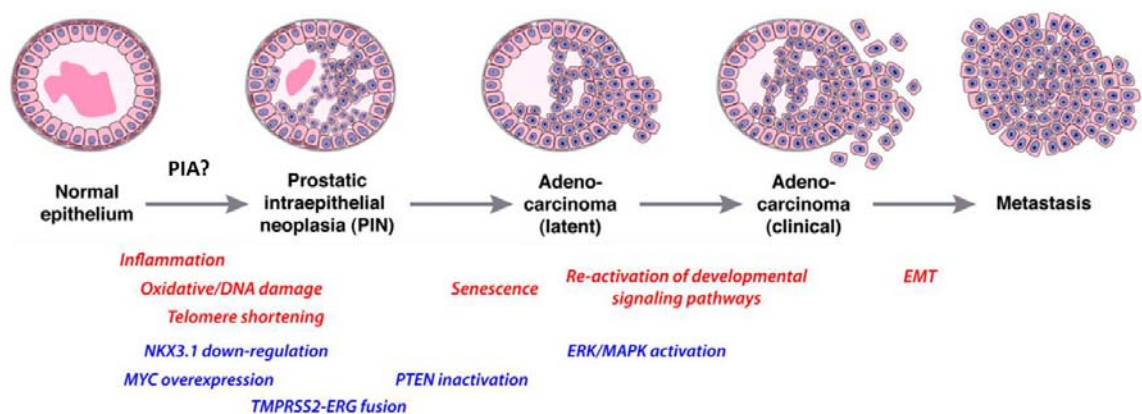


Figure 1.1.1 Human prostate cancer carcinogenesis

Schematic illustration showing the initiation and progression of prostate cancer, with the **molecular processes** and **gene/pathway aberrations** associated with each stage of cancer development. Proliferative inflammatory atrophy (PIA) may be a precursor to PIN. EMT = epithelial mesenchymal transformation. Adapted from Shen and Abate-Shen, 2010 [46].

The temporal sequence of other genetic aberrations and their cause and consequence, during stages of prostate cancer initiation and progression,

remains unclear. Integrated genomic analyses and molecular profiling of prostate cancers are contributing to our understanding of the molecular mechanisms involved in cancer development, latency and prognosis, and are discussed further in section 1.2.

1.1.2 Androgen signalling in prostate homeostasis and tumourigenesis

The *AR* gene, a member of the steroid hormone receptor family of genes, is located on the X chromosome at locus Xq11-12. Upon expression, it can be activated by androgens to undertake its role as a transcription factor, forming transcriptional complexes at gene promoters to up- or down-regulate target gene expression [47]. The AR protein is approximately 110 kDa in size, consisting of an N-terminal trans-activating domain (NTD), DNA-binding domain (DBD), hinge region and C-terminal ligand binding domain (LBD). In the absence of androgen, this LBD is bound by Hsp-90 and AR circulates in the cytosol. Testosterone diffuses across the cell membrane and is converted to the more potent DHT by 5 α -reductase. DHT-bound AR dissociates from Hsp-90 due to conformational changes to promote hetero- or homo-dimerization of AR. This active complex is targeted for translocation into the nucleus, where it interacts with cofactors and repressors at the promoter of target genes to regulate their transcription [47] (Figure 1.1.2). AR also activates proliferation and cell survival signals through interactions with MAPK and PI3K/Akt pathways [48].

AR plays a critical role in normal prostate development, regulating the expression of molecules involved in differentiation, proliferation, apoptosis and secretion, to maintain prostate homeostasis. AR regulates genes in a context specific manner, depending on the sequence and location of androgen response elements (AREs) associated with target genes [49]. Androgen signalling balances cell proliferation and survival with apoptotic signals and, therefore, has a major role in the development and progression of prostate cancer where this balance is lost [48]. The critical role of androgen signalling in prostate cancer was demonstrated by the regression of hormone naïve prostate cancer following androgen ablation, either by castration or oestrogen injection [2]. AR is not found to be mutated in untreated prostate cancer [50] but undergoes gain-of-function during cancer development, by mechanistic changes in AR signalling.

Paracrine androgen-regulated growth signals from the stroma are required for homeostasis of normal prostate epithelial cells. However, malignant prostate epithelial cells adopt an autocrine mechanism of androgen-stimulated growth regulation, leading to the hyper-proliferation of luminal epithelial cells in cancer lesions [51]. Thus, AR drives the growth, proliferation and survival of prostate cancer cells and its activity correlates with androgen-dependent disease progression.

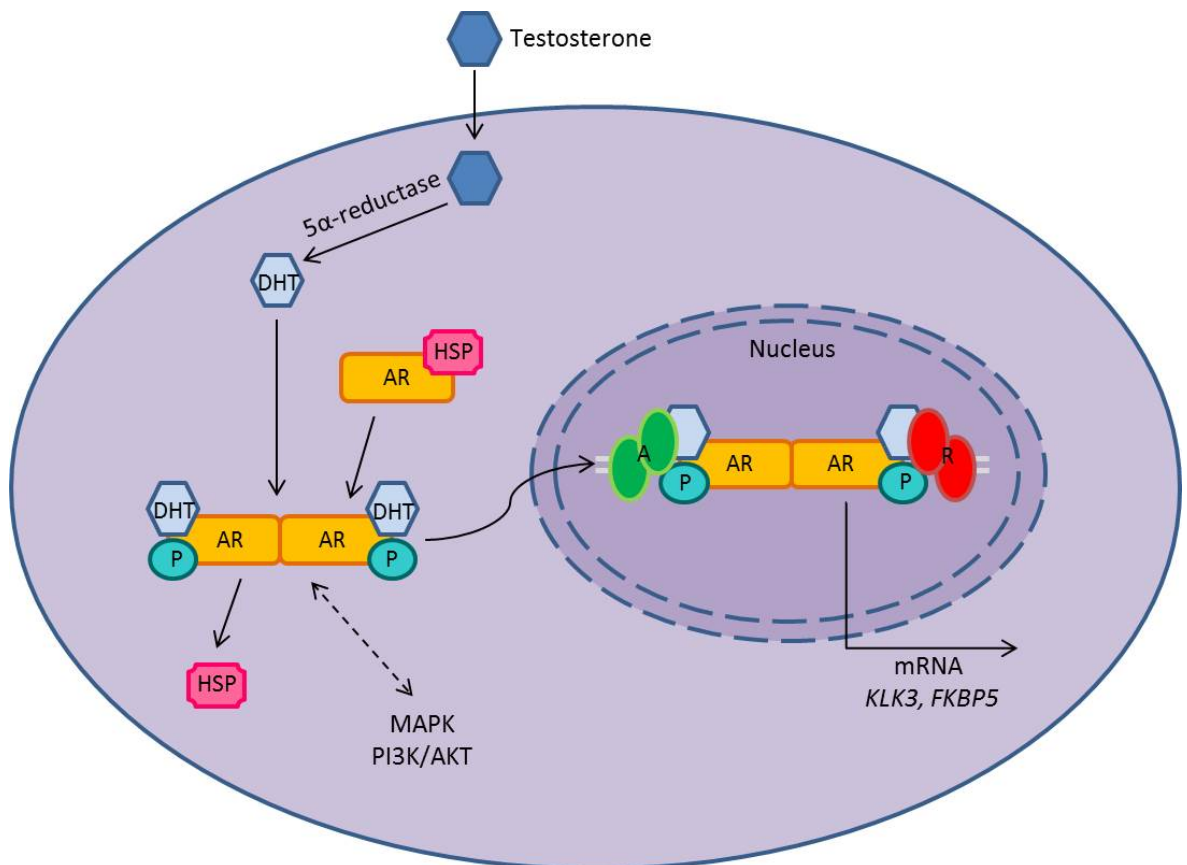


Figure 1.1.2 Androgen receptor signalling

Androgen receptor (AR) is activated by 5 α -dihydrotestosterone (DHT) and translocates into the nucleus where it regulates the transcription of target genes, including *KLK3*, which codes for PSA, and *FKBP5*. Abbreviations: HSP - heat shock protein 90; P - phosphate; A - co-activators; R - co-repressors

1.1.3 Systemic factors associated with prostate cancer

There is a direct correlation between prostate cancer development and aging, which is the greatest risk factor for prostate cancer. Although, the exact age-related molecular events that result in prostate cancer remain to be determined, genetic alterations pertaining to inflammation, oxidative stress and cellular senescence in the prostate have been associated with aging [52-54]. In

addition to age, a combination of environmental, ethnic and hereditary factors, determines cancer incidence, which varies between different populations [46]. Although the incidence of pre-neoplastic lesions is reported to be similar across the world [55], there is a much higher incidence of prostate cancer in American and Western European men compared to Asian populations. Studies have shown that the incidence of prostate cancer in Asian men increases when they migrate to Western countries [56], highlighting the importance of dietary and lifestyle factors for prostate cancer risk. However, no preventable risk factors are currently clearly linked to prostate cancer.

Within the last decade, significant evidence has emerged linking chronic inflammation with prostate carcinogenesis [57-59], and *in vivo* studies have shown that chronic inflammation promotes PIN development in rats and mice [60-62]. Furthermore, chemokines CXCL1, IL-15 and CCL4 have been reported as prognostic biomarkers for disease recurrence following prostatectomy [63], providing further evidence for the role of inflammation in prostate cancer. Various environmental factors, including diet, bacterial and viral infections, physical trauma and hormonal deregulation can contribute to chronic inflammation [64]. Diet, hormonal deregulation and inflammation also promote oxidative stress and DNA damage, which has been associated with aging and prostate cancer risk [65, 66]. Prostate susceptibility to the effects of reactive oxygen species (ROS) is likely attributed to the downregulation of major antioxidant enzymes, such as the glutathione S-transferase encoded by *GSTP1*, shown to be hyper-methylated and epigenetically silenced in prostate cancer [67].

Links between diet and oxidative stress have led researchers to investigate the potential of antioxidant supplements in prostate cancer prevention studies. One prevention trial tested effects of the antioxidant lycopene, present in tomatoes. Reduced DNA damage and serum PSA was observed in prostate cancer patients who consumed tomatoes daily for 3 weeks prior to prostatectomy, suggesting therapeutic benefits of lycopene consumption [68]. In contrast, the Selenium and vitamin E Cancer prevention Trial (SELECT), found that supplementation of selenium and vitamin E, alone or in combination, had no significant effect on prostate cancer risk [69]. Other studies, which tested vitamin C, vitamin E and β -carotene supplementation, found no benefit from vitamin C supplements and

only two subgroups of men had reduced risk of prostate cancer following increased intake of vitamin E and β -carotene: male smokers who took vitamin E supplements, and men with low dietary intake of β -carotene who were supplemented with β -carotene [70]. Despite the association of increased oxidative stress with prostate cancer initiation, a number of confounding dietary, lifestyle and genetic factors are likely to influence the efficacy of antioxidant supplementation and dietary intervention in prostate cancer prevention.

1.1.4 Diagnosis and treatment of prostate cancer

1.1.4.1 PSA testing and Gleason score

Since the 1980s, detection of prostate cancer has been facilitated by serum prostate-specific antigen (PSA) testing. The *KLK3* gene encodes PSA and its expression is positively and exclusively regulated by AR [71]. It was identified as a sensitive biomarker for prostate cancer diagnosis, disease progression and relapse following therapy [72] and is currently the only clinically approved biochemical biomarker for prostate cancer diagnosis. Normal blood serum PSA levels are low, while PSA levels correlating with low-, intermediate- and high-risk prostate cancers are <10 ng/ml, 10-20 ng/ml and >20 ng/ml, respectively.

PSA testing is combined with histopathological analysis of prostate tissue biopsies to determine prognosis and aid treatment choice. Tumours are graded in terms of severity and are given a Gleason score between 2 and 10, which is the sum of two morphologic scores for the tumour. Each morphologic score ranges from 1 to 5, with 5 defined as the least well-formed glandular structure [73]. Combined Gleason scores of ≤ 6 , 7 and 8-10 respectively represent low-, intermediate- and high-risk prostate cancer.

Widespread PSA screening has increased the number of tumours diagnosed at early stages of prostate cancer [74] but this has led to concerns of overtreatment in men whose cancer may have remained indolent. Active surveillance (distinct from watchful-waiting which signifies intention for symptomatic intervention in future, rather than radical treatments), has been

introduced into prostate cancer management for patients with low-risk, clinically localised disease and may also be considered for localised intermediate-risk prostate cancer [75]. This involves follow up with PSA testing, repeat biopsies and imaging to monitor signs of disease progression. Early detection and treatment intervention are essential for cancers that will progress to locally advanced and metastatic disease. However, diagnostic biomarkers that distinguish these cancers from indolent disease require to be developed in order to effectively manage prostate cancer treatment.

1.1.4.2 Targeting androgen receptor signalling to treat prostate cancer

While non-invasive, intracapsular (organ-confined) tumours can be successfully treated by prostatectomy or local radiotherapy, androgen deprivation therapy (ADT) remains the primary treatment of choice for locally advanced and/or metastatic prostate cancer. Adjuvant ADT is also prescribed in combination with radiotherapy for localised high-risk prostate cancer and locally advanced disease [76]. Androgen ablation can be achieved surgically by bilateral orchiectomy, or chemically through treatment with gonadotropin-releasing hormone agonists or antagonists, oestrogens or anti-androgens. The reduction in systemic testosterone levels induces programmed cell death in androgen-dependent prostate cells [77] and mediates prostate cancer regression. Luteinising hormone-releasing hormone (LHRH) agonists are predominantly used to reduce testosterone levels in patients. LHRH agonists achieve chemical castration by downregulating LHRH receptor activity in the pituitary gland, which leads to depletion of circulating LH and consequential inhibition of testosterone production in the testes [78].

However, ADT is a double-edged sword. Despite initial tumour regression, almost all men with advanced-stage prostate cancer relapse and develop castration-resistant prostate cancer (CRPC) following ADT. Patients experience a rising level of serum PSA and metastatic disease progression, often characterised by persistent AR signalling [79, 80]. Adrenal steroid production and intra-tumoural *de novo* steroidogenesis have been suggested to contribute to AR reactivation [81]. This has led to the development of second generation hormone therapies to overcome castration resistance mechanisms in prostate cancer. These include abiraterone, a potent inhibitor of androgen biosynthesis,

and enzalutamide, a second-generation antiandrogen that blocks AR transcriptional activity through high affinity binding to AR. These novel agents have brought survival benefits to some patients but unfortunately do not obviate cancer progression [82].

1.1.5 Castration-resistant prostate cancer

The invariable progression of advanced prostate cancers following treatment with ADT is predominantly associated with the reactivation of AR signalling. It has been proposed that a proportion of cells survive ADT and undergo growth arrest at G1 for a period of time. Regrowth and prostate cancer progression can then occur through cells adapting to low levels of circulating androgens [83] or developing androgen-independent mechanisms of AR activation [84]. In this way, AR appears to be oncogenic in a castrate environment. Mechanisms for the continuation or re-activation of AR signalling, involved in the failure of ADT and progression from HNPC to CRPC, are described in Table 1.1-1.

A recent study by Sharma et al [80] identified a signature of 16 genes at which AR binding was consistently enriched in CRPC, emphasising the role of AR signalling in disease progression. The signature included MYC, STAT and E2F, previously shown to play a role in CRPC development [85-88] and potentially useful as prognostic biomarkers.

Despite growing evidence for the role of AR signalling in the emergence and progression of CRPC, the failure of second generation ADT in a majority of patients highlights the complexity of resistance mechanisms. The transition from an androgen-dependent to androgen-independent molecular state within prostate cancer cells is also associated with AR-independent mechanisms for growth and survival [89]. Following treatment with ADT, prostate luminal epithelial cells undergo apoptosis, while androgen-independent basal stem and transit amplifying cells remain [90], and it is possible that these cells can give rise to AR-independent CRPC. Exome sequencing of 50 aggressive CRPCs identified 88 canonical pathways that were significantly mutated, including p53, Rb/E2F, JNK/MAPK, PTEN, PI3K/Akt and Wnt/ β -catenin pathways [91], which

have the potential to drive cell growth and survival in resistant cells, in an AR-independent manner. More recent developments in our understanding of the molecular mechanisms contributing to CRPC are described in section 1.2.2.

Table 1.1-1 Mechanisms for the continuation or reactivation of the AR signalling pathway in CRPC [84]

Mechanism	LD/LI	Description
Level of ligand	LD	Despite castration, a low level of androgen remains in the prostate which is capable of activating AR and promoting tumourigenesis. Androgens may be produced within the adrenal gland or via an intracrine mechanism in the prostate. It is apparent that ADT cannot cause 100% ablation of androgens within the prostate.
Level of AR protein	LD	AR protein levels are increased and amplification of the AR gene is seen in some cases. In other cases, increased AR mRNA expression is consistent in both hormone-naïve and castration-resistant prostate cancer cells. Up-regulation of AR protein levels increases cell sensitivity to low androgen concentration and results in up-regulation of AR-dependent gene expression.
Activating AR mutations	LD	AR mutations have been observed in 5-50% of CRPC cases and most commonly cause a gain in function. These receptors are often more sensitive to endogenous ligand or other steroid hormones/anti-androgens.
Changes in co-regulatory molecules	LI	AR co-regulatory molecules include co-activators that enhance and co-repressors that reduce AR function. Some co-regulatory molecules influence AR activity in a ligand-dependent manner. If the ratio of co-activators to corepressors changes in a low androgen-level environment, AR signal transduction can be altered resulting in aberrant transactivation activity and AR reprogramming.
Ligand independent activation	LI	There is evidence of crosstalk between other signal transduction pathways and AR, which may indirectly activate AR signalling, bypassing the need for ligand interaction. For example, HER-2/ <i>neu</i> is noticeably overexpressed in CRPC compared to HNPC [92, 93], which may act through MAPK and PI3K/Akt pathways to promote AR stability and transcriptional activity. Constitutively active AR variants which lack a LBD have also been identified [89, 94].

LD = ligand-dependent; LI = ligand-independent; LBD = ligand binding domain

1.2 Molecular profiling of human prostate cancer

The heterogeneity of prostate cancers reflects the genetic complexity of this disease, which needs to be better understood in order to improve diagnostic methods and treatment decisions for patients. Over the last five years a concerted effort has been made to profile the genetic mutations, copy number alterations and molecular expression patterns associated with cancer grade and prognosis. Integrated analysis using multiple modality platforms and large data sets is paving the way in prospective genomics. Data sets generated by microarray and, more recently, next generation sequencing (NGS) of prostate cancer tissue have uncovered mutations and gene expression changes associated with primary, metastatic and castration-resistant disease. Furthermore, NGS data from primary and metastasised prostate cancer tissue has been used to map the genetic phylogeny of prostate cancer in some patients, and work is ongoing to unravel the evolution of prostate cancer.

1.2.1 Genetic phylogeny of prostate cancer

To fully establish precision medicine in the clinic, the mechanism of prostate cancer development requires further investigation. A recent study by Cooper et al. carried out in-depth genome-wide DNA sequencing analysis of multiple primary prostate cancer samples taken from three patients [95]. To track the evolution of prostate cancer, copy number data was used to identify shared mutations or ERG fusions between cancer clone lineages, and differences that indicated breakpoints and branching into subclonal populations. Fluorescence *in-situ* hybridisation (FISH) was carried out to visualise mutations, such as different TMPRSS2-ERG fusions, to see whether they co-existed or were part of a lineage that underwent separate clonal expansion in a distinct cell population. Phylogenetic maps were constructed to illustrate common 'trunk' mutations, breakpoints and branching of distinct subclones, highlighting the multifocal nature of prostate cancer.

Interestingly, high levels of substitution mutations were observed in morphologically normal tissue that was not immediately adjacent to cancer tissue [95], indicative of clonal expansion. Some mutations present in morphologically normal tissue were shared with cancer clones, while others

were not yet detected in cancer tissue. There appears to be ongoing mutational processes, branching evolution and cancer clone mixing in primary prostate cancer tissue, suggesting that this may provide the basis for prostate cancer development and the multifocality of this disease [95]. Evidence of high levels of somatic mutations in morphologically normal tissue suggests the importance of targeting and ablating surrounding ‘normal’ cells, in addition to cancer, during focal therapy. Furthermore, the intra-tumoural heterogeneity of prostate cancer illustrates the continuing challenge posed to researchers investigating novel diagnostic biomarkers and targeted therapies.

Lethal prostate cancer is likely to arise from competing subclones within primary prostate tumours, which are able to metastasise and develop resistance to therapy. Deep sequencing analyses of multiple samples from individual patients with lethal metastatic prostate cancer, including primary tumour, hormone-naïve and castration-resistant metastasis, have uncovered molecular events involved in the evolution of metastatic disease and illustrated the complexity of metastatic spread [96, 97]. Multiple primary tumour subclones were found to be involved in metastasis [96], supporting the hypothesis of polyclonal seeding and contradicting an earlier hypothesis that single primary cancer cells are responsible for each metastasis [98]. In one study, inter-metastatic spread was observed in 5/10 patients [96], suggesting polyclonal seeding also occurs between metastatic sites. Some of this clonal expansion was attributed to resistance mechanisms driven by ADT, as subclones harboured alterations in *AR* or *AR* pathway component genes, involved in *AR*-dependent mechanisms of resistance, or *MYC* amplification or *CTNNB1* mutation, involved in alternative mechanisms to bypass ADT [96].

Clonal differences, within both primary tumours and metastasis, indicate that sub-populations of cells are likely to respond differently to treatments. Moreover, new mutations in cancer clones arise as a result of therapy and the development of resistance mechanisms [96, 97, 99]. An example of these phenomena was identified in an iliac metastasis, which was clonal prior to ADT treatment but contained two subclonal populations when castration-resistant [97]. One of these subclones had evolved from the hormone-naïve clonal population but the second subclonal population was derived from a distant metastatic site. Hong et al. surmised that the iliac metastasis was receding and,

hence, responsive to ADT, while the subclone from the second metastatic site was mechanistically predisposed to be resistant to ADT and could therefore invade the iliac metastatic niche following treatment.

Larger studies are required to validate these findings. However, these new observations are reshaping our understanding of prostate cancer development and the paths of evolution leading to lethal, metastatic and treatment resistant disease.

1.2.2 Classification of prostate cancers by genetic profiling

By understanding the molecular mechanisms of aggressive and treatment resistant prostate cancer, we can identify better prognostic markers at early stages of disease to predict clinical outcome and tailor treatment decisions accordingly. Currently, Gleason score is considered the best prognostic marker of cancer grade. In a bid to reduce the risk of overtreatment of prostate cancer, active surveillance is an option for patients with low (Gleason score ≤ 6) to intermediate risk (Gleason score 7) localised prostate cancer [75]. However, a number of patients diagnosed with low Gleason score prostate cancer will progress to aggressive disease (or have higher risk disease not detected due to sampling errors) and may, therefore, benefit from early treatment intervention. A large amount of prostate cancer research is now focussed on identifying subsets of prostate cancer patients based on their molecular profiles and correlating these with cancer aggressiveness, treatment response and survival outcome.

One study [100] analysed a microarray data set of 281 samples from a Swedish watchful-waiting cohort [101]. Markert and colleagues employed a method of bioinformatics analysis which studied the expression of gene sets known to be under- or over-expressed in embryonic stem cells (ESCs) to identify subsets of prostate cancer with an ESC-like signature. This has previously been shown to positively correlate with aggressive cancers and poor prognosis [102, 103]. The expression of other gene sets associated with induced pluripotent stem cells (iPSCs) and the polycomb repressive complex-2 (PRC2) signatures were also analysed. Unsupervised clustering of these, and other transcriptional signature profiles associated with prostate cancer, distinguished five molecular subtypes:

1) ESC, p53-, PTEN-; 2) TMPRSS2-ERG fusion; 3) Cytokine, Ras, Mesenchyme; 4) Transitional; and 5) PRC2 (normal-like). Patients in cluster 1 had the poorest survival outcome, and this was also associated with *MYC* activation, increased inflammatory signals, indicated by cytokine expression, and increased proliferation [100]. These findings were corroborated using mRNA expression data from 185 samples obtained from a cohort of patients at the Memorial Sloan Kettering Cancer Centre who underwent radical prostatectomy [41].

In other studies, clustering data according to DNA copy number alteration (CNA) defined low- and high-risk prostate cancer more reliably than Gleason score [41] and high CNA burden has been associated with biochemical relapse of prostate cancer [104]. CNAs associated with poor prognosis include *MYC* amplification and *PTEN* loss [46, 100], and may be robust prognostic markers to stratify risk in prostate cancer patients.

The application of molecular profiling analyses is also required to identify clinically targetable molecular alterations in individuals who already have aggressive metastatic and castration-resistant prostate cancer. Pursuing the vision of precision therapy for prostate cancer, the Prostate Cancer Dream Team grant has facilitated the establishment of a multi-institutional clinical sequencing infrastructure, co-ordinated by Arul Chinnaiyan and Charles Sawyers. The team's objective is to integrate whole-exome and transcriptome sequencing analysis of tumour biopsies from large cohorts of patients with metastatic CRPC, to characterise genomic alterations and how they differ from primary prostate cancer.

A prospective study of a metastatic CRPC cohort of 150 patients identified the greatest proportion of genetic mutations in *AR* (62.7%), *TP53* (53.3%), *PTEN* (40.7%) and *ETS* fusions (56.7%) [99]. Furthermore, comparison to primary prostate cancer data showed that mutations in *AR* were exclusive to castration-resistant disease and over 70% of CRPC cases had aberrations in *AR* pathway genes, indicating that these tumours remained *AR*-dependent. However, this means around 30% of CRPC cases are likely to be *AR*-independent and 65% of cases were found to harbour alterations, other than *AR* aberrations, that may be targeted therapeutically. The authors highlighted aberrations in PI3K, Wnt, cell-

cycle and DNA repair pathway genes and predicted benefits of prescribing patients with clinically-available therapies to target these signalling pathways.

1.3 PTEN and Wnt signalling in prostate cancer

The AR signalling pathway plays a fundamental role in the development of prostate cancer and is often central to the emergence of castration-resistant disease. However, the deregulation of a number of other pathways significantly contributes to disease progression and prognosis. In particular, there is increasing evidence that PTEN loss and Wnt/ β -catenin pathway activation are associated with aggressive prostate cancer. Pathways do not act linearly but co-operate and interact, influencing the transcription and translation of their own and other pathway components through downstream signalling events and feedback loops. The role of β -catenin signalling in prostate cancer requires further exploration, and mechanisms by which PTEN loss and β -catenin activation may co-operate are yet to be characterised in this disease.

1.3.1 PTEN-mediated tumour suppression

The PTEN (Phosphatase and TENsin homolog on chromosome 10) tumour suppressor, discovered in 1997 [105-107], is a protein and phospholipid phosphatase, best known for its role in the regulation of phosphoinositide signalling [108]. Phosphoinositide-3-kinase (PI3K) is predominantly activated and recruited to the membrane by receptor tyrosine kinase (RTK) signalling, and in turn regulates serine/threonine protein kinase (Akt) via phosphorylation of phosphatidylinositol (4,5)-triphosphate (PIP₂) and generation of the second messenger phosphatidylinositol (3,4,5)-triphosphate (PIP₃). Akt is activated following phosphorylation by PIP₃, phosphoinositide dependent kinase 1 (PDK1) and mammalian target of rapamycin complex 2 (mTORC2), and regulates a number of downstream effectors that contribute to cell survival, proliferation and migration. This includes the inhibition of pro-apoptotic signalling via BCL2-associated agonist of cell death (BAD) and BCL2-interacting mediator of cell death (BIM); the downregulation of p27 and GSK3 β to facilitate cell cycle entry and proliferation; and activation of mTOR signalling, which drives protein/lipid

synthesis and cell growth [109]. PTEN dephosphorylates the 3'-phosphate group of PIP3, produced by PI3K activity, to produce PIP2. By decreasing levels of PIP3, Akt is no longer recruited to the membrane for activation. In this way, PTEN negatively regulates PI3K/Akt signalling, facilitating apoptosis and downregulating cell cycle progression and proliferation (Figure 1.3.1).

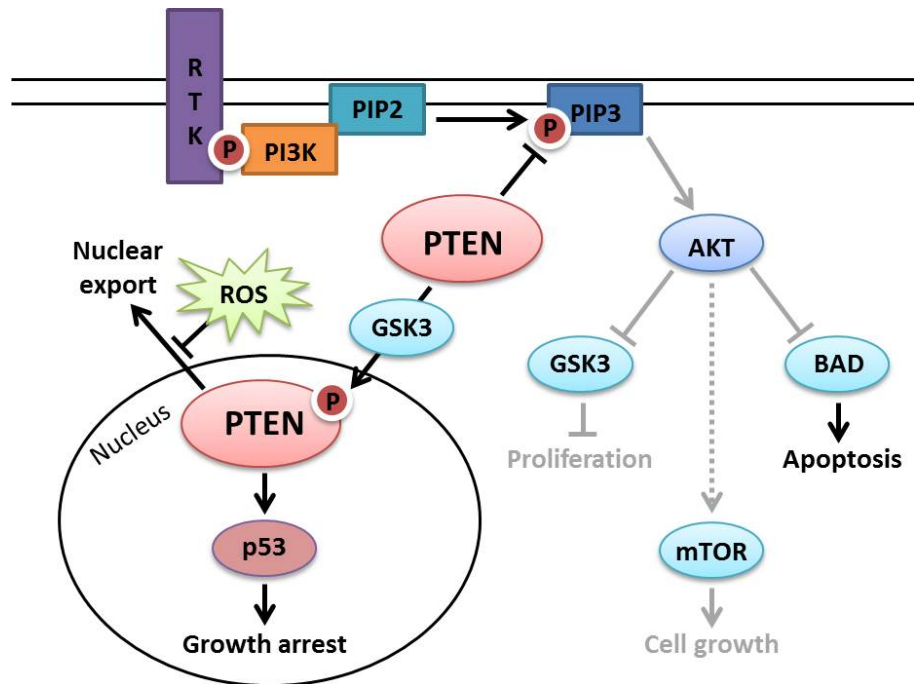


Figure 1.3.1 Mechanisms of PTEN tumour suppression

PTEN regulates tumour suppression via phosphatase-dependent inactivation of PI3K/Akt signalling, and via phosphatase-independent p53-mediated tumour suppression. Phosphoinositide-3-kinase (PI3K) converts phosphatidylinositol (4,5)-kinase (PIP2) to phosphatidylinositol (3,4,5)-kinase (PIP3). PIP3 in turn activates Akt leading to cell survival, growth and proliferation through inhibition and activation of downstream targets, including glycogen synthase kinase 3 (GSK3), mammalian target of rapamycin (mTOR) and BCL2-associated agonist of cell death (BAD). PTEN inhibits Akt activation in a phosphatase-dependent manner, by dephosphorylating PIP3, and promotes apoptosis and tumour suppression. Phosphorylated PTEN translocates to the nucleus, where it facilitates p53-mediated tumour suppression in a phosphatase-independent manner. ROS blocks nuclear export of PTEN, leading to PTEN accumulation in the nucleus.

While predominantly localised in the cytoplasm, nuclear accumulation of PTEN can be promoted by GSK3 β -mediated phosphorylation at Ser380/Thr383/Thr388 residues in the PTEN C-tail domain [110]. Phosphorylation increases the stability and alters the conformation of PTEN, preventing membrane interaction and PTEN phosphatase activity [111]. Oxidative stress is able to regulate PTEN localisation by inhibiting export of PTEN from the nucleus. This facilitates the role of PTEN in p53-mediated tumour suppression, whereby nuclear PTEN interacts with p53 in a phosphatase-independent manner to drive G₁ growth

arrest [112]. Furthermore, nuclear PTEN protects genomic stability by regulating chromosomal integrity and DNA repair [113]. Thus, PTEN functions as a tumour suppressor by both phosphatase-dependent and phosphatase-independent mechanisms (Figure 1.3.1).

PTEN is essential for cellular differentiation during embryogenesis [114] and plays an integral role in the regulation of apoptosis, cell cycle control, cell adhesion and migration [115]. Given its critical role in homeostasis and tumour suppression, PTEN is tightly regulated by multiple transcriptional, post-transcriptional, translational and post-translational mechanisms, which influence its function, stability and cellular localisation (recently reviewed by Bermudez Brito et al. [111] and Jerde [116]). A number of kinases, such as Sprouty2 and the MAPK pathway (via c-Jun) regulate PTEN transcription, while various miRNAs and the *PTEN* pseudogene, a long non-coding RNA that sequesters miRNAs to positively regulate *PTEN*, contribute to its post-transcriptional regulation. At the protein level, PTEN is further regulated by phosphorylation, oxidation and ubiquitination. The extensive signalling network that regulates PTEN, together with the numerous cellular events regulated by PTEN, highlights the complexity of PTEN-mediated tumour suppression.

1.3.2 PTEN loss in prostate cancer

Chromosome 10q23, containing the *PTEN* gene, is commonly mutated and often undergoes loss of heterozygosity (LOH) in human cancers [108]. PTEN is down-regulated in almost 50% of advanced metastatic prostate cancer due to decreased expression, mutation or biallelic deletion of the *PTEN* gene [41, 99, 117]. The role of *Pten* loss in prostate cancer has been well characterised in mouse model studies, demonstrating that *Pten* is critical for tumour suppression. *Pten* haploinsufficiency has been shown to initiate PIN development in the mouse prostate [114], while homozygous deletion resulted in progression to invasive adenocarcinoma [118]. Furthermore, *Pten* null prostate tumours regressed in response to ADT but a subset of cancer cells continued to proliferate in the absence of androgens [118]. In human prostate cancer, the complete loss of *PTEN* is associated with advanced and aggressive disease, and frequently observed in CRPC [99]. *PTEN* loss correlates with deregulation of PI3K/Akt signalling, with just over 40% of primary prostate cancers and 100% of

metastatic disease harbouring alterations in this pathway [41], fuelling cell survival and proliferation. This has led to the development of several inhibitors to target PI3K/Akt and mTOR signalling in cancer, although variations in their efficacy have been observed due to the emergence of resistance [109]. This may be explained in part by crosstalk between AR and PI3K pathways, shown to cross regulate each other by reciprocal feedback [119]. When PI3K signalling was inhibited, there was activation of both AR and MAPK signal transduction pathways, two pro-survival pathways capable of driving cancer progression.

As *Pten* haploinsufficiency is capable of driving prostate cancer initiation in mice, it is likely that PTEN loss plays a role in earlier stages of cancer development through co-operation with other molecular aberrations. PTEN itself interacts with AR as a scaffold protein, preventing AR nuclear translocation and promoting AR degradation [120]. Therefore, loss of PTEN may contribute to increased AR stability and activation in prostate cancer. Moreover, a number of non-mutational processes can contribute to the loss of PTEN function through deregulation of signalling events that regulate PTEN expression, stability and localisation, such as oxidative stress, which is elevated in cancer, and aberrant microRNAs. MicroRNAs have been found to down-regulate *PTEN* expression in prostate cancer cells, including miR-153 [121], miR-19b, miR23b, miR-26a and miR-92a [122] and many others are associated with loss of PTEN expression in other human cancers, such as miR-17 [123], miR-18a [124] and miR-21 [125]. Furthermore, reactivation of developmental signalling pathways is associated with prostate cancer progression [46], and there is growing evidence for the role of developmental signalling in PTEN regulation [116].

1.3.3 Canonical Wnt signalling

Wnts are a family of secreted cysteine-rich proteins. The *Wnt* (or *Wingless*) gene was first identified in *Drosophila melanogaster*, and named so because its mutation prevented wing development and caused defects in the segmentation of larvae [126]. Similar effects were observed following the mutation of *ARM* (or *Armadillo*), the *D. melanogaster* orthologue of *CTNNB1* (β -catenin), discovered to be key effector of the canonical Wnt signalling pathway [126]. Wnt proteins are expressed in a gradient pattern during embryo development, leading to differential activation of β -catenin, which controls the development of the

anterior-posterior axis. Wnt signalling continues to be required for stem cell maintenance and homeostasis in adult tissue, and organs such as the intestine depend highly on Wnt/ β -catenin activation for self-renewal processes [127]. As one of the essential signalling pathways required throughout early development and adult life, it is unsurprising that the disruption of this pathway leads to several types of human cancer, including colorectal, breast, liver and prostate cancer [128].

β -catenin stabilisation is regulated by a destruction complex, incorporating adenomatous polyposis coli (APC) protein, Axin1 scaffold protein, glycogen synthase kinase-3 (GSK3B) and casein kinase 1 (CK1). In the absence of Wnt ligand, GSK3B and CK1 phosphorylate serine residues in β -catenin, targeting β -catenin for ubiquitination by β -TrCP ubiquitin ligase and proteasomal degradation. Wnt binding to frizzled receptors (FZD) and low-density lipoprotein receptor-related proteins (LRP) disrupts the destruction complex by recruiting dishevelled and the APC/Axin complex to the membrane. β -TrCP dissociates from the destruction complex and β -catenin is no longer ubiquitinated [129]. Stabilised β -catenin accumulates and translocates into the nucleus to carry out its role as a transcriptional co-activator of T-cell factor/lymphoid enhancer factor (TCF/LEF) and AR-regulated genes (Figure 1.3.2).

β -catenin/TCF/LEF target genes include *c-MYC* [130], the metalloproteinase *MMP7* [131] and *CCND1* (cyclin D1) [132]. *C-Myc* is a multifunctional protein with important roles in cell cycle control, ribosomal biogenesis, protein synthesis, mitochondrial function and metabolism, and negatively regulates growth arrest and cell adhesion [133]. *MMP7* (also known as Matrilysin-1) is involved in the degradation of extra-cellular matrix proteins and regulation of cell surface proteins [134], and cyclin D1 is part of the cell cycle machinery, contributing to cell cycle progression [135]. Thus, Wnt/ β -catenin target genes are involved in a variety of processes from tissue development and regeneration to cell cycle, survival and metabolism.

Further to its role as central effector of the canonical Wnt signalling cascade, a large proportion of β -catenin is associated with cadherin cell adhesion complexes at cell junctions (Figure 1.3.2), where it plays an integral role in cell-cell interactions. Changes in cadherin/ β -catenin complexes may increase levels

of free β -catenin in cells, contributing to activation of canonical Wnt signalling [136].

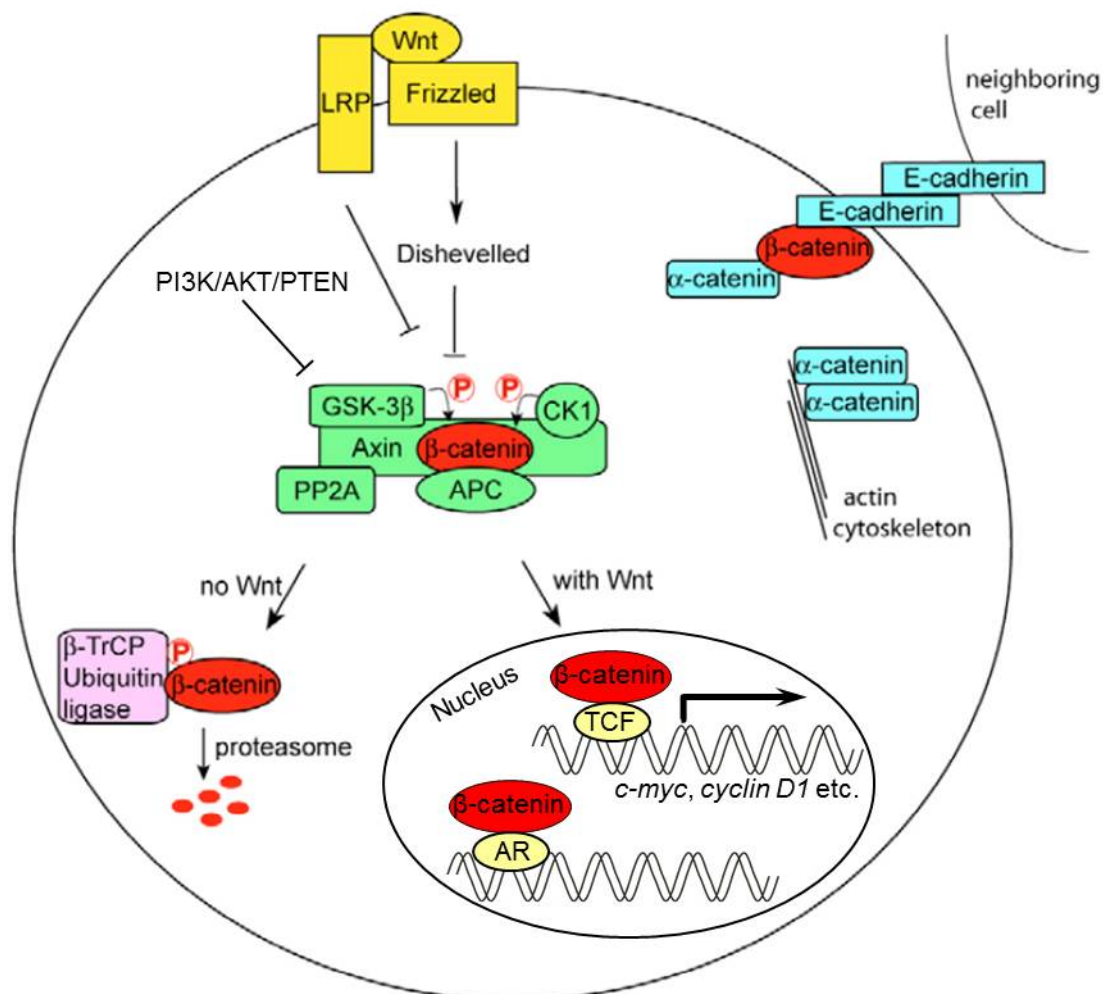


Figure 1.3.2 Canonical Wnt signalling pathway

In the absence of Wnt, β -catenin is phosphorylated by GSK3 β and CK1 and targeted for proteasomal degradation by the APC/Axin destruction complex. In the presence of Wnt, the destruction complex is disrupted and β -catenin is no longer degraded. Stabilised β -catenin translocates to the nucleus where it regulates the expression of target genes, including *c-Myc* and *cyclin D1*. Activation of PI3K/Akt, due to down-regulation of PTEN, has been shown to inhibit the destruction complex via GSK3 β phosphorylation, leading to Wnt-independent β -catenin activation. β -catenin also plays an integral role in cell adhesion in complex with α -catenin and E-cadherin. (Adapted from Xu and Kimelman, 2007 [137], with permission of Company of Biologists Ltd).

1.3.4 β -catenin and prostate cancer

β -catenin is essential for normal prostate development but not required for homeostasis in the adult prostate [138]. Over the past two decades, researchers have compiled substantial evidence for β -catenin activation in prostate cancer, although its role as a proto-oncogene is not well defined. Deregulation of

Wnt/ β -catenin signalling can be attributed to a variety of causes which continue to be investigated. Mutations in *exon3* of the β -catenin gene (*CTNNB1*) have been found in approximately 5% of prostate cancer patients [139-141]. *Exon3* contains the GSK3 β phosphorylation site, without which β -catenin can evade regulation by APC and TrCP. Thus, β -catenin escapes degradation, resulting in its stabilisation and accumulation in the nucleus. In a small study of 22 prostate cancer samples, mutually exclusive mutations were also observed in *APC* (9.1%) and *TrCP1* (13.6%)[142]. Furthermore, exome sequencing of lethal metastatic prostate cancer has identified significant Wnt pathway mutations, including *APC*, *CTNNB1* and *MYC*, that potentially contribute to the emergence and progression of CRPC [91, 143]. More recently, mutations in genes coding for *APC* (8.7%), β -catenin (4%), R-spondin 2 (1.3%) and E3 ubiquitin protein ligases, *RNF43* (2.7%) and *ZNRF3* (2.0%) were identified in another cohort of patients with metastatic CRPC [99], contributing to Wnt pathway deregulation in aggressive prostate cancer.

Overall there is a low mutation rate of Wnt pathway components in prostate cancer, which does not reflect the extent to which β -catenin localisation and expression is altered, particularly in high-grade, advanced stage disease. Studies have shown between 40% and as many as 80% of tumours with high Gleason scores ≥ 7 express increased levels of β -catenin as compared to BPH and low-grade cancer [44, 45, 141, 144]. Therefore, changes in β -catenin expression itself, the expression of Wnt ligands in the prostate tumour microenvironment [145, 146], or altered expression of other Wnt/ β -catenin pathway components (Figure 1.3.3) may contribute to the activation of endogenous Wnt/ β -catenin signalling. Recently, *APC* hyper-methylation has been reported as a reliable biomarker in the identification of high-risk prostate cancer [147] and likely to be indicative of activated Wnt/ β -catenin signalling.

While the role of Wnt/ β -catenin signalling has been well characterised in colorectal, lung and pancreatic carcinogenesis, few studies have investigated its role in the prostate. To date, published data indicates that stabilisation and activation of β -catenin in the mouse prostate causes neoplastic transformation [148], high-grade PIN [149] and cancer progression to invasive adenocarcinoma, when combined with large probasin promoter directed SV40-large T-antigen expression [150], *Pten* loss [138] and *AR* amplification [151]. This suggests that

β -catenin activation is capable of driving prostate cancer initiation but requires co-operation with other molecular events to promote cancer progression.

Several Wnt pathway inhibitors have already been developed and there is increasing data to suggest benefits for their use in prostate cancer management, where pharmacological targeting of Wnt/ β -catenin signalling is clinically relevant. Tankyrase inhibitors, which reactivate the destruction complex, and porcupine (PORCN) inhibitors, which block Wnt ligand secretion, are currently being evaluated in various cancer models [128].

1.3.4.1 β -catenin co-operation with Pten loss and PI3K pathway deregulation

Wnt/ β -catenin and PI3K/Akt mediated signalling are frequently deregulated in prostate cancer. Data from the MSKCC prostate adenocarcinoma study [41], accessed through cBioPortal for Cancer Genomics, demonstrates the clinical relevance of concurrent deregulation of these pathways (Figure 1.3.3). PTEN and PIK3CA, PIK3R1 and PIK3R2 alterations contribute to aberrant PI3K/Akt signalling, while the remaining genes are indicative of canonical Wnt pathway alterations. Over 70% of the primary tumours with mRNA expression data have alterations in one or more of the selected genes and 31% of these tumours display aberrations in both pathways (Figure 1.3.3A). It should also be noted that Wnt pathway genes alone are altered in 28% of primary tumours. In the metastatic tumour case set, 79% exhibit alterations in the selected genes but the number of these tumours harbouring mutations in both PTEN/PI3K and Wnt/ β -catenin extends to 93% (Figure 1.3.3B), and 95% of the metastasis have alterations in these pathways (Figure 1.3.3C). Furthermore, patients in the metastatic tumour case set had a significantly poorer survival outcome compared to the 21% with no aberrations in this gene set (Figure 1.3.3D). This strongly implies that deregulation, and potential crosstalk, of Wnt/ β -catenin and PTEN/PI3K/Akt pathways drives aggressive prostate cancer with poor prognosis.

Co-operation between Wnt/ β -catenin and PI3K/Akt pathways has already been shown to promote tumourigenesis in a bladder cancer [152] and prostate cancer [138] mouse model with combined β -catenin activation and Pten loss. However, mechanistically, it is unclear how these aberrations co-operate in tumourigenesis. Loss of PTEN activity results in the upregulation of Akt kinase

activity and some studies have suggested that this in turn inhibits GSK3B to activate β -catenin [153, 154]. However, β -catenin deletion did not affect prostate tumourigenesis in a *Pten* null prostate cancer mouse model [138], suggesting this mechanism is not required for prostate cancer initiation or progression. Meanwhile, the effects of β -catenin activation on PTEN or PI3K/Akt signalling have not been described.

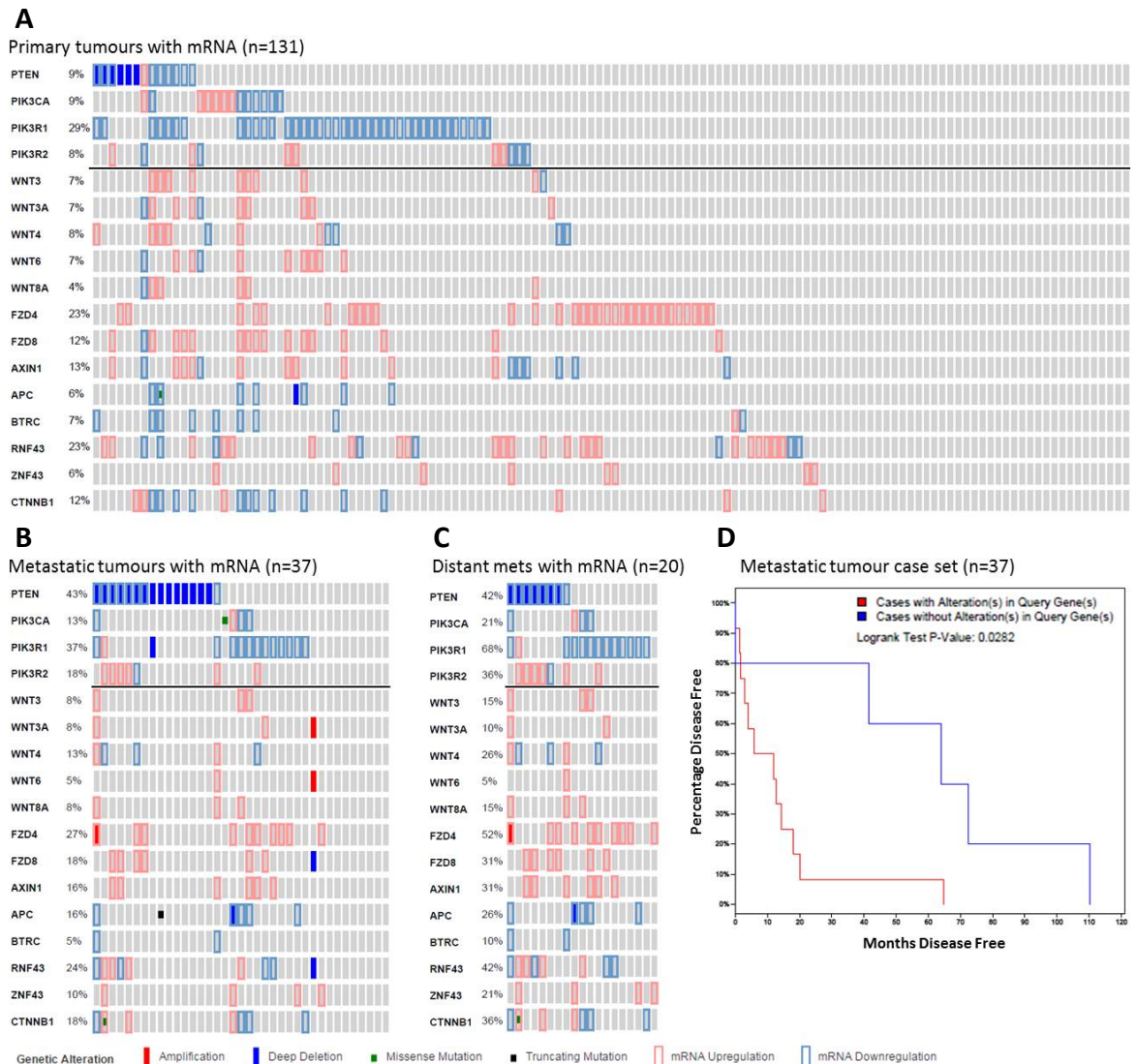


Figure 1.3.3 PTEN/PI3K and Wnt/ β -catenin pathway deregulation in aggressive prostate cancer (MSKCC prostate adenocarcinoma study data set [41] analysed in cBio Portal for Cancer Genomics)

Alterations in PI3K/Akt pathway regulators (above black line) and canonical Wnt pathway components (below black line) are shown in (A) 91 of 131 primary tumour cases with mRNA, (B) 29 of 37 metastatic prostate tumours and (C) 19 of 20 distant metastasis with mRNA. PTEN - phosphatase and tensin homologue; PIK3CA - phosphoinositide-3-kinase catalytic subunit (p110); PIK3R1 - phosphoinositide-3-kinase regulatory subunit 1 (p85 α); PIK3R2 - phosphoinositide-3-kinase regulatory subunit 2 (p85 β); FZD - frizzled receptor; BTRC - TrCP ubiquitin ligase; RNF43 and ZNF43 - E3 ubiquitin protein ligases; CTNNB1 = β -catenin. (D) Kaplan-Meier survival plot corresponding to metastatic prostate cancer case set (n=37) in (C). The red line represents cases with aberrations in the selected gene set and the blue line represents cases without aberrations in selected gene set. P value = 0.0282, analysed by Logrank Test.

1.3.4.2 β -catenin crosstalk with AR signalling

Androgen and Wnt signalling pathway enrichment has been associated with early-onset prostate cancer [155]. Furthermore, up-regulation of nuclear β -catenin immunohistochemical staining is commonly observed in CRPC. One study showed 38% of CRPC samples had abnormal β -catenin staining compared to only 23% of untreated prostate cancer [44], and recent genomic and transcriptomic analyses have identified significant Wnt/ β -catenin pathway aberration in CRPC [99, 156]. The reactivation of AR signalling is a hallmark of CRPC and can be a result of changes in AR co-regulatory molecules (Table 1.1-1). Therefore, alterations in β -catenin protein levels may influence AR signalling, through β -catenin's role as an AR cofactor [157], and play a role in prostate cancer progression and treatment resistance.

There is evidence that β -catenin increases AR transcriptional activity in an androgen-dependent manner [158]. A recent study by Lee et al. [151] identified a synergistic relationship between transgenic AR and β -catenin stabilisation, which drove aggressive prostate cancer in mice. Regression of these tumours in response to castration demonstrated that AR signalling was required for β -catenin-driven tumorigenesis and suggested the importance of AR and β -catenin co-regulation in prostate cancer initiation and progression. In correlation with these observations, prostate-targeted β -catenin activation has previously been shown to up-regulate AR signalling during development of hyperplastic lesions in mice [149]. However, downregulation of AR and AR target genes has been reported in high-grade PIN and progression to adenocarcinoma, as a consequence of constitutive Wnt/ β -catenin signalling in murine prostate tissue [149, 150], suggesting that β -catenin can also decrease AR transcriptional activity. An inverse correlation between β -catenin nuclear localisation and AR expression was also observed in human prostate cancer bone metastasis, suggesting that downregulation of AR may facilitate Wnt/ β -catenin signalling in this context [159].

Wnt/ β -catenin pathway activation has been shown to confer resistance to antiandrogen treatment *in vitro* [158] and constitutive β -catenin activation in the adult mouse prostate was shown to promote continuous growth post-castration [149], implicating the involvement of Wnt/ β -catenin signalling in the

progression from HNPC to CRPC. A LNCaP hollow fibre model, genomically similar to clinical samples, demonstrated reactivation of AR signalling and Wnt/ β -catenin pathway activation in CRPC [160]. Wang et al. observed increased expression of β -catenin and AR, which interacted and co-localised within the nucleus of castration-resistant tumour cells. This was not observed in tumours from non-castrated mice, and suggested that Wnt/ β -catenin activation, resulting from androgen ablation, may drive aberrant AR activity, contributing to CRPC progression. Furthermore, inhibition of nuclear β -catenin has been shown to inhibit AR signalling through disruption of β -catenin/AR target gene transcription, and blocked prostate tumour growth in mice and the proliferation of castration-resistant cells [161].

The studies described above provide evidence for both positive and negative regulation of AR signalling by β -catenin in prostate cancer. There is evidence that crosstalk between AR and β -catenin varies during stages of cancer progression in a context-dependent manner. While AR signalling is reported to be required for initiation of β -catenin-driven prostate tumorigenesis, it appears that the activation of Wnt/ β -catenin signalling is capable of promoting AR-dependent and AR-independent mechanisms of prostate cancer progression and castration-resistance. Further mechanistic insight is required to understand the relationship between AR and β -catenin in prostate cancer.

1.4 Mouse models of prostate cancer

Molecular profiling of genomic and transcriptomic aberrations, and their classification according to risk, is proving invaluable for the future of prostate cancer management. However, it is the translation of these aberrations into functional downstream effects that drives prostate cancer development and progression. Signalling pathways interact and co-operate, influencing the rate of cancer progression and aggressiveness of disease. The use of pre-clinical animal models facilitates investigation of prostate cancer drivers and pathway interactions in an *in vivo* context, also taking into account the influence of tumour-host interactions.

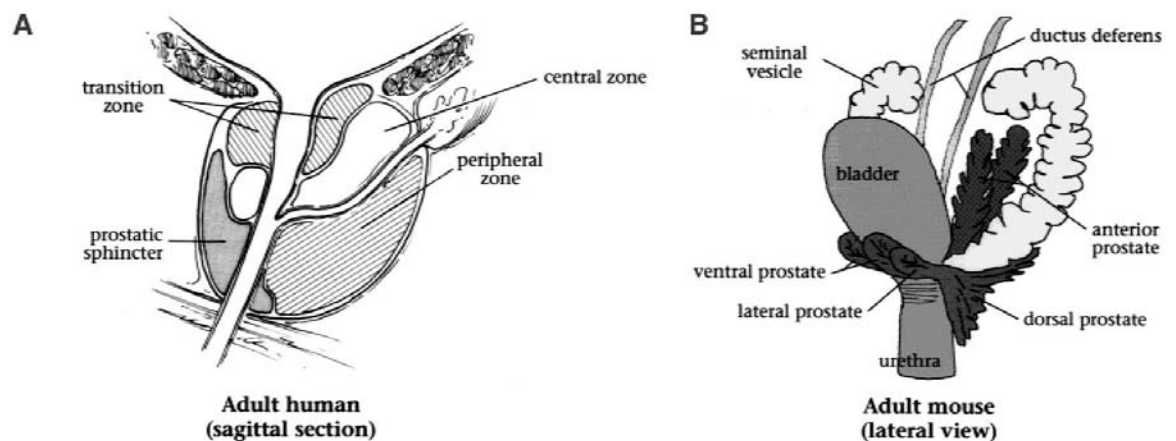


Figure 1.4.1 Human and mouse prostate anatomy

Diagrams illustrating the anatomy of (A) the adult human prostate in contrast to (B) the adult mouse prostate (adapted from Abate-Shen & Shen, 2000 [7]).

The human prostate gland is approximately the size of an acorn and consists of three distinct regions: the central zone, the peripheral zone and the transition zone (Figure 1.4.1A). This anatomy contrasts with that of the murine prostate which consists of the anterior, dorsal and lateral (or dorsolateral) and ventral lobes (Figure 1.4.1B). These lobes are distinguishable by their different gland morphology (Figure 1.4.2A-C). Murine prostate glands are composed of luminal, basal and neuroendocrine epithelial cells, with a central lumen containing secretions, and surrounded by stroma (Figure 1.4.2D). Unlike, human prostate morphology, basal cells are not in a continuous single-cell layer. Despite distinct differences between human and mouse prostate structure, the stages of cancer progression in the mouse closely mimic that in humans (Figure 1.4.3) [162].

Hence, xenograft, transgenic and knockout mouse models have proved to be suitable animal models for studying prostate development and carcinogenesis [7].

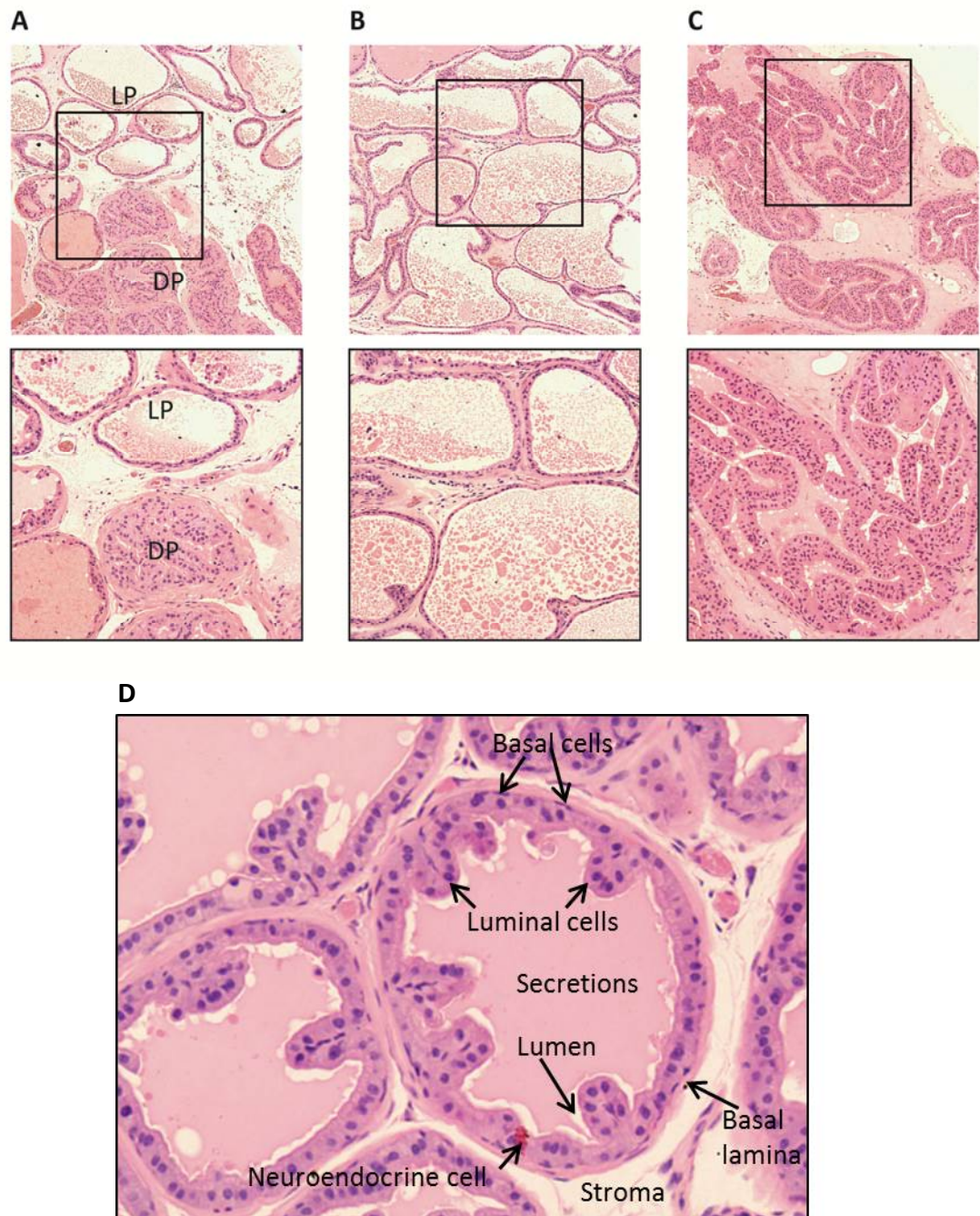


Figure 1.4.2 Pathology of normal mouse prostate

Haematoxylin and eosin staining of FFPE *wildtype* prostate tissue, showing normal histology of (A) the dorsal prostate (DP) and lateral prostate (LP), (B) ventral prostate and (C) anterior (coagulating) prostate glands at low (top panel) and high (bottom panel) power magnification. (D) Cell types and compartments in murine prostate tissue. (A-C Reproduced from Brzezinska et al, 2015 [162], with permission of Springer).

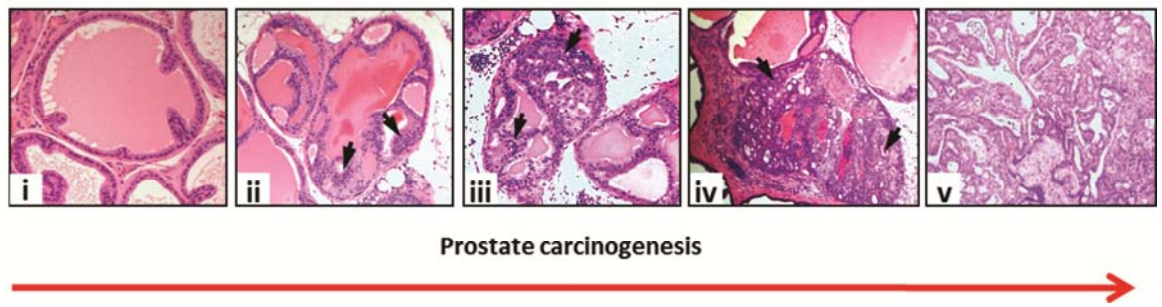


Figure 1.4.3 Murine prostate carcinogenesis

Images show murine prostate morphology during cancer initiation and development: i) normal glandular structure, ii) hyperplastic lesions (arrows), iii) PIN development (arrows), iv) high-grade PIN (arrows), v) adenocarcinoma and complete loss of glandular structure. (Reproduced from Brzezinska et al, 2015 [162], with permission of Springer).

Examples of whole body gene knockouts that have given rise to prostate adenocarcinoma in mice include concurrent heterozygous deletion of *Pten* with *Nkx3.1* [163] or *p27* [164], while combination with *Tp53* haploinsufficiency accelerated PIN development [165]. PIN lesions are observed in *Pten* haploinsufficient mice but do not progress to adenocarcinoma [114]. However, homozygous *Pten* deletion renders embryos unviable [114] and other knockout mutations result in developmental defects, limited lifespan or embryonic lethality, which precludes the study of their role in prostate cancer [7]. Such limitations have been overcome by using the conditional *Cre/LoxP* system [166], under the control of prostate-specific gene promoters, to manipulate gene expression in the prostate. *LoxP* sites contain sequences recognised and digested by Cre recombinase. These sites are inserted either side of a sequence that, when excised, will result in recombination and altered expression of the gene of interest. In this way, the effects of loss, stabilisation and overexpression of gene products can be studied only where there is expression of *Cre*.

To modulate genetic alterations in a prostate-specific manner, *Cre* expression must be regulated by a gene promoter specifically expressed in prostate tissue, such as the *PSA-Cre* [167], *-426/+28 Probasin-Cre* [168], *Probasin-Cre4 (PB-Cre4)* [169] or *Nkx3.1-Cre* [170] systems. The *PB-Cre4* and *Nkx3.1-Cre* models are both used in our laboratory. *Probasin* is a rat prostate-specific promoter, discovered to specifically target gene expression to prostate epithelial cells [171]. The *PB-Cre4* transgenic model was developed to drive high levels of *Cre* expression, using a small composite, androgen-regulated derivative of the *Probasin*

promoter, *ARR₂PB* [172]. The *Nkx3.1* homeobox gene is expressed specifically in the prostate during embryonic development and can be used to drive prostate-targeted *Cre* expression [170]. Recently the *Nkx3.1-Cre* system has been modified to generate the *Nkx3.1^{CreERT2}* tamoxifen-inducible system [23]. In this model, *Cre* is fused to a modified oestrogen receptor ligand-binding domain and activated by tamoxifen [173], facilitating the temporal control of genetic alterations.

There are a number of differences between *Probasin* and *Nkx3.1 Cre/LoxP* systems, each with benefits or limitations with regards to the timing and heterogeneity of *Cre* expression, breeding of mice, and the role of the promoter gene in the prostate. The expression of *Probasin* is androgen-regulated and peaks at sexual maturation [171], whereas *Nkx3.1* expression occurs during late embryogenesis and is maintained in the adult mouse [170]. Use of the constitutive *Nkx3.1* system poses a problem when studying genetic alterations that adversely affect prostate development, but can be overcome by using the *Nkx3.1^{CreERT2}* tamoxifen-inducible system to elicit *Cre* expression at a later time point. There is heterogeneous *Cre* expression in each model: *Probasin* is associated with basal epithelial cells; *Nkx3.1* with luminal epithelial cells [23]. As basal and luminal cell types have both been implicated in human prostate cancer [19], each model is clinically relevant. However, luminal epithelial cells are characterised by their expression of AR and more responsive to androgen manipulation, making this model preferable for CRPC studies.

Furthermore, constitutive *Nkx3.1-Cre* and inducible *Nkx3.1^{CreERT2}* mouse colonies can be expanded more quickly than *PB-Cre4* mice. *Probasin* recombines in oocytes resulting in progeny with recombined floxed alleles in multiple tissues, in addition to the prostate [174]. Therefore, *PB-Cre4*-positive females cannot be used for breeding. However, unlike *Nkx3.1*, manipulation of *Probasin* itself does not adversely affect prostate development or homeostasis. *Nkx3.1* is required for normal ductal morphogenesis and secretory protein production [170], and its loss has been shown to drive prostate cancer initiation [175]. The expression of *Cre*, regulated by the constitutive or tamoxifen-inducible *Nkx3.1* promoter, effectively results in heterozygous *Nkx3.1* expression and may contribute to cancer initiation and progression in prostate cancer models.

In this project the *PB-Cre4* (referred to as *Pb-Cre*) and *Nkx3.1^{CreERT2}* conditional *Cre/LoxP* systems have been crossed with floxed mouse models to generate mice with prostate-targeted *Pten* loss [176], β -catenin stabilisation [177] and red fluorescent protein (RFP) transgene expression [178]. *Pten* inactivation results from *LoxP* sites inserted either side of *exon5* of endogenous *Pten*, which contains the *Pten* phosphatase domain, commonly mutated in various human cancers [176]. To achieve β -catenin stabilisation, *LoxP* sites flanking *exon3* of the *Ctnnb1* gene are excised following *Cre* expression. *Exon3* contains the GSK3 β phosphorylation sites, required to maintain β -catenin association with the destruction complex in the absence of Wnt ligand. Therefore, *Exon3* deletion generates a dominant *Ctnnb1* allele and results in Wnt-independent β -catenin stabilisation and activation of nuclear β -catenin signalling [177].

The *Cre-LoxP* system has also been manipulated to introduce cell-specific transgene expression, such as the RFP “knock-in” *Cre*-reporter [178]. This was achieved by inserting the *RFP* reporter construct in the *ROSA26* locus, previously identified as an efficacious insertion site - ubiquitously expressed and non-essential for development [179]. The reporter construct contains a floxed ‘STOP’ sequence upstream of *RFP*, which blocks transcription in the absence of *Cre* recombinase. On expression of *Cre*, this sequence is excised, facilitating expression of *RFP*. This system was designed for use in lineage tracing experiments, such as those used to identify castration-resistant *Nkx3.1*-expressing cells (CARNs) as a luminal cell of origin for prostate cancer [23] (although yellow fluorescent protein was used as a *Cre*-reporter in these studies). The use of *RFP* as a *Cre*-reporter to identify CARNs in regressed and regenerated prostate tissue is described in Chapter 4.1.2.

1.5 Project aims and objectives

There is a plethora of evidence that aberrant activation of Wnt/ β -catenin signalling and PTEN loss co-occur in aggressive prostate cancer with the poorest prognosis [41, 100]. Furthermore, enrichment of genomic alterations in *CTNNB1* and *PTEN* is significantly higher in metastatic CRPC [99]. This warrants further investigation into the relationship between these aberrations to uncover molecular mechanisms that drive aggressive disease.

We formed two main hypotheses:

1. β -catenin activation, arising from β -catenin mutation or deregulation in Wnt/ β -catenin signalling, co-operates with *Pten* loss to drive aggressive prostate carcinogenesis in mice
2. β -catenin is able to reprogram AR signalling, through its role as an AR cofactor, and drive treatment resistant mechanisms that promote the progression of hormone naïve prostate cancer to castration resistant disease

The aim of this project is to investigate the role of β -catenin activation in prostate tumourigenesis, cancer progression and the emergence of castration-resistant disease, in the context of concurrent *Pten* loss. The project can be divided into the following objectives:

- I. Characterise the effects of β -catenin activation and *Pten* loss in a *Pb-Cre* prostate cancer mouse model
- II. Investigate the co-operation between β -catenin activation and *Pten* loss in prostate cancer and elucidate intrinsic and extrinsic events that may drive cancer progression
- III. Develop novel pre-clinical *in vivo* models for CRPC, using the *Nkx3.1^{CreERT2}* system, to characterise the role of β -catenin activation and *Pten* loss in the emergence of CRPC and identify mechanisms of treatment resistance

- IV. Investigate the impact of aberrant β -catenin activation on AR signalling in prostate cancer to understand if AR reprogramming confers resistance to ADT in this prostate cancer model

Chapter 2 – Materials and Methods

2.1 Materials

2.1.1 General reagents

Table 2.1-1 General reagents

Reagent	Manufacturer
Agarose	Melford
Aprotinin	Sigma
Bovine serum albumin (BSA)	Sigma
Citrate	Fisher Scientific
Collagenase	Sigma
Corn oil	Sigma
Cresyl violet	Sigma
Cryospray	CellPath
3,3-diaminobenzidine (DAB)	Thermo Scientific
Diethylpyrocarbonate (DEPC)	Sigma
Dispase	BD Biosciences
Dithiothreitol (DTT)	Thermo Scientific
Dulbecco's Modified Eagle's Medium (DMEM)	GIBCO
Enhanced chemiluminescence (ECL)	GE healthcare
Ethylene diamine triacetic acid (EDTA)	Fisher Scientific
Ethanol	Sigma
Fetal bovine serum (FBS)	GIBCO
Formaldehyde (36.5-38% solution)	Sigma
L-glutamine	GIBCO
Glycerol	Sigma
Glycine	Calbiochem
Glycogen	Ambion
HEPES	Sigma
Hydrogen chloride (HCl)	Sigma
Hydrogen peroxide (30% solution)	Fisher Scientific
Igepal	Sigma
Leupeptin	Sigma
Lithium chloride solution (LiCl) (8M)	Sigma
Matrigel	Invitrogen
β -Mercaptoethanol	Sigma

Methanol	Sigma
Methyl Cellulose	Sigma
MOPS SDS running buffer (20x)	Invitrogen
Normal goat serum	Abcam
OCT	CellPath
PVDF membrane	Millipore
Penicillin Streptomycin	GIBCO
Pepstatin	Sigma
Phenol:Chloroform:Isoamyl Alcohol 25:24:1	Sigma
Phenylmethylsulphonyl fluoride (PMSF)	Thermo Scientific
Protease Inhibitor Cocktail Set I	Calbiochem
Protease Inhibitor Cocktail Set III	Calbiochem
PhosSTOP™ Phosphatase Inhibitor Cocktail	Roche
RNase Inhibitor 500X	Sigma
RPMI-1640	GIBCO
Sodium bicarbonate (NaHCO ₃)	Sigma
Sodium butyrate (NaBu)	Sigma
Sodium chloride (NaCl)	Sigma
Sodium deoxycholate	Sigma
Sodium dodecyl sulphate (SDS)	Sigma
Sodium fluoride (NaF)	Sigma
Sodium hydroxide (NaOH)	Fisher Scientific
Sodium orthovanadate (Na ₃ VO ₄)	Sigma
Tris-HCl	Sigma
Triton X-100	Sigma
10X Trypsin	GIBCO
Trypsin/0.05% EDTA	Invitrogen
Tween-20	Sigma
Tween-80	Sigma

2.1.2 Treatments administered *in vivo* or *in vitro*

N-acetyl cysteine (NAC): 10 mM NAC (Sigma) was dissolved in drinking water and adjusted to pH 7.5 by dropwise addition of concentrated NaOH solution.

Tamoxifen: 1 g of Tamoxifen (Sigma) was resuspended in 5 ml ethanol absolute, vortexed and incubated at 37°C for ~2 hours to dissolve as much as possible. Tamoxifen was diluted to 20 mg/ml with 45 ml corn oil, vortexed and incubated at 37°C until all tamoxifen had dissolved. Stock was immediately aliquoted into amber bottles and stored at -20°C. Each aliquot was freeze/thawed up to 3 times, and then discarded.

Testosterone proprionate: Silastic® tubing was cut into 1 cm implants. One end was sealed with medical-grade glue and left to dry overnight. Implants were filled with 10 mg testosterone proprionate (Sigma) powder and the open end sealed with glue and left to dry overnight. Implants were stored in a sealed container at room temperature. Control (sham) implants were left empty and sealed with glue at both ends. Immediately prior to implantation, implants were soaked in PBS overnight.

LGK-974: A 0.375 mg/ml suspension of LGK-974 (MedKoo) was made in 0.5% Methyl Cellulose/0.5% Tween 80 vehicle. The suspension was vortexed and sonicated for 10 minutes to achieve a uniform (almost clear) suspension and stored at 4°. LGK-974 suspension must be protected from light and is only stable for one week.

ICG-001: ICG-001 (Tocris) powder was dissolved in ethanol absolute to generate a 50 mM stock solution. Aliquots were stored at -20°C

2.1.3 Antibodies

Table 2.1-2 Antibodies used for immunohistochemistry

Antibody	Species	Manufacturer	Dilution	Retrieval
Ki67*	Rabbit	Thermo Scientific	1:200	pH 6
β -catenin*	Mouse	BD Transduction Laboratories (610154)	1:750	pH 8
Pten	Mouse	Cell Signaling (#9556)	1:50	pH 6
Malondialdehyde	Rabbit	Abcam (ab6463)	1:500	pH 6
p21	Rabbit	Abcam (ab2961)	1:50	pH 6
Akt (P Ser473)	Rabbit	Cell Signaling (#4060)	1:50	pH 8
Active Rac1-GTP	Mouse	New East Biosciences (26903)	1:500	pH 6
RFP	Rabbit	Rockland (600-401-379)	1:50	pH 6
AR (N-20)	Rabbit	Santa Cruz (sc-816)	1:150	pH 6
Myc (N-262)	Rabbit	Santa Cruz (sc-764)	1:50	pH 6
F4/80*	Rat	Serotec (MCA-497)	1:150	Prot K
NIMP*	Rat	Abcam (ab2557)	1:50	Prot K

*IHC carried out by Histology Services

Table 2.1-3 Reverse Phase Protein Array antibodies

Antibody	Species	Manufacturer	Dilution
Survivin	Rabbit	Cell Signaling (#2808)	1:250
β -tubulin	Rabbit	Abcam (ab6046)	1:5000
p44/42 MAPK (ERK1/2)	Rabbit	Cell Signaling (#9102)	1:500
Prohibitin	Rabbit	Santa Cruz (sc-28259)	1:5000
Src	Rabbit	Cell Signaling (#2109)	1:500
p21 CIP/WAF1 (P Thr145)	Mouse	Cell Signalling (#2946)	1:2000
Smad3 (P Ser423/425)	Rabbit	Cell Signaling (#9520)	1:1000
Calpain2	Rabbit	Cell Signaling (#2539)	1:1000
PKC α (P Thr638)	Rabbit	Abcam (ab32502)	1:1000
PTEN	Rabbit	Cell Signaling (#9552)	1:500
AMPK α (P Thr172)	Rabbit	Cell Signaling (#2535)	1:500
Akt (P Ser473)	Rabbit	Cell Signaling (#4060)	1:500
Stat1 (P Ser727)	Rabbit	Invitrogen (Biosource, 44-382G)	1:500
PKC γ (P Thr514)	Rabbit	GeneTex (GTX25778)	1:250
mTOR (P Ser2448)	Rabbit	Cell Signaling (#2971)	1:250
ErbB-3/Her3/EGFR	Rabbit	Cell Signaling (#4754)	1:500
GSK3B	Rabbit	Cell Signaling (#9315)	1:500

Antibodies correspond to selected RPPA data included in heat map (Figure 3.2.9)

Table 2.1-4 Immunoblotting antibodies

Antibody	Species	Manufacturer	Dilution
β-catenin	Mouse	BD Transduction Laboratories (610154)	1:1000
PTEN	Rabbit	Cell Signaling (#9552)	1:1000
PTEN (P Ser380)	Rabbit	Cell Signaling (#9551)	1:1000
Akt	Rabbit	Cell Signaling (#9272)	1:1000
Akt (P Ser473)	Rabbit	Cell Signaling (#4060)	1:1000
Cyclin D1	Mouse	Santa Cruz (sc-246)	1:1000
Survivin (FL-142)	Rabbit	Santa Cruz (sc-10811)	1:1000
mTOR	Rabbit	Cell Signaling (#2972)	1:1000
mTOR (P Ser2448)	Rabbit	Cell Signaling (#2971)	1:1000
Hamartin/TSC1	Rabbit	Cell Signaling (#4906)	1:1000
Tuberin/TSC2	Rabbit	Cell Signaling (#3612)	1:1000
TSC2 (P Thr1462)	Rabbit	Cell Signaling (#3617)	1:1000
S6K	Rabbit	Cell Signaling (#9202)	1:1000
S6K (P Thr421/424)	Rabbit	Cell Signaling (#9204)	1:1000
S6	Rabbit	Cell Signaling (#2212)	1:1000
S6 (P Ser240/244)	Rabbit	Cell Signaling(#2215)	1:1000
AMPKα	Rabbit	Cell Signaling (#2603)	1:1000
AMPKα (P Thr172)	Rabbit	Cell Signaling (#2523)	1:1000
AMPKB1/2	Rabbit	Cell Signaling (#4150)	1:1000
AMPKB1/2 (P Ser108)	Rabbit	Cell Signaling (#4181)	1:1000
PKA (P Thr197)	Rabbit	Abcam (ab75991)	1:5000
PKA substrate (P Ser/Thr)	Rabbit	Cell Signaling (#9621)	1:1000
AR (N-20)	Rabbit	Santa Cruz (sc-816)	1:1000
Hsp-70	Mouse	Abcam (ab3148)	1:2000
GAPDH-HRP	Mouse	Sigma (G9295)	1:10000
HRP-linked secondary	Mouse	Cell Signaling (#7076)	1:5000
HRP-linked secondary	Rabbit	Cell Signaling (#7074)	1:5000

Table 2.1-5 Immunoprecipitation antibodies

Antibody	Species	Manufacturer	Experiment	Quantity
AR (N-20)	Rabbit	Santa Cruz (sc-816)	co-IP	2 μg
HA-probe (Y-11)	Rabbit	Santa Cruz (sc-805 X)	ChIP	10 μg
AR (N-20) X	Rabbit	Santa Cruz (sc-816 X)	ChIP	10 μg
AR (H-280) X	Rabbit	Santa Cruz (sc-13062 X)	ChIP	10 μg

2.1.4 Primers

Primers used in TaqMan® qPCR assays were designed using the Roche Assay Design Centre (<https://lifescience.roche.com>) and used in combination with probes from the Universal ProbeLibrary (Roche).

Table 2.1-6 TaqMan qPCR primers

Target	Forward primer sequence	Reverse primer sequence	Probe Library number
<i>18S</i>	gcaattattcccatgaacg	gggacttaatcaacgcaagc	48
<i>Pten</i>	aggcacaagaggccctagat	ctgactgggaattgtgactcc	60
<i>Pten exon5*</i>	tcagtttgcaatgccaagg	agaatcaagttcaaattgtcttactcc	46
<i>Casc3*</i>	ctcagggcgtgcaatggt	gagaatggcggttctctacatc	45
<i>Tiam1</i>	ggaatatttgatgacactgttcca	ggtaggacactgggtaagacc	7
<i>Vav3</i>	cgcgtgctgaagtatcacc	ctccatagggtcatgggtgt	17
<i>Def20</i>	gaccagaaggatctgctctt	cctgagcagggtcccataaac	75
<i>Adcy8</i>	acctgactttcaattcctcagc	caacaccccagtgaaagaaa	68
<i>Apoc4</i>	gctgttcttggtcagctttag	gcccttaccaggctccag	108
<i>Pnliprp2</i>	gggtaccctgttctccta	tttgggacacccttgttctg	38
<i>Fbp1</i>	tataccccgccaacaagaaa	aagctatggggttgcactca	66
<i>Tcf3</i>	cgcagaccaaactgctcat	gggttcagggtgcgttctc	1
<i>Lef1</i>	tcctgaaatccccaccttct	tgggataaacaggctgacct	94
<i>Ccnd1</i>	tttctttccagagtcacaaagtgt	tgactccagaagggttcaa	72
<i>Wnt4</i>	actggactccctccctgtct	tgcccttgtcactgcaaa	62
<i>Wnt5a</i>	tgaagcaggccgtaggac	agccagcacgtcttgagg	92
<i>Wnt10b</i>	ttcacgagtgtcagcacca	aaagcactctcacggaaacc	70
<i>Myc</i>	cctagtgtgcatgaggaga	tccacagacaccacatcaattt	77
<i>AR</i>	ccagtcccaattgtgtcaaa	tccctggtagtgcctcaaacg	58
<i>Fkbp5</i>	tgttcaagaagttcgagagc	ccttcttgcctccagcttt	69
<i>ApoF</i>	gcctggctctaaggaatgct	aagctgaagagcccagacct	16

*Used for *Pten* DNA copy number qPCR

MicroRNA qPCR analysis was carried out using TaqMan® assays (Applied Biosystems).

Table 2.1-7 TaqMan MicroRNA assays (Applied Biosystems)

Assay	Product number (4427975/...)
hsa-mir-17	2308
hsa-miR-18a	2422
hsa-miR-19b	396
hsa-miR-21	397
snoRNA202 Control Assay	1232

Primers for CHIP qPCR were based on published primer sequences and used for SYBR® Green qPCR.

Table 2.1-8 CHIP-qPCR primers

Target	Forward primer sequence	Reverse primer sequence
<i>Fkbp5</i> *	acccccattttaatcggagaac	tttgaagagcacagaacaccct
<i>Tmprss2</i> *	gcaaaaagaaccgactcaatcc	ggagctgtacatacaccctgattg
<i>Gapdh</i> *	gcccttgagctaggactggata	cgattttcacctggcactgc
<i>ApoF</i> **	taaagccaggtgaccttcat	ctttgcaaataagccagga
Non Target (<i>Lcor</i>)*	attaagacacaaaggagagaggtcc	tgtcatgtatcaagtttccaaaacc

All primer sequences previously published for AR CHIP-qPCR *[180], **[181]

All primers were tested in no-template control reactions prior to use in qPCR experiments.

2.1.5 Cell lines

LNCaP and CWR-22 cell lines were authenticated by LCG standards.

CP1-4 cell lines were derived from prostate tumours harvested from *Pb-Cre Pten^{fl/+} Ctnnb1^{(ex3)Δ/+}* transgenic mice.

2.1.6 Solutions and buffers

Solution/buffer	Components
Phosphate buffered saline (PBS)	170 mM NaCl, 3.3 mM KCl, 1.8 mM Na ₂ HPO ₄ , 10.6 mM K ₂ HPO ₄ , pH 7.4
Tris-buffered saline-TWEEN (TBS-T)	25 mM Tris-HCl (pH 7.4), 137 mM NaCl, 5 mM KCl, 0.1% Tween-20
Citrate buffer, pH 6 (immunohistochemistry)	300 mM citrate powder dissolved in dH ₂ O and titrated to pH 6 with 2M HCl
EDTA buffer, pH 8 (immunohistochemistry)	1 mM EDTA dissolved in dH ₂ O and titrated to pH 8 with 2M HCl
Blocking buffer (immunohistochemistry)	5% normal goat serum, 1% BSA, 0.1% Triton X-100 in TBS
RPPA tissue lysis buffer	1% TritonX-100, 50 mM HEPES (pH 7.4), 150 mM NaCl, 1.5 mM MgCl ₂ , 1 mM EGTA, 100 mM NaF, 10 mM Na pyrophosphate, 1 mM Na ₃ VO ₄ , 10% glycerol, containing freshly added 1X protease and phosphatase inhibitors
RPPA 4X SDS sample buffer	40% glycerol, 8% SDS, 0.25 M Tris-HCl (pH 6.8), 1/10 β-mercaptoethanol (added immediately before use)
Cell lysis buffer (protein extraction)	50 mM Tris-HCl (pH 7.6), 150 mM NaCl, 1% Triton X-100, 0.5% Deoxycholate, 0.1% SDS, 1 mM NaF, 1 mM Na ₃ VO ₄ , 1X protease cocktail inhibitor mix 1, 50 µg/ml PMSF, 1X PhosSTOP
Tissue lysis buffer (protein extraction)	50 mM Tris-HCl (pH 7.6), 150 mM NaCl, 1% Triton X-100, 0.5% Deoxycholate, 0.1% SDS, 1 mM NaF, 1 mM Na ₃ VO ₄ , 1X protease cocktail inhibitor mix 1, 50 µg/ml PMSF, 2X PhosSTOP
Blocking buffer (immunoblotting)	5% skimmed milk powder in TBS-T
Transfer buffer (immunoblotting)	192 mM glycine, 25 mM Tris, 20% methanol
Cytokine array lysis buffer	10 µg/ml Aprotinin, 10 µg/ml Leupeptin, 10 µg/ml Pepstatin, 1% Triton X-100 in PBS
Collagenase solution	Non-sterile lyophilised collagenase type I dissolved in PBS to a concentration of 10 mg/ml; filtered through a 0.22 µm filter and 1 ml aliquots stored at -20°C
DEPC water	0.1% DEPC pipetted into dH ₂ O, mixed and incubated overnight at room temperature, then autoclaved

Cresyl Violet	1% Cresyl Violet powder dissolved in 50% ethanol/DEPC water and passed through 0.2 µm syringe filter; stored at 4°C
IP washing buffer	PBS/BSA (0.1% BSA, 0.02% NaN ₃ to preserve)
IP lysis buffer	50 mM Tris (pH 7.4), 150 mM NaCl, 1 mM EDTA, 1% Triton X-100, 1 mM PMSF, 1 mM Na ₃ VO ₄ , 1X protease inhibitor cocktail set III, 1X PhosSTOP
NETN buffer STRONG	20 mM Tris (pH 8.0), 1 mM EDTA, 900 mM NaCl, 0.5% NP-40
NETN buffer WEAK	20 mM Tris (pH 8.0), 1 mM EDTA, 100 mM NaCl, 0.5% NP-40
Tissue cross-linking solution	1% formaldehyde, 50 mM HEPES-KOH, 100 mM NaCl, 1 mM EDTA, 0.5 mM EGTA
ChIP cell lysis buffer (CLB)	10 mM Tris (pH 8.0), 10 mM NaCl, 0.2% Igepal, 10 mM NaBu, 50 µg/ml PMSF, 1 µg/ml Leupeptin
ChIP nuclear lysis buffer (NLB)	50 mM Tris (pH 8.0), 10 mM NaCl, 1% SDS, 10 mM NaBu, 50 µg/ml PMSF, 1 µg/ml Leupeptin
ChIP dilution buffer (IPDB)	20 mM Tris (pH 8.0), 150 mM NaCl, 2 mM EDTA, 1% Triton X-100, 0.01% SDS, 10 mM NaBu, 50 µg/ml PMSF, 1 µg/ml Leupeptin
ChIP wash buffer 1 (IPWB1)	20 mM Tris (pH 8.0), 50 mM NaCl, 2 mM EDTA, 1% Triton X-100, 0.01% SDS
ChIP wash buffer 2 (IPWB2)	10 mM Tris (pH 8.0), 250 mM LiCl, 1 mM EDTA, 1% Igepal, 1% Deoxycholate
Tris-EDTA (TE)	10 mM Tris-HCl (pH 8.0), 1 mM EDTA
ChIP elution buffer (IPEB)	100 mM NaHCO ₃ , 1% SDS

2.2 Methods

2.2.1 Animal studies

All animal work in this study was compliant with the Animal (Scientific Procedures) Act 1986 and approved by the Home Office (London, United Kingdom).

2.2.1.1 Transgenic models

All mice in this study were on a mixed background and were genotyped by Transnetyx™ using PCR analysis of ear notch tissue. To generate the *Pb-Cre Pten^{fl/+} Ctnnb1^{(ex3)Δ/+}* colony, *ARR2Probasin-Cre (Pb-Cre)* mice [169] were crossed with mice harbouring a *Pten^{fl/+}* allele [176] and progeny were further crossed with *Ctnnb1^{(ex3)Δ/+}* mice [177]. For controls, *wildtype*, *Pb-Cre Pten^{fl/+}* and *Pb-Cre Ctnnb1^{(ex3)Δ/+}* littermates were used. Mice were sacrificed at 3 months for cancer initiation studies and other cohorts aged to 6 months and clinical endpoints for tumourigenesis studies.

For tamoxifen induction optimisation, and visualisation of CARNs following regression and regeneration, *Nkx3.1^{CreERT2} RFP/+* mice were generated by crossing *Nkx3.1^{CreERT2}* mice [23] with mice harbouring the *rosa-26-RFP* transgene (*RFP/+*) [178]. The optimisation of tamoxifen induction of *Cre recombinase* was carried out as described in Chapter 4.1.1 and final procedure is described below (2.2.1.4). For controls, *Nkx3.1^{CreERT2} wildtype* littermates were used. Mice were sacrificed 2 weeks post-induction for tamoxifen optimisation experiments, and 6 weeks post-induction for prostate regression/regeneration experiments.

To generate the *Nkx3.1^{CreERT2} Pten^{fl/+}* (or *Pten^{fl/fl}*) *Ctnnb1^{(ex3)Δ/+}* colony, *Nkx3.1^{CreERT2}* mice were crossed with *Pten^{fl/+}* or *Pten^{fl/fl}* mice, and progeny were further crossed with *Ctnnb1^{(ex3)Δ/+}* mice. Tamoxifen induction of *Cre recombinase* was carried out as described below (2.2.1.4). For controls, *Nkx3.1^{CreERT2} wildtype*, *Nkx3.1^{CreERT2} Pten^{fl/+}* (or *Pten^{fl/fl}*) and *Nkx3.1^{CreERT2} Ctnnb1^{(ex3)Δ/+}* littermates were used. Mice were sacrificed 2 weeks post-induction for tamoxifen optimisation experiments, 2 months post-induction for cancer initiation studies and a further cohort was aged to clinical endpoint for tumourigenesis studies.

Clinical endpoints were determined by clinical signs including palpable tumour burden, haematuria, weight loss, and reduced activity, in keeping with terms of the project license. Following dissection, prostates were weighed ('wet' weight), tumours were drained of any cystic fluid infiltrate, and prostates were weighed again ('dry' weight). The prostate was then divided into left and right lobes, with one half placed in 10% neutral buffered formalin for 36-48 hours fixation, prior to paraffin-embedding by histology services, and the other half snap frozen in dry ice and stored at -80°C . Lymph nodes, spleen, liver, kidneys and lungs were routinely dissected and formalin-fixed for examination.

2.2.1.2 Haematological analysis of whole blood from mice

Whole blood was sampled from mice immediately post-mortem and transferred to an EDTA blood collection tube (BD). 220 μl of blood was sent to the Clinical Pathology Laboratory at the School of Veterinary Medicine (University of Glasgow) for full haematology analysis.

2.2.1.3 N-acetyl-cysteine treatment

Wildtype, *Pb-Cre Pten^{fl/+}*, *Pb-Cre Ctnnb1^{(ex3) Δ /+}* and *Pb-Cre Pten^{fl/+} Ctnnb1^{(ex3) Δ /+}* mice were administered with 10 mM NAC (pH 7.5) in drinking water *ad libitum* between 3 and 6 months of age. Fresh NAC water was made twice weekly. Mice were sacrificed at 6 months, following 3 months of treatment, to analyse the effects of NAC on prostate cancer progression.

2.2.1.4 Tamoxifen induction

Unless otherwise stated, the expression of *Cre recombinase* in *Nkx3.1^{CreERT2}* mice was induced at 12 weeks of age by intraperitoneal injection of 160 mg/kg tamoxifen, administered 4 times over an 11 day period (Thursday/Monday/Thursday/ Monday). The dose was calculated based on the average weight of male mice at 12 weeks being ~25 g and all mice were administered with 4 mg tamoxifen in a 200 μl volume. Details of the optimisation of the tamoxifen-induction protocol are given in Chapter 4.1.1.

2.2.1.5 RFP fluorescence imaging

RFP expression in dissected *Nkx3.1^{CreERT2} RFP/+* prostates was visualised using the IVIS® Spectrum *in vivo* imaging system (Perkin Elmer) and Living Image software. Fluorescence imaging mode was selected and acquisition settings were as follows: 3 seconds exposure time; binning factor 8; 620/520 emission/excitation filters.

2.2.1.6 Bilateral orchietomy (castration)

For all mouse experiments androgen deprivation was achieved by surgical removal of the testes. Time points vary between experiments and are detailed in results (Chapter 4).

2.2.1.7 Prostate regeneration

Prostates were regenerated 6 weeks post-castration by subcutaneous implantation of a 1 cm Silastic® implant containing 10 mg testosterone propionate powder. Based on a 25 g mouse, this is a dose of 400 mg/kg. Empty sham implants were used in control mice. Implants were soaked in PBS overnight prior to implantation. Mice were sacrificed 4 weeks after testosterone administration to analyse prostate regeneration.

2.2.1.8 LGK-974 (Porcupine inhibitor) treatment

Nkx3.1^{CreERT2} Pten^{fl/+} Ctnnb1^{(ex3) Δ /+} mice were castrated at 7-8 months post-induction when palpable tumour was detected. Following 10 days recovery post-surgery, mice were treated with 1.25 mg/kg LGK-974 once daily by gavage for 1 month. The dose was calculated based on the average weight of mice at this time point being ~30 g and all mice were administered with 37.5 μ g LGK-974 in a volume of 100 μ l. Control mice were administered with 100 μ l of drug vehicle (0.5% Methyl Cellulose/0.5% Tween 80). Mice were sacrificed when treatment ended to analyse the effects of combined Wnt inhibition and ADT.

2.2.2 Histology and immunohistochemistry

Processing and paraffin embedding of formalin-fixed tissue was carried out by Histology Services. Haematoxylin and eosin staining of tissue sections was

carried out on the Leica ST5020 Autostainer. Ki67, B-catenin, F4/80 and NIMP immunohistochemical (IHC) staining was also carried out by Histology Services using an automated procedure, as previously described [162], with a pre-treatment module (Dako) for heat-induced epitope retrieval (HIER) (Ki67 and B-catenin staining) and an autostainer (Dako). F4/80 and NIMP staining was carried out following retrieval by incubation with proteinase K (Prot K) for 10 minutes at room temperature and Rat ImmPRESS™ (Vector Laboratories) was used as the secondary antibody. All other immunohistochemical staining was carried out as described below.

Pten, Malondialdehyde, p21, phospho-Akt, RFP, AR and Myc IHC: FFPE tissue sections were deparaffinised by three 5 minute washes in xylene and rehydrated by two 10 minute washes in 100% ethanol, 95% ethanol and dH₂O respectively. HIER was carried out in preheated citrate (pH 6) or EDTA (pH 8) buffer using a pressure cooker to bring slides to a boil and maintain temperature for 3 minutes when the cooker is fully pressurised. Slides were cooled in retrieval buffer for 20 minutes at room temperature, before washing in dH₂O and incubating in 3% hydrogen peroxide for 10 minutes to quench endogenous peroxidases. Sections were washed in dH₂O, followed by a 5 minute wash in TBS-T. A hydrophobic pen was used to draw around tissue section and 100-400 µl immunohistochemistry blocking buffer was added to this area for 1 hour incubation at room temperature. Sections were then incubated in primary antibody (diluted in blocking buffer) overnight at 4 °C. Slides were washed three times in TBS-T for 5 minutes and incubated in EnVision™ secondary antibody solution (Dako) for 1 hour at room temperature. Secondary antibody was removed and sections washed three times in tap water before staining with DAB chromogen (UltraVision Detection system, Thermo Scientific). Sections were incubated in DAB for up to 10 minutes and staining was monitored closely. Slides were immediately immersed in dH₂O and washed, before counterstaining with haematoxylin using the Autostainer (Leica ST5020) and mounting using the automated Coverslipper (Leica).

Rac1-GTP IHC staining was carried out according to published protocol [182].

Details of the antibody source, dilution and retrieval method used for each IHC staining can be found in Materials 2.1.3, Table 2.1-2.

2.2.2.1 Haematoxylin and eosin image analysis

Slides were scanned with a digital slide scanner (Leica) and images exported for ImageJ analysis. A deconvolution macro (designed by David Strachan, Senior Scientific Officer in the Beatson Advanced Imaging Resource team) was used to separate 'blue' nuclei from 'red' cytoplasm in manually defined areas of haematoxylin and eosin stained prostate epithelial tissue. In this way the percentage of haematoxylin staining was measured in *Pb-Cre Pten^{fl/+} Ctnnb1^{(ex3)Δ/+}* prostate tissue (n=5) at a 6 month time point and compared to *Wildtype* (n=3), *Pb-Cre Pten^{fl/+}* (n=3) and *Pb-Cre Ctnnb1^{(ex3)Δ/+}* (n=5) littermate controls. This analysis was carried out to determine if differences in cancer progression could be objectively measured based on the percentage of nuclei in prostate epithelial tissue. The number of PINs and tumour area was then measured in *Pb-Cre Ctnnb1^{(ex3)Δ/+}* and *Pb-Cre Pten^{fl/+} Ctnnb1^{(ex3)Δ/+}* tissue sections. PIN lesions were defined as prostate glands in which more than half the lumen area was filled with hyper-proliferative epithelial cells but the basal lamina remained intact. Areas of tissue that had progressed beyond PIN to *in situ* carcinoma and invasive adenocarcinoma were manually annotated and measured in pixels. The total of all tumour areas annotated per tissue section was the tumour area.

2.2.2.2 Ki67 scoring

To quantify Ki67 staining, images were taken of at least 5 fields of view of prostate tissue sections (n=3 per genotype) at 200X magnification using an Olympus BX51 light microscope. Percentage of positively stained nuclei were counted using ImageJ software.

2.2.3 Zeptosens' reverse-phase protein array

To prepare tissue lysates, 40 mg frozen prostate tissue was placed in a 2 ml tube with ceramic beads (Precellys® CK28), 1 ml ice-cold RPPA lysis buffer was added to the tube and tissue was homogenised using a Precellys 24 tissue homogeniser (Bertin Technologies) for three 25 second cycles at 5000 rpm and 4°C. Vials were immediately transferred back to ice, homogenised lysate was transferred to a fresh microcentrifuge tube and centrifuged at 16100 x g for 10 minutes at 4°C. Supernatant was transferred to another microcentrifuge tube and protein

concentration measured using the Bradford Protein Assay (BioRAD). The protein concentration was adjusted to 4 mg/ml using lysis buffer and 1X RPPA SDS sample buffer was mixed with the lysate before boiling for 5 minutes. Samples were stored at -80° C prior to RPPA processing.

The Zeptosens's reverse-phase protein array (RPPA) was carried out by Neil Carragher's laboratory at the Edinburgh Centre for Cancer Research, as previously described [183]. Details of the antibodies used in the data described can be found in Materials 2.1.3, Table 2.1-3.

Data analysis was carried out by Gabriela Kalna (Head of Computational Biology at the Beatson Institute). Dataset was normalized by protein loading (<http://www.mdanderson.org>). Pairwise fold changes were used to identify a list of antibodies differentially expressed among four samples. Normalized relative fluorescence intensities (RFIs), for which at least one fold change was larger than 1.1, were median centred and presented in the form of a heat map with hierarchical clustering and Euclidean distance similarity measure.

2.2.4 Immunoblotting

To prepare cell lysates, culture dishes were placed on ice and cells were washed twice with ice cold PBS before scraping cells into cell lysis buffer (80 µl for 6 cm and 100 µl for 9 cm culture dishes). Lysates were transferred to a microcentrifuge tube, vortexed and incubated on ice for 15 minutes. Following centrifugation at 16100 x g for 15 minutes, supernatant was collected for protein analysis.

Tissue lysates were prepared by grinding ~40 mg of frozen tissue in liquid nitrogen to form a powder, which was transferred to a 2 ml tube with ceramic beads (Precellys® CK28). 1 ml of tissue lysis buffer was added before using a Precellys® 24 tissue homogeniser (Bertin Technologies), for three 25 second cycles at 5000 rpm and 4° C. Homogenised lysate was transferred to a fresh 1.5 ml tube and incubated on ice for 15 minutes. Lysates were then centrifuged for 15 minutes at 16100 x g, and the supernatant collected for protein analysis.

Protein concentration was determined using the Bradford Protein Assay (Bio-Rad). Absorbance at 595 nm was measured with a spectrophotometer, from which protein concentration was calculated. Protein concentrations were adjusted with lysis buffer so that all samples were of equal concentration, before NuPAGE® LDS sample buffer and DTT were added to each protein lysate to give a final concentration of 1X and 1 µM respectively. Samples were then boiled at 100°C for 5 minutes, before being loaded alongside a prestained protein ladder (PageRuler™, Thermo Scientific), and resolved by SDS/PAGE on 10% or 4-12% gradient polyacrylamide gels (NuPAGE®, Invitrogen) in 1X MOPS SDS running buffer (Invitrogen) in a XCell SureLock™ Mini-Cell tank (Invitrogen) for 45 minutes at 120mA and 200V. Proteins were electrophoretically transferred to PVDF membrane (Millipore) using semi-dry transfer unit for 90 minutes at 20V and 180mA. Membranes were blocked in 5% milk/TBS-T for 60 minutes, rinsed in TBS-T and probed with primary antibodies in 5% BSA/TBS-T solution overnight at 4°C. (See Materials 2.1.3, Table 2.1-4 for primary antibody information). Membranes were washed three times with TBS-T for 10 minutes and incubated with HRP-conjugated secondary antibody (1/5000 dilution in TBS-T) for 60 minutes at room temperature. Bands were visualised by ECL (GE Healthcare) detection reagent and exposure on X-ray film for 1-10 minutes.

2.2.5 RT-PCR

2.2.5.1 mRNA analysis

RNA was extracted from ~40 mg frozen prostate tissue samples using an RNeasy Mini Kit (Qiagen), according to manufacturer's instructions. Homogenisation was carried out in a 2 ml tube with ceramic beads (Precellys® CK28) using the Precellys® 24 homogeniser. On-column DNase digestion steps were included to remove genomic DNA contamination using 2.7 U/µl RNase-free DNase I (Qiagen). RNA was eluted in 50 µl nuclease-free water and quantitated by spectrophotometric analysis. 10 µg RNA was reverse transcribed to cDNA using a High Capacity cDNA Reverse Transcription Kit (Applied Biosystems), according to manufacturer's instructions, in a 20 µl reaction volume. qPCR was performed in duplicate in a 96-well plate in a reaction volume of 20 µl containing 1X TaqMan® Universal PCR Master Mix (Applied Biosystems), 0.2 µM each of forward and reverse primers, 0.1 µM Universal ProbeLibrary probe (Roche) and 100 ng cDNA.

The thermal cycling conditions were as follows: 50°C for 2 minutes, 95°C for 10 minutes to activate enzyme, followed by 40 cycles of denaturation at 92°C for 15 seconds and annealing/extending at 60°C for 1 minute (Applied Biosystems 7500 Fast Real-Time PCR System). 18S was used to normalise for differences in murine tissue RNA input, as its expression was consistent between wildtype and tumour tissue samples. (See Materials 2.1.4, Table 2.1-6 for gene target primer sequences and probes).

2.2.5.2 miRNA analysis

Total RNA was extracted from frozen prostate tissue or cell lines using a miRNeasy Mini Kit (Qiagen), according to manufacturer's instructions. On-column DNase digestion steps were included to remove genomic DNA contamination using 2.7 U/ μ l RNase-free DNase I (Qiagen). RNA was eluted in 50 μ l nuclease-free water and quantitated by spectrophotometric analysis. In preparation for the reverse transcription reaction, 10X RT primer pool was prepared with the RT primers included in each TaqMan® miRNA assay, listed in Materials 2.1.4, Table 2.1-7. miRNA from 1 μ g total RNA was reverse transcribed to cDNA using a TaqMan® MicroRNA Reverse Transcription Kit (Applied Biosystems), according to manufacturer's instructions. qPCR was performed in duplicate in a 10 μ l reaction volume containing 1X TaqMan® MicroRNA Assays, 0.08 μ l RT product, 1X TaqMan® Universal Master Mix. 384-well plates were used for tissue miRNA analysis in biological triplicate (Applied Biosystems QuantStudio 7 Flex Real-Time PCR System); a 96-well plate was used for cell line miRNA analysis (Applied Biosystems 7500 Fast Real-Time PCR System). The thermal cycling conditions were as follows: 95°C for 10 minutes, followed by 40 cycles of denaturation at 95°C for 15 seconds and annealing/extending at 60°C for 1 minute. *Sno202* was used to normalise for differences in tissue miRNA input, as its expression was consistent across samples.

2.2.6 Transcriptomic analysis

2.2.6.1 RNA-sequencing

RNA was extracted from frozen prostate tissue samples as described in 2.2.5.1 and quantitated by spectrophotometry. RNA quality was evaluated by RNA integrity number (RIN), calculated using an Agilent 2100 Bioanalyzer (Agilent

Technologies) with the Agilent RNA 6000 Nano Kit. All samples processed for RNA-sequencing had RIN values >7.3. Library preparation and sequencing was carried out by BGI (Beijing) using the following steps and reagents according to manufacturer's instructions. The library was prepared with poly(A) messenger RNA (mRNA) selection using Dynabeads® mRNA Purification kit (Invitrogen), and Fragment buffer (Ambion) was used to generate poly (A)-containing mRNA fragments of 200-250 bp. First strand cDNA synthesis was carried out using N6 primer, First Strand Master Mix and Super Script II reverse transcription (Invitrogen) (thermal cycling conditions: 10 minutes at 25 °C, 30 minutes at 42 °C, 15 minutes at 70 °C) and Second Strand Master Mix (Invitrogen) was added to synthesise second strand cDNA (2 hours at 16 °C). Purified cDNA (QIAquick PCR Purification Kit, Qiagen) underwent end repair (End Repair Mix, Illumina), A-tailing (A-Tailing Mix, Illumina) and adapter ligation (Adenylate 3'-ends DNA, Adapter and Ligation Mix, Illumina). Samples were run on a 2% agarose gel to select 300-350 bp fragments, which were purified using QIAquick Gel Extraction kit (Qiagen). cDNA fragments were enriched by PCR amplification using PCR Primer Cocktail and PCR Master Mix (Illumina). Prior to sequencing, the average fragment length was quantitated using a Agilent 2100 Bioanalyzer with Agilent DNA 100 reagents and the RNA yield was quantitated by qPCR to validate quality of library preparation. TruSeq PE Cluster Kit V3-cBot-HS (Illumina) was used for paired end cluster generation. The library was pair end sequenced on the Illumina® HiSeq 2000 platform, with 90 nucleotide reads and at least 6 Gb of reads generated per sample.

2.2.6.2 Data analysis

Bioinformatics analysis of RNA-sequencing data was carried out by Ann Hedley (Bioinformatician at the Beatson Institute). A FastQC package was used to assess the quality of raw reads and, having passed FastQC quality control parameters, reads were mapped to mouse genome mm10 (NCBI38) using TopHat v.1.4.1. The percentage of reads uniquely aligned to the mouse genome was calculated to measure the quality of data. Using R and DESeq2 software, the number of reads mapped to each gene was counted, and normalised to read length and number. Fold-change values were generated relative to control data to identify differentially expressed genes. The heat map comparing all significantly up- and downregulated genes (twofold change in expression, $P < 0.05$) in the *wildtype*,

Pb-Cre Ctnnb1^{(ex3)Δ/+}, *Pb-Cre Pten^{fl/+} Ctnnb1^{(ex3)Δ/+}* data was generated by hierarchical cluster analysis on a set of dissimilarities, using the *complete linkage* method to find similar clusters. This method was also used to generate a heat map showing differential expression of androgen responsive genes in *Nkx3.1^{CreERT2} Pten^{fl/+} Ctnnb1^{(ex3)Δ/+}* CRPC compared to HNPC tissue. The androgen-responsive gene set used for enrichment analysis in *wildtype*, *Pb-Cre Ctnnb1^{(ex3)Δ/+}*, *Pb-Cre Pten^{fl/+} Ctnnb1^{(ex3)Δ/+}* and *Nkx3.1^{CreERT2} Pten^{fl/+} Ctnnb1^{(ex3)Δ/+}* HNPC and CRPC data sets was previously published by Carver et al. [119].

2.2.6.3 Pathway enrichment analysis

Differential gene expression values generated from RNA sequencing data were uploaded into GeneGo MetaCore™ for pathway analysis. The MetaCore Canonical Pathway Maps ontology was used to identify pathway enrichment in *Pb-Cre Ctnnb1^{(ex3)Δ/+}* and *Pb-Cre Pten^{fl/+} Ctnnb1^{(ex3)Δ/+}* prostate tissue compared to wildtype, and in *Nkx3.1^{CreERT2} Pten^{fl/+} Ctnnb1^{(ex3)Δ/+}* CRPC tumours compared to HNPC controls. Each pathway was tested for enrichment in significantly up- and downregulated genes (P value <0.05) using a hypergeometric distribution test. Pathways are significantly enriched when they have a $-\log(\text{P value}) > 1.3$ (P value <0.05) and false discovery rate (FDR) <0.05. Data was overlaid onto MetaCore Pathway Maps to show up- or downregulation of specific genes within significantly enriched pathways, as indicated by thermometer symbols (red = up-regulation; blue = down-regulation).

2.2.7 Cytokine array

Protein lysates were prepared from ~40 mg *Pb-Cre Ctnnb1^{(ex3)Δ/+}*, *Pb-Cre Pten^{fl/+} Ctnnb1^{(ex3)Δ/+}*, *Pb-Cre Pten^{fl/fl} Ctnnb1^{(ex3)Δ/+}* and *Pb-Cre Pten^{fl/fl}* prostate tumour tissue harvested from mice at clinical endpoint. Frozen tissue was ground in liquid nitrogen using a pestle and mortar and transferred to a 2 ml tube with ceramic beads (Precellys® CK28) for homogenisation in 900 µl cytokine array lysis buffer (minus 1% Triton X-100). Samples were homogenised in a Precellys® 24 tissue homogeniser (Bertin Technologies) at 4°C (3 cycles of 5000 rpm for 25 seconds) and supernatant transferred to a fresh microcentrifuge tube. Triton X-100 (100 µl of 10% stock) was added to final concentration of 1% and samples were frozen at -80°C overnight and thawed the following day to complete lysis.

Protein concentration was measured by Bradford assay (Bio-Rad). Samples were analysed using the Proteome Profiler Array: Mouse Cytokine Array Panel A (R&D Systems). The assay was carried out according to manufacturer's instructions and repeated in biological triplicate. Membranes were blocked in Array Buffer (AB) 6 for 1 hour at room temperature. During this time tissue protein samples were prepared by taking 200 µg protein lysate and diluting to 200 µg/ml in AB6. 0.5 ml of AB4 and 15 µl reconstituted Detection Antibody Cocktail was added to each sample and incubated at room temperature for 1 hour. Blocking buffer was removed from membranes and sample/antibody mixtures added for incubation overnight at 4°C. Each membrane was washed three times in 20 ml 1X Wash Buffer for 10 minutes on a rocking platform shaker. Membranes were incubated in Streptavidin-HRP (diluted 1:2000 in AB6) for 30 minutes at room temperature and washed as above. Protein expression spots were visualised following application of Chemi Reagent Mix and 1-10 minutes exposure to X-ray film. Films were scanned in and densitometry analysis carried out using ImageJ software to calculate relative levels of protein expression, normalised to control spots (A1, A2, A23, A24, F1, F2).

2.2.8 Laser-capture microdissection

Frozen prostate tissue (snap frozen immediately after dissection) was embedded in OCT on dry ice, with freezing accelerated by cryospray (CellPath). A cryostat (cleaned with RNase Zap prior to cutting sections for RNA extraction) was used to cut 5x 20 µm sections, which were mounted onto nuclease-free PET-membrane 1,4 µm slides (Leica) and stored in 50 ml tubes at -80°C until required. In order to visualise tissue histology and Pten expression, serial sections either side of these 5 sections were cut and mounted onto glass slides for Cresyl Violet staining and Pten IHC staining. Cresyl Violet staining was carried out as follows: 30 seconds each in 70% ethanol and 50% ethanol, 45 seconds in Cresyl Violet, 2 washes in DEPC water, and 30 seconds each in 50% ethanol, 70% ethanol, 95% ethanol and 2x 100% ethanol. Pten IHC was carried out as follows: Frozen sections were incubated in 5% paraformaldehyde for 5 minutes, washed three times in PBS and three times in dH₂O. Slides were blocked in 3% hydrogen peroxide for 10 minutes, washed in dH₂O, and sections outlined in hydrophobic pen. Sections were blocked for 1 hour in IHC blocking buffer and incubated overnight in Pten primary antibody (1:50, Cell Signaling

#9559). Signal was amplified with EnVision™ anti-mouse secondary antibody (Dako) and visualised using DAB chromogen. Slides were haematoxylin counterstained and mounted using the autostainer (Leica ST5020). Images of Cresyl Violet and Pten staining were taken using the Olympus BX51 light microscope at 40X magnification and compiled to assemble image of whole tissue section, which was used as a guide for LCM. Microdissection was carried out using the Leica LCM system. Sections mounted on membrane slides were kept on dry ice until required. Prior to microdissection, sections were stained with Cresyl Violet as described above, with all solutions kept on ice. When processing slides for RNA extraction, all solutions following the DEPC water washes contained 1X RNase inhibitor (Sigma). Excess ethanol was removed before cutting sections. Sections viewed at 50X magnification and epithelial or stromal areas were selected for microdissection, cut by the laser and collected into separate microcentrifuge lids (0.2 ml tubes). For some samples, areas were selected based on low or high Pten expression, as observed from immunohistochemical staining of serial sections, and were collected into separate microcentrifuge lids. For RNA extraction samples, 20 µl RLT buffer (RNeasy Micro Kit, Qiagen) containing 10% β-mercaptoethanol, was put into the lid of 0.2 ml microcentrifuge tubes and, once sample was collected, a further 30 µl RLT buffer was added to resuspend tissue and transferred into the tube. Samples were frozen at -80°C until whole set was collected for RNA isolation. For DNA extraction samples, 15 µl ALT buffer (QIAamp DNA Micro Kit, Qiagen) was put into the lid of 0.2 ml microcentrifuge tubes. Samples for RNA extraction and DNA extraction were processed separately, as described below.

2.2.8.1 *Pten* RNA expression analysis

Samples collected from serial sections of *Pb-Cre Ctnnb1^{(ex3)Δ/+}* and *Pb-Cre Pten^{fl/+} Ctnnb1^{(ex3)Δ/+}* prostate tissue were pooled for RNA extraction. RNA was extracted from the micro-dissected prostate tissue using a RNeasy Micro Kit (Qiagen), according to manufacturer's instructions. On-column DNase digestion steps were included to remove genomic DNA contamination using 2.7 U/µl RNase-free DNase I (Qiagen). RNA was eluted in 12 µl nuclease-free water. 8 µl RNA was reverse transcribed to cDNA using an Arcturus RiboAmp HS Plus RNA amplification kit for Random Priming 1st-Strand cDNA Synthesis, according to manufacturer's instructions. cDNA was measured by Qubit™ fluorometric

analysis using a Quant-iT™ BR Kit for dsDNA, as per manufacturer's instructions, and 4 ng cDNA was used for each qPCR reaction. TaqMan® qPCR was carried out as described in method 2.2.5.1 and 18s was used to normalise for differences in RNA input. (See materials 2.1.4, Table 2.1-6 for primer sequences and probes).

2.2.8.2 *Pten* copy number analysis

Samples collected from serial sections of *wildtype*, *Pb-Cre Pten^{fl/+}*, *Pb-Cre Pten^{fl/fl}*, *Pb-Cre Cttnb1^{(ex3)Δ/+}* and *Pb-Cre Pten^{fl/+} Cttnb1^{(ex3)Δ/+}* prostate tissue were pooled for DNA extraction. DNA was isolated from micro-dissected tissue using a QIAamp DNA Micro Kit (Qiagen), according to manufacturer's instructions for the 'Isolation of Genomic DNA from Laser-Micro-dissected Tissues'. DNA concentration was measured by Qubit™ fluorometric analysis using a Quant-iT™ HS Kit for dsDNA, according to manufacturer's instructions. TaqMan® qPCR was carried out as described in method 2.2.5.1, with 4 ng of DNA per reaction, and *Casc3* was used to normalise for differences in DNA input. (See materials 2.1.4, Table 2.1-6 for primer sequences and probes).

2.2.9 Primary cell line derivation and culture

CP3 and CP4 cell lines were derived from *Pb-Cre Pten^{fl/+} Cttnb1^{(ex3)Δ/+}* prostate tumours, using a method adapted from Lukacs et al [184]. Immediately following dissection prostate tumour tissue was placed in DMEM* medium. Tissue was minced with a scalpel blade, transferred into 10 ml of 1 mg/ml collagenase in DMEM* medium and incubated with rotation at 37°C for 2 hours. Following centrifugation at 400 x g for 5 minutes at room temperature, supernatant was removed and tissue resuspended in 2 ml Trypsin/0.5% EDTA. Cells were trypsinised for 5 minutes at 37°C. Trypsin was inactivated following addition of 3 ml DMEM containing 500 U DNase I and the cell suspension passed through an 18G and 20 G needle, five times each. Trypsinisation steps were then repeated and cells were filtered through a 40 µm filter into a 50 ml tube. Cells were pelleted by centrifugation at 400 x g for 5 minutes at room temperature and resuspended in 1 ml DMEM* for counting with a haemocytometer. Cells were diluted to $\sim 0.5 \times 10^6$ cells/ml in DMEM* and mixed with matrigel in a 2:3 ratio (cells:matrigel). 3D cell cultures were set up with 200 µl of the mixture pipetted evenly around the rim of wells in a 12 well plate and incubated for 30

minutes at 37°C to solidify the Matrigel. 800 µl warm DMEM* was added to the centre of each well and a half medium change was performed every three days. Spheres were cultured at 37°C for 7-10 days before passaging and expanding. To passage spheres, medium was removed and matrigel was digested in 0.5 ml of 1 mg/ml dispase solution for 1 hour at 37°C. Spheres were collected in a 15 ml tube and centrifuged at 233 x g for 5 minutes. Dispase was removed, the pellet resuspended in 1 ml Trypsin/0.5% EDTA (warmed at 37°C) and incubated at 37°C for 5 minutes. DMEM* was added to inhibit trypsin and spheres were dissociated by pipetting up and down. Cells were centrifuged at 500 x g for 2 minutes, resuspended in 2 ml and counted. 3D cultures were set up as already described. Cells were expanded in 3D culture until passage 4 and then expanded in 2D culture for use in experiments. 2D CP cell cultures were maintained in DMEM*. When ~80% confluent cells were passaged as follows: cells were washed in PBS, trypsinised in 1X trypsin/PE, resuspended in DMEM* and reseeded in fresh flasks or culture dishes.

*supplemented with 10% FBS, 1% 100X glutamine, 1% 100X penicillin/streptomycin

CP1 and CP2 cell lines, also derived from *Pb-Cre Pten^{fl/+} Ctnnb1^{(ex3)Δ/+}* prostate tumours, were generated by Meiling Gao.

To assess Pten status cell pellets were sent to Transnetyx™ for genotyping using standard PCR assays to detect *wildtype* and *Pten floxed* alleles. Tail tip and prostate tumour tissue from mice used to generate CP3 and CP4 cell lines was also sent to Transnetyx™ for genotyping for comparison with the cell lines.

2.2.9.1 CP1 ICG-001 treatment

CP1 cells were cultured to 70% confluency and treated with 25 µM ICG-001 or equivalent volume of ethanol vehicle control in DMEM (10% FBS; 1X glutamine) for 24 hours at 37°C. Whole cell lysates were prepared for analysis by immunoblotting (as described in 2.2.4) and total RNA extracted for miRNA analysis (as described in 2.2.5.2).

2.2.10 RNAscope®

Wnt5a RNAscope®, a form of *in situ* hybridisation, was carried out by Histology Services using the RNAscope® 2.0 High Definition kit (Advanced Cell Diagnostics) according to the manufacturer's protocol. *Nkx3.1^{CreERT2} Pten^{fl/+} Ctnnb1^{(ex3)Δ/+}* HNPC (n=3) and CRPC (n=4) FFPE prostate tissue sections were deparaffinised and rehydrated prior to pre-treatment retrieval steps to unmask target RNA. The Wnt5a probe, containing 20 Wnt5a-specific double Z probe pairs, was then hybridised to target RNA and the hybridisation signals were amplified by 6 sequential amplification steps using the RNAscope Detection Reagents. These reagents contain amplifiers which hybridise to binding sites formed by the probe pairs. These were detected by DAB staining and visualised following counterstaining with haematoxylin. Whole sections were scanned using a Leica digital slide scanner and representative images were taken at 40X and 200X magnification using SlidePath software (Leica Biosystems).

2.2.11 Immunoprecipitation

Dynabeads® M-280 sheep anti-rabbit IgG magnetic beads (Novex™, Life Technologies) were resuspended thoroughly by vortexing. 30 µl of bead suspension (6-7 x 10⁸ beads/ml) per sample was transferred into a microcentrifuge tube and placed on a magnetic stand for 2 mins before pipetting off supernatant. Beads were washed three times in excess volume of IP washing buffer and resuspended in 500 µl IP washing buffer by vortexing. 2 µg AR (N-20) antibody (sc-816, Santa Cruz) was added to the washed beads prior to incubation with slow tilt rotation mixing, overnight at 4°C. The next day, fresh whole cell lysates were prepared from adherent cells (70-80% confluent) cultured in 9 cm dishes. Culture dishes were placed on ice, cells were washed twice with ice cold PBS and scraped into 100 µl IP lysis buffer. Lysis buffer cell suspensions were transferred to a microcentrifuge tube, homogenised by vortexing and incubated on ice for 15 minutes before centrifugation at 16100 x g for 15 minutes. Supernatant was collected and protein concentration was measured by Bradford assay (Bio-Rad). Tubes containing antibody-bound beads were placed on a magnetic stand for 2 minutes and supernatant containing excess antibody was removed and discarded. In preparation for immunoprecipitation, beads were washed three times in excess IP washing buffer. Whole cell protein lysates were

adjusted to 100 µg in a total volume of 1 ml using PBS or 0.1M phosphate buffer (pH 7-8) and added to the beads. Samples were incubated, with slow tilt rotation mixing, for 60 minutes at 4°C. Tubes containing immunoprecipitated protein were placed on a magnetic stand for 2 minutes to collect the Ig-coated beads-protein target complex at the tube wall. The supernatant was discarded and beads were washed twice in high salt NETN buffer (STRONG) and once in low salt NETN buffer (WEAK). Beads were resuspended in 47.5 µl 1X sample buffer, boiled for 5 minutes at 100°C to elute protein from beads. Eluted supernatant was transferred to a fresh tube, 1 µM DTT reducing agent was added and samples were boiled for another 5 minutes at 100°C ready for Western blot analysis. Proteins were resolved, electrophoresed and visualised as described in section 2.2.5.

2.2.12 Chromatin immunoprecipitation assay

The method described below is the final standardised ChIP protocol used for cell lines and tissue. Optimisation procedures are described in Chapter 4.4.

2.2.12.1 Chromatin preparation

Cell line fixation: LNCaPs were grown on 3x 15cm culture dishes to yield ~1 x 10⁸ cells. When 70-80% confluent, medium was removed and replaced with 15 ml serum-free RPMI. 1% formaldehyde was added dropwise to each plate and incubated at room temperature with gentle agitation for 10 minutes. Cross-linking was quenched with 125 mM glycine and incubated for 5 minutes at room temperature. Culture dishes placed on ice and fixed cells were washed twice with ice cold PBS, then scraped into PBS and transferred to a 50 ml Falcon tube. Cells were washed in 40-50 ml PBS, centrifuged at 245 x g for 5 minutes at 4°C. The pellet was resuspended in 1.5 ml ice-cold PBS and centrifuged at 680 x g for 5 minutes at 4°C ready for lysis steps (see below).

Tissue fixation: Fresh or frozen prostate tissue was minced into small pieces (<0.5 cm³), added to 50 ml freshly prepared tissue cross-linking solution in a 100 ml glass bottle, and incubated at room temperature with stirring for 15 minutes. 125 mM Glycine was added dropwise and incubated for 5 minutes at room temperature to quench fixation. Tissue was rinsed with ice-cold PBS and

homogenised with a motorised tissue grinder. Cells were resuspended in 40 ml PBS, filtered through a 100 µm cell strainer into a fresh 50 ml tube and centrifuged at 1060 x g for 3 minutes at 4°C. The cell pellet was washed in 40 ml PBS, cells were counted, and the cell pellet was collected by centrifugation ready for lysis steps.

Cell lysis and chromatin sonication: Cell pellets were gently resuspended in 600 µl cell lysis buffer (CLB) by pipetting up and down and incubated for 10 minutes on ice. Lysates were centrifuged at 1060 x g for 5 minutes at 4°C to collect nuclei and supernatant was discarded. Nuclei were resuspended in 1.2 ml of nuclei lysis buffer (NLB) and incubated on ice for 10 minutes before 0.72 ml of IP dilution buffer (IPDB) was added. CLB, NLB and IPDB volumes are based on $\sim 1 \times 10^8$ cell sample and were adjusted according to cell number. Lysed nuclei samples were divided into ~ 0.5 ml aliquots and sonicated using the Bioruptor sonicator on high setting 30s on/30s off. Cell line samples were sonicated for 20 minutes (2x 10 minutes) and tissue samples were sonicated for 25 minutes (2x 10 minutes + 1x 5 minutes) (N.B. ice was replaced every 10 minutes). Under these conditions, the DNA was sheared to approximately 200-500 bp fragments. Samples were centrifuged at 15700 x g for 5 minutes at 4°C, the supernatant was then pooled in a 15 ml Falcon and IPDB added to bring the ratio of NLB:IPDB to 1:4.

Chromatin pre-clearing: 100 µl of normal rabbit IgG was added to the pooled chromatin sample and incubated for 1 hour at 4°C on a rotating wheel. Samples were briefly centrifuged and 200 µl of the homogeneous protein G-agarose suspension (100 µl bead volume) was added prior to incubation for 3 hours (to overnight) at 4°C on a rotating wheel.

2.2.12.2 Chromatin-immunoprecipitation (ChIP)

Pre-cleared chromatin was centrifuged at 1530 x g for 2 minutes at 4°C and 0.675 ml used per ChIP assay. This was added to 0.675 ml NLB/IPDB (NLB:IPDB = 1:4) and 10 µg ChIP-grade antibody in 2 ml PCR clean tubes. HA antibody was used as a ChIP control. (See Materials 2.1.3, Table 2.1-5 for antibody details). Samples were incubated overnight at 4°C with rotation. 10% input control (67.5 µl) was stored at -20°C. ChIP samples were centrifuged at 15700 x g for 5

minutes at 4°C and transferred to a new 1.5 ml microcentrifuge tube. 50 µl homogenous protein G-agarose suspension (25 µl bead volume) was added and samples were incubated for 4 hours at 4°C with rotation. Samples were then centrifuged 15700 x g for 20 seconds at 4°C and the supernatant discarded. The bead pellet was washed twice with 750 µl of IP wash buffer 1 (IPWB1), each time vortexing briefly and centrifuging samples at 5100 x g for 2 minutes at 4°C. The pellet was washed similarly, once with 750 µl of IP wash buffer 2 (IPWB2) and twice with 750 µl of TE pH8.0. Beads were resuspended in 200µl IP elution buffer (IPEB) and input sample volume was adjusted to 200 µl with IPEB. 100 µg/ml RNase A and 200 µg/ml proteinase K were added to samples and incubated overnight in a thermocycler at 65°C and 900 rpm. Samples were centrifuged at 5100 x g for 2 minutes at room temperature and supernatant eluate transferred to a fresh microcentrifuge tube. 200 µl TE buffer and 400 µl Phenol:Chloroform:Isoamyl alcohol was added to each sample and mixed thoroughly. Phase lock tubes (5Prime) were centrifuged for 1 minute at 14000 x g to pellet solvent, prior to samples being transferred to these tubes. Samples were centrifuged for 5 minutes at 14000 x g and upper phase collected in a fresh microcentrifuge tube. 16 µl of 5 M NaCl (200 mM final concentration) and 40 µg glycogen were added to each sample and vortexed before adding 1 ml ice cold ethanol absolute. Samples were stored at -80°C for at least 30 minutes, then centrifuged at maximum speed for 15 minutes at 4°C. The precipitated pellet containing DNA was washed with ice cold 80% ethanol and centrifuged again for 10 minutes at 4°C. The supernatant was discarded; the pellet was dried for 10 minutes; and DNA was eluted in 50 µl 10mM Tris-HCl pH 8, following 10 minutes incubation at 50°C to allow DNA to dissolve.

To test sonication efficiency, input DNA was run alongside DNA HyperLadder™ IV (100 bp) on a 2% agarose gel, containing 1:10000 SYBR® Safe DNA gel stain. DNA smears were visualised on a UV transilluminator.

2.2.12.3 Quantitative PCR analysis

SYBR® Green qPCR was performed in duplicate in a reaction volume of 20 µl containing 1X Fast SYBR® Green Master Mix (Applied Biosystems), 0.3 µM each of forward and reverse primers and 2 µl DNA (1:10 diluted input DNA and 1:2 diluted CHIP DNA). The thermal cycling conditions were as follows: enzyme

activation at 95 °C for 20 seconds, followed by 40 cycles of denaturation at 95 °C for 3 seconds and annealing/extending at 60 °C for 30 seconds (Applied Biosystems 7500 Fast Real-Time PCR System). Melting curve analysis was performed from 70 °C to 95 °C in 0.3 °C intervals to demonstrate primer specificity and confirm absence of primer dimer formation. (See materials 2.1.4, Table 2.1-8 for primer sequences used for ChIP qPCR). Relative DNA enrichment of target genes was normalised to DNA input as follows: Ct value for DNA input was adjusted to 100%, i.e. for 10% input, the Ct value was adjusted 10-fold ($Ct_{input} - \log_2(10)$). % input = $100 \times 2^{(Adjusted\ input\ Ct - ChIP\ Ct)}$

2.2.13 Statistics

Data are presented as mean \pm SEM or SD, as noted in the figure legend. GraphPad Prism software was used to produce graphs and carry out statistical analysis. Where statistically significant differences have been observed, details of the statistical tests used are provided in figure legends.

Chapter 3 - β -catenin activation drives prostate tumourigenesis and co-operates with Pten loss to advance cancer progression

3.1 Introduction

Prostate cancer patients with the poorest prognosis have tumours with an embryonic stem cell (ESC) signature, *MYC* activation and loss of *PTEN*. This expression profile has also been associated with tumours in younger patients [41, 100]. *MYC* is a β -catenin target and the deregulation of Wnt/ β -catenin signalling, frequently observed in prostate cancer, could be a contributing factor for *MYC* activation. The deregulation of Wnt/ β -catenin signalling can be attributed to a variety of causes, including mutations in *exon3* of the β -catenin gene (*CTNNB1*) in approximately 5% of cases [139, 140]. However, the mutation rate of Wnt/ β -catenin pathway components in prostate cancer is low. Instead, changes in the expression of β -catenin and Wnt pathway components, including the expression of Wnt ligands in the prostate tumour microenvironment, contribute to β -catenin activation.

The MSKCC prostate cancer data set [41] (available in the cBioPortal for Cancer Genomics) shows that the combined deregulation of *PTEN/PI3K* and Wnt/ β -catenin pathways is clinically relevant. Almost 93% of the metastatic tumour case set and 95% of the metastatic lesions themselves have alterations in both *PTEN/PI3K* and Wnt pathway components (Figure 1.3.4). These data suggest the deregulation of Wnt/ β -catenin and *PTEN/PI3K* pathways, and their co-operation, play a role in aggressive prostate cancer phenotypes.

Direct crosstalk between Wnt/ β -catenin and *PI3K/Akt* pathways may be important in promoting prostate tumourigenesis. It has previously been reported that loss of *PTEN* activity results in the upregulation of Akt kinase activity, leading to phosphorylation and inactivation of *GSK3B* by phospho-Akt and the resultant activation of β -catenin [154]. However, effects of β -catenin activation on *PTEN/PI3K/Akt* signalling have not been described.

We initiated this project to investigate the role of aberrant Wnt/ β -catenin signalling in prostate cancer tumourigenesis and progression, alone and in combination with *Pten* loss, using pre-clinical *in vivo* models. It is vital that we gain a better understanding of the molecular mechanisms and pathway interactions associated with Wnt/ β -catenin activation and *PTEN* loss in order to elucidate novel therapeutic strategies to treat this subset of patients.

Data from our lab has demonstrated a significant co-occurrence of PTEN loss and high levels of nuclear β -catenin in an independent cohort of 209 prostate cancer patients. Samples were analysed in a tissue microarray, comparing immunohistochemical staining of (Gleason grade 3 to 5) prostate cancer tissue to benign prostatic hyperplasia (BPH) (Figure 3.1.1).

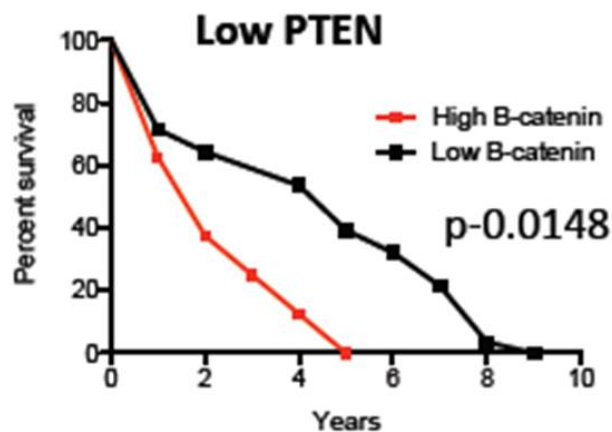
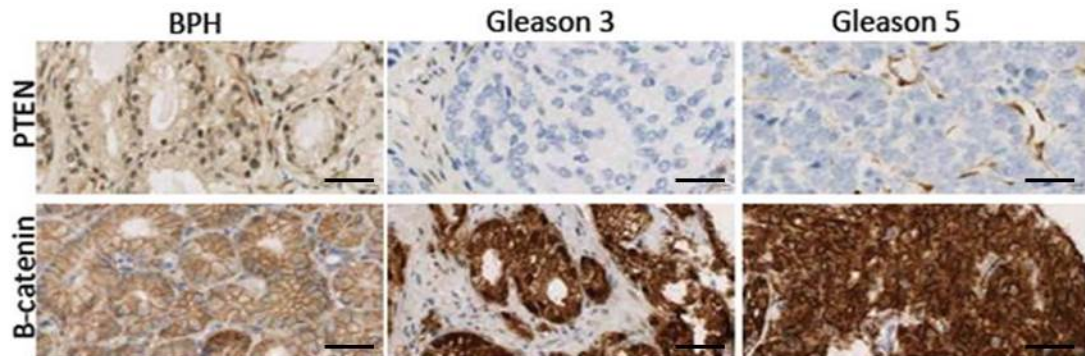


Figure 3.1.1 Clinical relevance of studying Wnt/ β -catenin and PTEN in prostate cancer
Tissue microarray analysis was carried out on samples from a cohort of 209 prostate cancer patients with local ethical committee approval (MREC 01/0/36). The top panel shows representative immunohistochemical staining of PTEN and β -catenin in Benign Prostatic Hyperplasia (BPH), Gleason grade 3 and Gleason grade 5 FFPE prostate tissues. Scale bar: 100 μ m. Survival plot shows the reduced survival of patients with low PTEN and high β -catenin compared to patients with low PTEN and low β -catenin. Data provided by Imran Ahmad (unpublished).

Furthermore, analysis of survival data showed that patients with low levels of PTEN and high levels of nuclear β -catenin have a significantly poorer prognosis compared to patients with low levels of PTEN and low levels of β -catenin (Figure 3.1.1) (Imran Ahmad, unpublished data). This provides further evidence that concurrent loss of PTEN and expression of high levels of nuclear β -catenin are associated with aggressive prostate cancer.

3.2 Wnt/ β -catenin pathway activation and Pten loss co-operate to drive aggressive prostate cancer

Increased stromal-derived Wnt has been reported in prostate cancer [146]. This can be responsible for the activation of Wnt/ β -catenin signalling in cancer epithelial cells. In order to demonstrate the effect of increased stromal Wnt on tumour epithelial cells, Wnt3A-secreting L cells and Pten null murine prostate cancer cells were orthotopically co-injected into the prostates of CD-1 nude mice (Figure 3.2.1).

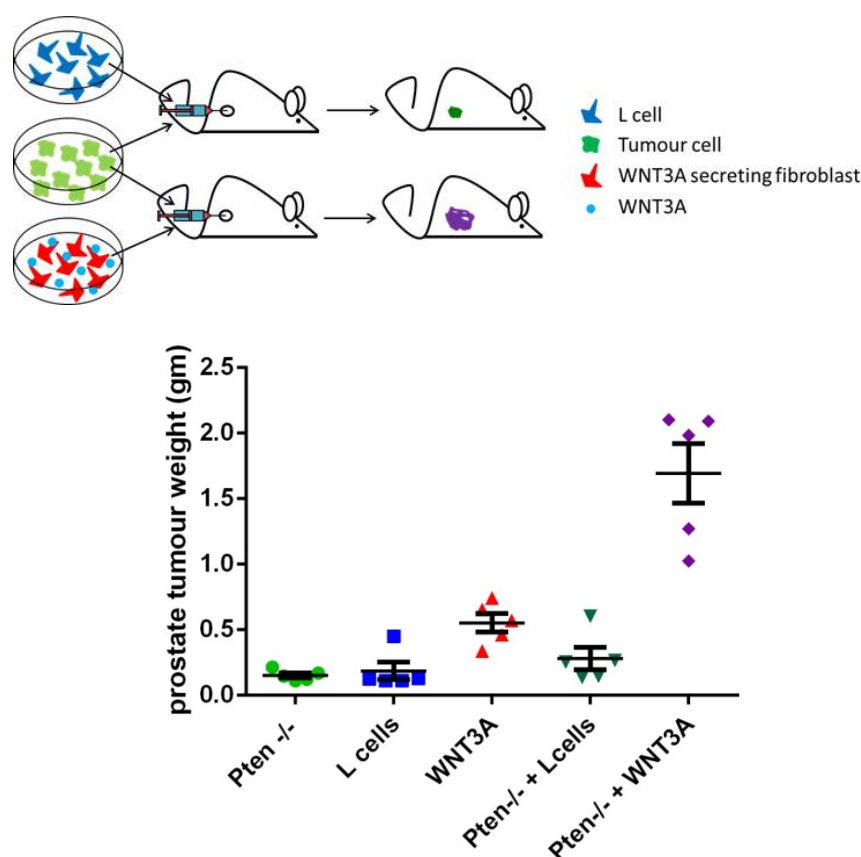


Figure 3.2.1 Increased circulating Wnt co-operates with Pten loss to drive aggressive prostate cancer

Proof-of-concept experiment to show the effect of co-injecting Wnt3A-secreting L cells with *Pten* null murine tumour cells in a CD-1 orthotopic prostate model, compared to relevant controls as shown in the experiment schematic. *Pten* null tumour cells were derived from a GEMM tumour driven by the complete loss of *Pten*. Mice were sacrificed 4 weeks after orthotopic injection of cells into the prostate. Prostate tumour weights from mice orthotopically co-injected with Wnt3A-secreting L cells and *Pten* null murine tumour cells were compared to controls. Data provided by Rachana Patel (unpublished).

These mice developed significantly larger prostate tumours compared to controls (Figure 3.2.1) (Rachana Patel, unpublished data). Thus, concurrent activation of Wnt/ β -catenin and Pten loss was required to drive aggressive prostate cancer,

not observed when Wnt3A-secreting L cells or Pten null cells were injected alone.

This data provided evidence of a direct cooperation between Wnt/ β -catenin pathway activation and Pten loss which we continued to study in a genetically engineered mouse model. We hypothesised that loss of Pten would co-operate with β -catenin activation to drive aggressive prostate carcinogenesis in mice.

3.2.1 Characterisation of an *in vivo* prostate cancer model with β -catenin activation and concurrent Pten loss

To model the effects of high levels of nuclear β -catenin and Pten loss in an *in vivo* prostate cancer model, we used a conditional *Cre-loxP* system modulated by *Pb-Cre* [169]. This system places *Cre recombinase* under the control of a modified rat prostate-specific *probasin (Pb)* promoter. *Probasin*, and hence *Cre*, is expressed in the prostate during post-natal development and responsive to increasing levels of androgens [169]. *Pb-Cre* mice were crossed with *Pten^{fl/fl}* mice to generate mice with a conditional knockout *Pten* allele, with *exon5* flanked by *loxP* sequences (*Pb-Cre Pten^{fl/+}*) [176] and with *Ctnnb1^{(ex3) Δ /+}* mice [177] to generate a conditional dominant *Ctnnb1* allele, with *exon3* flanked by *loxP* sequences (*Pb-Cre Ctnnb1^{(ex3) Δ /+}*). These mice were then inter-crossed to generate mice with simultaneous heterozygous excision of *Pten exon5* and *Ctnnb1 exon3* (*Pb-Cre Pten^{fl/+} Ctnnb1^{(ex3) Δ /+}*).

Exon5 of the *Pten* gene is the site of many known tumour-associated mutations and excision of *exon5* renders *Pten* inactive, resulting in loss of *Pten* protein in *Cre*-expressing tissue [176]. *Exon3* of the *Ctnnb1* gene contains the GSK3 β phosphorylation site which, in the absence of Wnt ligand, targets β -catenin for degradation. When *exon3* is excised, β -catenin is no longer targeted for degradation. It is stabilised and accumulates in the nucleus, able to carry out its role as a transcriptional co-activator. Following expression of *cre recombinase*, there is heterozygous loss of *Pten*, with activation of PI3K/Akt, in a subset of prostate epithelial cells, while β -catenin is activated and mimics canonical Wnt pathway activation in the absence of Wnt ligand.

Mice were aged and sacrificed at clinical endpoint, determined by clinical signs including palpable tumour burden, haematuria, weight loss and reduced activity, in keeping with the terms of the project licence. Survival analysis found that *Pb-Cre Pten^{fl/+} Ctnnb1^{(ex3)Δ/+}* mice had a significantly poorer survival outcome than mice with β-catenin activation alone (*Pb-Cre Ctnnb1^{(ex3)Δ/+}*) (Figure 3.2.2). β-catenin activation alone was sufficient to drive prostate cancer, as *Pb-Cre Ctnnb1^{(ex3)Δ/+}* mice also developed adenocarcinoma comparable at endpoint to *Pb-Cre Pten^{fl/+} Ctnnb1^{(ex3)Δ/+}* mice (Figure 3.2.3), but with a longer latency (Figure 3.2.2). *Pb-Cre Ctnnb1^{(ex3)Δ/+}* mice survived up to 384 days whereas all *Pb-Cre Pten^{fl/+} Ctnnb1^{(ex3)Δ/+}* mice were taken within 274 days. Heterozygous loss of *Pten* alone (*Pb-Cre Pten^{fl/+}*) did not result in prostate cancer (Figure 3.2.4) and, therefore, did not adversely affect survival (Figure 3.2.2).

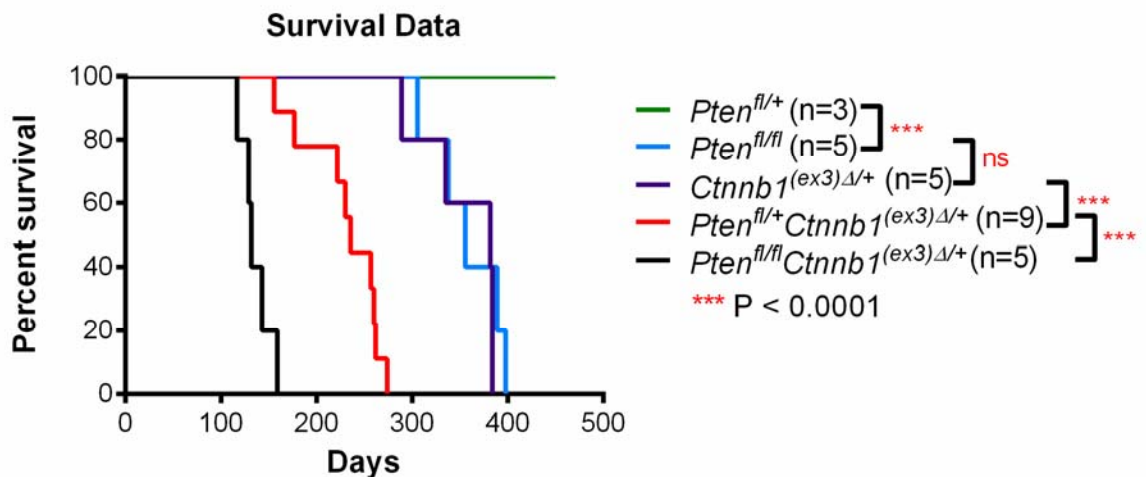


Figure 3.2.2 Co-operation between β-catenin activation and Pten loss results in poor survival outcome *in vivo*

Kaplan-Meier survival curve for *Pb-Cre Pten^{fl/+}*, *Pb-Cre Ctnnb1^{(ex3)Δ/+}*, *Pb-Cre Pten^{fl/+} Ctnnb1^{(ex3)Δ/+}*, *Pb-Cre Pten^{fl/fl}*, and *Pb-Cre Pten^{fl/fl} Ctnnb1^{(ex3)Δ/+}* mice (***) P < 0.001, data analysed by log-rank test). *Pb-Cre Pten^{fl/fl}* survival data provided by Rachana Patel.

As a result of mating combinations, *Pb-Cre Pten^{fl/fl} Ctnnb1^{(ex3)Δ/+}* mice, with homozygous loss of *Pten* and β-catenin activation, were also generated and aged to clinical endpoint. We observed an additive effect of complete loss of *Pten*, as these mice only survived up to 159 days, over 100 days less than mice with heterozygous loss of *Pten* and β-catenin activation (Figure 3.2.2). The additional loss of *Pten* had a ‘dose-dependent’ effect for driving tumour progression and suggested that *Pten* tumour suppression may play a role in increasing the latency of tumours driven by β-catenin activation alone. Survival data for *Pb-Cre*

Pten^{fl/fl} mice, with homozygous *Pten* deletion alone, was generated by Rachana Patel and used for comparison with the other genotypes. These mice had a similar survival outcome to mice with β -catenin-driven prostate cancer (Figure 3.2.2).

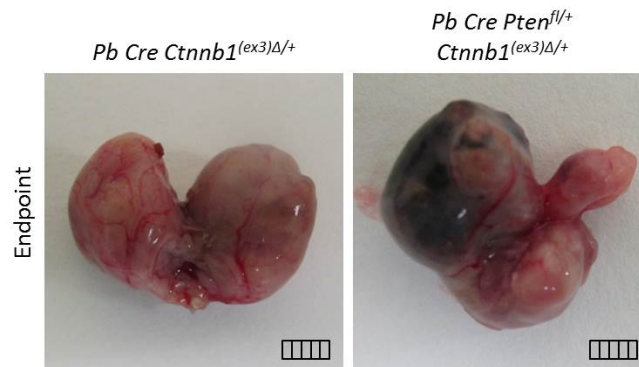


Figure 3.2.3 β -catenin activation alone drives prostate tumourigenesis
Representative images of prostate tumours dissected from *Pb-Cre Ctnnb1*^{(ex3) Δ /+} and *Pb-Cre Pten*^{fl/+} *Ctnnb1*^{(ex3) Δ /+} mice at clinical endpoint. Ruler scale: 5 mm.

Unlike homozygous *Pten* loss, heterozygous loss of *Pten* did not result in prostate cancer (Figure 3.2.4 & 3.2.5). However, it significantly contributed to the progression of β -catenin-driven prostate cancer. To further investigate how *Pten* loss and β -catenin activation co-operate to drive aggressive prostate cancer, we focussed on the effects of heterozygous *Pten* loss in combination with β -catenin activation.

Mice were sacrificed at 3 month and 6 month time points to study prostate cancer initiation and progression in *Pb-Cre Ctnnb1*^{(ex3) Δ /+} and *Pb-Cre Pten*^{fl/+} *Ctnnb1*^{(ex3) Δ /+} prostate tissue compared to *wildtype* and *Pb-Cre Pten*^{fl/+} controls. Macroscopic tumour was evident in anterior and dorsal-lateral prostate lobes of *Pb-Cre Pten*^{fl/+} *Ctnnb1*^{(ex3) Δ /+} mice at 3 months, and prostate weights were significantly greater than those from *wildtype* and *Pb-Cre Pten*^{fl/+} mice (Figure 3.2.4). The prostates of *Pb-Cre Ctnnb1*^{(ex3) Δ /+} mice appeared slightly enlarged compared to *wildtype* but the higher standard deviation of weights in this group meant there was no significant difference compared to *wildtype* or *Pb-Cre Pten*^{fl/+} *Ctnnb1*^{(ex3) Δ /+} prostate weights at 3 months (Figure 3.2.4).

At 6 months, *Pb-Cre Ctnnb1*^{(ex3) Δ /+} prostate lobes were enlarged with white or necrotic lesions in the dorsal-lateral lobe, and the prostate weight was

significantly greater than *wildtype* (Figure 3.2.4). By 6 months *Pb-Cre Pten^{fl/+} Ctnnb1^{(ex3)Δ/+}* mice had developed substantial tumour burden in the anterior prostate lobes, which tended to be solid with little tumour infiltrate (Figure 3.2.4). Furthermore, despite a large variation in the weights of *Pb-Cre Pten^{fl/+} Ctnnb1^{(ex3)Δ/+}* prostates, statistical analysis using the Mann Whitney test indicated a significant tendency for *Pb-Cre Pten^{fl/+} Ctnnb1^{(ex3)Δ/+}* prostate weights to be greater than *Pb-Cre Ctnnb1^{(ex3)Δ/+}* (Figure 3.2.4).

The average weight of *Pb-Cre Ctnnb1^{(ex3)Δ/+}* prostates increased over 2-fold from 0.15 g at 3 months to 0.35 g at 6 months, while that of *Pb-Cre Pten^{fl/+} Ctnnb1^{(ex3)Δ/+}* increased just over 5-fold from 0.18 g at 3 months to 0.95 g at 6 months (Figure 3.2.4). Together with the survival data (Figure 3.2.2), this demonstrated that concurrent heterozygous loss of *Pten* and β -catenin activation resulted in a faster growing tumour with shorter latency compared to tumours driven by β -catenin activation alone.

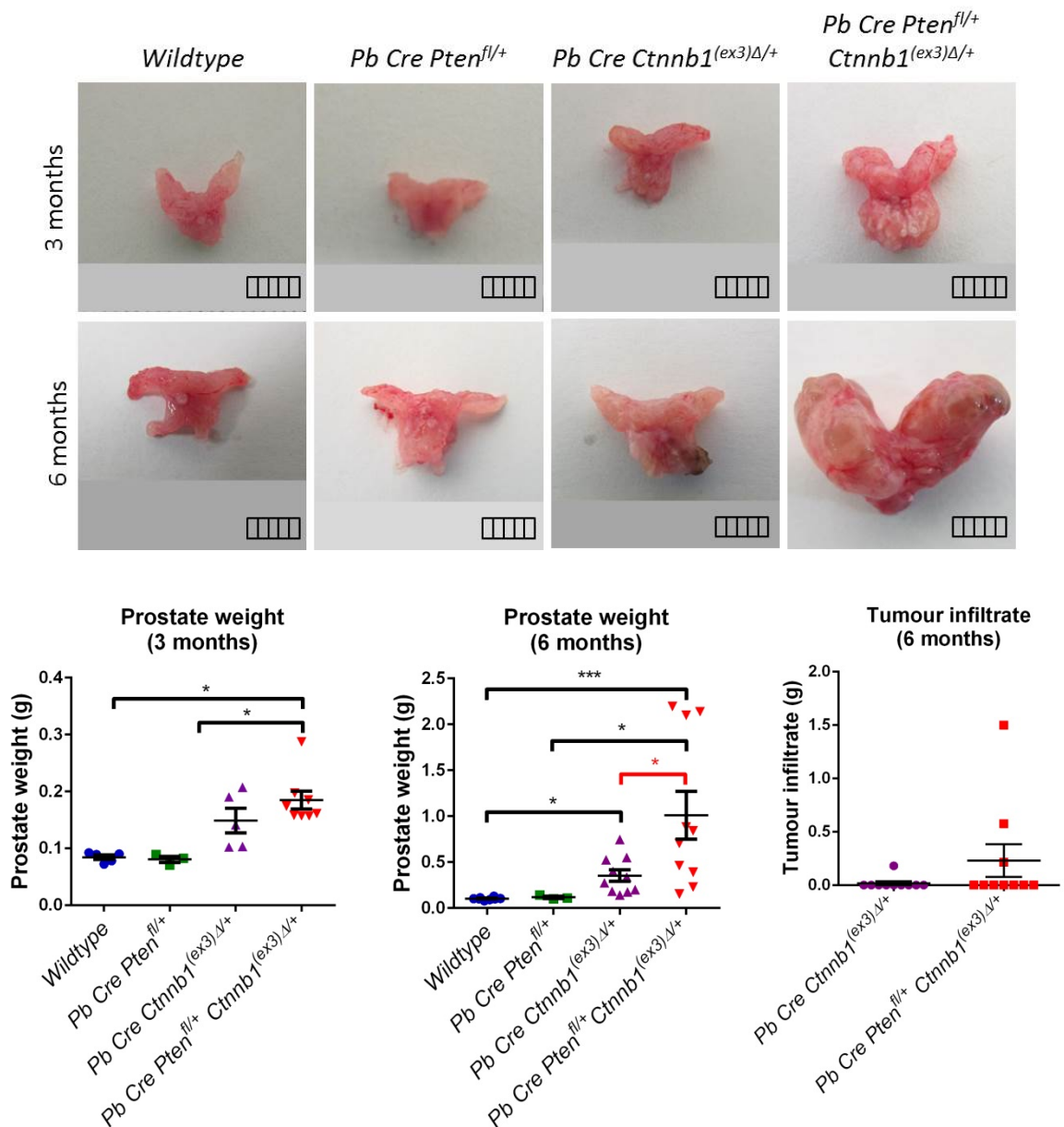


Figure 3.2.4 Co-operation between β -catenin activation and *Pten* loss drives prostate tumour growth

Representative images of prostates dissected from *wildtype*, *Pb-Cre Pten^{fl/+}*, *Pb-Cre Ctnnb1^{(ex3)Δ/+}* and *Pb-Cre Pten^{fl/+} Ctnnb1^{(ex3)Δ/+}* mice at 3 months and 6 months of age. Ruler scale: 5 mm. The graphs show the 'dry' weights of prostates sampled from mice at 3 months and 6 months and the amount of tumour infiltrate in *Ctnnb1^{(ex3)Δ/+}* and *Pten^{fl/+} Ctnnb1^{(ex3)Δ/+}* prostates at 6 months. (***) $P < 0.001$, ** $P < 0.01$, * $P < 0.05$; data analysed by one-way ANOVA Kruskal-Wallis test, with Dunn's multiple comparison test. * P value in red was generated by Mann Whitney test). Data presented as mean \pm SEM.

We continued to characterise the *Pb-Cre Pten^{fl/+} Ctnnb1^{(ex3)Δ/+}* model by studying the histopathology of prostate tissue from mice sacrificed at 6 months compared to controls (Figure 3.2.5). Heterozygous loss of *Pten* expression combined with β -catenin activation resulted in aggressive, invasive adenocarcinoma in the majority of the prostate tissue. Low levels of *Pten*, high nuclear β -catenin and a large proportion of Ki67 positive cells were detected (Figure 3.2.5).

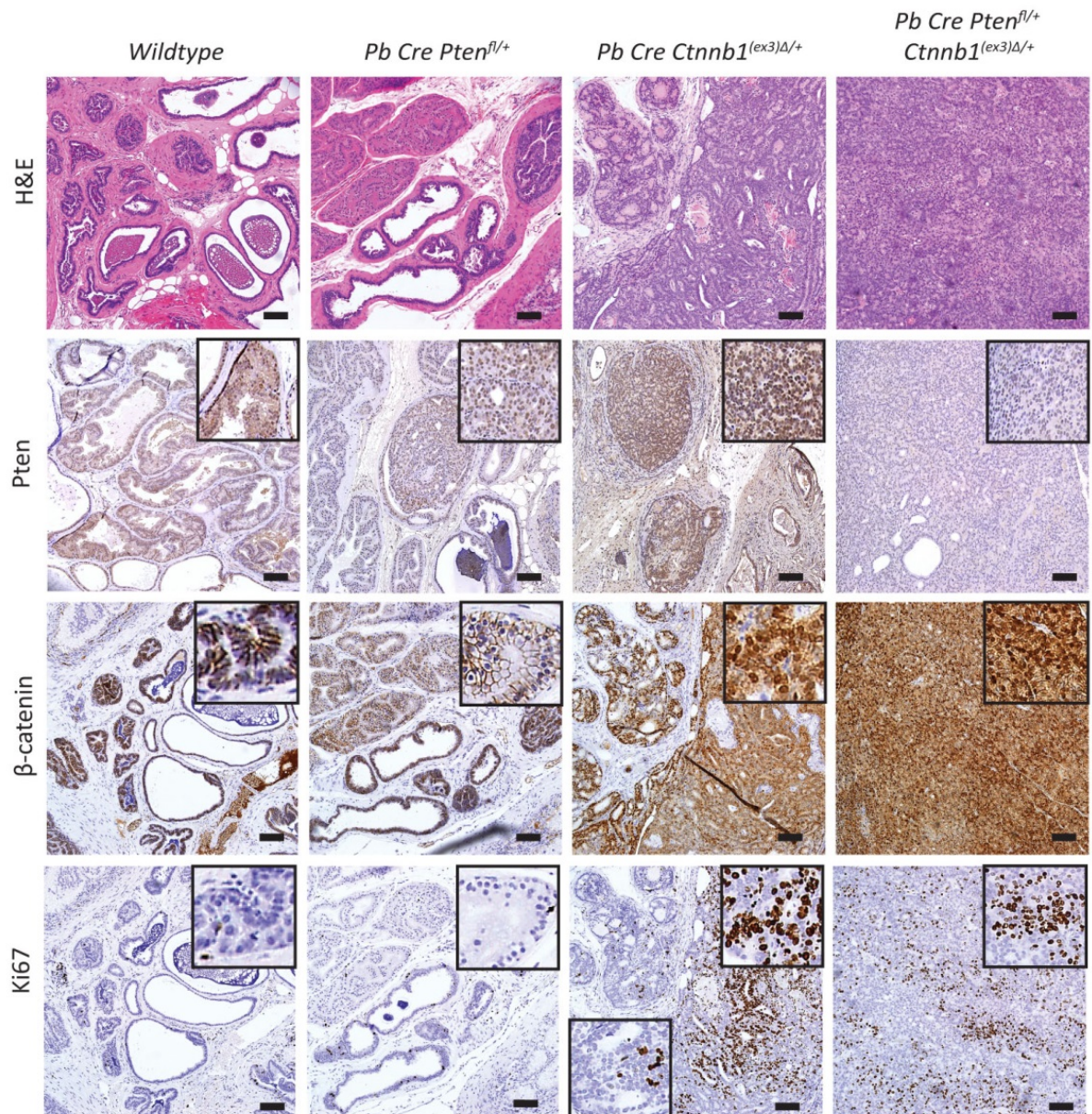


Figure 3.2.5 Histopathological characterisation of *Pb-Cre Pten^{fl/+} Ctnnb1^{(ex3)Δ/+}* mouse model
 Representative haematoxylin and eosin staining, and Pten, β-catenin and Ki67 immunohistochemical staining of FFPE sections of *wildtype*, *Pb-Cre Pten^{fl/+}*, *Pb-Cre Ctnnb1^{(ex3)Δ/+}* and *Pb-Cre Pten^{fl/+} Ctnnb1^{(ex3)Δ/+}* prostate tissue from mice sacrificed at 6 months. To illustrate the variation observed in *Pb-Cre Ctnnb1^{(ex3)Δ/+}* Ki67 levels, two representative inserts are included: lower left = PIN, upper right = tumour. Scale bar: 100 μm. Insert box: 100 μm².

In contrast, heterozygous loss of *Pten* (*Pb-Cre Pten^{fl/+}*) did not result in tumour and the morphological structure of glands was similar to *wildtype*, with few prostatic intraepithelial neoplasia (PIN) lesions observed at 6 months. Pten, β-catenin and Ki67 staining were also comparable to *wildtype*. In contrast, *Pb-Cre Ctnnb1^{(ex3)Δ/+}* mice, with β-catenin activation alone, developed PIN and *in situ* carcinoma by 6 months. While levels of nuclear β-catenin were similar to *Pb-Cre Pten^{fl/+} Ctnnb1^{(ex3)Δ/+}*, levels of ki67 varied, being high within regions of

carcinoma and low in PINs, and *Pten* levels were higher than *wildtype* (Figure 3.2.5).

In order to address the variation observed in weights of *Pb-Cre Pten^{fl/+} Ctnnb1^{(ex3)Δ/+}* prostates and identify differences between these and *Pb-Cre Ctnnb1^{(ex3)Δ/+}* prostates, we investigated alternative methods of measuring histological tumour burden in these mice.

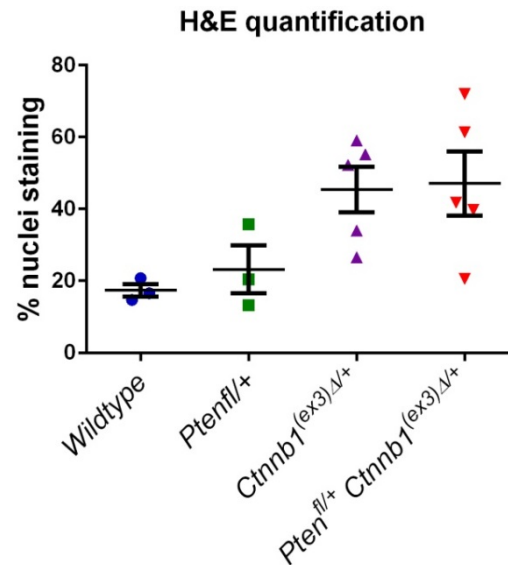


Figure 3.2.6 Analysis of haematoxylin and eosin staining to measure tumour burden

Percentage nuclei staining was measured in haematoxylin and eosin stained of FFPE sections of prostate tissue from *wildtype* (n=3), *Pb-Cre Pten^{fl/+}* (n=3), *Pb-Cre Ctnnb1^{(ex3)Δ/+}* (n=5) and *Pb-Cre Pten^{fl/+} Ctnnb1^{(ex3)Δ/+}* (n=5) mice sacrificed at 6 months. Slides were scanned using a Leica digital slide scanner and analysis was carried out using a deconvolution macro in ImageJ software. The tissue area to be measured was annotated and the software measured the percentage of the area that was positively stained with haematoxylin (purple) as a measure of the percentage of nuclei in that area. Data presented as mean \pm SEM.

Higher tumour density would be indicative of more advanced tumour grade. In order to measure this objectively and identify if there were differences between *Pb-Cre Ctnnb1^{(ex3)Δ/+}* and *Pb-Cre Pten^{fl/+} Ctnnb1^{(ex3)Δ/+}* prostate tissue at 6 months, we developed a deconvolution macro with ImageJ software to measure the percentage of nuclear (haematoxylin) staining in manually annotated areas of prostate epithelial tissue. We observed an average 2.5-fold increase in the percentage of nuclei in *Pb-Cre Ctnnb1^{(ex3)Δ/+}* and *Pb-Cre Pten^{fl/+} Ctnnb1^{(ex3)Δ/+}* prostate tissue compared to *wildtype* (Figure 3.2.6), demonstrating that this may be an effective method of objectively quantifying tumour burden. However, the standard deviation was high across groups and no significant

difference between *Pb-Cre Ctnnb1^{(ex3)Δ/+}* and *Pb-Cre Pten^{fl/+} Ctnnb1^{(ex3)Δ/+}* was observed.

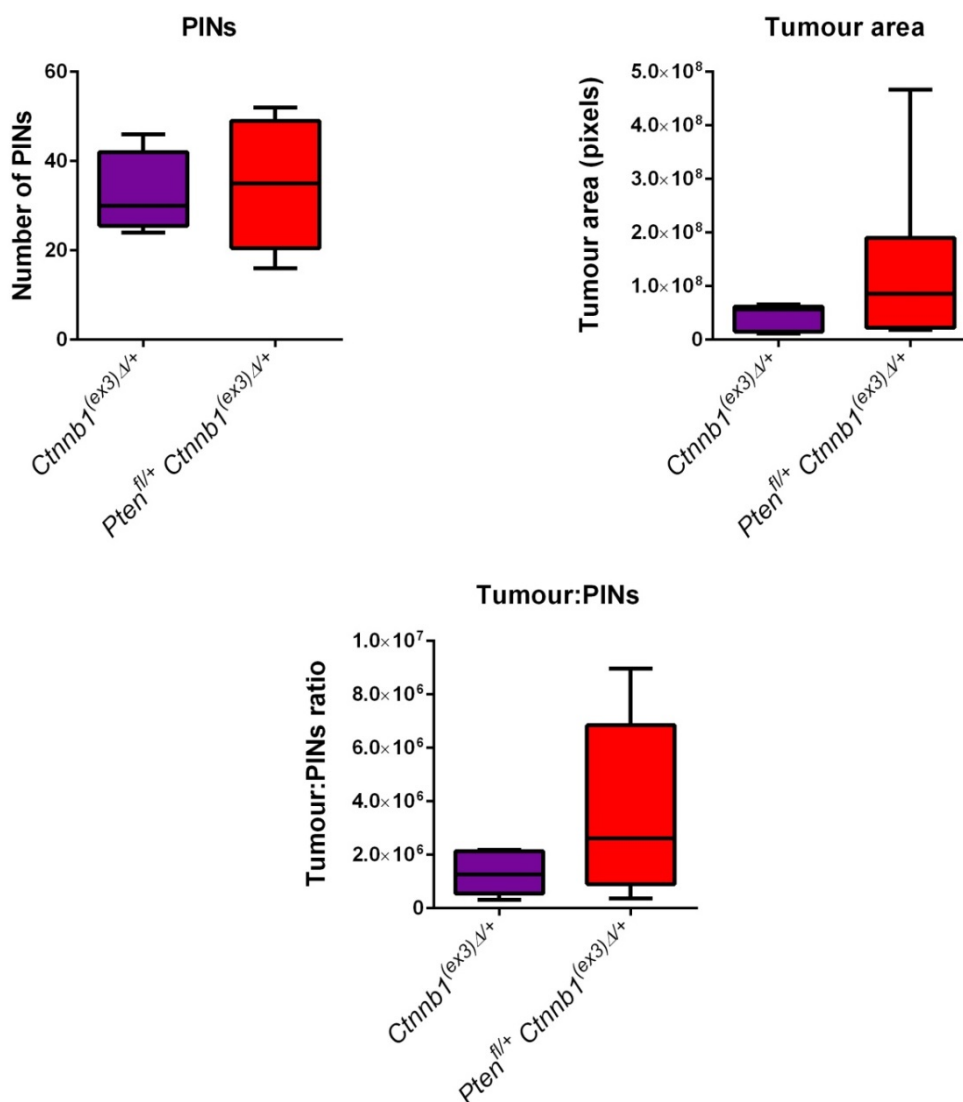


Figure 3.2.7 Analysis of PIN number and tumour area in *Pb-Cre Ctnnb1^{(ex3)Δ/+}* and *Pb-Cre Pten^{fl/+} Ctnnb1^{(ex3)Δ/+}* prostates

The graphs show box and whiskers plots of the number of PIN lesions, tumour area and tumour area to PIN number ratio measured in haematoxylin and eosin stained, FFPE prostate tissue sections from *Pb-Cre Ctnnb1^{(ex3)Δ/+}* (n=5) and *Pb-Cre Pten^{fl/+} Ctnnb1^{(ex3)Δ/+}* (n=6) mice sacrificed at 6 months. PINs were defined as hyper-proliferative prostate glands, in which more than half the lumen area was filled with epithelial cells but which had not merged with other hyperproliferative glands. ImageJ software was used to annotate the tumour regions and the pixel area was used as a measure of tumour area.

Further analysis was carried out on the whole sections that had been imaged with the Leica digital slide scanner to compare the total number of PIN lesions and tumour area in *Pb-Cre Ctnnb1^{(ex3)Δ/+}* and *Pb-Cre Pten^{fl/+} Ctnnb1^{(ex3)Δ/+}* prostate tissue. There were a similar number of PIN lesions identified between the two groups (Figure 3.2.7). However, larger tumours were present in *Pb-Cre Pten^{fl/+} Ctnnb1^{(ex3)Δ/+}* prostate tissue and there was far less variation in the tumour area of *Pb-Cre Ctnnb1^{(ex3)Δ/+}* prostate samples compared to *Pb-Cre Pten^{fl/+} Ctnnb1^{(ex3)Δ/+}* (Figure 3.2.7). The two data sets were combined, normalising tumour area to PIN number to give a tumour to PIN ratio. No statistically significant difference was observed between the two groups but data for each had a more normal distribution and greater difference between means compared to independent PIN number and tumour area data sets.

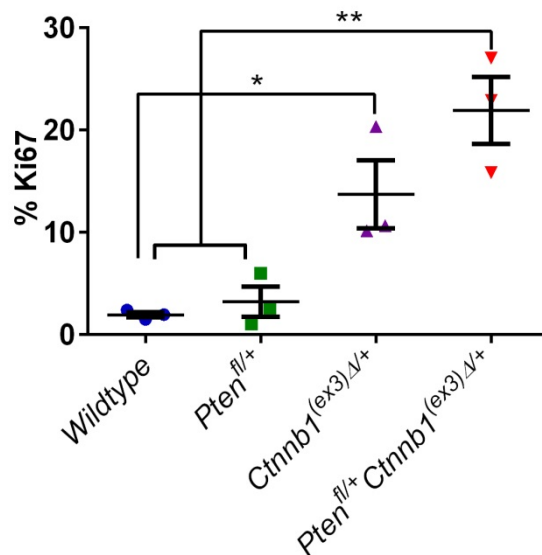


Figure 3.2.8 Ki67 scoring to quantify levels of proliferation in *Pb-Cre Pten^{fl/+} Ctnnb1^{(ex3)Δ/+}* and control prostate tissue

Quantification of Ki67 staining of *wildtype*, *Pb-Cre Pten^{fl/+}*, *Pb-Cre Ctnnb1^{(ex3)Δ/+}* and *Pb-Cre Pten^{fl/+} Ctnnb1^{(ex3)Δ/+}* prostate tissue from mice sacrificed at 6 months. The percentage of stained nuclei was calculated for n=3 of each genotype, as an average value of the percentage of stained nuclei in 5 fields of view at 200X magnification. (** P < 0.01, * P < 0.05; analysed by one-way ANOVA (P = 0.0012), with Tukey multiple comparison test). Data presented as mean ± SEM. No significant difference was observed between levels of Ki67 staining in *Pb-Cre Ctnnb1^{(ex3)Δ/+}* and *Pb-Cre Pten^{fl/+} Ctnnb1^{(ex3)Δ/+}* prostate tissue.

Having also observed variation in the levels of proliferation across the genotypes, the percentage of Ki67 staining was measured in biological triplicate for each genotype. *Pb-Cre Ctnnb1^{(ex3)Δ/+}* prostate tissue had a significantly higher percentage of Ki67 staining compared to *wildtype* tissue, while levels of

Ki67 were significantly higher in *Pb-Cre Pten^{fl/+} Ctnnb1^{(ex3) Δ /+}* prostate tissue compared to both wildtype and *Pb-Cre Pten^{fl/+}* (Figure 3.2.8). Despite there being a trend towards higher levels of Ki67 in *Pb-Cre Pten^{fl/+} Ctnnb1^{(ex3) Δ /+}* compared to *Pb-Cre Ctnnb1^{(ex3) Δ /+}*, no significant difference was observed between the two groups.

To explore the changes in molecular events associated with the development of β -catenin-driven prostate cancer and the co-operation with Pten loss, we carried out a Reverse Phase Protein Array (RPPA) screen with 138 antibody markers, in collaboration with Dr Neil Carragher at the Edinburgh Centre for Cancer Research. At this stage, limited samples were available for analysis, so we conducted the screen on one sample set, later validating changes of interest by western blot analysis in biological triplicate.

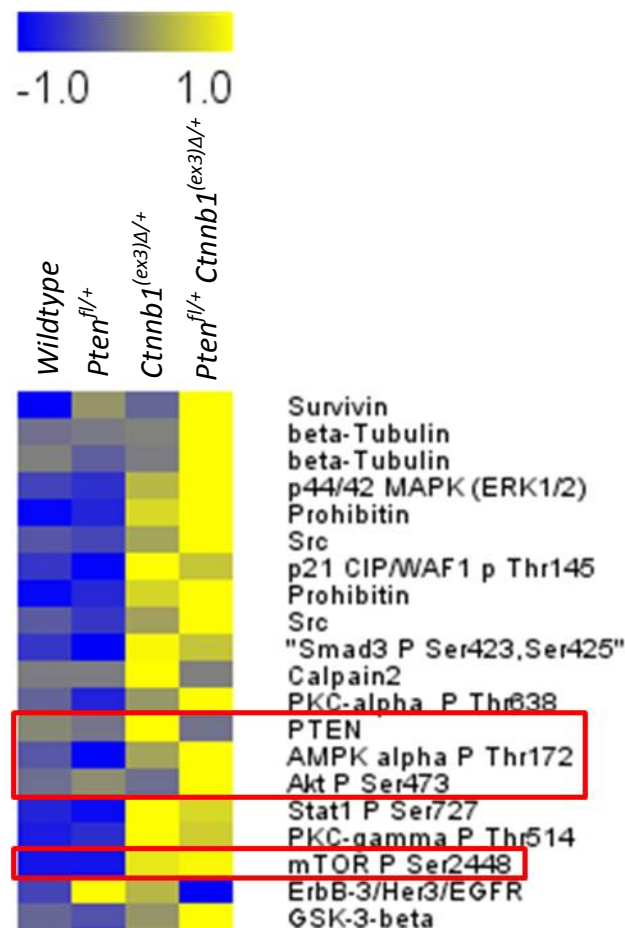


Figure 3.2.9 Reverse-Phase Protein Array screen to identify changes in protein levels associated with β -catenin activation and Pten loss in prostate cancer

Protein was extracted from prostate tissue of *wildtype*, *Pb-Cre Pten^{fl/+}*, *Pb-Cre Ctnnb1^{(ex3) Δ /+}* and *Pb-Cre Pten^{fl/+} Ctnnb1^{(ex3) Δ /+}* mice sacrificed at 6 months. Protein lysates were sent for Reverse-Phase Protein Array analysis by Neil Carragher's laboratory at the Edinburgh Centre for Cancer Research. The heat map shows levels of proteins found to be altered between samples. Further pathway analysis was carried out on proteins in red boxes.

From the RPPA, we identified a number of changes, including a significant increase in Pten protein expression in *Ctnnb1*^{(ex3) Δ /+} prostate tissue (Figure 3.2.9). Furthermore, I observed an interesting variation in Pten protein expression across sections of prostate tissue from *Pb-Cre Ctnnb1*^{(ex3) Δ /+} mice at 6 months. High levels of nuclear Pten were present in PIN lesions, while lower levels were observed in tumour regions of the same section (Figure 3.2.10).

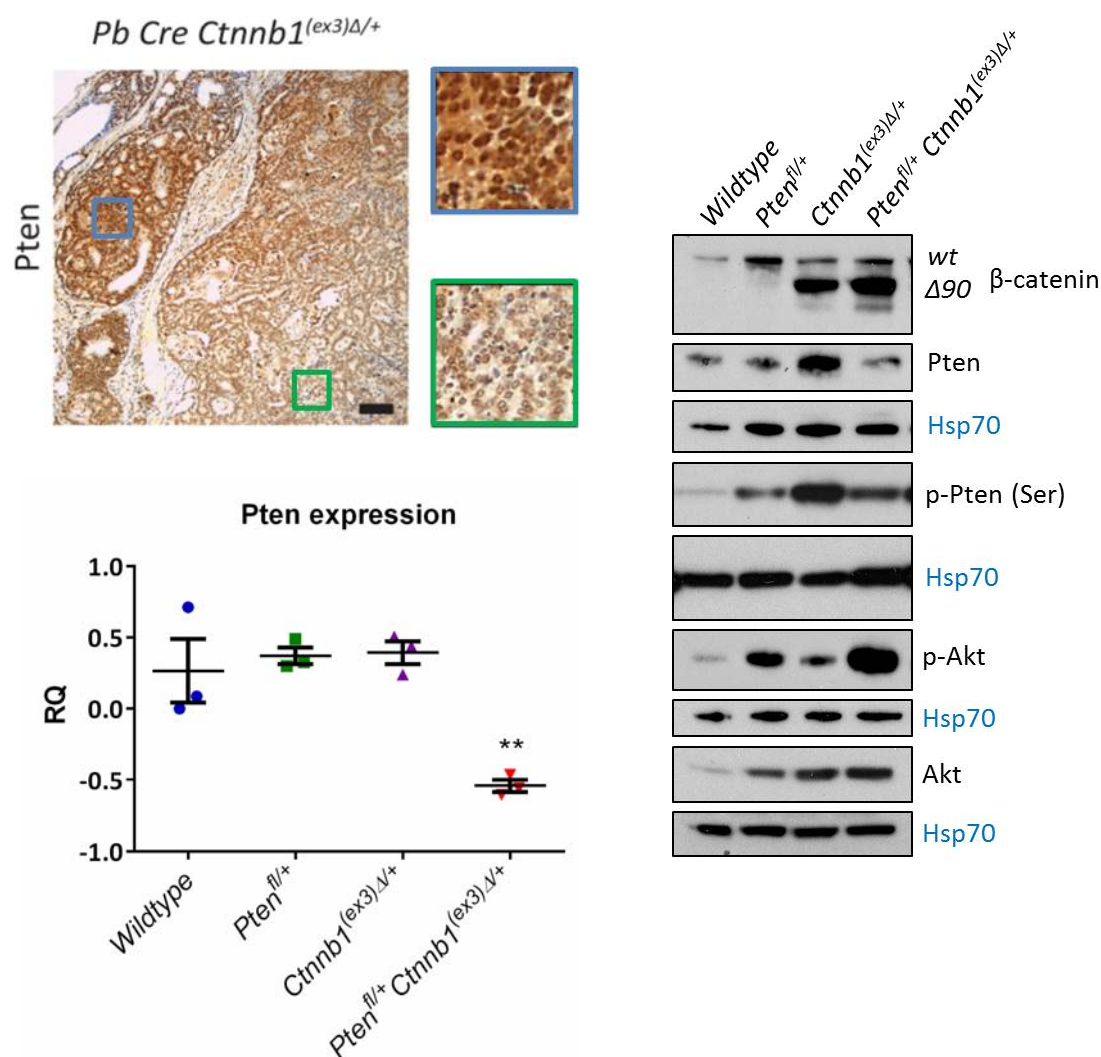


Figure 3.2.10 Pten and Akt pathway analysis

The tissue section image is representative of Pten immunohistochemical staining of FFPE sections of *Pb-Cre Ctnnb1*^{(ex3) Δ /+} prostate tissue, with inserts showing high levels of nuclear Pten in PIN lesions (blue) but less nuclear Pten in the tumour (green). Scale bar: 100 μ m. Insert box: 100 μ m². Quantitative RT-PCR analysis was carried out on RNA extracted from prostate tissue of *wildtype*, *Pb-Cre Pten*^{fl/+}, *Pb-Cre Ctnnb1*^{(ex3) Δ /+} and *Pb-Cre Pten*^{fl/+} *Ctnnb1*^{(ex3) Δ /+} mice at 6 months and the graph shows the relative *Pten* mRNA expression in samples. RQ = relative quantity (log scale). Normalised to *18S* housekeeping gene. (** P < 0.01; analysed by one-way ANOVA, with Tukey multiple comparison test). The Western blot panel is representative of analysis of β -catenin, Pten, phospho-Pten (Ser-380), phospho-Akt (Ser-473) and total Akt protein levels in protein lysates extracted from prostate tissue of *wildtype*, *Pb-Cre Pten*^{fl/+}, *Pb-Cre Ctnnb1*^{(ex3) Δ /+} and *Pb-Cre Pten*^{fl/+} *Ctnnb1*^{(ex3) Δ /+} mice at 6 months (n=3). Hsp70 was used as a loading control.

Western blot analysis, confirmed the presence of mutant ($\Delta 90$) β -catenin in *Pb-Cre Ctnnb1^{(ex3) Δ /+}* and *Pb-Cre Pten^{fl/+} Ctnnb1^{(ex3) Δ /+}* prostate tissue and showed overall levels of Pten protein were much higher in *Ctnnb1^{(ex3) Δ /+}* prostate tissue compared to *wildtype*, *Pten^{fl/+}* and *Pten^{fl/+} Ctnnb1^{(ex3) Δ /+}*. Analysis of mRNA from the same set of samples did not show a corresponding increase in *Pten* mRNA expression in *Pb-Cre Ctnnb1^{(ex3) Δ /+}* prostate tissue (Figure 3.2.10). However, the increase in Pten protein did correspond with increased levels of phospho-Pten (Ser-380) (Figure 3.2.10), which facilitates stabilisation and nuclear localisation of Pten [110].

Pten mRNA and protein expression was significantly reduced in *Pb-Cre Pten^{fl/+} Ctnnb1^{(ex3) Δ /+}* prostate tissue compared to *wildtype* and *Pten^{fl/+}* (Figure 3.2.10). These appeared to be below the expression levels associated with *Pten* haploinsufficiency. There was a corresponding increase in phospho-Akt levels, while total Akt levels remained unchanged (Figure 3.2.10). RPPA data also showed high levels of the anti-apoptotic protein survivin in *Pten^{fl/+} Ctnnb1^{(ex3) Δ /+}* prostate tissue, corresponding to *Pten* loss (Figure 3.2.9). Heterozygous loss of *Pten* alone resulted in an increase in phospho-Akt (Figure 3.2.10) and survivin (Figure 3.2.9) but this was not sufficient to drive tumourigenesis (Figure 3.2.5). Despite high levels of *Pten*, Akt activation was also observed in *Ctnnb1^{(ex3) Δ /+}* prostates, in which phospho-Akt levels were elevated above those observed in *wildtype* tissue (Figure 3.2.10). This is likely due to the accumulation of phospho-Pten in the nucleus, relieving repression of PI3K/Akt at the cell membrane.

Overall, these data demonstrate that β -catenin activation is sufficient to initiate tumourigenesis in cells with intact *Pten* expression and is associated with stabilisation and nuclear accumulation of Pten in PIN lesions. However, lower levels of *Pten* observed in tumour lesions indicate that cells must overcome *Pten* tumour suppression for cancer to progress from PIN to adenocarcinoma. Hence, we observed a more aggressive phenotype in tumours harbouring concurrent β -catenin activation and heterozygous *Pten* loss.

3.2.2 ROS-driven proliferation and Pten-modulation overcome tumour suppression in β -catenin-driven prostate cancer

We wanted to further investigate the biological significance of increased levels of nuclear Pten in PIN lesions of prostate tissue from *Pb-Cre Ctnnb1^{(ex3) Δ /+}* mice (Figure 3.2.10) and assess how β -catenin activation may be modulating these effects. Previous work from our lab has shown that nuclear Pten induces p53-mediated G1 arrest in a phosphatase-independent manner [110]. It has previously been shown that ROS is able to drive the nuclear accumulation of phosphorylated Pten, resulting in p21 expression and p53-mediated tumour suppression [112]. Quenching of ROS with N-acetyl-cysteine (NAC) treatment overcame growth arrest and tumour suppression, leading to hyper-proliferation of epithelial cells and increased development of PIN lesions in the prostate [110].

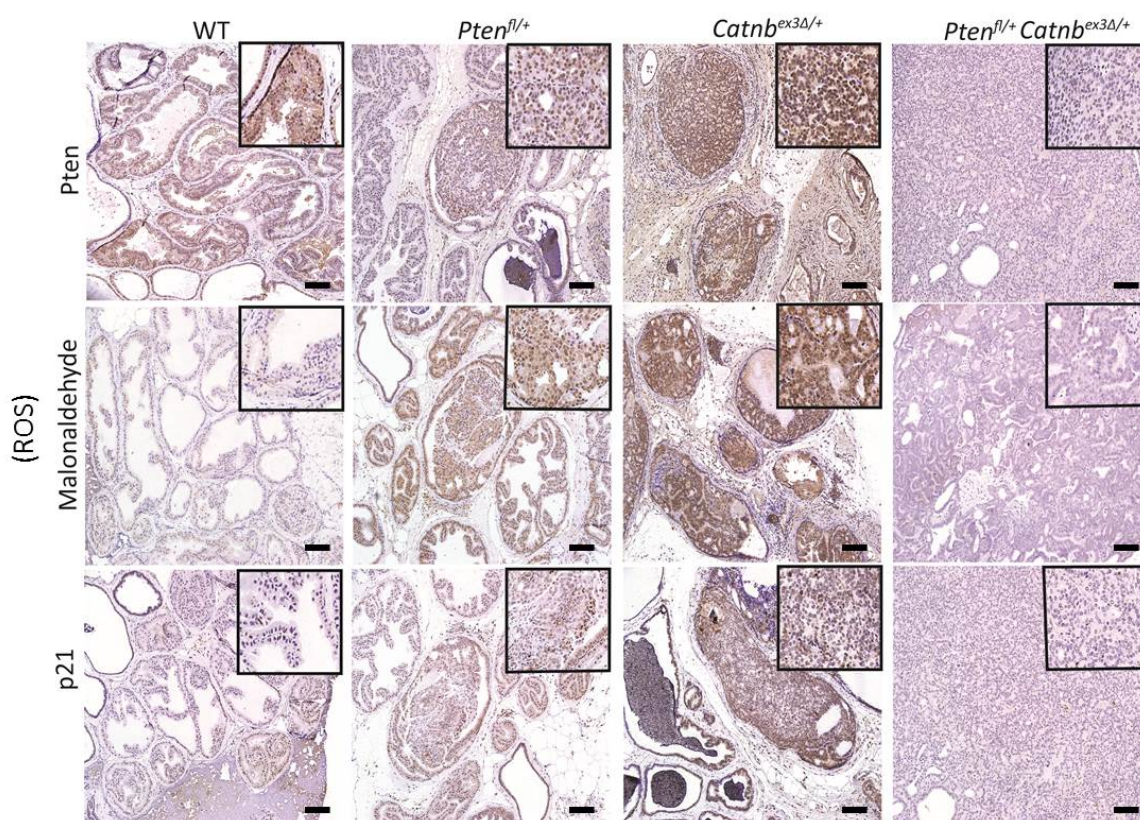


Figure 3.2.11 Nuclear Pten observed in *Pb-Cre Ctnnb1^{(ex3) Δ /+}* PIN lesions corresponds with elevated levels of ROS and p21

Representative images of Pten, malondialdehyde (ROS) and p21 immunohistochemical staining of FFPE *wildtype*, *Pb-Cre Pten^{fl/+}*, *Pb-Cre Ctnnb1^{(ex3) Δ /+}* and *Pb-Cre Pten^{fl/+} Ctnnb1^{(ex3) Δ /+}* sections of prostate tissue, harvested from mice at 6 months. Data provided by Rachana Patel (unpublished). Scale bar: 100 μ m. Insert box: 100 μ m².

We carried out immunohistochemical staining for Pten, the ROS marker malondialdehyde and p21 in *wildtype*, *Pb-Cre Pten^{fl/+}*, *Pb-Cre Ctnnb1^{(ex3) Δ /+}* and

Pb-Cre Pten^{fl/+} Ctnnb1^{(ex3)Δ/+} fixed prostate tissue sections. Increased levels of nuclear Pten, observed in *Pten^{fl/+}* and *Ctnnb1^{(ex3)Δ/+}* PIN lesions, correlated with increased levels of ROS (malondialdehyde staining) and nuclear p21, and was not observed in *Pb-Cre Pten^{fl/+} Ctnnb1^{(ex3)Δ/+}* tumour tissue (Figure 3.2.11). This led us to hypothesise that the longer latency of tumour development in *Pb-Cre Ctnnb1^{(ex3)Δ/+}* mice (Figure 3.2.2-3.2.4) was due to ROS-dependent Pten and p53-mediated tumour suppression during early stages of tumourigenesis, which must be overcome for cancer progression.

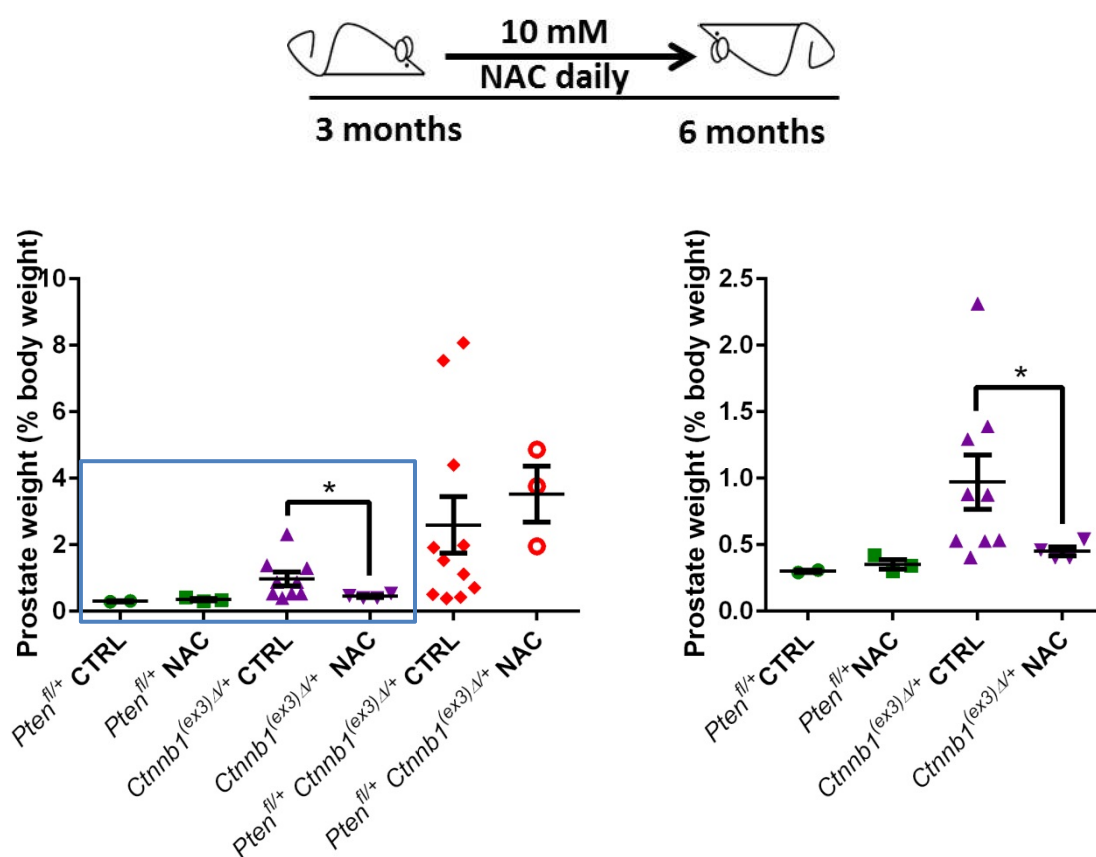


Figure 3.2.12 N-acetyl cysteine (NAC) treatment decreased tumour burden in *Pb-Cre Ctnnb1^{(ex3)Δ/+}* mice

Schematic shows the timeline for NAC treatment in mice. The graphs show prostate weights of *Pb-Cre Pten^{fl/+}*, *Pb-Cre Ctnnb1^{(ex3)Δ/+}* and *Pb-Cre Pten^{fl/+} Ctnnb1^{(ex3)Δ/+}* mice after 3 months treatment with 10 mM NAC, compared to vehicle control treated mice. Prostate weights are presented as a percentage of body weight to negate any variations in body weight between groups. NAC (or vehicle) treatment commenced when mice were 3 months old and all mice were taken after 3 months of treatment. Differences between *Pten^{fl/+}* and *Ctnnb1^{(ex3)Δ/+}* data (blue box) are shown more clearly in the graph on the right. (* p value <0.05; analysed by unpaired, two-tailed t-test with Welch's correction). Data presented as mean \pm SEM.

To test this hypothesis, we treated *Pb-Cre Pten^{fl/+}*, *Pb-Cre Ctnnb1^{(ex3)Δ/+}* and *Pb-Cre Pten^{fl/+} Ctnnb1^{(ex3)Δ/+}* mice with 10 mM NAC antioxidant in drinking water, administered continuously for 3 months, to quench ROS (Figure 3.2.12). Initial

analysis of NAC treated and control groups showed a significant decrease in the prostate weight of *Pb-Cre Ctnnb1^{(ex3)Δ/+}* NAC treated mice, and smaller standard deviation, compared to controls (Figure 3.2.12). No significant difference in prostate weight was observed between *Pb-Cre Pten^{fl/+} Ctnnb1^{(ex3)Δ/+}* NAC treated and control mice (Figure 3.2.12).

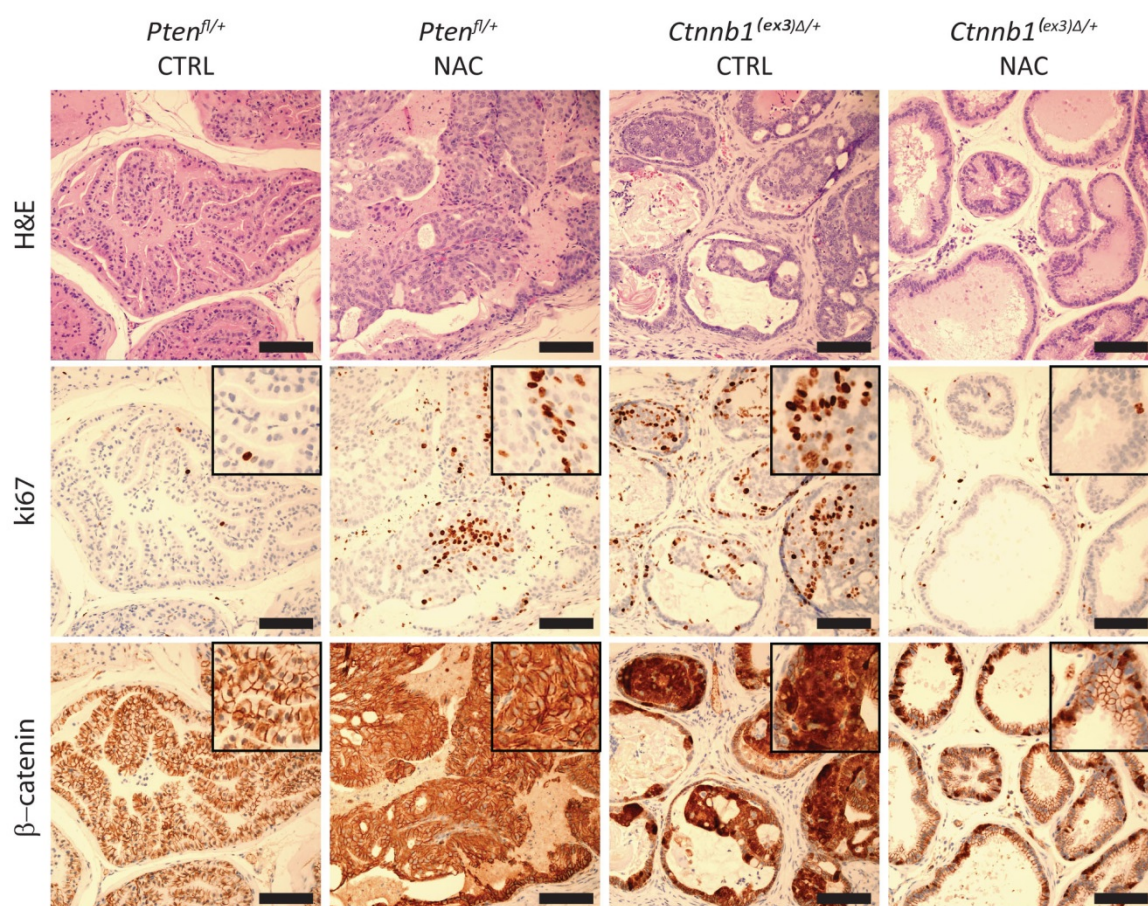


Figure 3.2.13 NAC treatment had a pro-proliferative effect on *Pb-Cre Pten^{fl/+}* prostate cells but was chemopreventive in *Pb-Cre Ctnnb1^{(ex3)Δ/+}* mice

Haematoxylin & eosin staining, ki67 and β -catenin immunohistochemical staining of FFPE *Pb-Cre Pten^{fl/+}* and *Pb-Cre Ctnnb1^{(ex3)Δ/+}* prostate tissue comparing samples from NAC treated mice to controls. Scale bar: 100 μ m. Insert box: 100 μ m².

We had predicted quenching ROS would decrease Pten phosphorylation and nuclear Pten, relieving growth arrest and facilitating cell growth and proliferation. While NAC treatment in *Pb-Cre Pten^{fl/+}* mice increased levels of proliferation (Ki67) in prostate tissue, NAC treatment in *Pb-Cre Ctnnb1^{(ex3)Δ/+}* mice had a chemo-preventative effect, and resulted in fewer PIN lesions and reduced proliferation (Ki67) compared to age-matched, vehicle-treated controls (Figure 3.2.13). We also observed a decrease in levels of nuclear β -catenin in these mice compared to controls (Figure 3.2.13), suggesting that NAC treatment

restricted the proliferation of cells harbouring mutant (nuclear) β -catenin. Thus, ROS appears to be required for the proliferation of β -catenin-mutant prostate cancer cells. Both genotypes displayed a decrease in nuclear Pten, ROS and p21 levels following NAC treatment (Figure 3.2.14), but with contrasting effects.

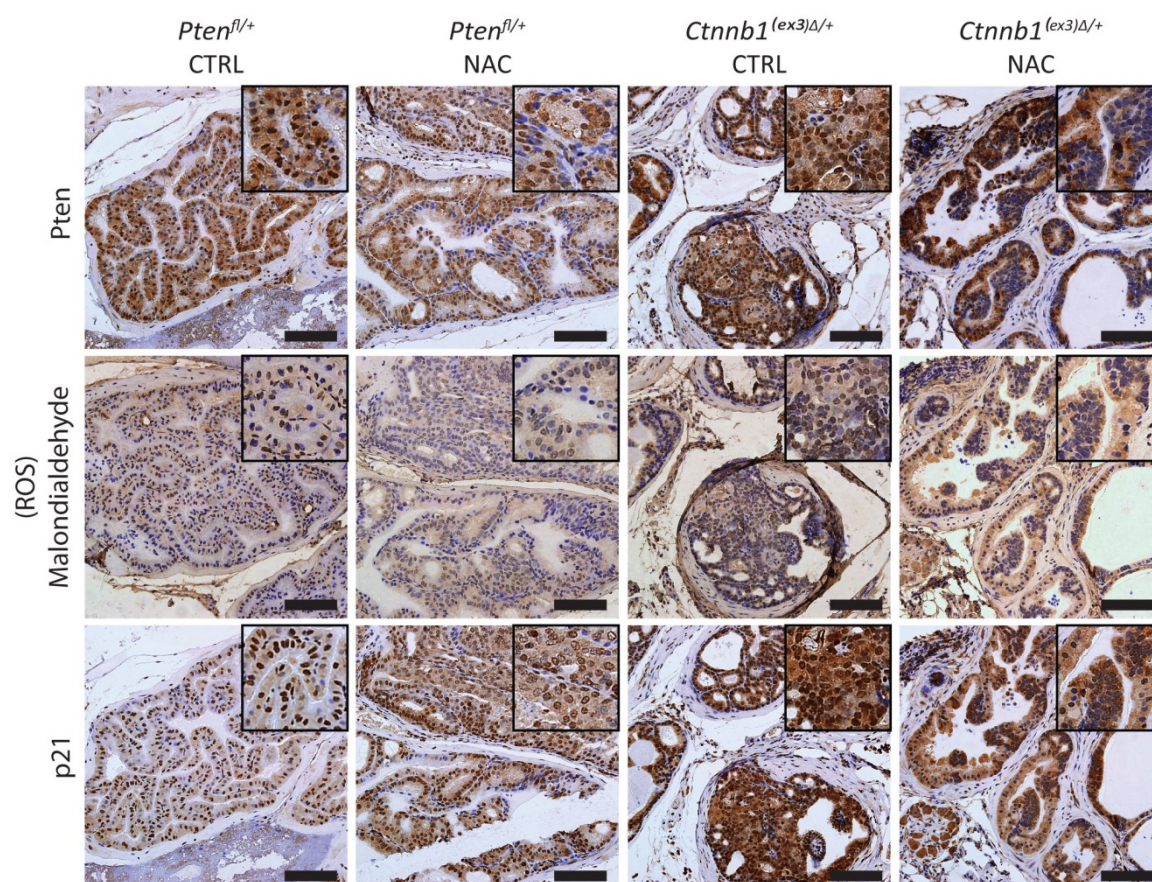


Figure 3.2.14 Effects of NAC treatment on Pten, ROS and p21 in *Pb-Cre Pten^{fl/+}* and *Pb-Cre Ctnnb1^{(ex3) Δ /+}* prostate tissue

Pten, malondialdehyde (ROS) and p21 immunohistochemical staining of FFPE *Pb-Cre Pten^{fl/+}* and *Pb-Cre Ctnnb1^{(ex3) Δ /+}* prostate tissue comparing samples from NAC treated mice to controls. Scale bar: 100 μ m. Insert box: 100 μ m².

Histopathological analysis of *Pb-Cre Pten^{fl/+} Ctnnb1^{(ex3) Δ /+}* prostates showed that NAC treatment had not halted tumour progression, nor had it accelerated cell growth and proliferation in these mice (Figure 3.2.15). Despite control *Pb-Cre Pten^{fl/+} Ctnnb1^{(ex3) Δ /+}* prostate tissue having lower levels of ROS and nuclear Pten in comparison to *Pb-Cre Ctnnb1^{(ex3) Δ /+}*, the positive effect of NAC treatment was still observed by a reduction in ROS levels, and loss of nuclear Pten and p21 (Figure 3.2.16). Haematoxylin and eosin staining showed the development of adenocarcinoma and similar levels of Ki67 staining across the prostate tissue sections in control and NAC treated mice (Figure 3.2.15). Although a large

number of cells with nuclear β -catenin remained, there did appear to be a small reduction in levels of nuclear β -catenin following NAC treatment (Figure 3.2.15), suggesting quenching of ROS had restricted proliferation in β -catenin-mutant cells, as observed in *Ctnnb1*^{(ex3) Δ /+} prostate tissue (Figure 3.2.13).

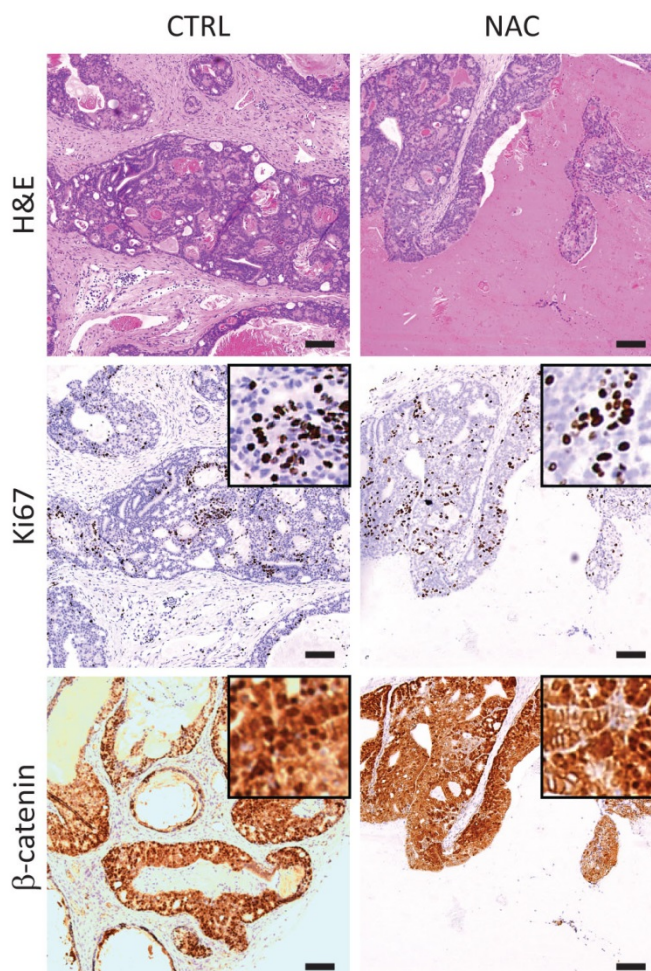


Figure 3.2.15 NAC treatment had little effect on prostate cancer progression in *Pb-Cre Pten*^{fl/+} *Ctnnb1*^{(ex3) Δ /+} mice

Haematoxylin & eosin staining, ki67 and β -catenin immunohistochemical staining of FFPE *Pb-Cre Pten*^{fl/+} *Ctnnb1*^{(ex3) Δ /+} prostate tissue comparing samples from NAC treated mice to controls. Scale bar: 100 μ m. Insert box: 100 μ m².

There was a reduction in Pten levels in all three genotypes following NAC treatment (Figure 3.2.14 & 3.2.16). In *Pten* haploinsufficient *Pb-Cre Pten*^{fl/+} and *Pb-Cre Pten*^{fl/+} *Ctnnb1*^{(ex3) Δ /+} prostates, both nuclear and cytoplasmic Pten expression decreased compared to controls. However, in *Pb-Cre Ctnnb1*^{(ex3) Δ /+} prostates, we observed a loss of nuclear Pten, while high levels of cytoplasmic Pten expression remained (Figure 3.2.14). To investigate the downstream effect of these changes on Pten phosphatase activity, we looked at Akt activation in these samples.

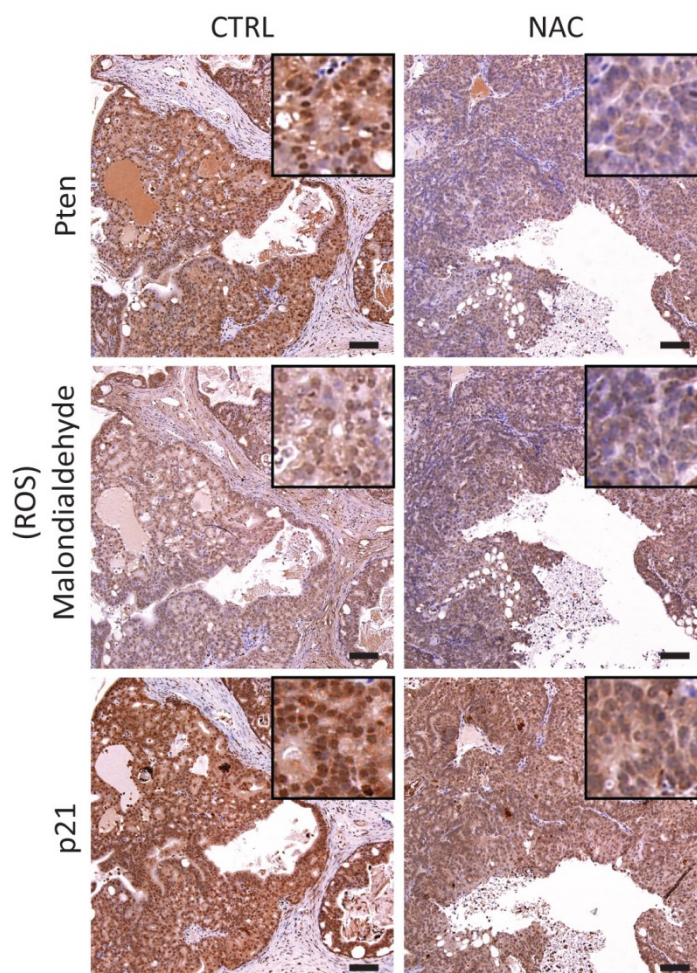


Figure 3.2.16 Effects of NAC treatment on Pten, ROS and p21 in *Pb-Cre Pten^{fl/+} Cttnb1^{(ex3)Δ/+}* prostate tissue

Pten, malondialdehyde (ROS) and p21 immunohistochemical staining of FFPE *Pb-Cre Pten^{fl/+} Cttnb1^{(ex3)Δ/+}* prostate tissue comparing samples from NAC treated mice to controls. Scale bar: 100 μm . Insert box: 100 μm^2 .

Immunohistochemical staining of phospho-Akt (Ser-473) showed significant Akt activation in *Pb-Cre Pten^{fl/+}* prostates, with patches of intense phospho-Akt staining following NAC treatment (Figure 3.2.17). The pro-proliferative effect of NAC treatment in *Pten* haploinsufficient prostate tissue is caused by overcoming G1 growth arrest and tumour suppression. It is likely that cells are compensating for the heterozygous loss of Pten and somehow increase ROS levels to maintain a tumour suppressive state via nuclear Pten-mediated G1 growth arrest. This explains the low incidence of PIN and tumour resulting from *Pten* haploinsufficiency. However, when ROS levels are decreased there is loss of G1 growth arrest and increased proliferation.

In contrast, a low level of phospho-Akt was present in prostates of *Pb-Cre Cttnb1^{(ex3)Δ/+}* control mice (also detected by western blot (Figure 3.2.10)),

despite high levels of Pten, but was completely ablated following NAC treatment, even in a region of hyperplasia (Figure 3.2.17). NAC treatment caused a reduction in nuclear Pten levels, due to quenching of ROS, and Pten levels increased in the cytoplasm, inhibiting activation of Akt at the cell membrane. Low levels of Akt activation may provide a survival benefit to cells in *Pb-Cre Ctnnb1^{(ex3)Δ/+}* control prostates, despite high levels of nuclear Pten in PIN lesions. This ROS-dependent mechanism may be required to co-operate with pro-proliferative downstream effectors of β-catenin activation to initiate tumourigenesis. Phospho-Akt staining was present but less intense in *Pb-Cre Pten^{fl/+} Ctnnb1^{(ex3)Δ/+}* prostates of NAC treated mice compared to controls demonstrating the influence of β-catenin activation in this cohort.

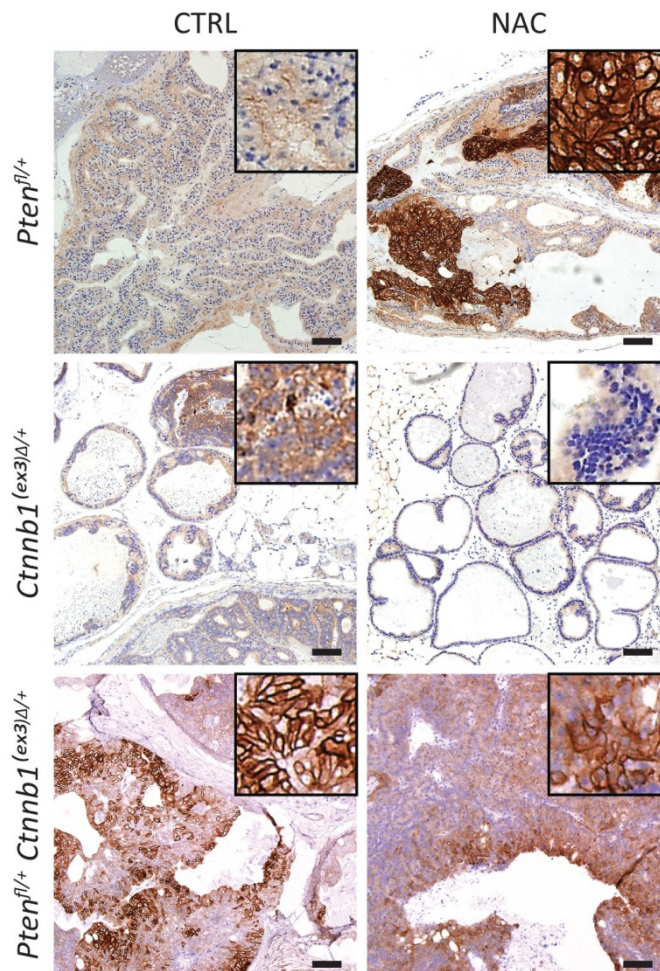


Figure 3.2.17 Differential effects of NAC treatment on phospho-Akt expression in *Pb-Cre Pten^{fl/+}*, *Pb-Cre Ctnnb1^{(ex3)Δ/+}* and *Pb-Cre Pten^{fl/+} Ctnnb1^{(ex3)Δ/+}* prostate tissue
 Phospho-Akt immunohistochemical staining of FFPE *Pb-Cre Pten^{fl/+} Ctnnb1^{(ex3)Δ/+}* prostate tissue comparing samples from NAC treated mice to controls. Scale bar: 100 μm. Insert box: 100 μm².

These data illustrate the association of β -catenin activation with elevated levels of pro-proliferative ROS that modulates Pten localisation in order to overcome tumour suppression. However, it was not clear how ROS was being produced following β -catenin activation.

Similar effects of NAC treatment have been observed by Myant et al. in a colorectal cancer mouse model, in which β -catenin activation was triggered by APC loss [182]. ROS-mediated proliferation was required for cancer initiation in these mice, and was concordant with upregulation of Rac1 signalling.

Therefore, we tested the levels of Rac1 activity in relation to levels of ROS in prostate tissue from *wildtype*, *Pb-Cre Pten^{fl/+}*, *Pb-Cre Ctnnb1^{(ex3) Δ /+}* and *Pb-Cre Pten^{fl/+} Ctnnb1^{(ex3) Δ /+}* mice sampled at 6 months. Immunohistochemical staining of Rac1-GTP (active Rac1) showed a positive correlation between levels of ROS (malondialdehyde) and Rac1-GTP. The highest levels of ROS were detected in PIN lesions of *Pb-Cre Ctnnb1^{(ex3) Δ /+}* prostate tissue and significantly decreased in tumour regions of *Pb-Cre Ctnnb1^{(ex3) Δ /+}* and *Pb-Cre Pten^{fl/+} Ctnnb1^{(ex3) Δ /+}* mice (Figure 3.2.18).

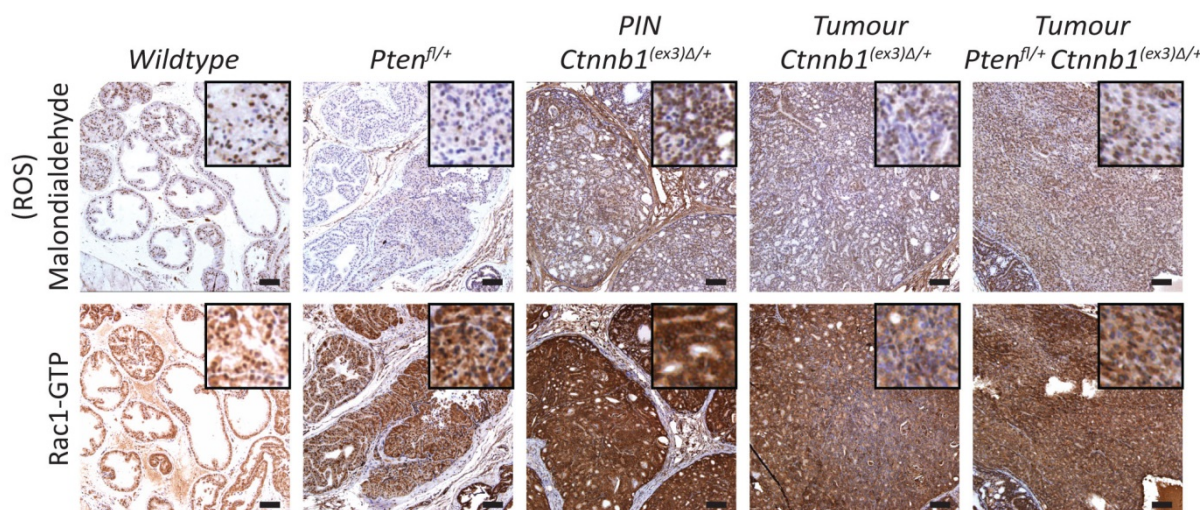


Figure 3.2.18 High levels of ROS positively correlate with Rac1 activity in *Pb-Cre Ctnnb1^{(ex3) Δ /+}* PIN lesions

Malondialdehyde (ROS) and Rac1-GTP immunohistochemical staining of FFPE prostate tissue from *wildtype*, *Pb-Cre Pten^{fl/+}*, *Pb-Cre Ctnnb1^{(ex3) Δ /+}* and *Pb-Cre Pten^{fl/+} Ctnnb1^{(ex3) Δ /+}* mice sacrificed at 6 months. To illustrate the variation observed between PIN and tumour regions of *Pb-Cre Ctnnb1^{(ex3) Δ /+}* prostate tissue, a representative image is included for each region. Scale bar: 100 μm . Insert box: 100 μm^2 .

Work by Myant et al. [182] showed a significant correlation between elevated levels of Rac1 and Tiam1, Vav3 and c-Myc in human colorectal cancer, and

attributed increased Rac1 activity to the increased expression of the Rac1-GEFs, *Tiam1* and *Vav3*, driven by β -catenin/Myc signalling. Using RT-PCR, I analysed *Tiam1* and *Vav3* expression in prostate tissue from *wildtype*, *Pb-Cre Pten^{fl/+}*, *Pb-Cre Ctnnb1^{(ex3) Δ /+}* and *Pb-Cre Pten^{fl/+} Ctnnb1^{(ex3) Δ /+}* mice sampled at 6 months but did not observe any significant differences between the genotypes (Figure 3.2.19).

As Rac1-GTP levels are highest in PIN lesions of *Pb-Cre Ctnnb1^{(ex3) Δ /+}* prostates (Figure 3.2.18), I hypothesised that the levels of the Rac1-GEFs are highest at earlier stages of tumourigenesis, and that β -catenin activation alone could regulate these changes. Analysis of RNA from *Pb-Cre Ctnnb1^{(ex3) Δ /+}* prostate tissue collected at 3, 6 and 12 month time points and showed a significant increase in levels of *Tiam1* and *Vav3* expression at 3 months compared to *wildtype* (Figure 3.2.20). At 6 months, there was a drop in both *Tiam1* and *Vav3* expression, and levels were equivalent to those observed in *wildtype* samples. Elevated levels of *Tiam1* were again observed in endpoint tumour samples. RT-PCR analysis of *Tiam1* and *Vav3* at 3, 6 and 12 month time points in *wildtype* samples showed that there was no significant age-associated variation in their expression (Figure 3.2.21). Hence, the high levels of *Tiam1* and *Vav3* expression at 3 months are a specific consequence of β -catenin activation.

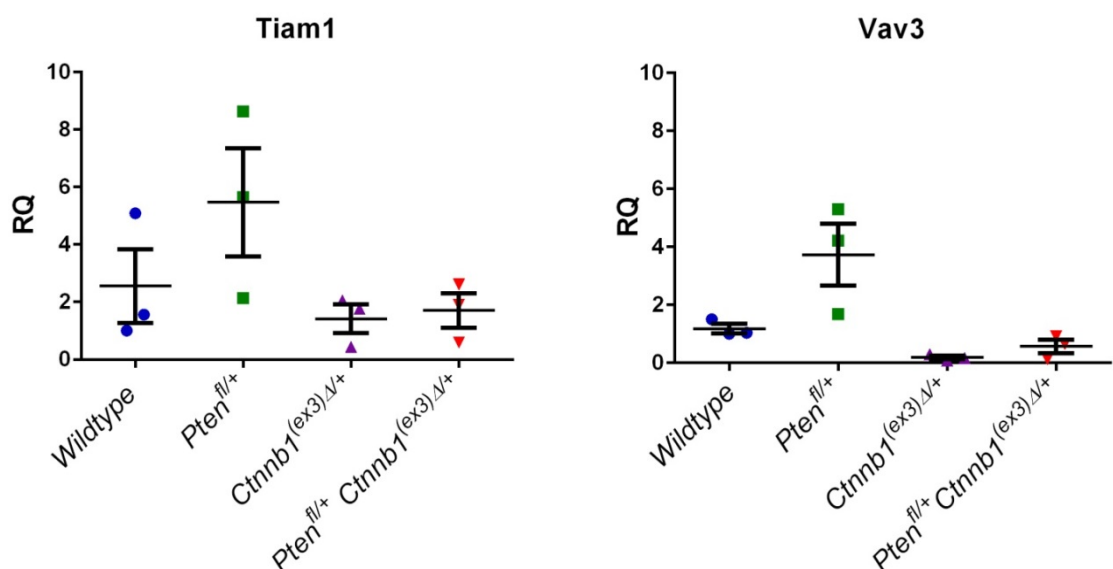


Figure 3.2.19 Rac-GEFs, *Tiam1* and *Vav3*, are not significantly altered in prostate tissue with β -catenin activation at 6 months

TaqMan RT-qPCR analysis of *Tiam1* and *Vav3* mRNA expression levels (RQ) in *wildtype*, *Pb-Cre Pten^{fl/+}*, *Pb-Cre Ctnnb1^{(ex3) Δ /+}* and *Pb-Cre Pten^{fl/+} Ctnnb1^{(ex3) Δ /+}* mouse prostates tissue at 6 month time point. Normalised to *18S* housekeeping gene. (Analysis by one-way ANOVA, with Tukey multiple comparison test showed no significant difference in expression levels).

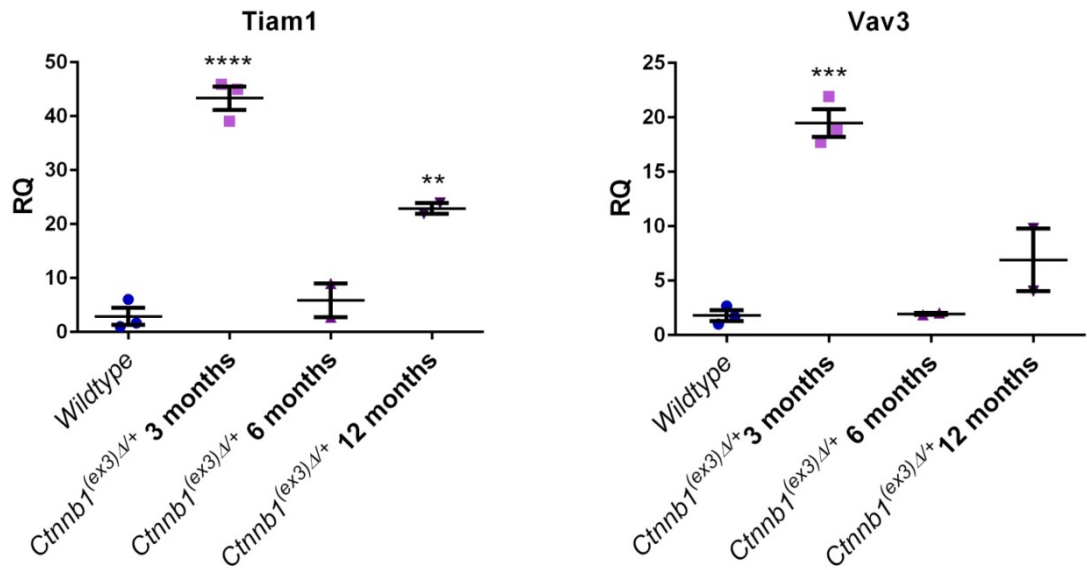


Figure 3.2.20 *Tiam1* and *Vav3* are significantly upregulated in *Pb-Cre Ctnnb1*^{(ex3)Δ/+} prostate tissue at 3 months

TaqMan RT-qPCR analysis of *Tiam1* and *Vav3* mRNA expression levels (RQ) in *wildtype* prostate tissue at 6 months and *Pb-Cre Ctnnb1*^{(ex3)Δ/+} prostates tissue at 3, 6 and 12 month time points. Normalised to *18S* housekeeping gene. (**** $P < 0.0001$, *** $P < 0.001$, ** $P < 0.01$; analysis by one-way ANOVA, with Tukey multiple comparison test).

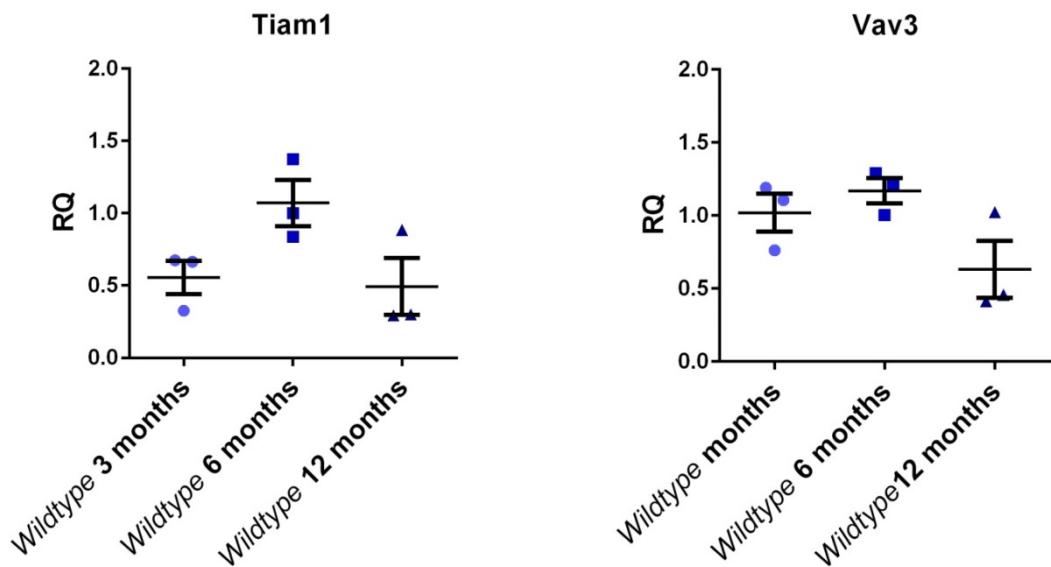


Figure 3.2.21 Levels of *Tiam1* and *Vav3* expression do not vary significantly between 3, 6 and 12 month time points in *wildtype* prostate tissue

TaqMan RT-qPCR analysis of *Tiam1* and *Vav3* mRNA expression levels (RQ) in *wildtype* prostate tissue at 3, 6 and 12 month time points. Normalised to *18S* housekeeping gene. (Analysis by one-way ANOVA, with Tukey multiple comparison test showed no significant difference in expression levels).

The increased expression of Rac1-GEFs, Tiam1 and Vav3 indicates that β -catenin activation upregulates the expression of *Tiam1* and *Vav3*. These Rac-GEFs convert inactive Rac1-GDP to its active Rac1-GTP state which is able to interact with NOX signalling machinery at the cell membrane [182]. Rac1-GTP activates the NOX complex, resulting in oxidation of NADPH to NADP^+ and production of oxygen free radicals. Thus, β -catenin activation may result in NOX-mediated ROS production in *Pb-Cre Ctnnb1^{(ex3) Δ /+}* prostate tissue.

3.2.3 Progressive loss of Pten correlates with advanced cancer stage in β -catenin-driven prostate cancer

Our work has established that Pten-mediated tumour suppression is required to delay the progression of prostate cancer driven by aberrant β -catenin activation. We further investigated Pten status during tumour progression and observed a progressive loss of Pten over 3, 6 and 12 month (endpoint) time points in *Pb-Cre Ctnnb1^{(ex3) Δ /+}* prostate tissue (Figure 3.2.22). In some regions of tumour tissue sampled from *Pb-Cre Ctnnb1^{(ex3) Δ /+}* mice at endpoint, Pten expression was lower than the levels of Pten in *Pb-Cre Pten^{fl/+} Ctnnb1^{(ex3) Δ /+}* tumour tissue sampled at 6 months (Figure 3.2.22)

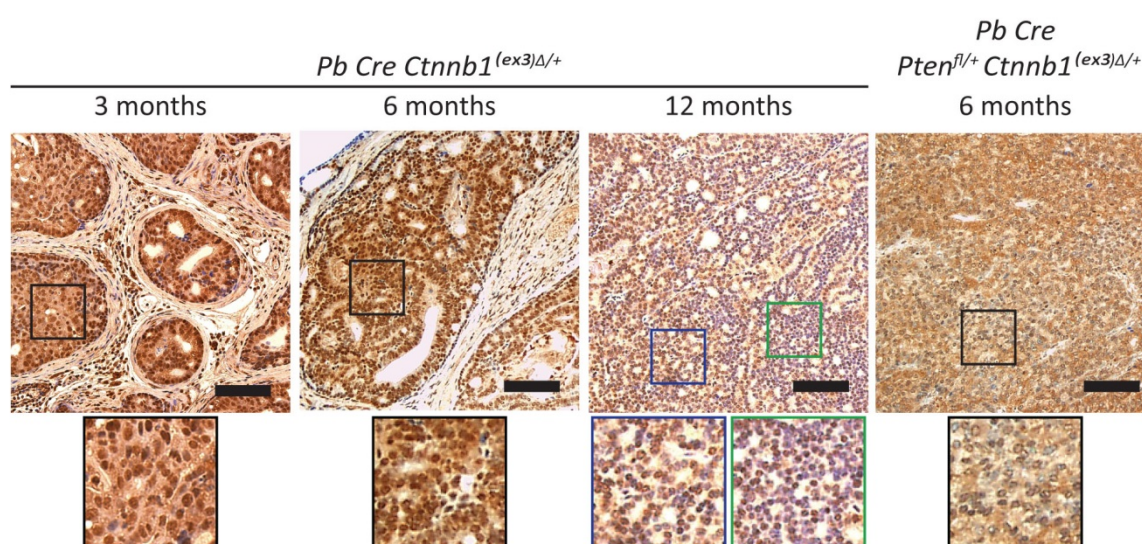


Figure 3.2.22 Progressive loss of Pten in tumours driven by β -catenin activation
Representative Pten immunohistochemical staining of FFPE sections of *Pb-Cre Ctnnb1^{(ex3) Δ /+}* prostate tissue sampled at 3, 6 and 12 months, and *Pb-Cre Pten^{fl/+} Ctnnb1^{(ex3) Δ /+}* prostate tissue sampled at 6 months. Scale bar: 100 μm . Insert box: 100 μm^2 .

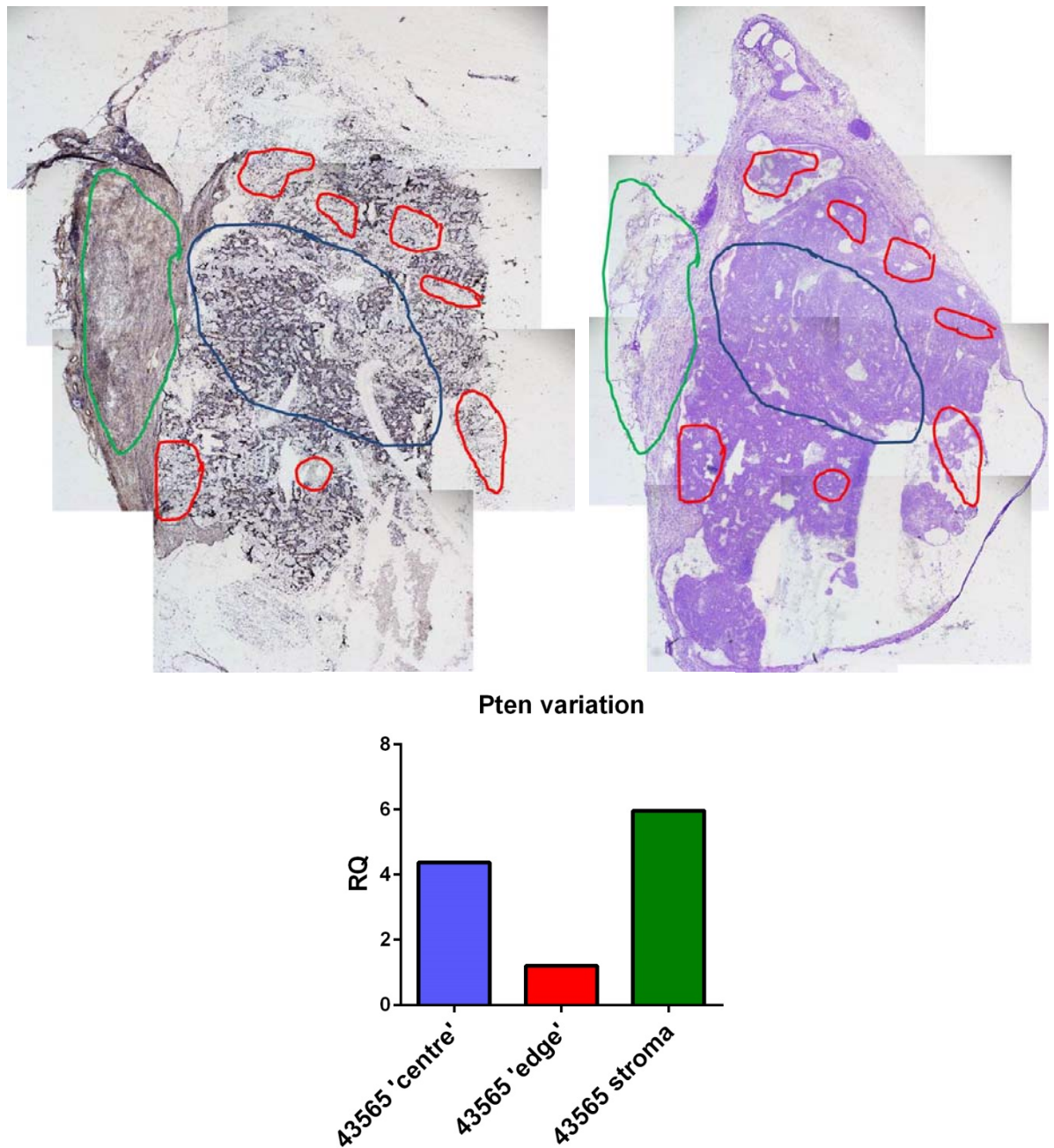


Figure 3.2.23 Pten expression is heterogeneous in epithelial and stromal regions of prostate tumour

Images show Pten immunohistochemical staining (left) and cresyl violet staining (right) of frozen sections of prostate tissue from a *Pb-Cre Pten^{fl/+} Ctnnb1^{(ex3)Δ/+}* mouse (6 month time point). These were two serial sections cut following the five serial sections used for LCM. Images were taken at 40X magnification and compiled to assemble an image of whole tissue section. Pten IHC was used to determine regions of low (red) and high (blue) Pten in epithelial tissue and cresyl violet staining highlights cell nuclei to aid identification of epithelial and stromal (green) regions of tissue. The red, blue and green annotated regions were isolated using LCM and put in separate tubes, pooled across the five LCM tissue sections. Graph shows the relative quantity of *Pten* expression at the tumour edge, centre and stroma correlates with Pten IHC (colours correspond to regions annotated in above images).

We wanted to investigate if the loss of Pten protein expression correlates with a reduction in *Pten* mRNA expression. Due to the heterogeneous expression of Pten across tissue sections, with varying levels of Pten observed between PIN, tumour and stroma, we decided to employ laser capture microdissection (LCM) to isolate tumour epithelial tissue from 6 month *Pb-Cre Cttnb1^{(ex3)Δ/+}* and *Pb-Cre Pten^{fl/+} Cttnb1^{(ex3)Δ/+}* mice and endpoint *Pb-Cre Cttnb1^{(ex3)Δ/+}* mice. RNA was extracted from these regions of tissue for downstream quantitative analysis of *Pten* mRNA expression by RT-PCR.

Differences in *Pten* mRNA expression were found to correlate with levels of Pten staining across areas of one *Pb-Cre Pten^{fl/+} Cttnb1^{(ex3)Δ/+}* prostate tumour. Regions of low Pten at the tumour edge correlated with low *Pten* expression and higher levels of Pten at the centre correlated with high *Pten* expression, comparable to levels observed in the stroma region (Figure 3.2.23). This example highlights the variations within a tissue sample that can mask specific changes of interest if analysing RNA from the whole tissue section. For all samples, a further serial tissue section was cut following five serial sections used for LCM, and used for immunohistochemical Pten staining. For many samples, it was difficult to identify areas of epithelial tissue on the cresyl violet stained LCM slides that corresponded to high or low Pten levels observed in this serial section. The structure of tissue in frozen sections is also not conserved in the same way as fixed tissue sections and varied slightly through the five serial sections. It was, therefore, challenging to isolate tissue based on Pten expression status, but possible to distinguish epithelia from stroma (Figure 3.2.23).

Analysis of RNA extracted from *Pb-Cre Cttnb1^{(ex3)Δ/+}* and *Pb-Cre Pten^{fl/+} Cttnb1^{(ex3)Δ/+}* tumour epithelial tissue confirmed that there was significantly less *Pten* expressed in *Pb-Cre Cttnb1^{(ex3)Δ/+}* tumour tissue at 12 months than at 6 months. Furthermore, the relative quantity of *Pten* expressed at 12 months was comparable to *Pten* expression in *Pb-Cre Pten^{fl/+} Cttnb1^{(ex3)Δ/+}* mice (Figure 3.2.24). This confirms the progressive loss of Pten protein correlates with loss of *Pten* transcript in tumours driven by aberrant β-catenin activation.

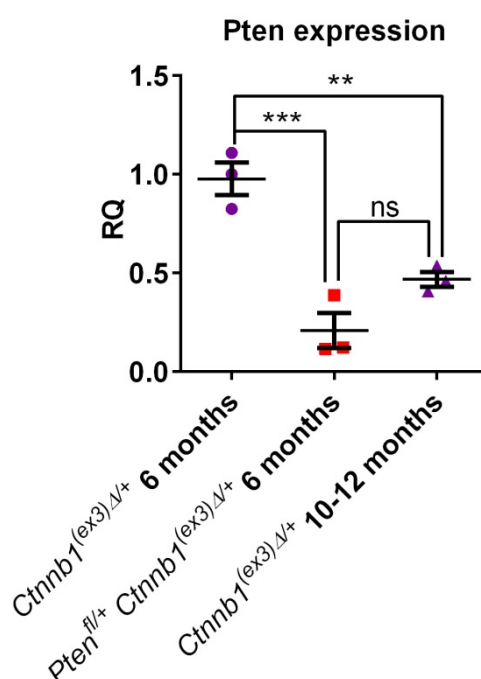


Figure 3.2.24 *Pten* expression significantly decreases in *Pb-Cre Ctnnb1*^{(ex3)Δ/+} tumour epithelial tissue between 6 and 12 months

LCM was used to isolate tumour epithelial tissue from prostates of *Pb-Cre Ctnnb1*^{(ex3)Δ/+} mice at 6 and 12 months (endpoint) and *Pb-Cre Pten*^{fl/+} *Ctnnb1*^{(ex3)Δ/+} mice at 6 months. TaqMan RT-qPCR analysis was carried out on RNA extracted from this tissue to compare the relative quantity (RQ) of *Pten* expression. Normalised to 18S housekeeping gene. (***) $P < 0.001$, ** $P < 0.01$; analysis by one-way ANOVA, with Tukey multiple comparison test). Data presented as mean \pm SEM.

In order to understand how *Pten* is progressively lost in association with aberrant β -catenin activation, we analysed *Pten* gene copy number in the same samples to determine if loss of *Pten* at the genomic level was responsible for loss of *Pten* expression. It was first necessary to determine *Pten* copy number in *wildtype*, *Pten* heterozygous and *Pten* null prostate epithelial tissue. LCM was used to isolate DNA from prostate epithelial tissue of *Pb-Cre Pten*^{fl/fl} (*Pten* null) mice at clinical endpoint (~10 months), and *Pb-Cre Pten*^{fl/+} (*Pten* heterozygous) and *wildtype* mice at 10-12 months. In *Pb-Cre Pten*^{fl/+} and *Pb-Cre Pten*^{fl/fl} mice, *Pten* exon5 is flanked by *loxP* sites. The expression of *cre recombinase* results in *Pten* exon5 deletion and subsequent loss of *Pten* expression. It was, therefore, possible to quantify *Pten* copy number by using primers to specifically amplify *Pten* exon5 DNA and determine the relative quantity in samples by qPCR.

As expected, *Pten* copy number decreased in *Pten* heterozygous prostate tissue and was significantly lower in *Pten* null prostate tissue, with approximately 3-fold and 5-fold reduction in levels of *Pten* exon5 DNA compared to *Pten*^{fl/+} and *wildtype*, respectively (Figure 3.2.25). This data provided a standard curve with

which to compare *Pten* copy number in *Pb-Cre Ctnnb1^{(ex3)Δ/+}* and *Pb-Cre Pten^{fl/+} Ctnnb1^{(ex3)Δ/+}* prostate tissue.

We observed no statistically significant difference between *Pten* copy number in 6 month and 10-12 month *Ctnnb1^{(ex3)Δ/+}* prostate epithelial tissue compared to *wildtype* (Figure 3.2.25). However, samples in each *Ctnnb1^{(ex3)Δ/+}* group do overlap with *Pten^{fl/+}* copy number data and a 2-fold increase in *Pten* DNA was observed in stromal tissue compared to epithelial tissue in endpoint *Ctnnb1^{(ex3)Δ/+}* prostate tumours (Figure 3.2.26). This suggests *Ctnnb1^{(ex3)Δ/+}* tumours may have lost one *Pten* allele. By applying LCM to specifically study tumour epithelial cells, we were able to demonstrate that the progressive loss of *Pten* expression observed in *Ctnnb1^{(ex3)Δ/+}* prostate tissue may be partly due to heterozygous genomic loss of *Pten* but suggests that β-catenin activation drives other molecular changes that further down-regulate *Pten* expression.

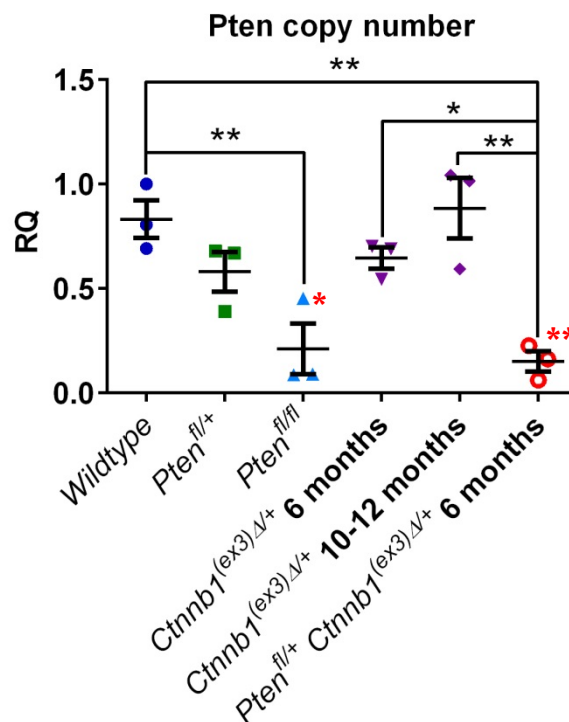


Figure 3.2.25 *Pten* copy number in *Pten^{fl/+} Ctnnb1^{(ex3)Δ/+}* prostate tumour epithelia tissue is comparable to homozygous *Pten* loss

LCM was used to isolate tumour epithelial tissue from prostates of *wildtype*, *Pb-Cre Pten^{fl/+}*, *Pb-Cre Pten^{fl/fl}* mice at 10-12 months, *Pb-Cre Ctnnb1^{(ex3)Δ/+}* mice at 6 and 12 months (endpoint) and *Pb-Cre Pten^{fl/+} Ctnnb1^{(ex3)Δ/+}* mice at 6 months. TaqMan qPCR analysis was carried out on DNA extracted from this tissue to compare the relative quantity (RQ) of *Pten* exon5. Normalised to *Casc3* housekeeping gene. (** $P < 0.01$; * $P < 0.05$; black* - analysis by one-way ANOVA, with Tukey multiple comparison test; red* - analysis by unpaired, one-tailed student t-test compared to *Pten^{fl/+}*). Data presented as mean \pm SEM.

However, *Pten* copy number was significantly decreased in *Pten^{fl/+} Ctnnb1^{(ex3)Δ/+}* tissue compared to *wildtype* and *Pten^{fl/+}*, beyond levels concordant with heterozygous loss of *Pten* and, instead, comparable to *Pten* null prostate epithelial tissue (Figure 3.2.25). This suggests that, in the context of *Pten* haploinsufficiency, β -catenin activation leads to loss of heterozygosity (LOH) in *Pten*, and correlates with low levels of *Pten* expression in tumour epithelial tissue (Figure 3.2.5 & 3.2.24).

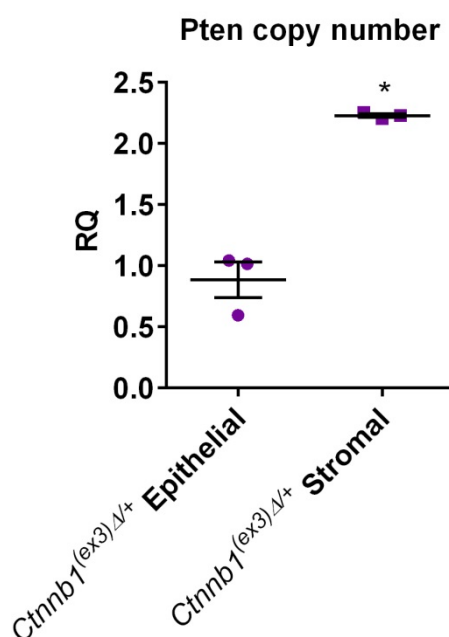


Figure 3.2.26 *Pten* copy number is significantly higher in the stroma compared to epithelia of *Ctnnb1^{(ex3)Δ/+}* prostate tissue

LCM was used to isolate tumour epithelial tissue and stroma from prostates of *Pb-Cre Ctnnb1^{(ex3)Δ/+}* mice at 12 months (endpoint). TaqMan qPCR analysis was carried out on DNA extracted from this tissue to compare the relative quantity (RQ) of *Pten* exon5. Normalised to *Casc3* housekeeping gene. (* $P < 0.05$; analysis by unpaired, two-tailed t-test with Welch's correction). Data presented as mean \pm SEM.

We generated four cell lines (referred to as CP1-4) from four independent *Pb-Cre Pten^{fl/+} Ctnnb1^{(ex3)Δ/+}* prostate tumours (Figure 3.2.27). As these tumours had a *Pten* heterozygous background, we were initially surprised to detect no *Pten* in CP1, CP2 and CP3 cells by western blot analysis (Figure 3.2.28). Only CP4 cells maintained *Pten* expression but β -catenin expression was consistent across all four cell lines (Figure 3.2.28). This suggested that the cell lines were derived from different sub-populations of tumour epithelial cells within *Pb-Cre Pten^{fl/+} Ctnnb1^{(ex3)Δ/+}* tumours, harbouring differential *Pten* status. Alternatively, it was

possible that the loss of *Pten* in cell lines could be a consequence of culturing the cells *in vitro* and may not represent *Pten* status of tumour cells *in vivo*.

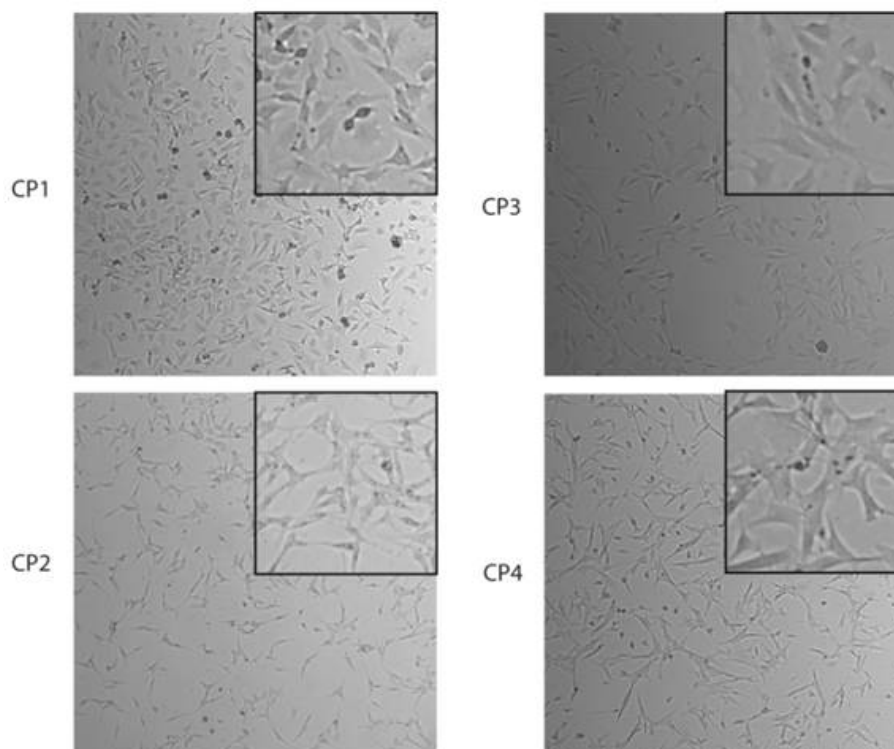


Figure 3.2.27 Primary cell lines derived from *Pb-Cre Pten^{fl/+} Ctnnb1^{(ex3)Δ/+}* prostate tumours CP1 and CP2 cell lines were previously derived from *Pb-Cre Pten^{fl/+} Ctnnb1^{(ex3)Δ/+}* prostate tumours by Meiling Gao. CP3 and CP4 were later derived from prostate tumours of the same genotype. All four cell lines have similar morphology. Images of main panels taken at 50X magnification and inserts at 100X magnification.

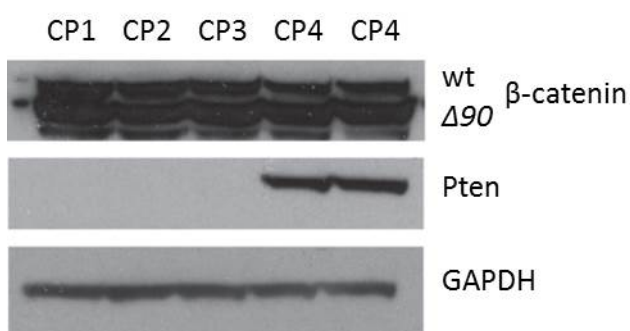


Figure 3.2.28 *Pten* is completely lost in CP cell lines 1-3 but present in CP4 cells Western blot analysis of β -catenin and *Pten* protein levels in protein lysates extracted from CP1, CP2, CP3 and CP4 cell lines. The two CP4 lanes show results from consecutive passages. GAPDH was used as a loading control.

To determine their *Pten* status, CP1-4 cell pellets were sent to Transnetyx for PCR analysis using the standard primers for genotyping the *Pb-Cre Pten^{fl/+} Ctnnb1^{(ex3)Δ/+}* mouse colony. Tumour tissue, from which CP3 and CP4 were

derived, and the corresponding mouse tail tips were also sent for genotyping. Analysis of CP cell lines 1-3 showed complete loss of *wildtype* and *loxP Pten* alleles, while CP4 cells retained the *wildtype Pten* allele (Table 3.2-1), corresponding to Pten protein levels in the four cell lines (Figure 3.2.28). *Cre* and *wildtype Ctnnb1* DNA was present in all cell lines and *Ctnnb1 Exon3 LoxP* was not detected, confirming that all four cell lines were derived from *Pb-Cre* positive cells in which cre-mediated recombination had taken place (Table 3.2-1).

Table 3.2-1 Transnetyx genotyping results for CP cell lines, tumour tissue and tail tips

Sample	<i>Cre</i>	<i>Ctnnb1 Exon3 LoxP</i>	<i>Ctnnb1 WT</i>	<i>Pten Exon5 LoxP</i>	<i>Pten WT</i>
CP1 cells	+	-	+	-	UD
CP2 cells	+	-	+	-	-
CP3 cells	+	-	+	-	-
CP3 tumour	+	UD	+	UD	-
CP3 tail	+	+	+	+	+
CP4 cells	+	-	+	-	+
CP4 tumour	+	+	+	+	-
CP4 tail	+	+	+	+	+

UD=undetermined (signal between positive and negative ranges)

Genotyping of DNA extracted from CP3 and CP4 mouse tail tips confirmed that the germline harboured the *Cre* transgene, one *Ctnnb1* allele with *loxP* sites at *Exon3* and one *Pten* allele with *loxP* sites at *Exon5*. However, genotyping of the tumour tissue used to derive CP3 cells uncovered the loss of *wildtype Pten* in the tumour itself (Table 3.2-1), indicating that LOH occurred prior to generation of the CP3 cell line and was not a consequence of culturing cells *in vitro*. Loss of *wildtype Pten* in CP4 tumour tissue also suggested LOH had occurred, but was contradictory to the positive expression of Pten protein in CP4 cells. It should be noted that the tumour tissue genotyped will not be completely representative of the tissue used to generate the cell lines. However, it is also likely that cancer cells evolve during the establishment of cell lines.

These cell line data corroborate findings from *Pten* transcript and gene analysis of *Pb-Cre Pten^{f/+} Ctnnb1^{(ex3)Δ/+}* tumour epithelial tissue (Figure 3.2.24 & 3.2.25) and demonstrate that LOH in *Pten* occurs within tumours initiated by aberrant β-

catenin activation and *Pten* haploinsufficiency. It is likely that the level of LOH varies between cells and tumours, leading to differential expression of *Pten* across the tissue. This makes it possible to generate cell lines such as CP4 which retain *wildtype Pten* and, hence, *Pten* expression.

While we elucidated that LOH was responsible for the low levels of *Pten* expression in *Pb-Cre Pten^{fl/+} Ctnnb1^{(ex3)Δ/+}* prostate tumours, this was not the case in *Pb-Cre Ctnnb1^{(ex3)Δ/+}* tumours. Therefore, we investigated other mechanisms of *Pten* transcript regulation in tumours driven by aberrant activation of β-catenin alone.

We searched the miRBase database and identified a number of microRNAs involved in *Pten*-regulation. These included *miR-17*, *miR-18a*, *miR-19b* and *miR-21*, which negatively regulate *Pten* expression. Using TaqMan microRNA assays, we carried out RT-PCR expression analysis of these microRNAs in total RNA extracted from *wildtype* and *Ctnnb1^{(ex3)Δ/+}* prostate tissue. This experiment was carried out on samples collected at 3, 6 and 12 month time points in order to assess temporal changes in miRNA expression. We hypothesised that the negative regulation of *Pten* expression would be more apparent at later stages of tumour progression, between 6-12 months, correlating with tumour development and the progressive loss of *Pten* that we had identified in *Pb-Cre Ctnnb1^{(ex3)Δ/+}* prostates.

In keeping with our hypothesis, at 3 months no significant differences in *miR-17*, *18a*, *19b* or *21* (Figure 3.2.29) expression were observed between *Ctnnb1^{(ex3)Δ/+}* and *wildtype* prostate tissue. However, in *Ctnnb1^{(ex3)Δ/+}* prostate tissue at 6 months there was a significant increase in *miR-17*, *18a*, *19b* and *21* expression (Figure 3.2.29), all associated with the negative regulation of *Pten*. These differences in *miR-18a* and *19b* were maintained in *Ctnnb1^{(ex3)Δ/+}* prostate tissue at 12 months. We noted no significant age-related changes in miRNA expression in *wildtype* prostate tissue (Figure 3.2.29), meaning that the changes in miRNA expression in *Ctnnb1^{(ex3)Δ/+}* prostate tissue were a consequence of aberrant β-catenin activation.

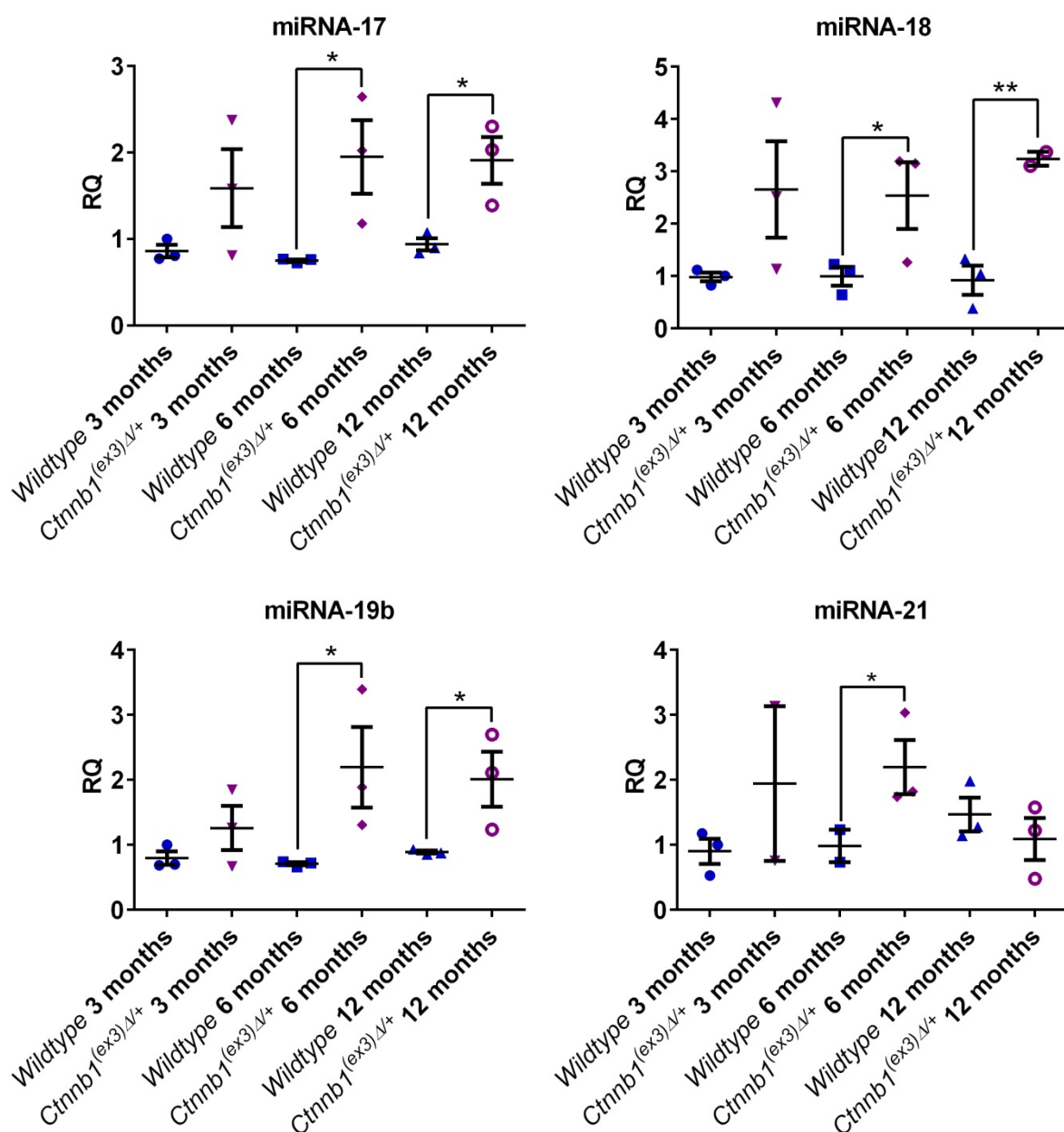


Figure 3.2.29 Upregulation of *miRNA-17*, *-18*, *19b* and *-21* expression is associated with aberrant β -catenin activation

TaqMan microRNA assays for *miR-17*, *-18a*, *-19b* and *-21* were used to measure the relative quantity (RQ) of these miRNAs expressed in wildtype and *Pb-Cre Ctnnb1*^{(ex3)Δ/+} prostate tissue at 3, 6 and 12 month time points. Expression data was normalised to *SnoRNA-202* housekeeping gene and the data is shown relative to *wildtype* 3 months. (** $P < 0.01$, * $P < 0.05$; analysed by unpaired, one-tailed t-test with Welch's correction).

From this experiment it was not possible to determine if expression changes were a direct consequence of β -catenin activation or an indirect effect associated with tumour development. To test whether transcriptional β -catenin activity can directly regulate the expression of *Pten*-regulatory miRNAs, we analysed miRNA expression in CP1 cells following treatment with 25 μ M ICG-001 inhibitor or vehicle control for 24 hours.

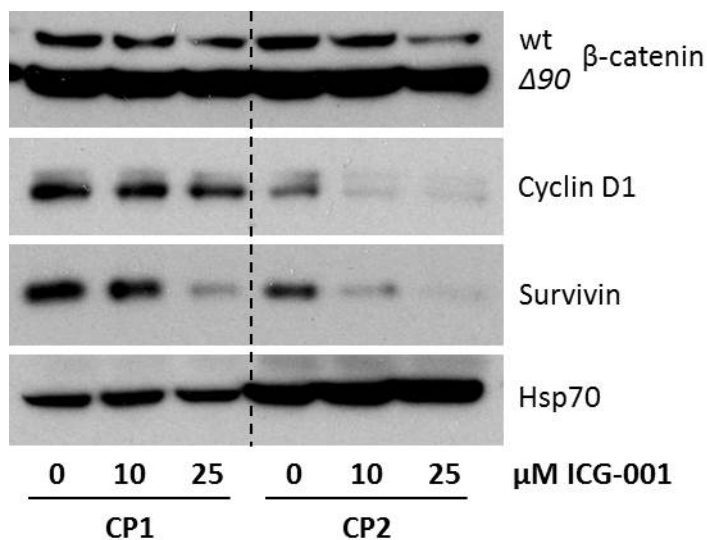


Figure 3.2.30 Western blot analysis of CP1 and CP2 cells treated with ICG-001 inhibitor
Western blot analysis of β -catenin, Cyclin-D1 and Survivin protein levels in protein lysates extracted from CP1 and CP2 cell lines following 24 hours treatment with 0 μ M (vehicle control), 10 μ M or 25 μ M of ICG inhibitor. GAPDH was used as a loading control.

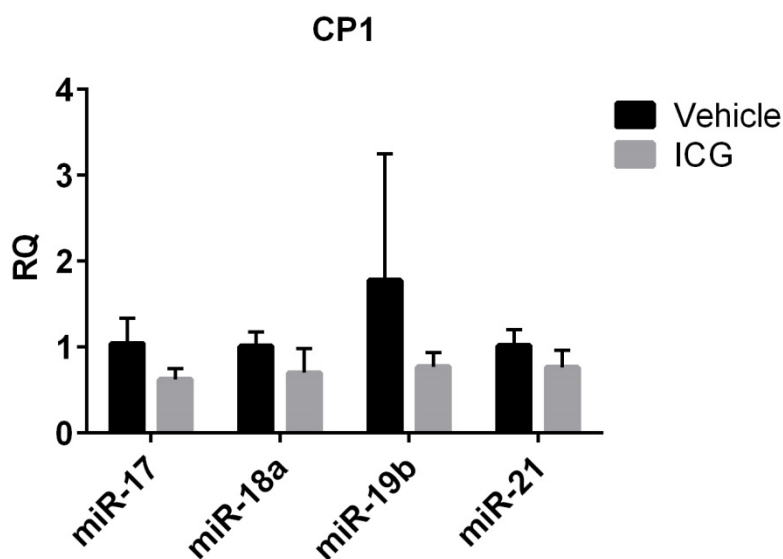


Figure 3.2.31 Preliminary data suggests that blocking β -catenin transcriptional activity decreases expression of *miRNA-17*

TaqMan microRNA assays for *miR-17*, *-18a*, *-19b*, and *-21* were used to measure the relative quantity (RQ) of these miRNAs expressed in CP1 cells following 24 hours treatment with 25 μ M of ICG inhibitor compared to treatment with ethanol vehicle control. Expression data was normalised to *SnoRNA-202* housekeeping gene and the data is shown relative to vehicle control. This is preliminary data from n=1 experiment and results need to be validated.

ICG-001 is a small molecule inhibitor that down-regulates β -catenin/TCF signalling by specifically binding to cyclic AMP response element-binding protein. Western blot analysis of protein lysates prepared from ICG-001-treated CP1 and

CP2 cells confirmed that 25 μ M of ICG-001 inhibitor downregulated protein expression of the β -catenin/TCF target genes, Cyclin-D1 and survivin (Figure 3.2.30). Preliminary data showed that *miR-17* expression was downregulated following β -catenin/TCF inhibition in CP1 cells (Figure 3.2.31) but it was unclear whether there was a significant effect on expression of *miR-18*, *19b* or *21*. Validation of these interesting results is warranted in repeat experiments.

Further work is required to determine whether expression of *Pten*-regulatory miRNAs is directly regulated by β -catenin. However, it is likely that the upregulation of *miR-17*, *18a*, *19b* and *21* are collectively contributing to loss of *Pten* expression in *Pb-Cre Ctnnb1^{(ex3) Δ /+}* prostate tissue in advanced stages of prostate cancer.

3.3 Tumour intrinsic events that facilitate co-operation between β -catenin activation and *Pten* loss in prostate cancer

We proceeded to investigate intrinsic molecular alterations arising from β -catenin activation and *Pten* loss that may potentially contribute to their co-operation. Changes in phospho-Akt (Ser-473), phospho-mTOR (Ser-2448) and phospho-AMPK (Thr-172) protein expression were identified in the RPPA screen (Figure 3.2.9). Therefore, we proceeded to investigate changes in mammalian target of rapamycin (mTOR) and AMP-activated protein kinase (AMPK) signalling pathways that could be contributing to prostate cancer development and progression.

Further downstream analysis of the mTOR signalling pathway found that there was phosphorylation of TSC2 (Thr1462) by phospho-Akt in *Pb-Cre Pten^{fl/+}*, *Pb-Cre Ctnnb1^{(ex3) Δ /+}* and *Pb-Cre Pten^{fl/+} Ctnnb1^{(ex3) Δ /+}* samples (Figure 3.3.1), so that Rheb was no longer inhibited from activating mTORC1 signalling. Total mTOR levels were elevated in *Pb-Cre Pten^{fl/+}* and *Pb-Cre Pten^{fl/+} Ctnnb1^{(ex3) Δ /+}* samples compared to *wildtype* and to a lesser extent in *Pb-Cre Ctnnb1^{(ex3) Δ /+}* samples. Similar levels of phospho-mTOR were detected in the three groups. However, increased total and phosphorylated levels of the downstream pathway effectors,

S6 kinase (S6K) and its substrate, S6, were most apparent in *Pb-Cre Pten^{fl/+} Ctnnb1^{(ex3)Δ/+}* prostate tissue compared to control groups, with only low levels of phospho-S6K and phospho-S6 present in *Ctnnb1^{(ex3)Δ/+}* prostate (Figure 3.3.1).

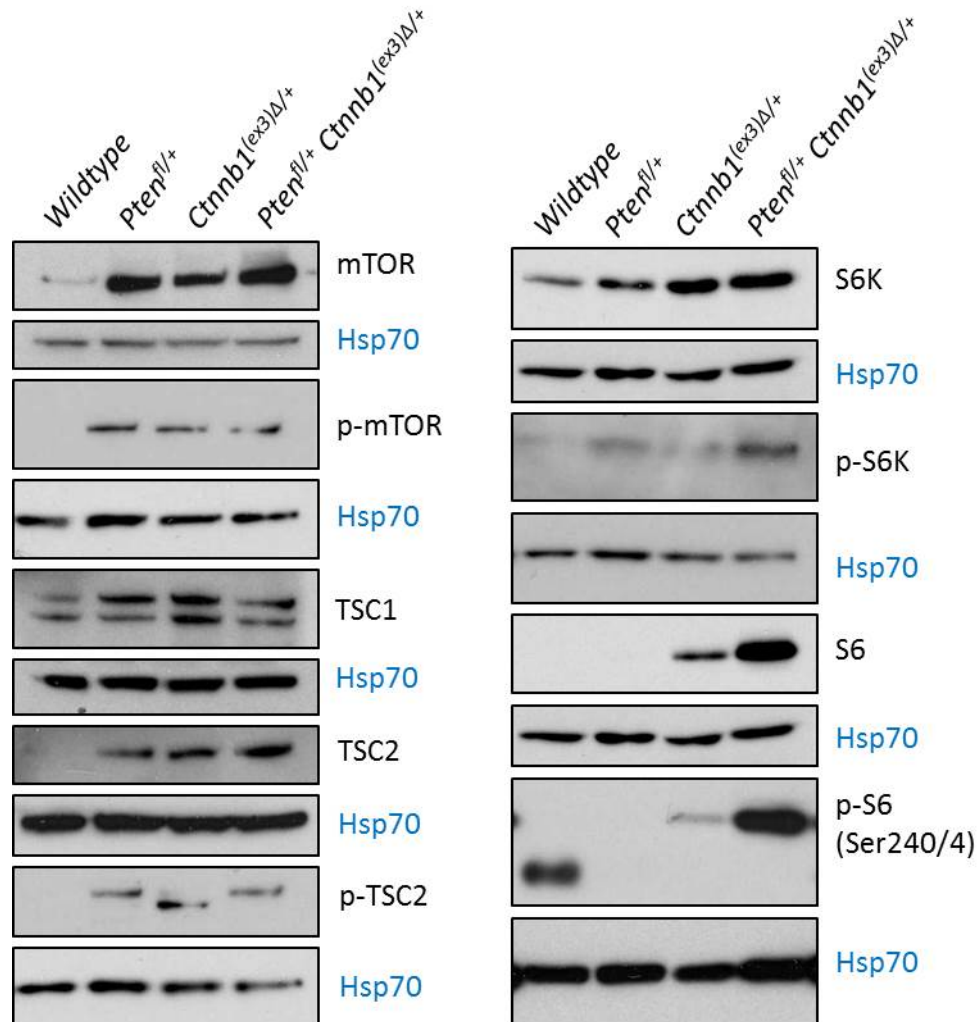


Figure 3.3.1 mTOR pathway analysis

Representative western blot analysis of mTOR, phospho-mTOR (Ser-2448), TSC1, TSC2, phospho-TSC2 (Thr1462), S6K, phospho-S6K (Thr421/Ser424), S6 and phospho-S6 (Ser-240/244) protein levels in protein lysates extracted from prostate tissue of *wildtype*, *Pb-Cre Pten^{fl/+}*, *Pb-Cre Ctnnb1^{(ex3)Δ/+}* and *Pb-Cre Pten^{fl/+} Ctnnb1^{(ex3)Δ/+}* mice at 6 months (n=3). Hsp70 was used as a loading control.

S6K regulates mRNA biogenesis and translation and it is well established that phosphorylation and activation of S6K drives increased protein synthesis and also lipid synthesis for the production of cell membrane [185], required in proliferating cells. Activation of the mTOR pathway will also positively regulate energy metabolism to maintain cellular ATP requirements.

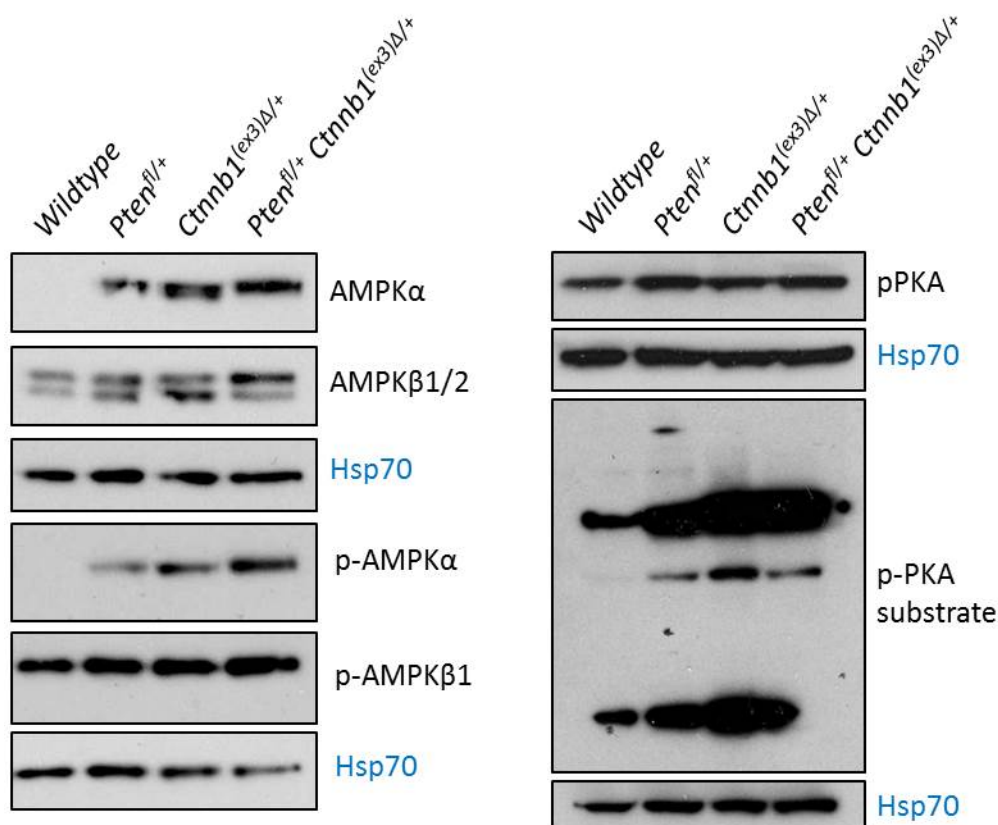


Figure 3.3.2 AMPK and PKA pathway analysis

Representative western blot analysis of total AMPK α , total AMPK β 1/2, phospho-AMPK α (Thr172) and phospho-AMPK β 1 (Ser108) protein levels, and phospho-PKA (Thr197) and phospho-PKA substrate levels in protein lysates extracted from prostate tissue of *wildtype*, *Pb-Cre Pten^{fl/+}*, *Pb-Cre Ctnnb1^{(ex3)Δ/+}* and *Pb-Cre Pten^{fl/+} Ctnnb1^{(ex3)Δ/+}* mice at 6 months (n=3). Hsp70 was used as a loading control.

AMPK functions upstream of mTOR and is activated in response to cellular stresses such as hypoxia, low energy and DNA damage, inhibiting mTOR signalling through promotion of TSC2 activity or direct allosteric inhibition of mTORC1 [185]. Thus, upregulation in mTOR signalling activity should correspond with low levels of AMPK signalling activity. I therefore further characterised the phosphorylation status of AMPK subunits. The highest levels of phospho-AMPK α were present in *Pb-Cre Pten^{fl/+} Ctnnb1^{(ex3)Δ/+}* samples, as suggested by the RPPA screen, with lower but significant levels also detected in *Pb-Cre Pten^{fl/+}* and *Pb-Cre Ctnnb1^{(ex3)Δ/+}* samples (Figure 3.3.2).

AMPK activation is likely to be a consequence of the high energy requirements of rapidly proliferating *Pten^{fl/+} Ctnnb1^{(ex3)Δ/+}* cancer cells, which will generate high levels of AMP. This is also likely to activate PKA signalling. Phosphorylation of PKA was similar across the genotypes but showed increased activity, measured

by increased levels of phospho-PKA substrate, in *Ctnnb1*^{(ex3) Δ /+} prostate tissue compared to *Pten*^{fl/+} *Ctnnb1*^{(ex3) Δ /+} and *Pten*^{fl/+} alone (Figure 3.3.2). AMPK and PKA activation highlight the increase in cellular stresses and energy requirements within prostate tissue with elevated β -catenin activation.

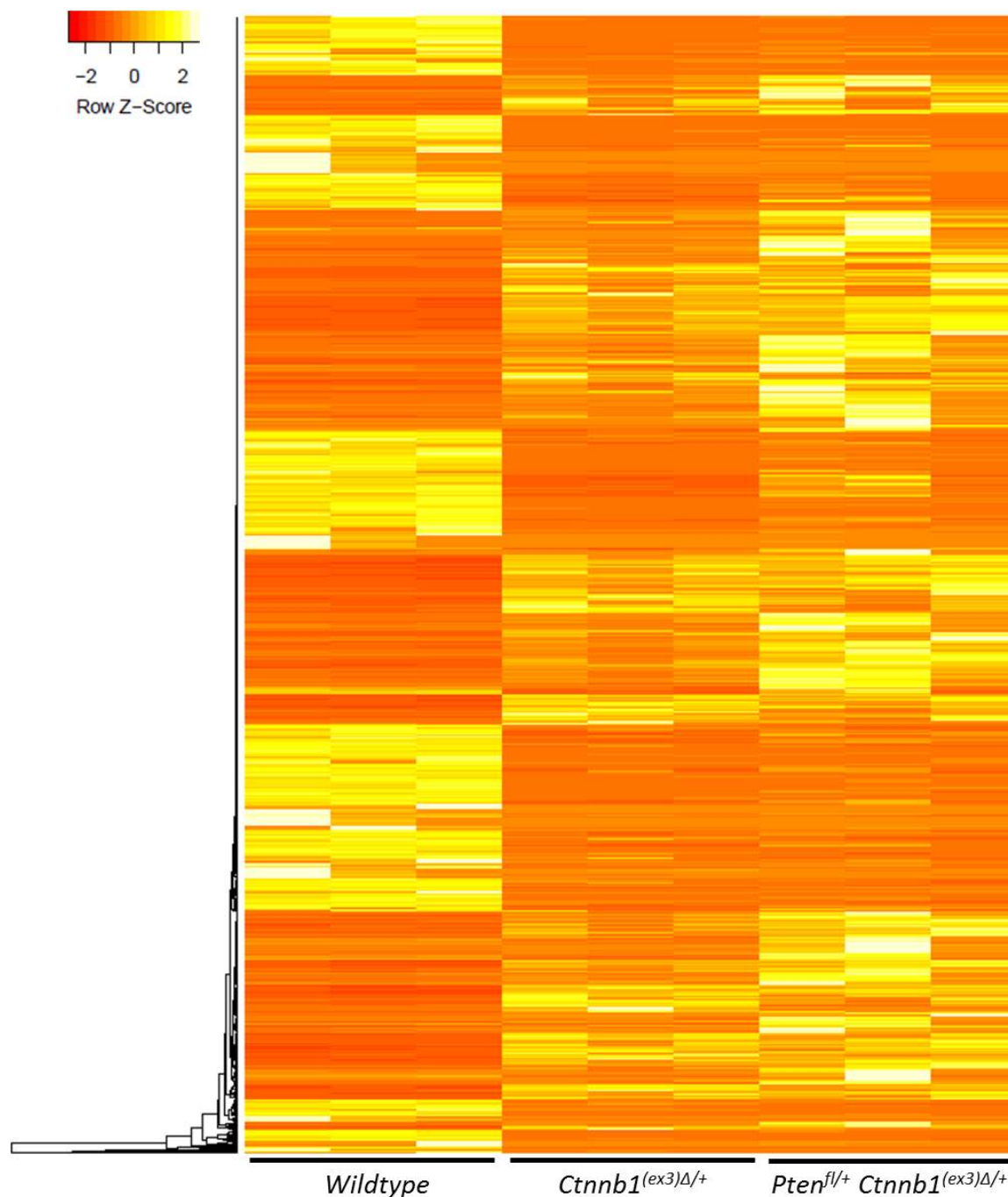


Figure 3.3.3 *Pb-Cre Ctnnb1*^{(ex3) Δ /+} and *Pb-Cre Pten*^{fl/+} *Ctnnb1*^{(ex3) Δ /+} tumours have similar gene expression patterns

RNA extracted from *wildtype* prostate tissue (12 months) and *Pb-Cre Ctnnb1*^{(ex3) Δ /+} and *Pb-Cre Pten*^{fl/+} *Ctnnb1*^{(ex3) Δ /+} tumour tissue (endpoint) underwent RNA sequencing and gene expression analysis. The heat map shows significant ($P < 0.05$) expression changes in 1638 genes in *Ctnnb1*^{(ex3) Δ /+} and/or *Pten*^{fl/+} *Ctnnb1*^{(ex3) Δ /+} tumours compared to *wildtype*.

To better characterise the molecular changes associated with β -catenin activation in *Pb-Cre Ctnnb1^{(ex3) Δ /+}* and *Pb-Cre Pten^{fl/+} Ctnnb1^{(ex3) Δ /+}* tumours, we carried out transcriptomic analysis of RNA from tumours sampled at clinical endpoint. We found the expression of over 1600 genes was significantly altered in the tumour prostate tissue compared to *wildtype*. The heat map represents these changes (Figure 3.3.3) and illustrates the overall similarity in gene expression pattern between *Pb-Cre Ctnnb1^{(ex3) Δ /+}* and *Pb-Cre Pten^{fl/+} Ctnnb1^{(ex3) Δ /+}* tumours.

From RNA sequencing data, I selected 5 genes that were significantly upregulated in β -catenin driven tumours. RT-PCR was used to analyse their expression in RNA extracted from *Pten^{fl/+} Ctnnb1^{(ex3) Δ /+}* prostate tissue compared to *Ctnnb1^{(ex3) Δ /+}*, *Pten^{fl/+}* and *wildtype* controls, all sampled at 6 months. There was a significant increase in expression of alpha-defensin 20 (*Defa20*), adenylate cyclase 8 (*Adcy8*), apolipoprotein C-IV (*Apoc4*) and pancreatic lipase-related protein 2 (*Pnliprp2*) in both *Pten^{fl/+} Ctnnb1^{(ex3) Δ /+}* and *Ctnnb1^{(ex3) Δ /+}* prostate tissue compared to *Pten^{fl/+}* and *wildtype* (Figure 3.3.4). *Defa20*, the most highly expressed gene, is associated with antimicrobial innate immune response, and is known to be released from neutrophils [186]. *Adcy8* catalyses the biosynthesis of cyclic-AMP (cAMP) from ATP to activate PKA-mediated signalling [187]. *Apoc4* and *Pnliprp2* are both involved in lipid metabolism: *Apoc4* is a lipid-binding protein which can facilitate stabilisation and solubilisation of lipoproteins for lipid metabolism and cholesterol transport [188]; *Pnliprp2* plays a role in fat digestion and absorption [189]. We surmised that expression of *Adcy8*, *Defa20*, *Apoc4* and *Pnliprp2* is upregulated by β -catenin signalling and independent of *Pten* loss because there was no significant difference between the level of gene expression in tissue with β -catenin activation alone or with additional *Pten* loss.

Although RNA sequencing data showed significant changes in expression of the gluconeogenesis regulatory enzyme, fructose biphosphatase (*Fbp1*), no significant increase in *Fbp1* expression was observed in *Ctnnb1^{(ex3) Δ /+}* or *Pten^{fl/+} Ctnnb1^{(ex3) Δ /+}* tissue compared to controls at 6 months (Figure 3.3.4). It should be noted that RNA sequencing analysis was carried out on endpoint tumour samples, whereas RT-PCR validation of gene expression changes was conducted on samples taken at a 6 month time point. There are likely to be temporal changes in gene expression associated with the stage of tumour development.

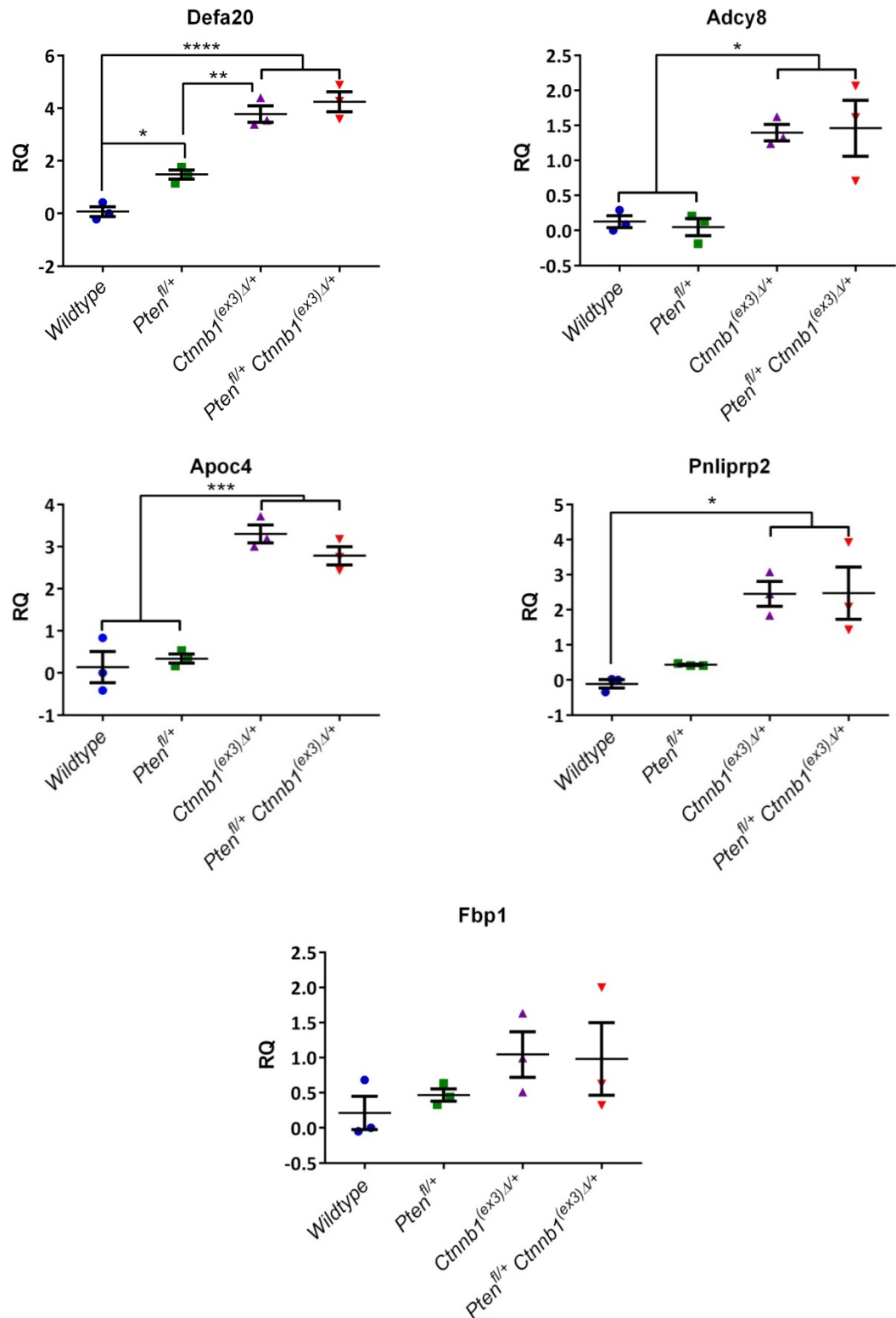


Figure 3.3.4 Validation of expression changes observed in genes associated with innate immune response, cAMP biosynthesis, lipid metabolism and glycolysis

TaqMan RT-PCR analysis of alpha-defensin 20 (*Defa20*), adenylate cyclase 8 (*Adcy8*), apolipoprotein C-IV (*Apoc4*), pancreatic lipase-related protein 2 (*Pnliprp2*) and fructose bisphosphatase (*Fbp1*) mRNA expression levels in *wildtype*, *Pb Cre Pten*^{fl/+}, *Pb Cre Ctnnb1*^{(ex3)Δ/+} and *Pb Cre Pten*^{fl/+} *Ctnnb1*^{(ex3)Δ/+} mouse prostates tissue at 6 month time point. Normalised to 18S housekeeping gene. Relative quantity (RQ) presented as log scale due to high expression differences. (**** P < 0.0001, *** P < 0.001, ** P < 0.01, * P < 0.05; analysis by one-way ANOVA, with Tukey multiple comparison test).



Figure 3.3.5 MetaCore pathway analysis of gene expression changes in *Pb-Cre Ctnnb1^{(ex3)Δ/+}* tumour tissue compared to *wildtype*

MetaCore pathway analysis software was used to elucidate the signalling pathways associated with gene expression changes identified in RNA sequencing data. This histogram shows the most significantly altered pathways in *Pb-Cre Ctnnb1^{(ex3)Δ/+}* prostate tumours taken at clinical endpoint compared to *wildtype* prostate tissue (orange line), ranked according to statistical significance and ordered from most significant to least significant. Significance of pathway alterations observed in *Pb-Cre Pten^{fl/+} Ctnnb1^{(ex3)Δ/+}* tumour tissue compared to *wildtype* (blue line) included for reference. ($-\log(P \text{ value}) > 2 = P < 0.01$).

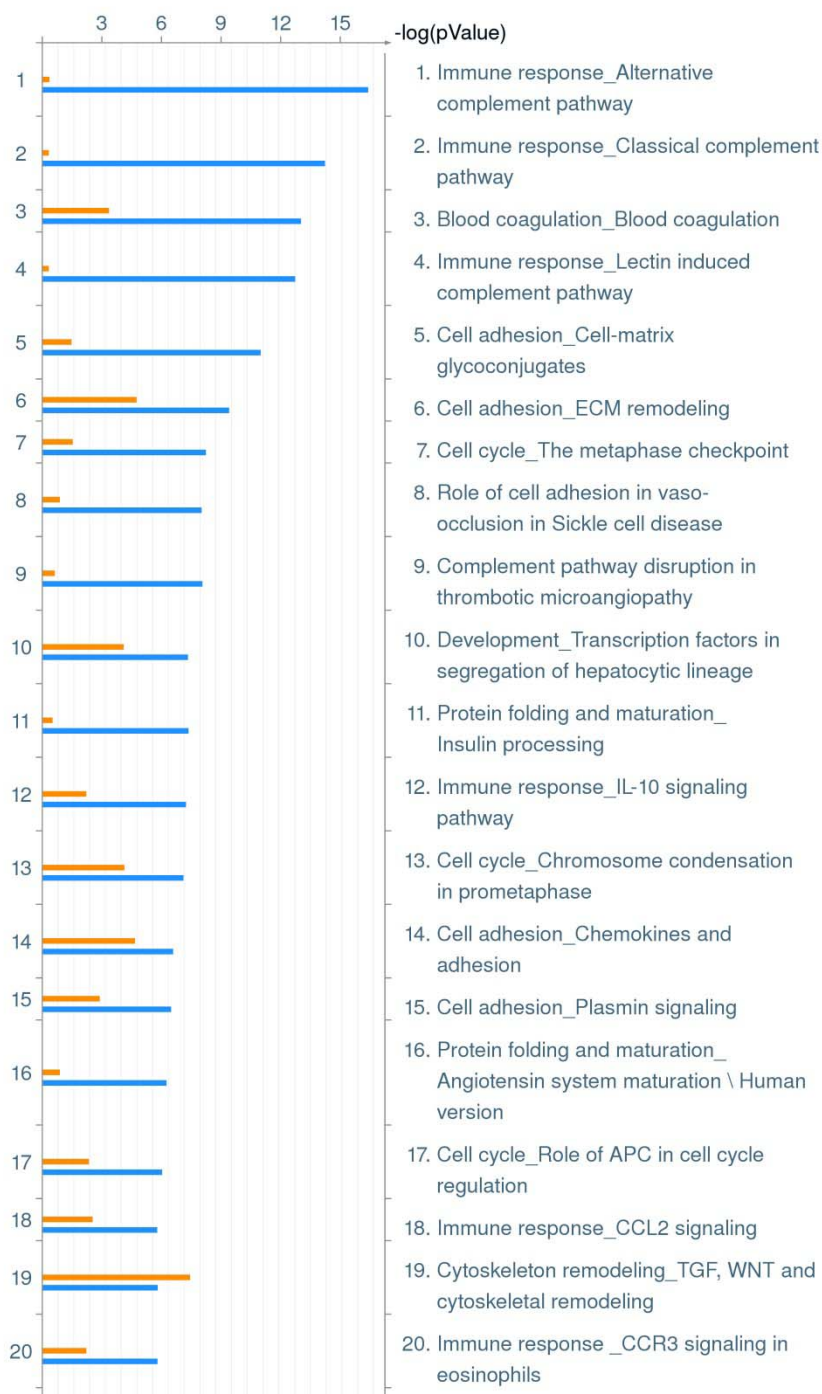


Figure 3.3.6 MetaCore pathway analysis of gene expression changes in *Pb-Cre Pten^{fl/+} Cttnb1^{(ex3)Δ/+}* tumour tissue compared to *wildtype*

This histogram shows the most significantly altered pathways in *Pb-Cre Pten^{fl/+} Cttnb1^{(ex3)Δ/+}* prostate tumours taken at clinical endpoint compared to *wildtype* prostate tissue (blue line), ranked according to statistical significance and ordered from most significant to least significant. Significance of pathway alterations observed in *Pb-Cre Cttnb1^{(ex3)Δ/+}* tumour tissue compared to *wildtype* (orange line) included for reference. ($-\log(P \text{ value}) > 2 = P < 0.01$).

Only 203 genes were significantly altered in *Pb-Cre Pten^{fl/+} Cttnb1^{(ex3)Δ/+}* compared to *Pb-Cre Cttnb1^{(ex3)Δ/+}* tumours. MetaCore pathway analysis software was used to examine the similarities and differences in pathway alterations associated with these tumours.

In *Pb-Cre Ctnnb1^{(ex3)Δ/+}* tumours, gene expression changes in TGF, Wnt and cytoskeletal remodelling pathways, and glycolysis and gluconeogenesis pathways were more significantly enriched when compared to *Pb-Cre Pten^{fl/+} Ctnnb1^{(ex3)Δ/+}* tumours (Pathways 1, 3, 13 and 14; Figure 3.3.5). Most of the other pathways that were significantly enriched in *Pb-Cre Ctnnb1^{(ex3)Δ/+}* tumours were enriched to the same or greater extent in *Pten^{fl/+} Ctnnb1^{(ex3)Δ/+}* tumours, such as cell adhesion, development and cell cycle (Pathways 4-7; Figure 3.3.5). In *Pb-Cre Pten^{fl/+} Ctnnb1^{(ex3)Δ/+}* tumours, the most significant alterations occurred in immune response pathways (Pathways 1, 2 and 4; Figure 3.3.6) that were not enriched in *Ctnnb1^{(ex3)Δ/+}* tumours, and the blood coagulation pathway (Pathway 3; figure 3.3.6).

3.4 Tumour extrinsic events that facilitate co-operation between β-catenin activation and Pten loss in prostate cancer

The significant enrichment of immune response pathways, identified in prostate tumours driven by concurrent β-catenin activation and Pten loss, suggested that many gene expression changes were associated with tumour extrinsic events. Such events may also provide an explanation for variations between weights of β-catenin-driven tumours (Figure 3.2.4, 3.2.6, 3.2.7). Furthermore, we frequently observed weight loss (and haematuria) in mice harbouring these aggressive prostate tumours, demonstrating the systemic consequences of tumour development. It is important to develop our understanding of the tumour-host interaction, which is fundamental in facilitating tumour progression, and how this is influenced by the mutations driving prostate cancer.

To characterise tumour extrinsic events that may influence cancer progression and host survival, we studied innate immune cell infiltration into prostate tissue during cancer development and progression, carried out haematological analysis of whole blood from tumour-bearing mice and analysed the cytokines present in advanced-stage prostate tumours.

To examine the effect of age on macrophage and neutrophil infiltration, we carried out F4/80 and NIMP immunohistochemical staining of *wildtype* prostate tissue to respectively identify macrophages and neutrophils at 3, 6 and 12 month time points. Few macrophages were present in the stroma at 3 and 6 months but infiltration increased at 12 months. Macrophages were not observed in epithelial tissue (Figure 3.4.1) and neutrophils were not normally present in the stroma or epithelial tissue at any time point (Figure 3.4.2).

We proceeded to examine macrophage and neutrophil infiltration in *Pb-Cre Pten^{fl/+}*, *Pb-Cre Ctnnb1^{(ex3)Δ/+}* and *Pb-Cre Pten^{fl/+} Ctnnb1^{(ex3)Δ/+}* prostate tissue compared to *wildtype*. There was significant macrophage infiltration (F4/80 immuno-reactivity) during PIN development in *Ctnnb1^{(ex3)Δ/+}* and *Pten^{fl/+} Ctnnb1^{(ex3)Δ/+}* tissue at 3 months and sustained presence of macrophages in stroma and epithelial tissue during cancer progression (Figure 3.4.1). The age-associated increase in basal levels of macrophages (observed in *wildtype* prostate tissue at 12 months) may contribute to the high levels of macrophages present in *Ctnnb1^{(ex3)Δ/+}* tumours at 12 months (Figure 3.4.1).

Significant neutrophil infiltration (positive for NIMP staining) was observed in *Ctnnb1^{(ex3)Δ/+}* and *Pten^{fl/+} Ctnnb1^{(ex3)Δ/+}* tissue at 3 months, and was highest within regions of PIN and *in situ* carcinoma (Figure 3.4.2). In contrast to macrophage infiltration, only small patches of neutrophils were detected in advanced adenocarcinoma and were absent from large regions of *Pten^{fl/+} Ctnnb1^{(ex3)Δ/+}* tumours at 6 months (lower panel) and *Ctnnb1^{(ex3)Δ/+}* tumours at 12 months (lower panel) (Figure 3.4.2). Neutrophils observed in *Ctnnb1^{(ex3)Δ/+}* tumours at 12 months (upper panel; Figure 3.4.2) are likely to be associated with regions of fluid infiltrate.

While few macrophages or neutrophils were observed in *Pten^{fl/+}* prostate tissue at 3 and 6 months, both were present at 12 months (Figure 3.4.1 and 3.4.2), correlating with development of PIN lesions at this time point. Overall, these data suggest that macrophages and neutrophils respond to abnormal epithelium that develops during stages of cancer initiation, and the timing of their infiltration correlates with PIN development. Further work is required to understand the impact of innate immune cell infiltration on cancer initiation and progression.

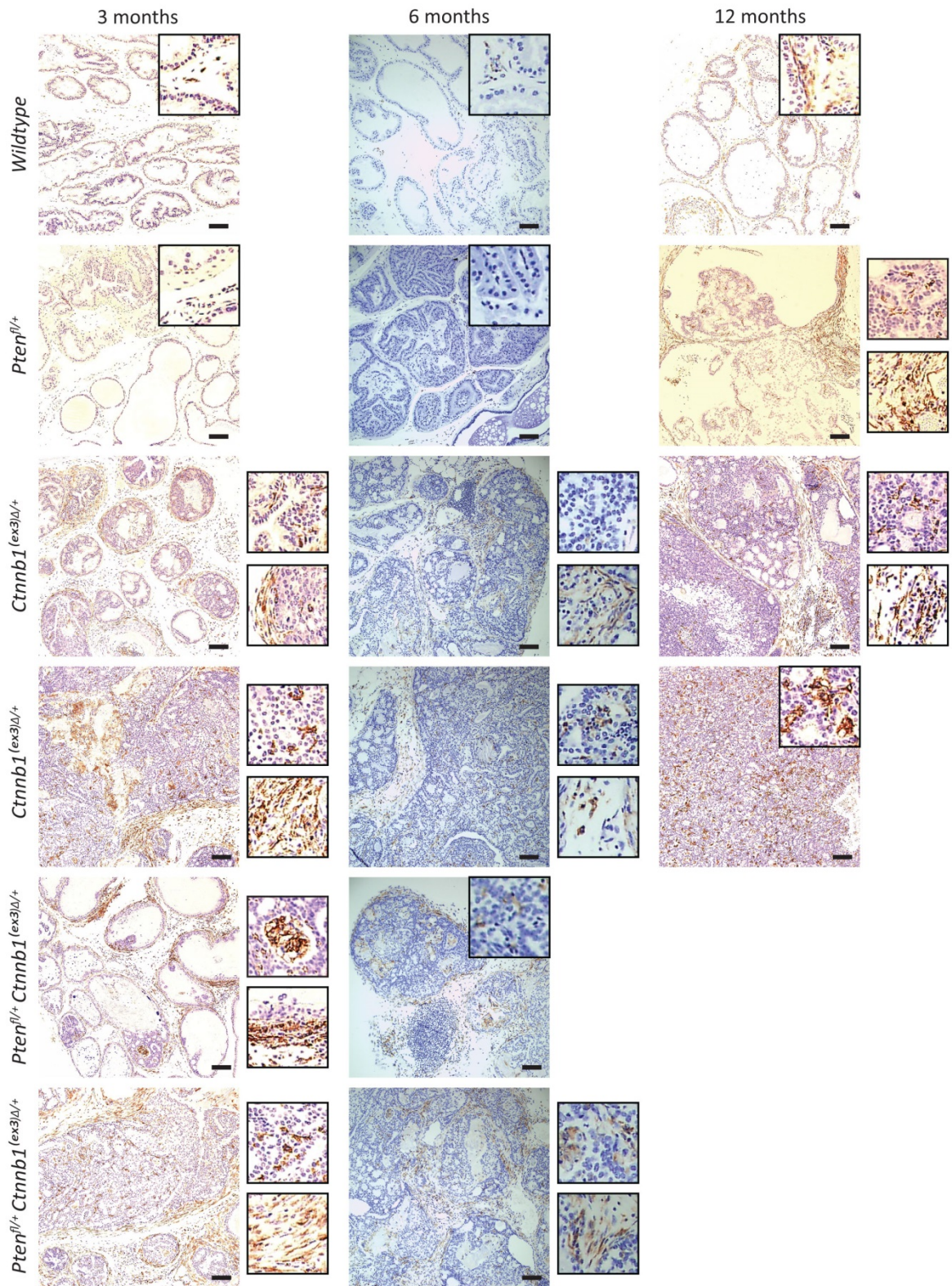


Figure 3.4.1 Characterisation of macrophage infiltration in prostate tissue with β -catenin activation and *Pten* haploinsufficiency

Representative F4/80 immunohistochemical staining of FFPE sections of *wildtype*, *Pb-Cre Pten^{fl/+}*, *Pb-Cre Ctnnb1^{(ex3)Δ/+}* and *Pb-Cre Pten^{fl/+} Ctnnb1^{(ex3)Δ/+}* prostate tissue from mice sacrificed at 3, 6 and 12 months. To illustrate the patterns of macrophage infiltration across the tissue sections, two different areas of *Pb-Cre Ctnnb1^{(ex3)Δ/+}* and *Pb-Cre Pten^{fl/+} Ctnnb1^{(ex3)Δ/+}* prostates are shown. Two representative inserts are included for some sections to show F4/80 staining within epithelial regions (top) and within stromal regions (bottom). Scale bar: 100 μ m. Insert box: 100 μ m². The 6 month panel of images were taken at a different time from those at 3 and 12 months.

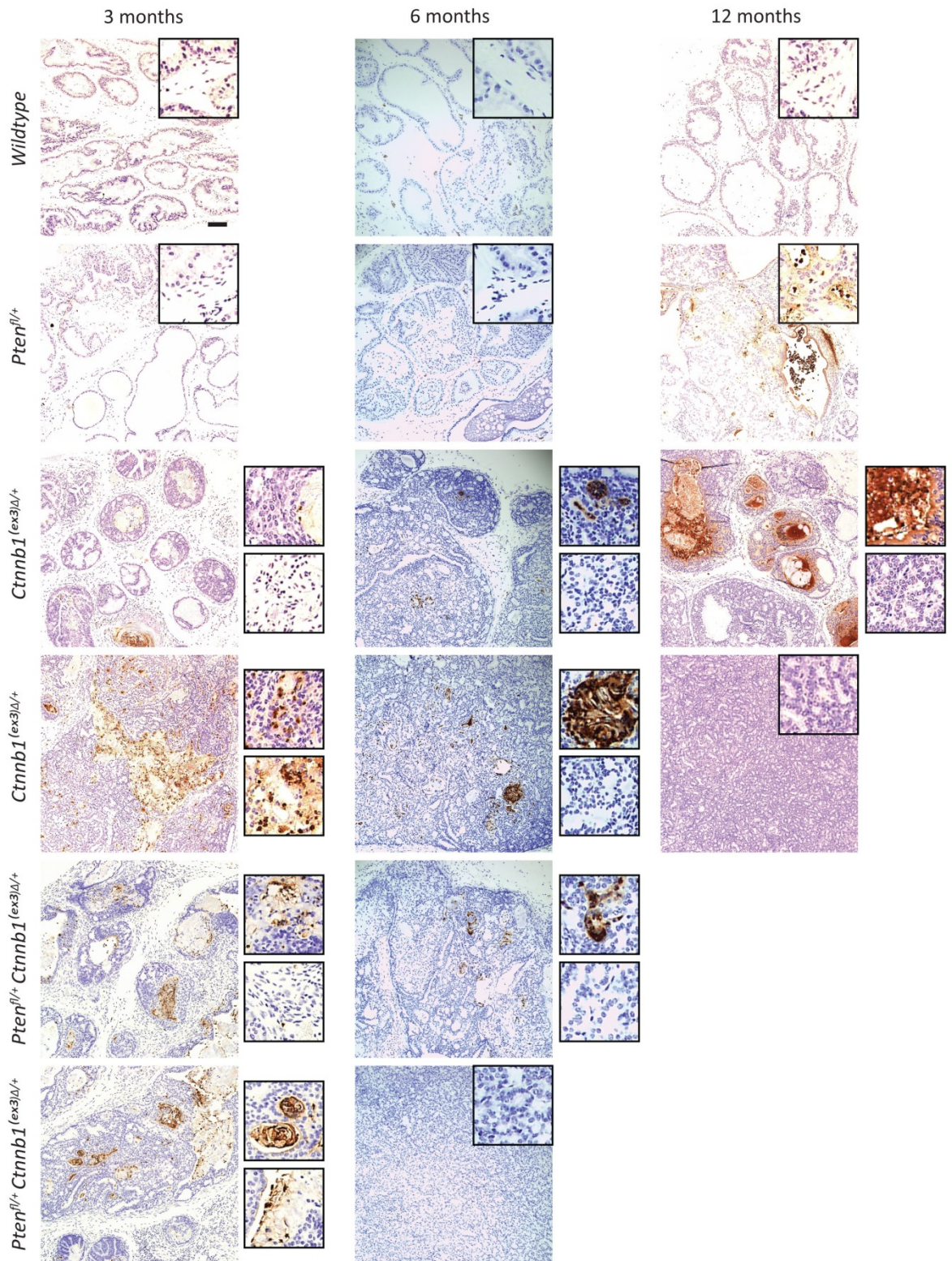


Figure 3.4.2 Characterisation of neutrophil infiltration in prostate tissue with β -catenin activation and *Pten* haploinsufficiency

Representative NIMP immunohistochemical staining of FFPE sections of *wildtype*, *Pb-Cre Pten^{fl/+}*, *Pb-Cre Ctnnb1^{(ex3)Δ/+}* and *Pb-Cre Pten^{fl/+} Ctnnb1^{(ex3)Δ/+}* prostate tissue from mice sacrificed at 3, 6 and 12 months. To illustrate the patterns of neutrophil infiltration across the tissue sections, two different areas of *Pb-Cre Ctnnb1^{(ex3)Δ/+}* and *Pb-Cre Pten^{fl/+} Ctnnb1^{(ex3)Δ/+}* prostates are shown. Two representative inserts are included for some sections to show the patchy nature of NIMP staining. Scale bar: 100 μm . Insert box: 100 μm^2 . The 6 month panel of images were taken at a different time from those at 3 and 12 months.

To extend our study to the systemic level, we carried out haematological analysis of whole blood sampled from tumour-bearing mice post-mortem. Due to some variations in haematology of whole blood between *wildtype* mice at 6 and 12 months, we compared results from tumour-bearing mice to their age-matched *wildtype* control. At this stage, haematology data was only available from one *Cttnb1^{(ex3)Δ/+}* mouse but has been included for reference in the following results.

The only statistically significant differences observed from red blood cell analysis were increased RBC distribution width (RDW) and decreased mean corpuscular volume (MCV) in mice bearing advanced *Pten^{fl/+} Cttnb1^{(ex3)Δ/+}* tumours compared to *wildtype* (Figure 3.4.3). The RDW measures the variation in RBC size and MCV is a measure of average RBC volume. Higher RDW indicates a greater variation in RBC sizes within the blood, while lower MCV suggests RBCs are smaller and may not be holding sufficient haemoglobin. This may be indicative of anaemia in these mice. However, only one mouse had low mean corpuscular haemoglobin concentration (MCHC) (Figure 3.4.3). It should be noted that RDW and MCV normally range between 15.9-20.3% and 42.7-56.0 fL respectively in C57BL/6 mice (Charles River 2012), so although we observed statistically significant differences, these may still be within the 'normal' range. Mice in the *Pb-Cre Pten^{fl/+} Cttnb1^{(ex3)Δ/+}* colony had a mixed background so the normal range of values may vary slightly from C57BL/6 mice.

White blood cell (WBC) analysis showed no overall difference in WBC numbers between mice. Only numbers of monocytes significantly increased in *Pten^{fl/+} Cttnb1^{(ex3)Δ/+}* mice compared to *wildtype*, although there was also a trend towards higher levels of neutrophils and eosinophils (Figure 3.4.4).

As we observed a dose-dependent effect of *Pten* loss on tumour progression and poor survival outcome (Figure 3.2.1), we also analysed whole blood from mice bearing late stage *Pten^{fl/fl} Cttnb1^{(ex3)Δ/+}* tumours to determine effects on the host compared to mice bearing single mutant *Pten^{fl/fl}* or *Cttnb1^{(ex3)Δ/+}* tumours. As in mice bearing *Pten^{fl/+} Cttnb1^{(ex3)Δ/+}* tumours, we observed a mild but statistically significant increase in RDW relative to age-matched *wildtype* control (Figure 3.4.5). There was a trend towards decreased MCV but this was not statistically significant (Figure 3.4.5). Overall, RBC data from blood of mice bearing *Pten^{fl/fl}* tumours was similar to age-matched *wildtype* controls.

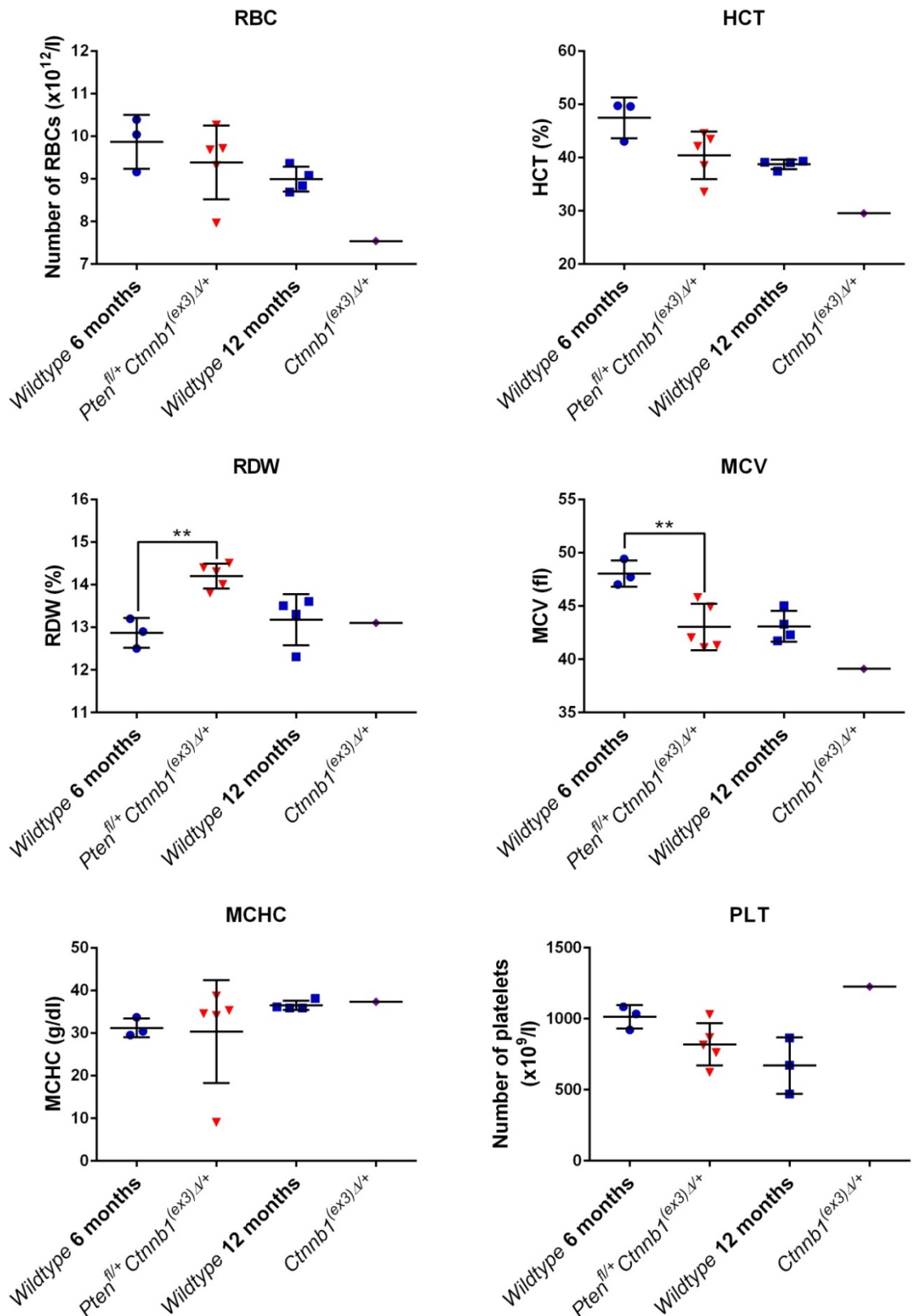


Figure 3.4.3 Analysis of circulating red blood cells and platelets in mice harbouring β -catenin-driven prostate tumours with heterozygous *Pten* loss

Full haematology analysis was carried out on whole blood, collected from mice post-mortem, by the University of Glasgow Veterinary School Clinical Pathology Laboratory. Graphs show the number of red blood cells (RBCs), percentage of haematocrit (HCT), RBC distribution width (RDW), mean corpuscular volume (MCV), mean corpuscular haemoglobin concentration (MCHC) and number of platelets (PLT) in endpoint *Pten*^{fl/+} *Ctnnb1*^{(ex3)Δ/+} mice (n=5) compared to *wildtype* at 6 months (n=3) and endpoint *Ctnnb1*^{(ex3)Δ/+} mice (n=1) compared to *wildtype* at 12 months (n=4). (** P < 0.01; analysed by unpaired, one-tailed t-test with Welch's correction). Data presented as mean \pm SD.

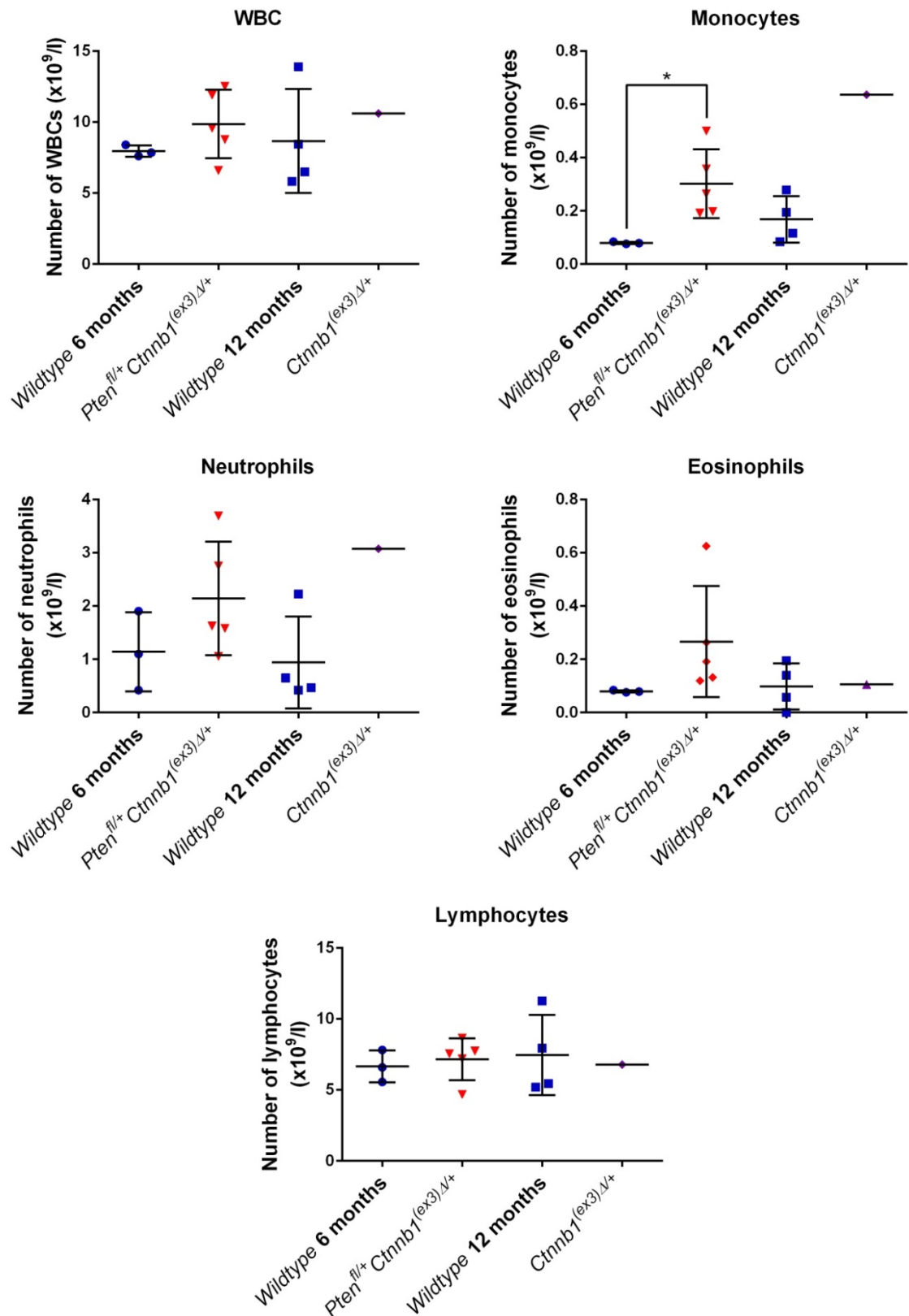


Figure 3.4.4 Analysis of circulating white blood cells in mice harbouring β -catenin-driven prostate tumours with heterozygous *Pten* loss

Full haematology analysis was carried out as described in Figure 3.4.3. Graphs show the overall number of white blood cells (WBCs), and number of monocytes, neutrophils, eosinophils and lymphocytes circulating in endpoint (~6 months) *Pten*^{fl/+} *Ctnnb1*^{(ex3)Δ/+} mice (n=5) compared to *wildtype* at 6 months (n=3) and endpoint (~12 months) *Ctnnb1*^{(ex3)Δ/+} mice (n=1) compared to *wildtype* at 12 months (n=4). (* $P < 0.05$; analysed by unpaired, one-tailed t-test with Welch's correction). Data presented as mean \pm SD.

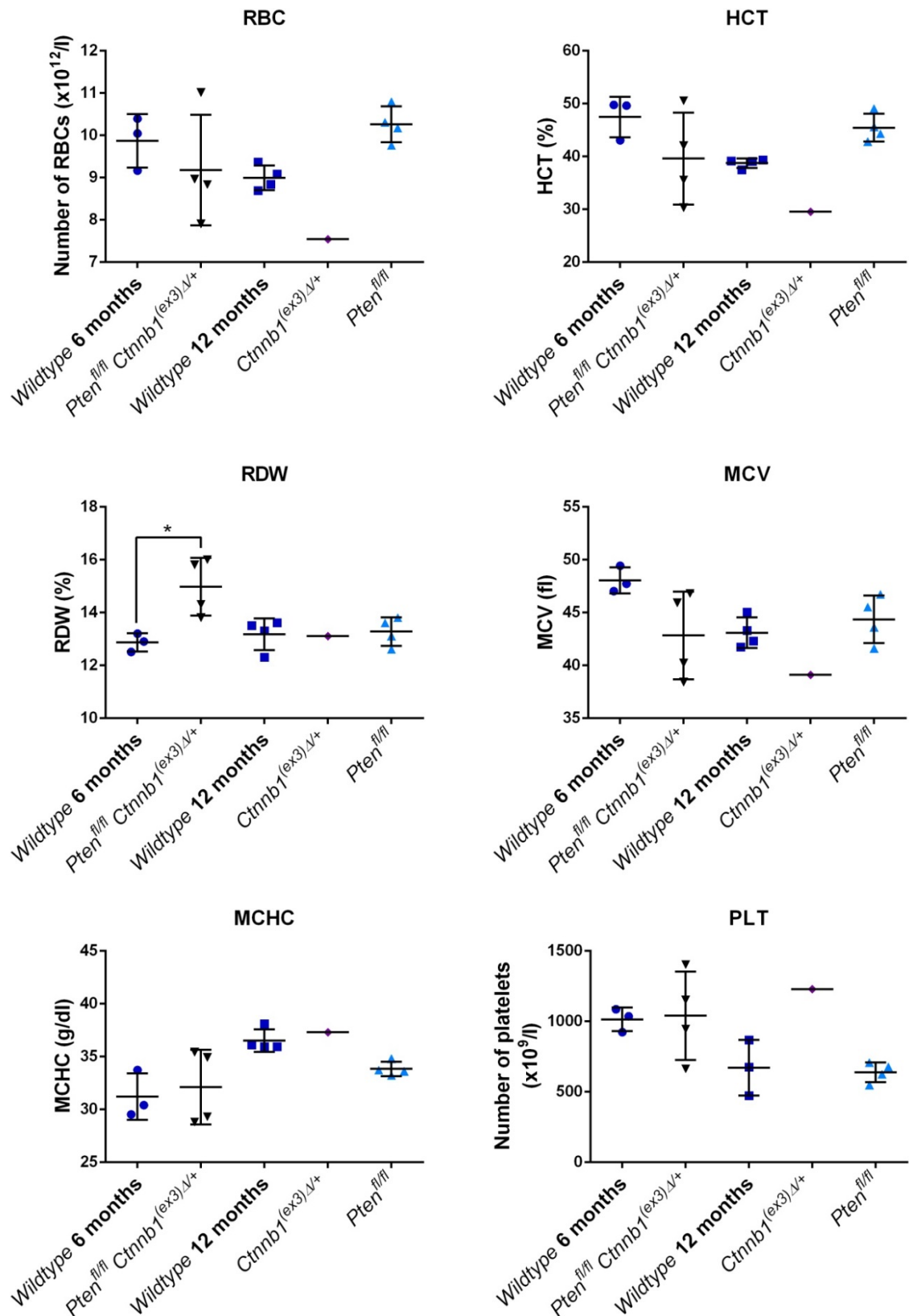


Figure 3.4.5 Analysis of circulating red blood cells and platelets in mice harbouring β -catenin-driven prostate tumours with homozygous *Pten* loss

Full haematology analysis was carried out as described in Figure 3.4.3. Graphs show the number of red blood cells (RBCs), percentage of haematocrit (HCT), RBC distribution width (RDW), mean corpuscular volume (MCV), mean corpuscular haemoglobin concentration (MCHC) and number of platelets (PLT) in endpoint (~6 months) *Pten^{fl/fl} Cttnb1^{(ex3)Δ/+}* mice (n=4) compared to *wildtype* at 6 months (n=3) and endpoint (~12 months) *Pten^{fl/fl}* (n=4) and *Cttnb1^{(ex3)Δ/+}* (n=1) mice compared to *wildtype* at 12 months (n=4). (* $P < 0.05$; analysed by unpaired, one-tailed t-test with Welch's correction). Data presented as mean \pm SD.

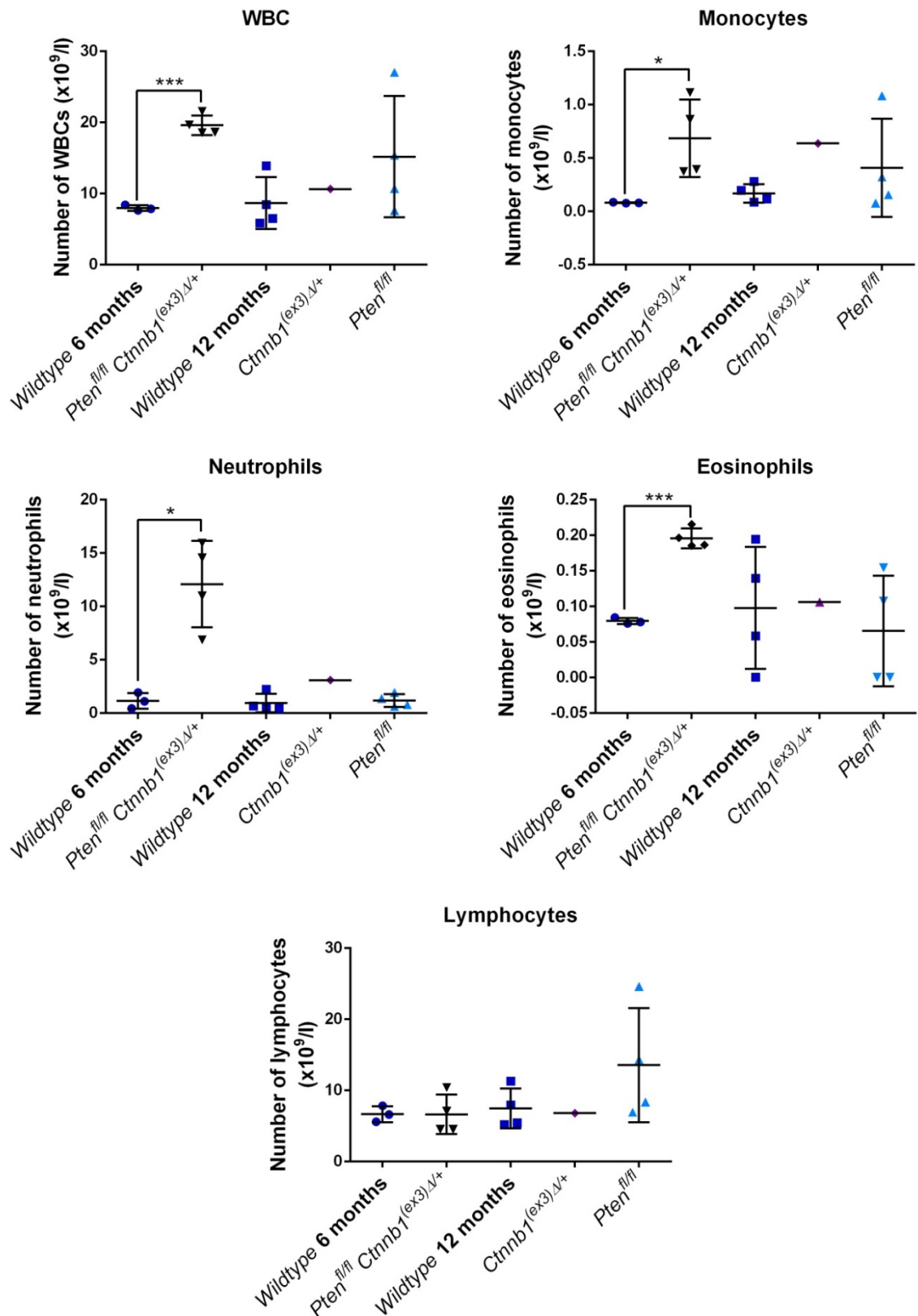


Figure 3.4.6 Analysis of circulating white blood cells in mice harbouring β -catenin-driven prostate tumours with homozygous *Pten* loss

Full haematology analysis was carried out as described in Figure 3.4.3. Graphs show the overall number of white blood cells (WBCs), and number of monocytes, neutrophils, eosinophils and lymphocytes circulating in endpoint *Pten^{fl/fl} Cttnb1^{(ex3)Δ/+}* mice (n=4) compared to *wildtype* at 6 months (n=3) and endpoint *Pten^{fl/fl}* (n=4) and *Cttnb1^{(ex3)Δ/+}* (n=1) mice compared to *wildtype* at 12 months. (***) $P < 0.001$, * $P < 0.05$; analysed by unpaired, one-tailed t-test with Welch's correction). Data presented as mean \pm SD.

Analysis of WBCs in whole blood showed a substantial increase in WBCs in *Pten^{fl/fl} Ctnnb1^{(ex3)Δ/+}* tumour-bearing mice compared to *wildtype*, specifically in monocytes, neutrophils and eosinophils (Figure 3.4.6), while neither *Pten^{fl/fl}* tumours nor *Ctnnb1^{(ex3)Δ/+}* tumour elicited this effect. Numbers of lymphocytes were similar in *wildtype* and tumour-bearing mice.

Blood processed for haematological analysis was sampled from mice that had reached clinical endpoint meaning that tumours had progressed to the same stage. However, only *Pb-Cre Pten^{fl/fl} Ctnnb1^{(ex3)Δ/+}* mice, which harboured the most aggressive tumours, elicited a significant systemic immune response. Our data suggest that the systemic effects of tumours are more related to the rate of tumour growth rather than the stage of tumour development or genotype of the tumour.

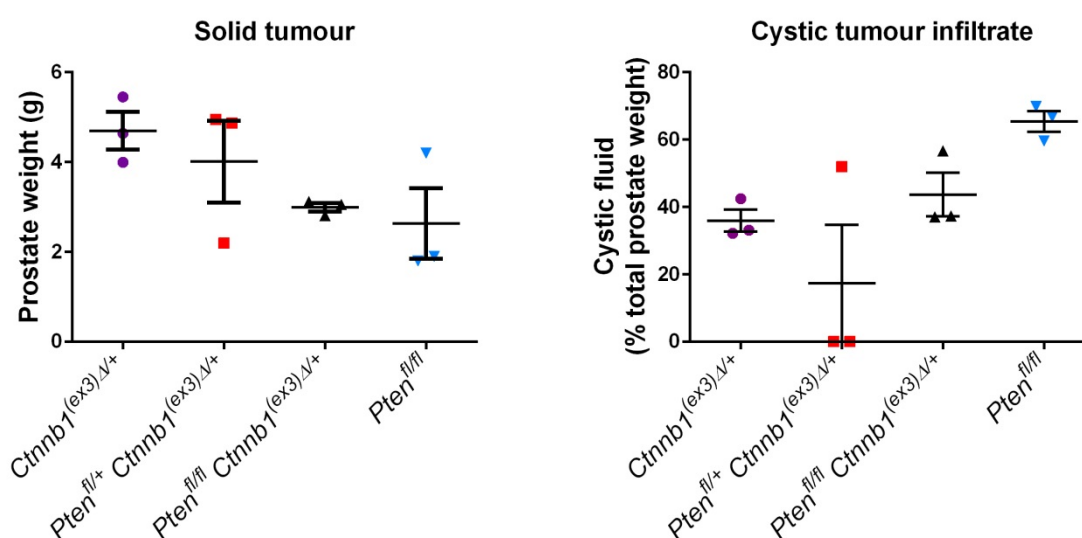


Figure 3.4.7 Endpoint prostate tumour weights and quantity of tumour infiltrate do not vary significantly between tumour genotypes

The graphs show the weight of solid prostate tumour tissue and the amount of cystic fluid within these tumours from *Pb-Cre Ctnnb1^{(ex3)Δ/+}*, *Pb-Cre Pten^{fl/+} Ctnnb1^{(ex3)Δ/+}*, *Pb-Cre Pten^{fl/fl} Ctnnb1^{(ex3)Δ/+}* and *Pb-Cre Pten^{fl/fl}* mice. Cystic fluid tumour infiltrate was calculated by subtracting dry prostate weight (cystic fluid removed) from wet prostate weight (cystic fluid present) and presented as a percentage of total (wet) prostate weight. Data presented as mean ± SEM. Protein extracted from these tumours was used for the cytokine array analysis (Figure 3.3.22 & 3.3.23).

To determine whether there were genotype-dependent differences in host-tumour interactions, we analysed cytokine expression, produced by tumour epithelia or immune cells, in late stage *Pb-Cre Ctnnb1^{(ex3)Δ/+}*, *Pb-Cre Pten^{fl/+} Ctnnb1^{(ex3)Δ/+}*, *Pb-Cre Pten^{fl/fl} Ctnnb1^{(ex3)Δ/+}* and *Pb-Cre Pten^{fl/fl}* tumours. The protein lysates analysed were extracted from tumours with similar solid tumour

weight (Figure 3.4.7). However, *Pten* null tumours contained approximately 20% more cystic tumour infiltrate than tumours with β -catenin activation, and two *Pten*^{fl/+} *Ctnnb1*^{(ex3) Δ /+} tumours were completely solid (Figure 3.4.7).

A mouse cytokine array kit was used to analyse cytokine expression in *Pb-Cre Ctnnb1*^{(ex3) Δ /+}, *Pb-Cre Pten*^{fl/+} *Ctnnb1*^{(ex3) Δ /+}, *Pb-Cre Pten*^{fl/fl} *Ctnnb1*^{(ex3) Δ /+} and *Pb-Cre Pten*^{fl/fl} tumours in biological triplicate. We identified 5 pairs of spots that showed differential expression between tumours (Figure 3.4.8). These corresponded to B lymphocyte chemoattractant (BLC/CXCL13), triggering receptor expressed on myeloid cells 1 (TREM-1), interleukin-16 (IL-16), macrophage inflammatory protein 2 (MIP-2/CXCL2) and interleukin-1 receptor antagonist (IL-1ra/IL-1F3).

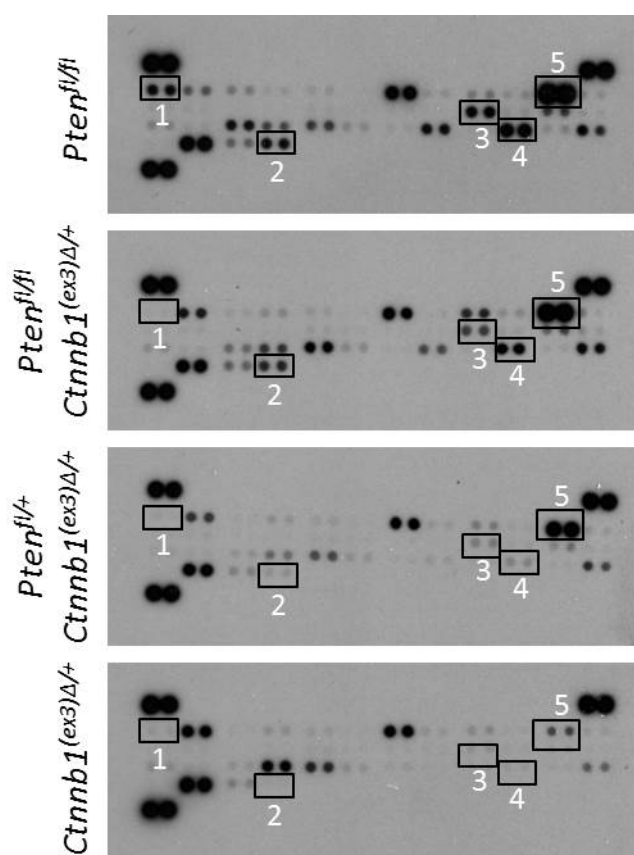


Figure 3.4.8 Protein array showing differential expression of cytokines associated with β -catenin activation and *Pten* loss in prostate tumour tissue

Protein array analysis showing the relative expression of cytokines in protein lysates extracted from *Pb-Cre Ctnnb1*^{(ex3) Δ /+}, *Pb-Cre Pten*^{fl/+} *Ctnnb1*^{(ex3) Δ /+}, *Pb-Cre Pten*^{fl/fl} *Ctnnb1*^{(ex3) Δ /+} and *Pb-Cre Pten*^{fl/fl} endpoint prostate tumour tissue. This image is representative of n=3 cytokine arrays; analysis carried out for each tumour genotype in biological triplicate. 1 = BLC/CXCL13, 2 = TREM-1, 3 = IL-16, 4 = MIP-2 (CXCL2), 5 = IL-1ra (IL-1F3).

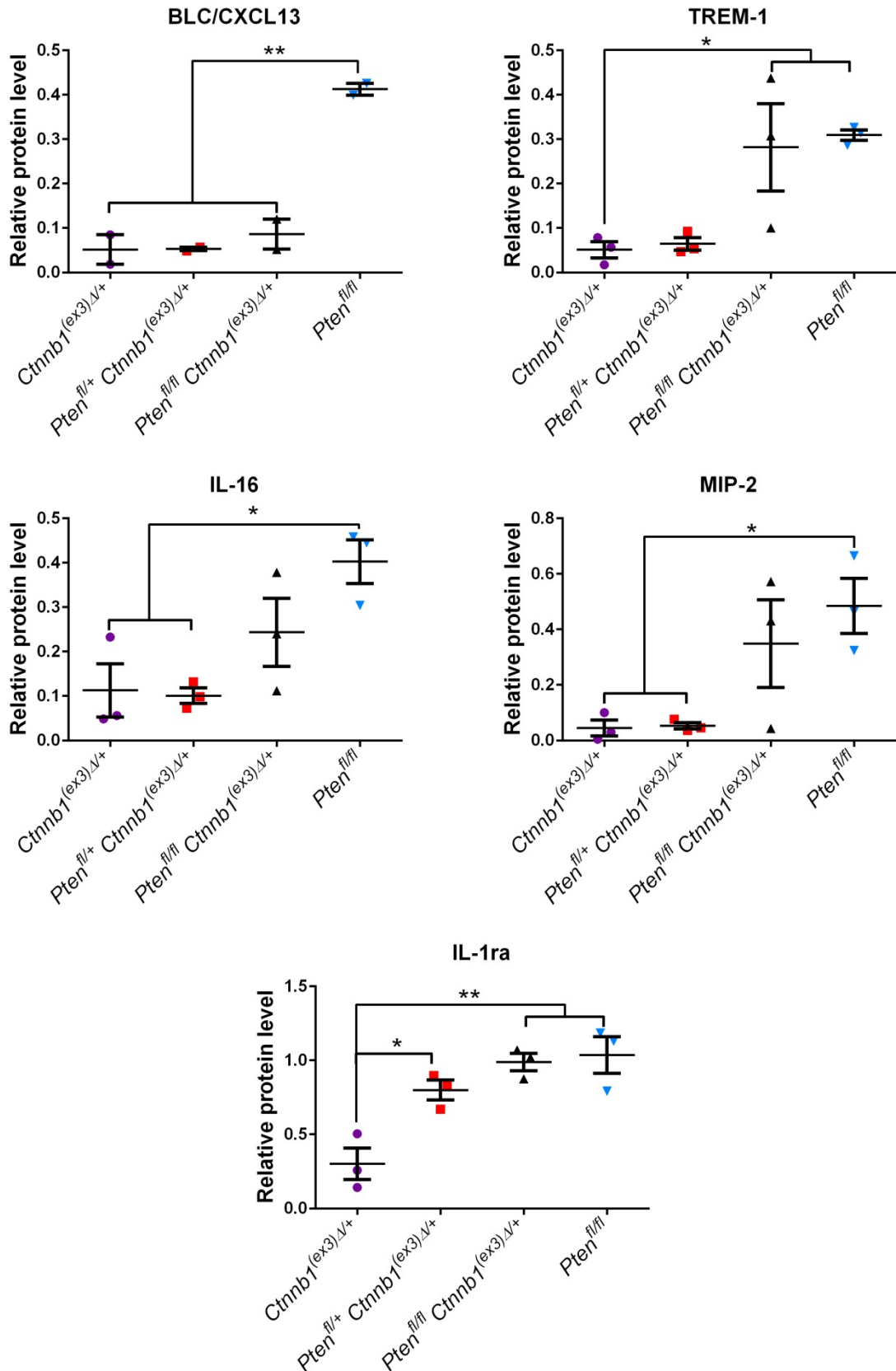


Figure 3.4.9 Cytokines BLC/CXCL13, TREM-1, IL-16, MIP-2 and IL-1ra differ significantly between *Pten* loss- and β -catenin-driven prostate tumours

ImageJ was used for densitometry analysis of spots 1-5 annotated in the cytokine array blots in Figure 3.4.8. Graphs show the relative protein levels of BLC/CXCL13, TREM-1, IL-16, MIP-2 and IL-1ra cytokines in *Pb-Cre Ctnnb1^{(ex3)Δ/+}*, *Pb-Cre Pten^{fl/+} Ctnnb1^{(ex3)Δ/+}*, *Pb-Cre Pten^{fl/fl} Ctnnb1^{(ex3)Δ/+}* and *Pb-Cre Pten^{fl/fl}* endpoint prostate tumour tissue. Results show analysis of n=3 cytokine arrays for each tumour genotype. (** P < 0.01, * P < 0.05; analysed by one-way ANOVA, with Tukey multiple comparison test). Data presented as mean \pm SEM.

ImageJ densitometry analysis was used to quantify the levels of these cytokines in each tumour. The most striking difference observed was the 4-fold increase in BLC levels in *Pten^{fl/fl}* tumours compared to the three other genotypes (Figure 3.4.9). This suggested that increased levels of BLC were a consequence of Pten loss in prostate tumours, while the presence of β -catenin activation, alone or in addition to heterozygous or homozygous *Pten* loss, prevented upregulation (or instigated downregulation) of BLC.

Low levels of TREM-1 were expressed in *Ctnnb1^{(ex3) Δ /+}* and *Pten^{fl/+} Ctnnb1^{(ex3) Δ /+}* tumours, while increased expression of TREM-1 was observed in *Pten* null tumours with and without β -catenin activation. However, there was a large standard deviation in TREM-1 expression in *Pten^{fl/fl} Ctnnb1^{(ex3) Δ /+}* tumours. The expression of IL-16 and MIP-2 in these tumours followed a similar pattern. The only cytokine which showed a difference in expression between *Ctnnb1^{(ex3) Δ /+}* and *Pten^{fl/+}* (or *Pten^{fl/fl}*) *Ctnnb1^{(ex3) Δ /+}* was IL-1ra; increased IL-1ra expression was associated with Pten loss whether alone or in combination with β -catenin activation (Figure 3.4.9).

Overall, low levels of BLC, TREM-1, IL-16, MIP-2 and IL-1ra were associated with β -catenin activation, while high expression of these cytokines was associated with Pten loss. Their expression pattern varied in tumours harbouring both mutations. Our data suggest that expression of certain cytokines is dictated by the underlying genetic mutations driving prostate cancer. These are likely to contribute to different phenotypes observed in prostate cancers, such as the increased percentage of cystic tumour infiltrate in *Pten^{fl/fl}* compared to *Ctnnb1^{(ex3) Δ /+}* tumours, and host-tumour interactions that may influence cancer response to therapy. Further work is necessary to characterise the role of intra-tumoural immune cells and the pro- and anti-tumourigenic effects associated with cytokine expression, to understand how the immune response is modulated during β -catenin-driven cancer initiation and progression.

3.5 Discussion

Concurrent aberrations in the canonical Wnt signalling pathway and PI3K/Akt signalling pathway leads to aggressive prostate cancer with poor prognosis [41, 100]. Our data demonstrate that aberrant activation of Wnt/ β -catenin signalling is sufficient to drive prostate tumourigenesis in mice. *Pten* status determines the latency of these tumours and β -catenin activation co-operates with *Pten* loss, in a dose-dependent manner, to drive the survival and proliferation of cancer cells. Thus, complete *Pten* loss and concurrent β -catenin activation generates the most aggressive prostate cancer and poorest host survival outcome.

There is extensive evidence that PTEN loss results in PI3K/Akt pathway activation [108] and activation of pro-survival signals, such as survivin [190], whereas Wnt/ β -catenin pathway activation drives pro-proliferative signals via downstream targets, such as *Myc* [130, 133]. Consistent with the literature, we observe elevated Akt activation and expression of survivin following *Pten* loss in prostate tissue, and increased proliferation when β -catenin was activated. Levels of phospho-Akt, survivin and cell proliferation were increased in *Pten*^{f1/+} *Ctnnb1*^{(ex3) Δ /+} prostate tissue compared to controls. In this way, *Pten* loss and β -catenin activation co-operate: *Pten* loss provides a survival advantage to cells via PI3K/Akt activation, while β -catenin activation is able to drive cell proliferation.

In prostate cells with β -catenin activation, we observed great pressure on cells to modulate *Pten* and employ mechanisms to downregulate its expression in order for cancer to progress. We have elucidated a mechanism by which β -catenin signalling modulates *Pten* localisation, via increased ROS production, to overcome *Pten* tumour suppression. At early stages of tumourigenesis, β -catenin activation correlates with increased ROS and nuclear accumulation of phospho-*Pten*. While *Pten* mRNA expression in *Ctnnb1*^{(ex3) Δ /+} prostates at 6 months was comparable to *wildtype*, protein levels were increased due to stabilisation of *Pten* following phosphorylation. Elevated ROS has previously been shown to promote phosphorylation and nuclear accumulation of PTEN, resulting in PTEN/p53 mediated tumour suppression [110, 112]. Quenching of ROS in prostate cells with heterozygous loss of *Pten* overcame *Pten*/p53-mediated

growth arrest leading to increased proliferation and development of PIN lesions, which corroborates previous work from our laboratory [110]. In this context, ROS promotes phosphorylation and stabilisation of Pten, while there is also sufficient inhibition of PI3K/Akt. In the absence of ROS, cells overcome growth arrest and proliferate, leading to Akt activation in a large number of cells. Conversely, NAC treatment in *Cttnb1*^{(ex3) Δ /+} mice decreases proliferation and halts tumour progression.

This observation is supported by previous reports of ROS-dependent proliferation of intestinal stem cells following Wnt/ β -catenin pathway activation and accumulation of nuclear β -catenin [182]. Myant et al. demonstrated that elevation of pro-proliferative ROS, downstream of β -catenin activation, arises via activation of Rac-GEFs, Tiam1 and Vav3. The upregulation of Rac-GEF expression activates the Rac1-GTPase and NOX signalling complex, increasing ROS production. Indeed, we have confirmed that *Tiam1* and *Vav3* mRNA levels, together with levels of Rac1-GTP and ROS, are increased in *Cttnb1*^{(ex3) Δ /+} prostate tissue during stages of cancer initiation. Thus, after Cre-mediated recombination of *Cttnb1*^{(ex3) Δ /+} in prostate cells, there is a wave of proliferation driven by the activation of β -catenin, Tiam1, Vav3 and Rac1-GTP, which elevate ROS production.

In the context of β -catenin activation, the dominant effect of increased ROS is pro-proliferative, demonstrated by the abrogation of proliferation and loss of nuclear β -catenin and phospho-Akt expression in NAC-treated *Pb-Cre Cttnb1*^{(ex3) Δ /+} mice. A reduction in nuclear β -catenin staining was also observed in NAC-treated *Pten*^{f1/+} *Cttnb1*^{(ex3) Δ /+} prostate tissue, despite *Pten* haploinsufficiency. In this way, ROS appears to be required for the proliferation of cells with nuclear β -catenin. ROS-mediated proliferation in *Cttnb1*^{(ex3) Δ /+} prostate cells seems counterintuitive to the simultaneous ROS-mediated accumulation of nuclear Pten, which promotes p53-mediated growth arrest. However, the increase in nuclear Pten relieves Pten phosphatase-mediated inhibition of PI3K/Akt signalling at the cell membrane. Activation of low levels of phospho-Akt is sufficient for cell survival, while β -catenin activation drives cell cycle progression and proliferation [133, 135], leading to evasion of Pten tumour suppression (Figure 3.5.1).

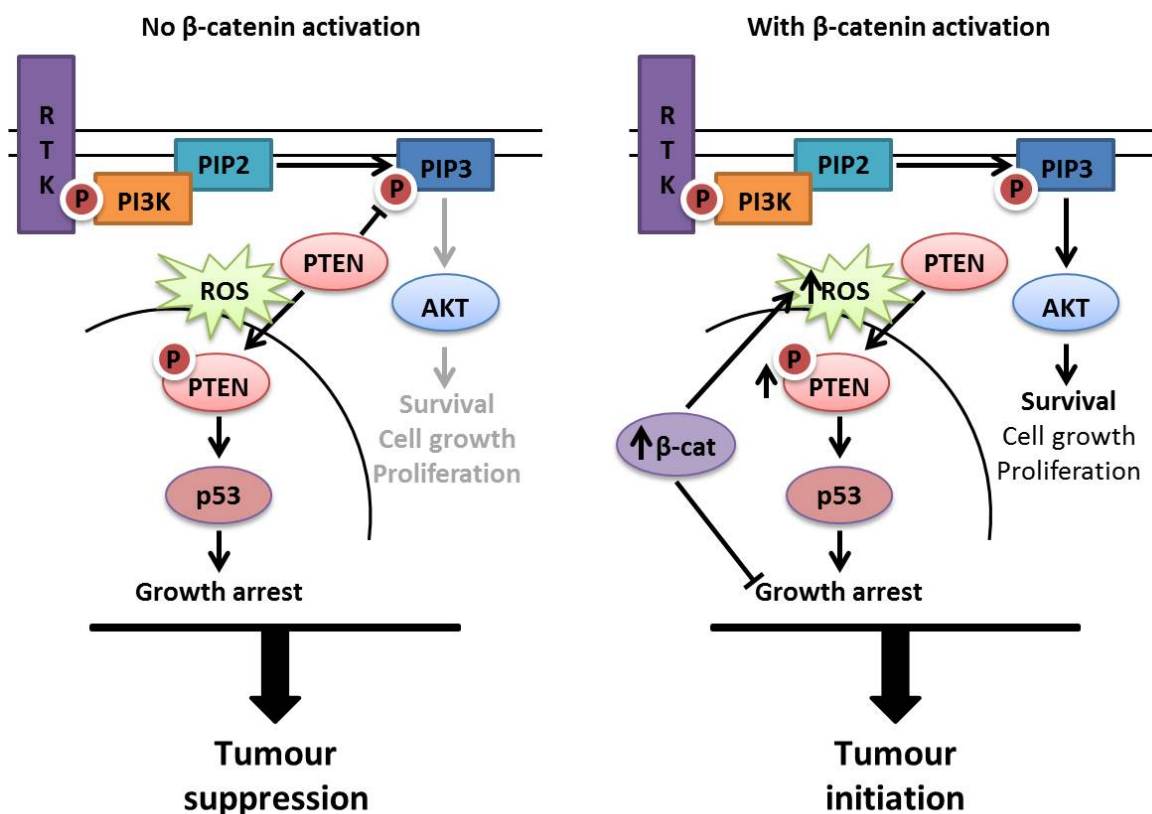


Figure 3.5.1 β -catenin activation modulates Pten localisation to overcome tumour suppression

Schematic illustrating the ROS-mediated mechanism by which β -catenin activation drives Pten nuclear localisation, facilitating Akt activation and cell survival, and leading to tumour initiation. RTK = receptor tyrosine kinase; PI3K = Phosphoinositide-3-kinase; PIP2 = phosphatidylinositol (4,5)-kinase; PIP3 = phosphatidylinositol (3,4,5)-kinase; Akt = protein kinase B; β -cat = β -catenin; ROS = reactive oxygen species.

While Pten/p53-mediated growth arrest is insufficient to stop tumourigenesis, it is likely to be responsible for delayed cancer progression and longer latency of tumours in *Pb Cre Ctnnb1^{(ex3) Δ /+}* mice. Therefore, concurrent heterozygous deletion of *Pten* relieves tumour suppression, via PI3K/Akt activation and reduced growth arrest, and co-operates with β -catenin activation, decreasing tumour latency and host survival (Figure 3.5.2).

Following initial evasion of Pten tumour suppression mechanisms by modulation of Pten localisation, we observed progressive loss of *Pten* expression in tumours driven by β -catenin activation alone (Figure 3.5.2). This may be partly due to changes in *Pten* at the genomic level as there was a decrease in DNA copy number in the epithelium compared to stroma of advanced-stage *Ctnnb1^{(ex3) Δ /+}* prostate tumours, indicating potential heterozygosity at the *Pten* gene locus (Figure 3.5.3). Therefore, at this point *Ctnnb1^{(ex3) Δ /+}* tumours may become

genotypically similar to early stages of *Pten*^{fl/+} *Cttnb1*^{(ex3) Δ /+} tumours. In addition, we identified increased expression of *microRNAs* 17, 18a, 19b and 21 in *Cttnb1*^{(ex3) Δ /+} prostate tumour tissue during later stages of cancer progression, correlating with reduced *Pten* expression (Figure 3.5.3). These miRNAs are known to negatively regulate *PTEN* expression and their aberrant expression has been implicated in various cancer types, including prostate cancer [111]. Increased expression of *miR-18a* in response to β -catenin/Myc activation has been reported in a breast cancer study [124] and β -catenin/STAT signalling is reported to up-regulate *miR-21* expression [191]. Preliminary data, from ICG-001 inhibition of β -catenin/TCF transcriptional activity in CP1 cells, suggest that increased *miR-17* expression may be a direct consequence of β -catenin activity, but further work is required to confirm whether β -catenin directly regulates *miR-17*, -18a, -19b and -21 in this prostate cancer model.

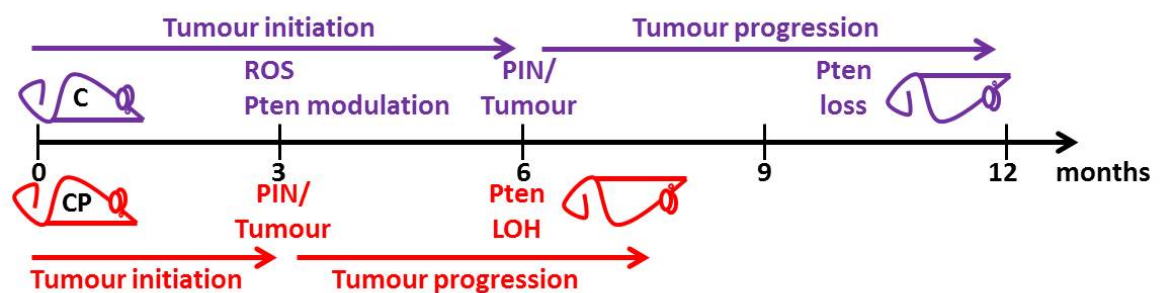


Figure 3.5.2 *Pten* status determines the latency of β -catenin-driven prostate cancer

Timeline of events involved in prostate tumour initiation and progression to clinical endpoint in *Pb-Cre Cttnb1*^{(ex3) Δ /+} (C) and *Pb-Cre Pten*^{fl/+} *Cttnb1*^{(ex3) Δ /+} (CP) mice. *Pten* loss = monoallelic *Pten* deletion and *Pten* mRNA downregulation; LOH = loss of heterozygosity.

In tumours with *Pten* haploinsufficiency and β -catenin activation, we observed a significant decrease in *Pten* expression, lower than levels expected from heterozygous *Pten* loss. We established that this was due to LOH in *Pten*, a common event in human prostate cancer, which tends to occur in late-stage tumours [41, 99, 117]. We hypothesise that the increased dependence cells have on *Pten*-mediated tumour suppression, following β -catenin activation, initially drives *Pten* transcription and puts pressure on the remaining *Pten* allele. Highly transcribed DNA will retain an open chromatin structure and is more likely to be damaged, leading to loss of the remaining functional *Pten* allele. It would be interesting to test whether further passaging of CP4 cells would eventually result in loss of *Pten* expression. If this were the case, we could study

differences between *Pten* positive and *Pten* negative passages to understand the mechanism for *Pten* LOH in association with β -catenin activation. Furthermore, β -catenin-driven LOH may not be restricted to *Pten*, and loss of *Pten* can, itself, contribute to aberrations in chromosomal integrity and DNA repair [113], and play a role in genomic instability.

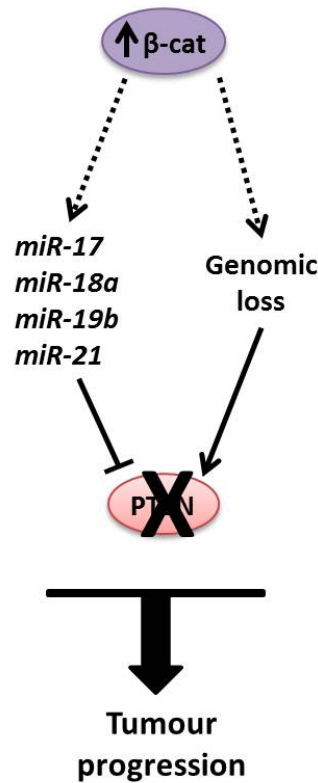


Figure 3.5.3 *Pten* is lost during the evolution of β -catenin-driven prostate cancer

Schematic illustrating that β -catenin activation leads to upregulation of *Pten*-regulatory microRNAs and genomic deletion of *Pten*, which result in *Pten* loss in advanced β -catenin-driven prostate cancer.

Pten LOH may provide some explanation for the variation in *Pten*^{fl/+} *Cttnb1*^{(ex3) Δ /+} prostate weights compared to *Cttnb1*^{(ex3) Δ /+} at 6 months. Although, analysis by Mann Whitney test showed a significant trend towards increased weight of *Pten*^{fl/+} *Cttnb1*^{(ex3) Δ /+} prostates, a number of samples were of similar weight to *Cttnb1*^{(ex3) Δ /+} prostates. Therefore, it is likely that the rate of *Pten* LOH in *Pten*^{fl/+} *Cttnb1*^{(ex3) Δ /+} prostate tumours is non-uniform, resulting in heterogeneity of *Pten* levels between tumours, which will influence the level of endogenous *Pten* tumour suppression and the stage of tumour progression. This hypothesis can be tested using fluorescence *in-situ* hybridisation (FISH) to compare *Pten* LOH between different sizes of *Pten*^{fl/+} *Cttnb1*^{(ex3) Δ /+} tumours at 6

months. Variations in the rate of *PTEN* LOH and tumour evolution are likely to contribute to *PTEN* haplodiploidy and heterogeneity observed in clinical samples.

Our work demonstrates that *Pten* loss occurs during tumour evolution (Figure 3.5.2), as a consequence of β -catenin activation, and provides an explanation (Figure 3.5.3) for the significant co-occurrence of nuclear β -catenin and *PTEN* loss in clinical samples. From mouse *in vivo* studies, we know that *Pten* loss does not depend on β -catenin activation to drive tumorigenesis [138]. I have shown that β -catenin activation regulates signalling events upstream of *Pten* and does depend on *Pten* loss to drive tumorigenesis. By increasing our understanding of how β -catenin modulates *Pten* tumour suppression, we may be able to identify methods to prevent *Pten* loss and halt tumour progression in β -catenin-driven prostate cancer.

To further investigate the pathway co-operation observed between *PTEN*/*PI3K* and *Wnt*/ β -catenin signalling, we studied the tumour-intrinsic and -extrinsic events involved in initiation and progression of β -catenin-driven prostate cancer. Murine prostate tumours with concurrent β -catenin activation and *Pten* loss are characterised by increased *mTOR* signalling. It is well established that *Pten* loss can upregulate *mTOR* signalling via *Akt* activation [185] but increased circulatory *Wnt* can also lead to *mTOR* activation via loss of *GSK3B* activity, preventing *TSC1/2* phosphorylation and relieving *mTOR* inhibition [192]. If co-operation between *Wnt*/ β -catenin pathway activation and *Pten* loss is driving *mTOR* signalling, *mTOR* may be a good target for therapy in this model. However, work in our laboratory failed to show inhibition of tumour growth in CP1 orthotopic tumours treated with *mTORC1/2* inhibitor (data not shown). Furthermore, it has previously been shown that transgenic mice with concurrent *AKT1* and *MYC* activation, or *MYC* activation alone, developed prostate tumours that were resistant to *mTOR* inhibitors [193], and a recent study revealed that *mTOR* inhibitors can in fact promote tumour growth and survival by providing an alternative source of nutrients to highly catabolic cancer cells [194]. This suggests β -catenin-driven tumours are highly adaptable to nutrient-depletion and evade dependence on *mTOR* activity for cell growth and energy metabolism.

Increased *AMPK* signalling, *PKA* pathway activation and expression of genes involved in *cAMP* biosynthesis and lipid metabolism were observed in prostate

tissue with β -catenin activation, irrespective of genomic *Pten* loss. Up-regulation of *Adcy8* is likely to generate increased levels of cAMP and AMP, resulting in both PKA and AMPK pathway activation [195], which we observe in β -catenin-driven prostate cancer. PKA activation inhibits glycogen and lipid synthesis and regulates a number of pathways contributing to cell survival and proliferation [187]. AMPK is activated by a decrease in ATP production and positively regulates fatty acid oxidation and lipolysis [195]. Activation of these pathways correlates with an increase in *Apoc4* and *Pnlprp2* expression, which play respective roles in stabilisation and solubilisation of lipoproteins for lipid metabolism and cholesterol transport [188], and in fat digestion and absorption [189]. Therefore, β -catenin-driven tumours enhance lipid metabolism due to higher energy requirements for cell survival and proliferation. If lipid and cholesterol uptake and metabolism are important for β -catenin-driven tumourigenesis, it is likely that conditions such as obesity and hypertension could be potential etiological factors in prostate cancer. A better understanding of their role may elucidate potential treatments or preventative strategies for β -catenin-driven prostate cancer.

Overall, there were a number of similarities between *Ctnnb1*^{(ex3) Δ /+} and *Pten*^{fl/+} *Ctnnb1*^{(ex3) Δ /+} tumours, indicating β -catenin's role as a driver mutation in prostate tumourigenesis. This included significant upregulation of *Defa20*, which is released from neutrophils as part of innate immune response [186], highlighting the involvement of tumour extrinsic factors and immune system interaction in β -catenin-driven tumourigenesis. To understand the pro-tumourigenic co-operation between Wnt/ β -catenin and PI3K/Akt pathway activation, we need to investigate the 203 genes differentially expressed in *Ctnnb1*^{(ex3) Δ /+} and *Pten*^{fl/+} *Ctnnb1*^{(ex3) Δ /+} prostate tumours, together with their associated pathways. Initial analysis of pathway enrichment has identified further tumour extrinsic events arising from co-operation between β -catenin activation and *Pten* loss that may contribute to development and progression of these tumours.

The significant enrichment of immune response pathways, in particular the classical, alternative and lectin-induced complement pathways, in advanced *Pten*^{fl/+} *Ctnnb1*^{(ex3) Δ /+} tumours was not observed in advanced *Ctnnb1*^{(ex3) Δ /+} tumours. The classical complement pathway is activated by antibody-antigen

complexes, whereas the alternate and lectin pathways are activated, independently of antigen-antibody reactions, in response to pathogens. The complement system forms part of the innate immune response and is involved in initiation of inflammation and host defence [196]. These pathway alterations may have a pro-tumourigenic effect as they are associated with aggressive tumours with short latency.

Furthermore, highly aggressive *Pten*^{fl/fl} *Ctnnb1*^{(ex3)Δ/+} tumours had the most dramatic impact on host immune response, demonstrated by the significant increase in monocytes, neutrophils and eosinophils in the blood of these mice. Systemic effects, such as these, may lead to detrimental effects on the host, and contribute to the underlying cause of prostate cancer-associated mortality.

While rate of tumour progression may impact upon host immune response, the effect of *Pten* loss itself may result in different tumour-host interactions to that of *Ctnnb1*^{(ex3)Δ/+} tumours. In corroboration with this hypothesis, I have shown that BLC/CXCL13, TREM-1, IL-16, MIP-2 and IL-1ra cytokines are all highly expressed in *Pten*^{fl/fl} but not in *Ctnnb1*^{(ex3)Δ/+} tumours. IL-1ra inhibits the effect of pro-inflammatory cytokines, IL1α and IL1β, which are mostly produced by neutrophils and macrophages [197]. Macrophage and neutrophil infiltration occurred during early stages of cancer development in *Ctnnb1*^{(ex3)Δ/+} and *Pten*^{fl/+} *Ctnnb1*^{(ex3)Δ/+} prostate tissue, relative to perturbations in epithelium and PIN development. Thus, it appears *Pten* loss further co-operates with β-catenin activation via tumour extrinsic mechanisms to evade immune response and facilitate tumour progression.

The expression of BLC was unusual in that the presence of *Ctnnb1*^{(ex3)Δ/+} mutation, regardless of *Pten* status, was associated with low levels of BLC/CXCL13, whereas expression was significantly increased in *Pten*^{fl/fl} tumours in the absence of β-catenin activation. The release of BLC/CXCL13 recruits B lymphocytes to tissue and is known to be expressed by tumour-associated myofibroblasts in human prostate cancer. Furthermore BLC/CXCL13 expression is positively associated with clinical severity [198]. Given that the clinical severity is greater in *Pten*^{fl/+} *Ctnnb1*^{(ex3)Δ/+} and *Pten*^{fl/fl} *Ctnnb1*^{(ex3)Δ/+} mouse models than *Ctnnb1*^{(ex3)Δ/+} or *Pten*^{fl/fl} alone, it is interesting that this does not correlate with BLC/CXCL13 expression and warrants further investigation.

In addition to heterogeneity of *Pten* LOH between tumours, already discussed, extrinsic factors are likely to contribute to the variations I observed in the rate of *Pten*^{fl/+} *Ctnnb1*^{(ex3) Δ /+} tumour development between mice. This may be attributed to the mixed background of mice, which is arguably more representative of human prostate cancer. It would be interesting to correlate *Pten* status with the expression of extrinsic factors, such as the chemokine IL-1ra, which may positively correlate with *Pten* loss and stage of tumour progression.

In summary, I have shown that concurrent activation of β -catenin and *Pten* loss drive aggressive prostate cancer *in vivo*. I have identified that β -catenin-driven tumourigenesis is dependent on overcoming *Pten*-mediated tumour suppression and loss of *Pten* occurs during evolution of these tumours. β -catenin activation and *Pten* loss drive tumourigenesis through co-operation between pro-survival and pro-proliferative tumour intrinsic signalling events, as well as up-regulation of cell growth, energy and lipid metabolism pathways. Furthermore, I provide evidence of tumour extrinsic co-operation between β -catenin activation and *Pten* loss via cytokines and mechanisms of immune response modulation.

Chapter 4 - Activation of β -catenin promotes treatment-resistant prostate cancer

4.1 Introduction

Androgen receptor (AR) signalling is integral to prostate homeostasis and the development of prostate cancer. Androgen deprivation therapy (ADT) remains the first-line treatment for locally advanced and metastatic prostate cancer. While the initial response to treatment is favourable, at least 20% of patients stop responding to treatment within 18 months and develop castration-resistant prostate cancer (CRPC). It is vital that we gain a better understanding of the mechanisms involved in the development of resistance to ADT, and the level of heterogeneity between patients. This will enable better stratification of patients for treatment and the identification of targets for intervention therapies, to be used alone or in combination with ADT.

The majority of studies on CRPC use human cell line or xenograft models, along with direct analysis of human prostate cancer tissue. To date, few genetically-engineered mouse models have been established to study CRPC, despite the benefits of studying a model which closely mimics the development and progression of human prostate cancer. One such transgenic mouse model uses the tamoxifen-inducible *Nkx3.1^{CreERT2}* system, developed in Michael Shen's laboratory [23]

The *Nkx3.1* homeobox gene is expressed specifically in the prostate during embryonic development [170]. The non-inducible *Nkx3.1 Cre-loxP* model has been used in our laboratory. However, if the gene undergoing mutation is required for prostate organogenesis, e.g. *β-catenin*, mutation during late-embryogenesis will impact on normal prostate development. The tamoxifen-inducible system overcomes this issue, as Cre-mediated recombination at *loxP* sites can be specifically induced in the adult mouse. Furthermore, induction of genetic alterations at later time points is more realistic of the later-onset of prostate cancer in humans.

Nkx3.1 is expressed in luminal epithelial cells, in contrast to *Probasin*, which is expressed in basal epithelial cells. These gene promoters will therefore drive *Cre* expression in distinct cell populations in our transgenic models. Each has distinct cell markers: p63, cytokeratin 5 and 14 are expressed in basal cells, while cytokeratin 18 and AR expression is characteristic of luminal cells [7].

Expression of both luminal and basal epithelial cell markers have been observed in human prostate cancer [19], meaning that both models are clinically relevant. However, as AR is a luminal cell marker, these cells are more androgen responsive and, hence, more responsive to effects of androgen ablation than *probasin*-expressing basal cells [23]. Thus, the *Nkx3.1 Cre-loxP* transgenic mouse is a good model to study the effects of manipulating AR signalling in prostate cancer.

The tamoxifen-inducible *Nkx3.1^{CreERT2}* system was used to identify castration-resistant *Nkx3.1*-expressing cells (CARNs) as a cell of origin for prostate cancer [23]. This model can be manipulated to interrogate the role of CARNs in CRPC, and provides a means to study prostate-specific targeted genetic alterations and the effects of castration, in different spatial and temporal contexts. Therefore, we established the *Nkx3.1^{CreERT2}* inducible system in our laboratory in order to develop new models for CRPC.

Alterations in Wnt/ β -catenin and PI3K/AKT signalling pathways are significantly enriched in CRPC [99]. A number of studies have shown higher levels of nuclear β -catenin present in CRPC compared to hormone naïve prostate cancer (HNPC) [44, 156]. Alterations in β -catenin protein levels may influence androgen receptor (AR) signalling, through β -catenin's role as an AR cofactor [157], and facilitate the escape from androgen-dependent to androgen-independent prostate cancer following ADT.

We hypothesised that β -catenin is able to reprogram AR signalling, through its role as an AR cofactor, and play a role in the progression of HNPC to castration-resistant disease. Using the tamoxifen-inducible *Nkx3.1^{CreERT2}* system, we have developed a novel CRPC model to study the effects of β -catenin activation (and *Pten* loss) on AR physiology in HNPC and CRPC, and other changes contributing to CRPC.

4.2 Manipulating the $Nkx3.1^{CreERT2}$ transgenic mouse model to study treatment resistant prostate cancer

4.2.1 Optimisation of the tamoxifen induction protocol

In the $Nkx3.1^{CreERT2}$ system, *Cre* is fused to a mutated ligand binding domain of the human oestrogen receptor and placed under the control of the *Nkx3.1* promoter (Figure 4.2.1). Hence, *Cre* is only activated in the presence of tamoxifen and only expressed in *Nkx3.1*-expressing cells. $Nkx3.1^{CreERT2} RFP^{+/-}$ and $Nkx3.1^{CreERT2} Ctnnb1^{(ex3)\Delta/+}$ models (Figure 4.2.1) were used to optimise tamoxifen induction and select the best regime for efficacious induction of *Cre* and excision of floxed alleles.

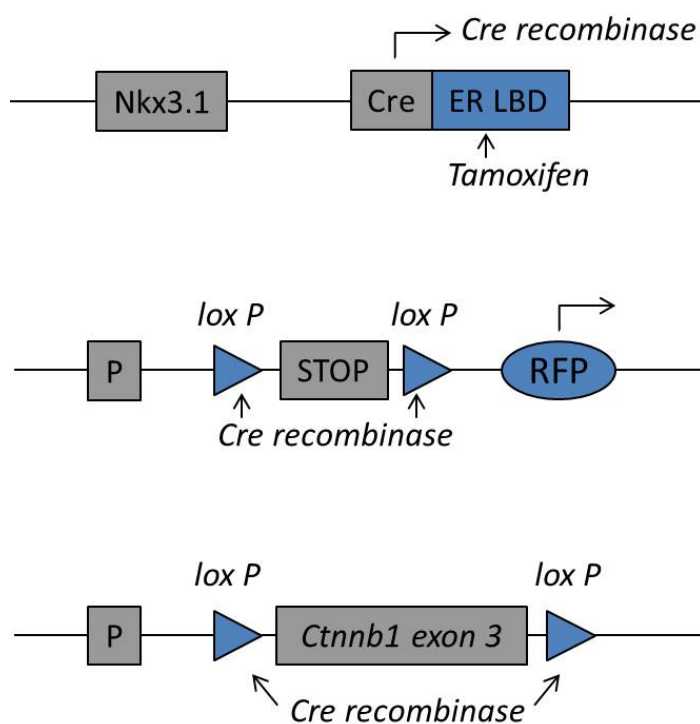


Figure 4.2.1 Schematic of the tamoxifen-inducible $Nkx3.1^{CreERT2}$ *Cre-loxP* system

In this system, a mutated ligand binding domain (LBD) of the human oestrogen receptor (ER) is fused to the *cre* gene, such that the chimeric *cre* is functionally activated following intraperitoneal injection with tamoxifen, and placed under the control of the prostate-specific *Nkx3.1* promoter. Mice expressing RFP ($Nkx3.1^{CreERT2} RFP^{+/-}$) or activated (nuclear) β -catenin ($Nkx3.1^{CreERT2} Ctnnb1^{(ex3)\Delta/+}$) were used for optimisation of the tamoxifen-induction protocol. In the $Nkx3.1^{CreERT2} RFP^{+/-}$ model, *loxP* sites are present either side of a stop cassette upstream of the *RFP* transgene. On expression of *cre recombinase*, the *loxP* sites are cleaved and the *RFP* transgene is expressed. In the $Nkx3.1^{CreERT2} Ctnnb1^{(ex3)\Delta/+}$ model, *loxP* sites are present either side of *exon3* of the β -catenin gene, resulting in the heterozygous deletion of *exon3* and activation of β -catenin following expression of *cre*.

Successful induction of *Cre* expression in the *Nkx3.1^{CreERT2} RFP^{+/-}* model results in the cleavage of *loxP* sites either side of a STOP cassette that prevents the expression of *RFP*. Removal of this STOP cassette facilitates RFP expression, which can be detected by fluorescence imaging (IVIS) and immunohistochemical staining. In the *Nkx3.1^{CreERT2} Ctnnb1^{(ex3)Δ/+}* model, successful *Cre* induction and recombination led to the loss of *Ctnnb1* exon3 and stabilisation of nuclear β -catenin, which can be detected by western blot analysis and immunohistochemical staining.

The published induction regime for *Nkx3.1^{CreERT2}* mice used one intraperitoneal injection of 225 mg/kg tamoxifen [23]. This induced efficient recombination when tested in *Nkx3.1^{CreERT2} RFP^{+/-}* mice (Figure 4.2.2A); however, mice did not tolerate this high dose well. We therefore tested three other regimes with lower doses of tamoxifen: 1) 120 mg/kg (3 mg) on day one and 90 mg/kg (2 mg) on days two to four (3,2,2,2 regime); 2) four doses of 160 mg/kg (4 mg) over 11 days, administered on Thursday/Monday/Thursday/Monday (4 mg T/M/T/M regime); and 3) one dose of 160 mg/kg (4 mg). In our colony, the average weight of male mice at 12 weeks was 25 g. We calculated doses accordingly (shown above in brackets), which were administered to all mice.

Unfortunately, IVIS fluorescence imaging of live *Nkx3.1^{CreERT2} RFP^{+/-}* mice could not detect RFP expression *in vivo*. However, we used the IVIS to image fluorescence in dissected prostates from mice sacrificed two weeks post-induction, and detected RFP expression following induction with the 3,2,2,2 regime (Figure 4.2.2B) and T/M/T/M regime (Figure 4.2.2C). We further confirmed RFP expression following the T/M/T/M regime using immunohistochemical staining, which correlated with the level of RFP detected by fluorescence imaging (Figure 4.2.2).

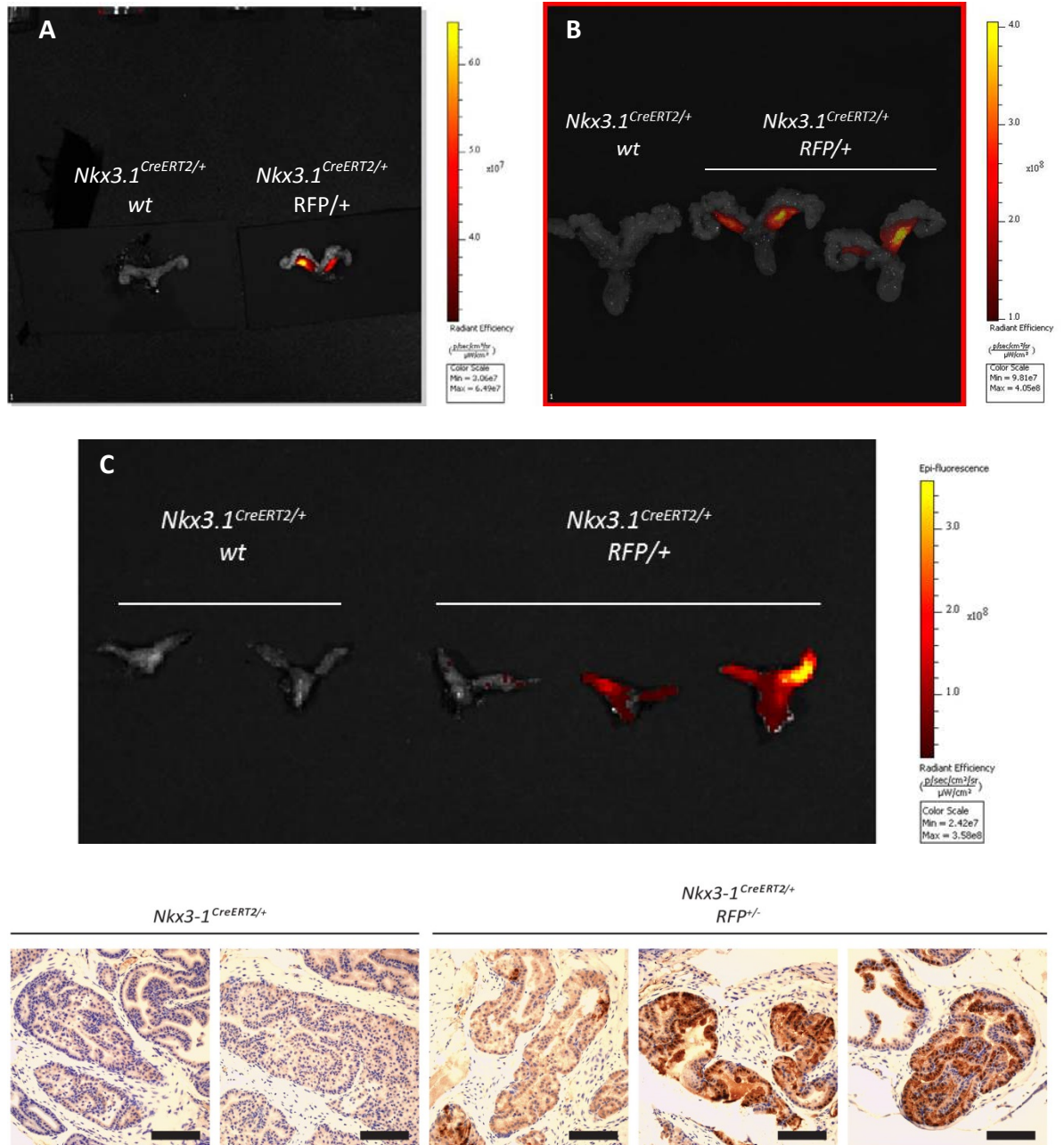


Figure 4.2.2 Detection of RFP expression in $Nkx3.1^{CreERT2}$ RFP^{+/-} prostate tissue following tamoxifen induction

Fluorescence imaging of the dissected prostate, using an *in vivo* imaging system (IVIS), detects recombination and expression of RFP in $Nkx3.1^{CreERT2}$ expressing cells two weeks after the following tamoxifen regimes: (A) 225mg/kg once; (B) 120mg/kg tamoxifen on day 1, followed by three doses of 90mg/kg on consecutive days (3,2,2,2 regime); (C) four doses of 160mg/kg over 11 days (4 mg T/M/T/M regime). The IHC images show representative staining for RFP, corresponding to prostates in C. Scale bar: 100 μm .

We detected expression of mutant ($\Delta Ex3$) β -catenin protein by western blot analysis following all induction regimes (Figure 4.2.3), showing that *exon3* of the *Ctnnb1* gene had been successfully deleted. Densitometry analysis showed comparable levels of expression following 3,2,2,2 and T/M/T/M regimes and slightly lower expression following the 4 mg once regime (Figure 4.2.3). When we carried out immunohistochemical analysis of nuclear β -catenin expression in tissue sections from the same prostates, we observed the highest levels in both anterior and dorsal-lateral prostate of mice induced by the T/M/T/M regime (Figure 4.2.4).

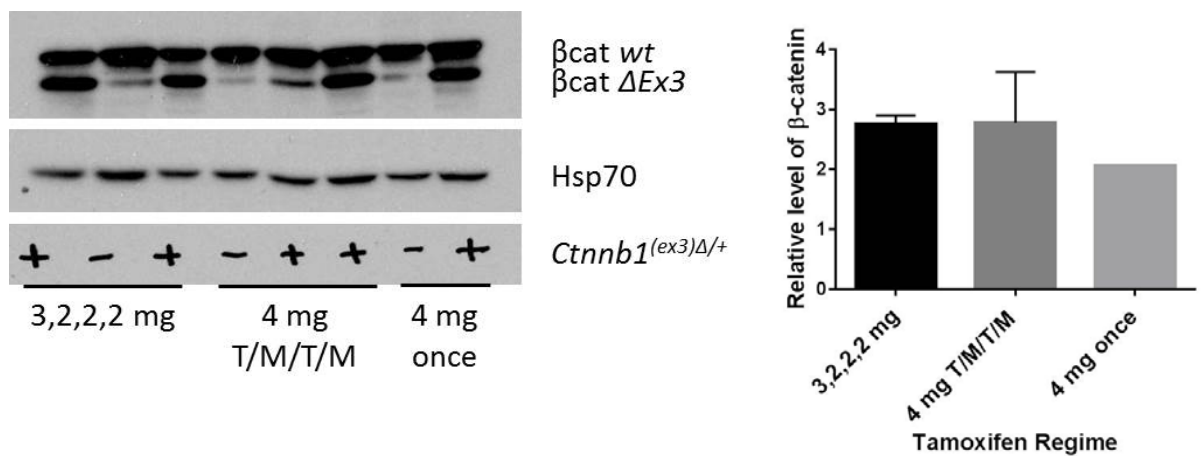


Figure 4.2.3 Detection of β -catenin exon 3 deletion in *Nkx3.1^{CreERT2} Ctnnb1^{(ex3) Δ /+}* prostate tissue following tamoxifen induction

Western blot analysis of *wildtype* and *exon3* mutant β -catenin levels in protein extracted from *Nkx3.1^{CreERT2} wildtype* and *Nkx3.1^{CreERT2} Ctnnb1^{(ex3) Δ /+}* prostate tissue two weeks after the following tamoxifen regimes: 120 mg/kg (3 mg) tamoxifen on day 1, followed by three doses of 90 mg/kg (2 mg) on consecutive days (3,2,2,2 regime); four doses of 160 mg/kg (4 mg) over 11 days (T/M/ T/M regime); and 160 mg/kg (4 mg) once. The amount in brackets corresponds to the dose given to a 25 g mouse. The level of β -catenin $\Delta Ex3$ bands was quantified relative to Hsp70 loading control using ImageJ.

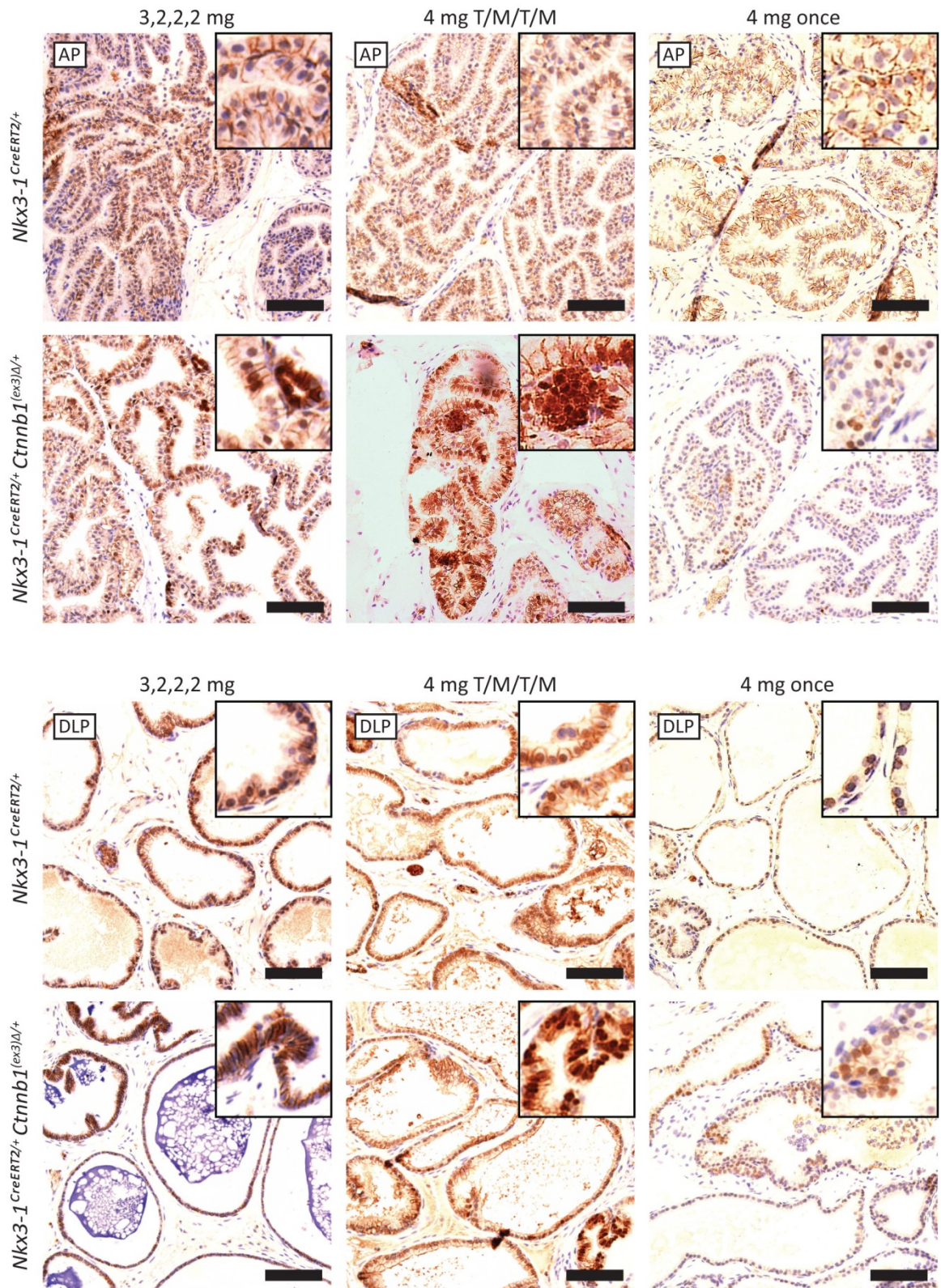


Figure 4.2.4 Detection of β -catenin activation in $Nkx3.1^{CreERT2} Ctnnb1^{(ex3)\Delta/+}$ prostate tissue following tamoxifen induction

Representative images of β -catenin immunohistochemical staining of FFPE sections of $Nkx3.1^{CreERT2}$ wildtype and $Nkx3.1^{CreERT2} Ctnnb1^{(ex3)\Delta/+}$ mouse prostate, two weeks after induction by 3,2,2,2 mg, 4mg T/M/T/M or 4 mg once tamoxifen regimes. The top panel compares levels of nuclear (activated) β -catenin in the anterior prostate (AP) and bottom panel shows the dorsal-lateral prostate (DLP). Scale bar: 100 μ m. Insert box: 100 μ m².

The higher dose of 4 mg injections given four times over 11 days (T/M/T/M regime) was well tolerated by mice and we proceeded to use this induction regime for future work.

We crossed $Nkx3.1^{CreERT2} Ctnnb1^{(ex3)\Delta/+}$ mice with Cre negative $Pten^{fl/fl}$ (or $Pten^{fl/+}$) mice to generate an $Nkx3.1^{CreERT2} Pten^{fl/+} Ctnnb1^{(ex3)\Delta/+}$ colony with respective controls. A limitation of the $Nkx3.1^{CreERT2}$ model is that Cre expression results in the heterozygous loss of $Nkx3.1$ itself, which has been associated with prostate cancer initiation. Therefore, all *wildtype* controls used were $Nkx3.1^{CreERT2}$ positive. Initial histological and immunohistochemical analysis of prostate tissue sampled from mice two months post-induction, showed PIN-like lesions, increased Ki67 staining and high levels of nuclear β -catenin staining in prostates from $Nkx3.1^{CreERT2} Ctnnb1^{(ex3)\Delta/+}$ and $Nkx3.1^{CreERT2} Pten^{fl/+} Ctnnb1^{(ex3)\Delta/+}$ mice, which were not present in $Nkx3.1^{CreERT2}$ *wildtype* and $Nkx3.1^{CreERT2} Pten^{fl/+}$ controls (Fig. 4.2.5). We were, therefore, satisfied that the tamoxifen regime was effective in initiating Cre recombination and prostate tumourigenesis in this model.

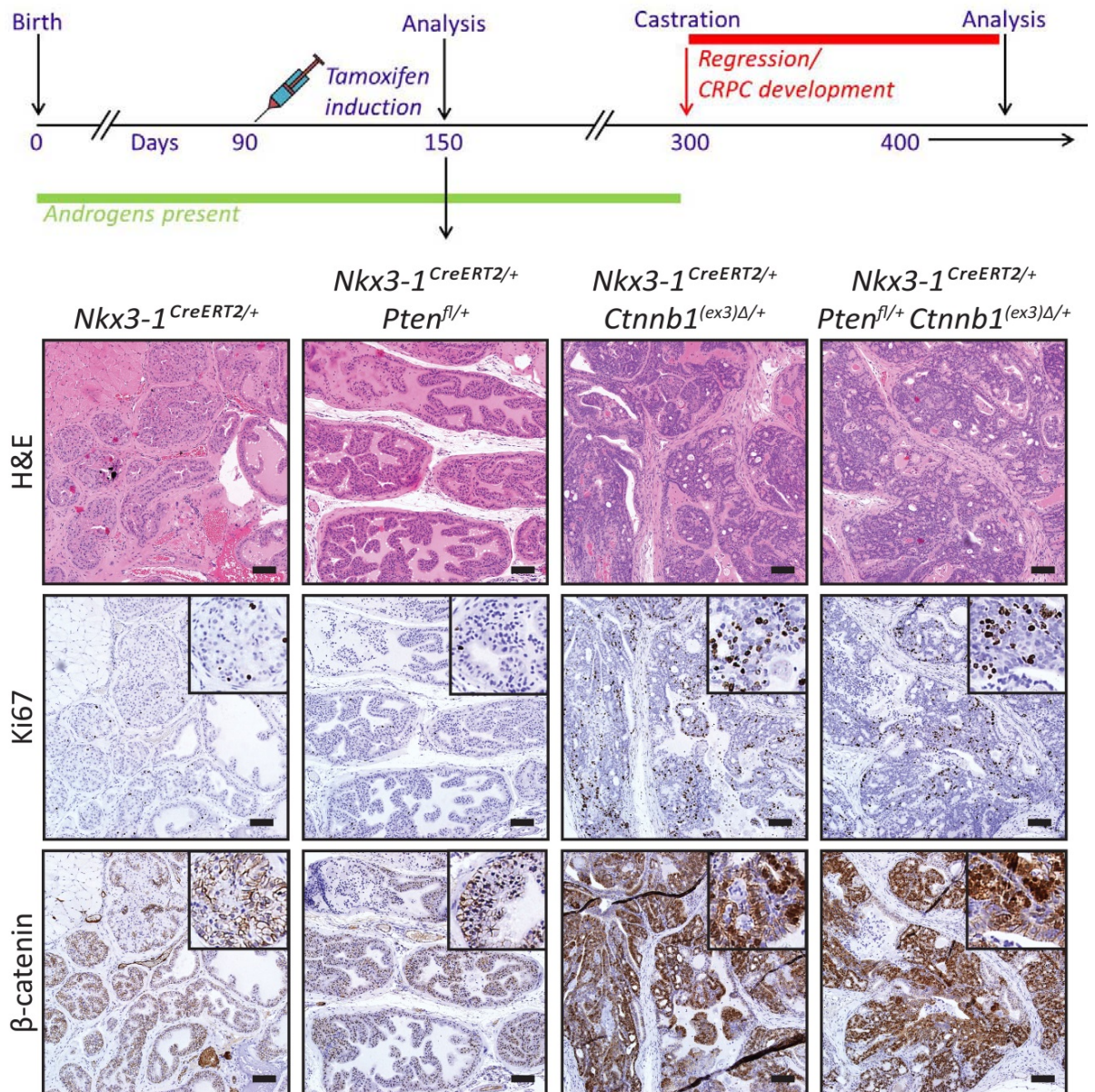


Figure 4.2.5 Using the inducible *Nkx3.1^{CreERT2}* *loxP* system to manipulate *Pten* (*Pten^{fl/+}*) and β -catenin (*Ctnnb1^{(ex3)Δ/+}*) and investigate effects of castration *in vivo*
 Timeline for *cre* induction and castration in *Nkx3.1^{CreERT2} Pten^{fl/+} Ctnnb1^{(ex3)Δ/+}* mice and respective controls. Mice were induced using the 4mg T/M/T/M tamoxifen regime and sacrificed 60 days after tamoxifen induction for histopathological analysis. The panel shows representative haematoxylin and eosin staining, and ki67 and β -catenin immunohistochemical staining of FFPE sections of *Nkx3.1^{CreERT2} wildtype*, *Nkx3.1^{CreERT2} Pten^{fl/+}*, *Nkx3.1^{CreERT2} Ctnnb1^{(ex3)Δ/+}* and *Nkx3.1^{CreERT2} Pten^{fl/+} Ctnnb1^{(ex3)Δ/+}* mouse prostate tissue. Scale bar: 100 μ m. Insert box: 100 μ m².

4.2.2 Nkx3.1 expression is retained in a sub-population of cells in regressed and regenerated prostate

To demonstrate the essential role of androgens for normal prostate growth and homeostasis, the effects of ADT were initially studied in *wildtype* mice. We observed significant regression of normal, adult mouse prostates following ablation of testicular androgens using surgical orchiectomy (Figure 4.2.6).

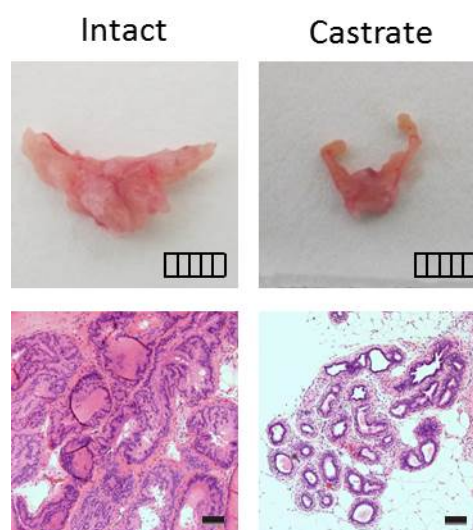


Figure 4.2.6 The effect of castration on wildtype mouse prostate

(Top panels) Representative images of intact and castrate wildtype prostate. Ruler scale: 5 mm. (Bottom panels) Representative haematoxylin and eosin staining showing the histology of FFPE sections of intact and castrate (regressed) prostate. Scale bar: 100 μ m

To study the effects of ADT and replacement of androgens following ADT, a working regression/regeneration model was established. In an initial pilot study, *wildtype* mice were castrated at 8 weeks of age and the prostate was allowed to regress for 6 weeks. A 1 cm Silastic implant containing testosterone propionate (or empty sham control) was inserted subcutaneously between the shoulders 6 weeks after castration, and mice were sampled 4 weeks after the implant was inserted. The size and weight of prostates from castrated (ADT) mice treated with testosterone were over three times greater than control mice with sham implants (Figure 4.2.7). This confirms the prostate's ability to regenerate in the presence of androgens.

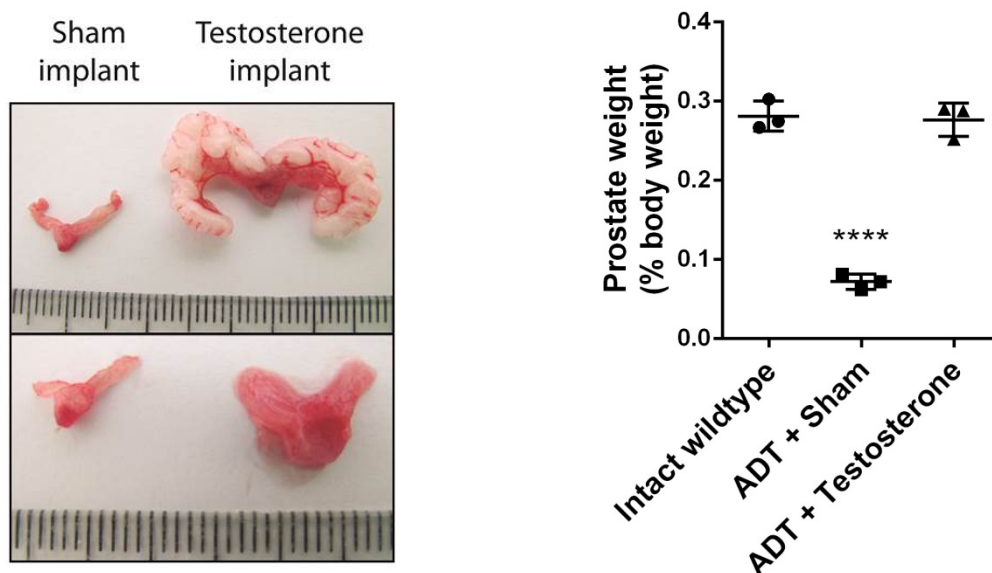


Figure 4.2.7 Manipulating androgen levels to study regression and regeneration of the mouse prostate

Wildtype mice were castrated at 8 weeks and the prostate was allowed to regress for 6 weeks before a 1 cm Silastic implant containing testosterone propionate (or empty sham control) was subcutaneously implanted to regenerate the prostate. Images are representative of the effect of testosterone administration on the prostate 1 month after the Silastic implants were inserted. The top panel of the image shows the regeneration of the seminal vesicles around the anterior prostate and bottom panel shows the regeneration of the dissected prostate compared to the regressed sham control. Ruler scale: 1 mm/increment. The graph shows weights of regenerated prostates as percentage body weight compared to prostates of control mice with sham implant and intact *wildtype* mice. (**** p value <0.0001; n=3, analysed by one-way ANOVA with Tukey multiple comparison test). Data are presented as mean \pm SD.

The *Nkx3.1^{CreERT2} RFP^{+/-}* model was used to study whether *Cre* expression could be induced post-castration and the effect of prostate regeneration after tamoxifen-induction. Following castration, prostates were allowed to regress for 1 month before tamoxifen-induction of *Cre*. Implants containing testosterone propionate (or empty sham control) were then inserted subcutaneously, 18 days after induction, and the experiment was ended one month later. This experiment was carried out in mice at 6-7 months (Figure 4.2.8), corresponding to a time point when most of our murine prostate cancer models have established tumours.

In mice which underwent castration, followed by tamoxifen-induction and insertion of a sham implant, a large proportion of cells in the regressed, androgen ablated prostate expressed RFP (Figure 4.2.8). This demonstrated that *Nkx3.1*-expressing cells remain in the absence of androgens when a majority of AR is inactive, in the cytoplasm, as shown by immunohistochemical staining (Figure 4.2.8). These CARNs are responsive to tamoxifen induction, resulting in expression of *Cre*, recombination at *loxP* and expression of RFP. The reintroduction of androgens regenerated the prostate and reactivated AR, which translocated to the nucleus (Figure 4.2.8). RFP immunohistochemical staining showed that patches of CARNs were present in the regenerated tissue (Figure 4.2.8). This suggests that these are stem cells, capable of regenerating the prostate following reactivation of AR signalling, which commonly occurs in CRPC. Regression and regeneration studies can be carried out in the inducible *Nkx3.1 Cre^{ERT2}* system, to manipulate AR signalling *in vivo*, in combination with induction of prostate-specific genetic alterations at any time point. In this way, we can study the role of CARNs in CRPC.

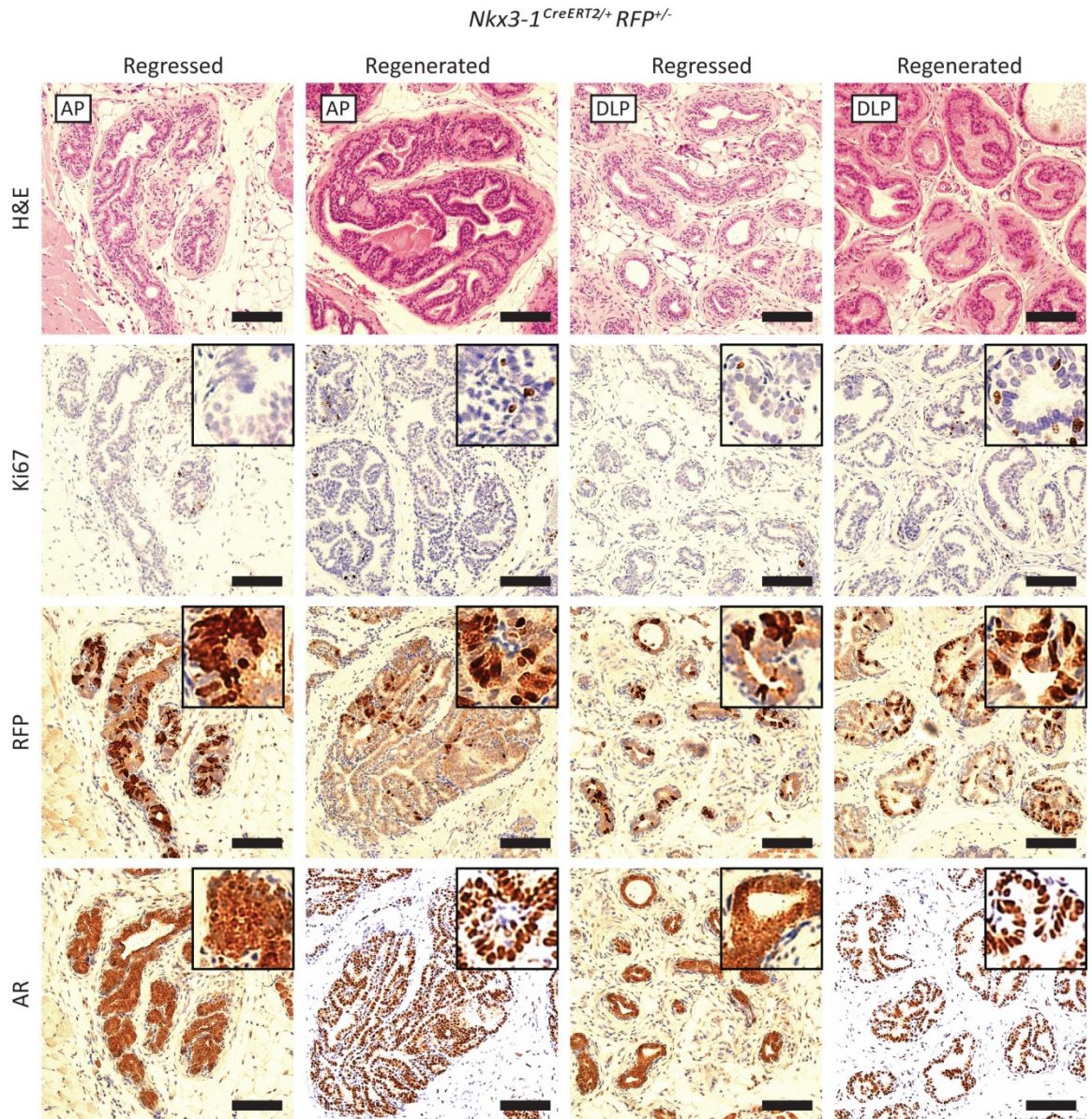
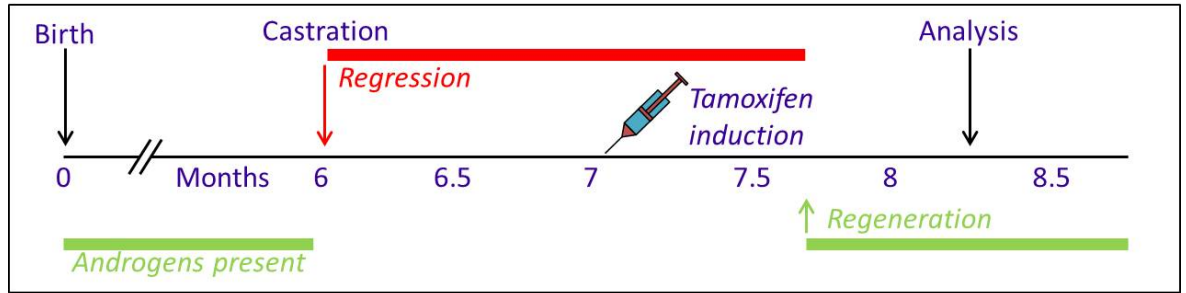


Figure 4.2.8 Detection of castration-resistant *Nkx3.1*-expressing cells (CARNs) in regressed and regenerated prostate

The timeline indicates the protocol used to study the regression and regeneration of *Nkx3.1^{CreERT2} RFP^{+/-}* mouse prostates. Following castration at 6 months, the prostate was allowed to regress for 1 month before administration of tamoxifen to induce expression of RFP. A Silastic implant containing testosterone propionate (or empty sham control) was subcutaneously implanted 18 days after tamoxifen induction to regenerate the prostate. The panel shows representative haematoxylin and eosin staining, and ki67, RFP and AR immunohistochemical staining of FFPE sections of *Nkx3.1^{CreERT2} RFP^{+/-}* mouse prostate tissue. AP=anterior prostate; DLP=dorsal-lateral prostate. Scale bar: 100 μ m. Insert box: 100 μ m².

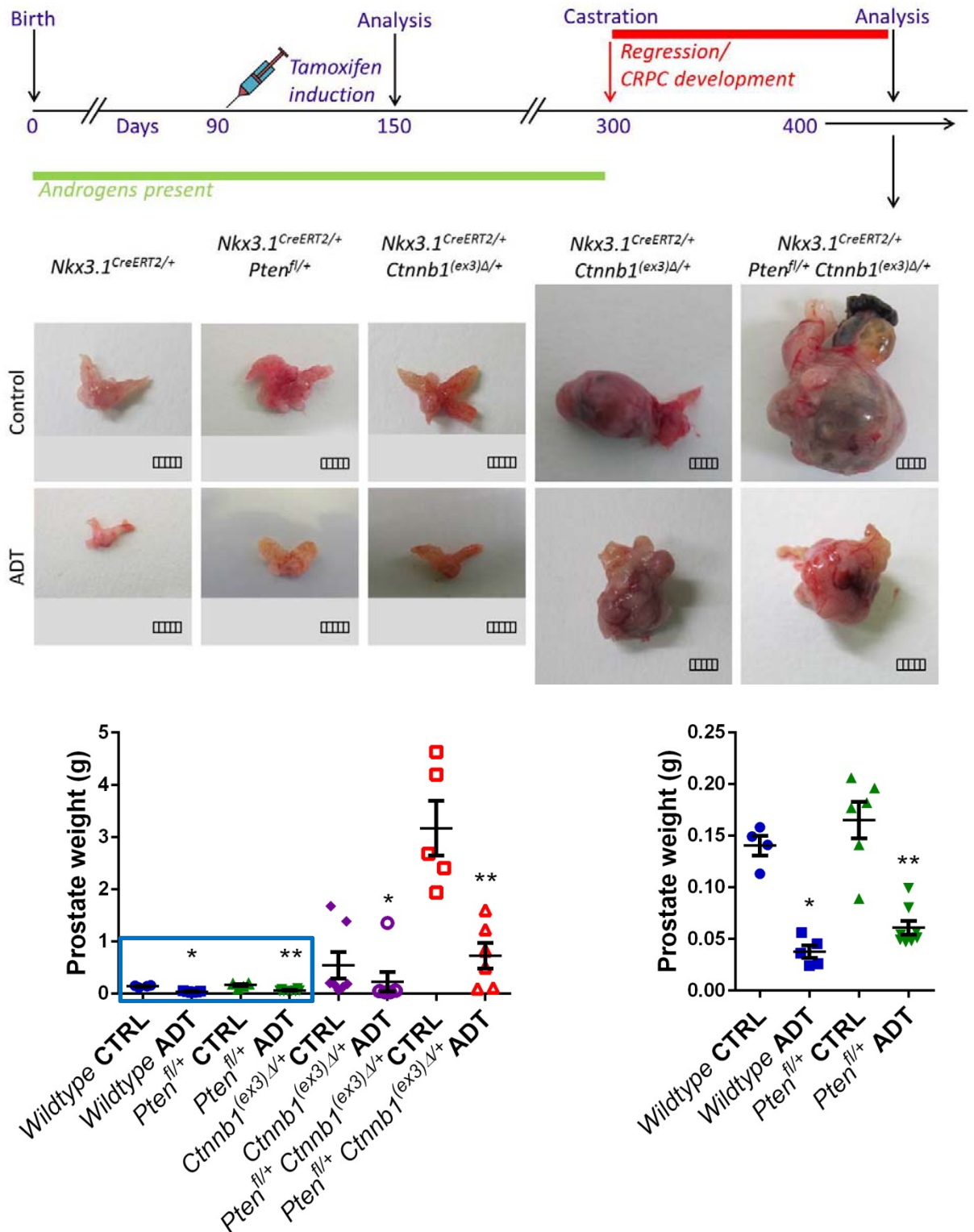
4.3 Tumours with β -catenin activation are resistant to androgen deprivation therapy – a novel pre-clinical model for castration resistant prostate cancer

4.3.1 Investigating the effect of castration in $Nkx3.1^{CreERT2} Pten^{fl/+} Ctnnb1^{(ex3)\Delta/+}$ genetically engineered mouse model

After initial analysis confirmed tumourigenesis as expected in $Nkx3.1^{CreERT2} Pten^{fl/+} Ctnnb1^{(ex3)\Delta/+}$ mice two months post-induction, mice were allowed to age. When palpable tumour was detected in $Nkx3.1^{CreERT2} Pten^{fl/+} Ctnnb1^{(ex3)\Delta/+}$ mice, they were castrated (see timeline; Figure 4.3.1). Palpable tumour was detected at 7 months post-induction (~300 days), so this was the time point established for castration of $Pten^{fl/+} Ctnnb1^{(ex3)\Delta/+}$ mice and controls. Intact and castrated $Pten^{fl/+} Ctnnb1^{(ex3)\Delta/+}$ mice were allowed to age to respective clinical endpoints and compared to age-matched $Nkx3.1^{CreERT2}$ *wildtype*, $Pten^{fl/+}$ and $Ctnnb1^{(ex3)\Delta/+}$ controls.

$Nkx3.1^{CreERT2} Pten^{fl/+} Ctnnb1^{(ex3)\Delta/+}$ mice developed large tumours and reached clinical endpoint approximately one year post-induction due to tumour burden, weight loss and haematuria. Tumours responded to ADT as indicated by the significant decrease in weights compared to controls (Figure 4.3.1). However, sizeable tumour burden remained in four out of six mice post-ADT. *Wildtype*, $Pten^{fl/+}$ and most $Ctnnb1^{(ex3)\Delta/+}$ prostates regressed significantly in response to ADT (Figure 4.3.1). A large tumour was present in only one of five $Nkx3.1^{CreERT2} Ctnnb1^{(ex3)\Delta/+}$ mice post-ADT and only two of five $Nkx3.1^{CreERT2} Ctnnb1^{(ex3)\Delta/+}$ control (without ADT) mice.

The body weight of castrated *wildtype* and $Pten^{fl/+}$ mice decreased significantly compared to intact mice of the same genotype (Figure 4.3.2). Body weight was lost as result of tumour burden in intact $Ctnnb1^{(ex3)\Delta/+}$ and $Pten^{fl/+} Ctnnb1^{(ex3)\Delta/+}$ mice, relative to intact *wildtype* mice. While castration in $Ctnnb1^{(ex3)\Delta/+}$ mice did not have a significant effect on body weight, the majority of castrated $Pten^{fl/+} Ctnnb1^{(ex3)\Delta/+}$ mice did lose weight in comparison to controls, despite overall analysis not showing a significant difference (Figure 4.3.2).



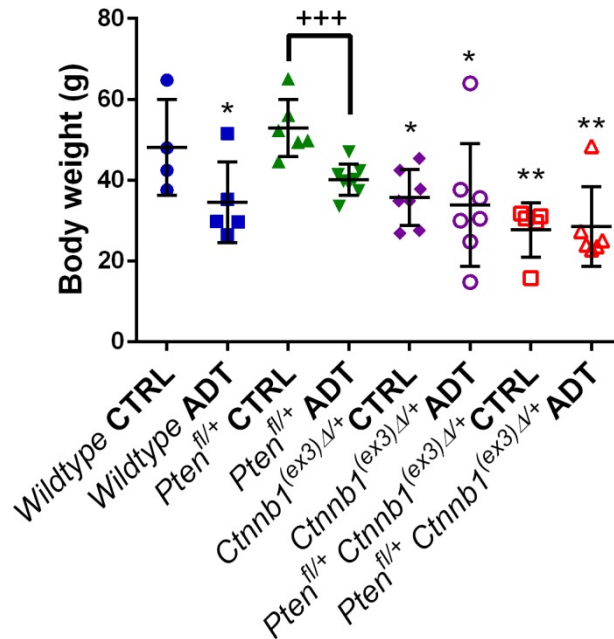


Figure 4.3.2 The effect of ADT on body weight of *Nkx3.1*^{CreERT2} *Pten*^{fl/+} *Ctnnb1*^{(ex3)Δ/+} mice compared to controls

The graph shows body weights of mice after prostate weight (including any tumour infiltrate) has been subtracted. (** p value <0.01, * p value <0.05; analysed by one-way ANOVA with Fisher LCD test, comparing all groups to *wildtype* control. ++ p value <0.01; analysed by Mann-Whitney test). Data are presented as mean ± SEM.

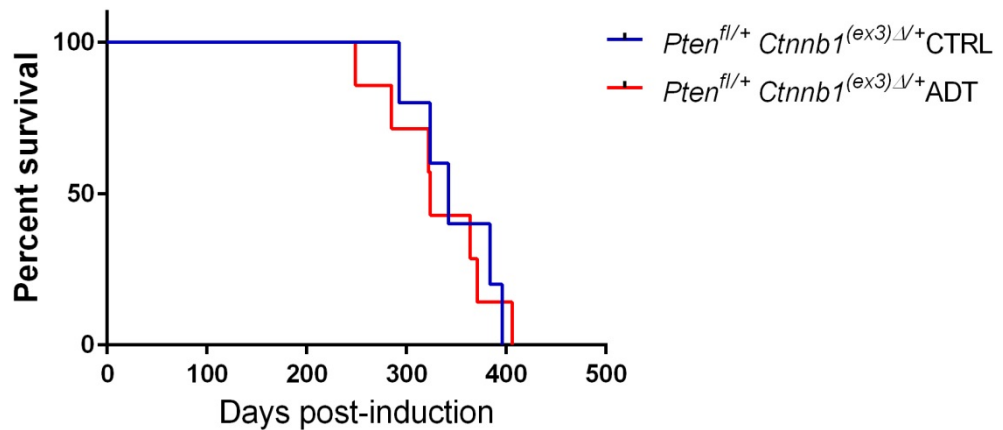


Figure 4.3.3 Treatment of *Nkx3.1*^{CreERT2} *Pten*^{fl/+} *Ctnnb1*^{(ex3)Δ/+} mice with ADT provides no survival benefit

Kaplan-Meier survival plot for *Nkx3.1*^{CreERT2} *Pten*^{fl/+} *Ctnnb1*^{(ex3)Δ/+} mice treated with ADT (n=7) compared to control (n=5).

Pten^{fl/+} *Cttnb1*^{(ex3) Δ /+} mice lived 5-6 months post-ADT but this was comparable to survival of untreated control mice (Figure 4.3.3). Despite decreased tumour burden in *Pten*^{fl/+} *Cttnb1*^{(ex3) Δ /+} mice post-ADT, mice lost weight and became weak and inactive. I, therefore, observed no survival advantage of ADT in these mice. This suggests that the extrinsic effects of prostate tumour burden, prior to ADT, including weight loss, compromise the host's ability to recover regardless of tumour regression in response to ADT.

Histopathological characterisation of prostate tissue, excised from endpoint *Nkx3.1*^{CreERT2} *Pten*^{fl/+} *Cttnb1*^{(ex3) Δ /+} mice and age-matched controls, was conducted to establish whether ADT simply halted tumour growth from the time of castration or if tumour cells were actively proliferating following ADT. In *Nkx3.1*^{CreERT2} *wildtype* prostate, H&E staining showed complete regression of the prostate glands following ADT and no Ki67 expression in control or ADT prostates, while β -catenin continued to be expressed at the membrane of regressed prostate tissue (Figure 4.3.4). *Nkx3.1*^{CreERT2} *Pten*^{fl/+} prostate histology was similar to *wildtype*. There was some evidence of hyperplasia and PIN in *Pten*^{fl/+} prostates but, overall, little Ki67 expression, and prostates regressed in response to ADT. In contrast, *Cttnb1*^{(ex3) Δ /+} control mice all developed carcinoma to varying extents. The central panel (Figure 4.3.4) shows the histology of a small *Cttnb1*^{(ex3) Δ /+} control prostate tumour, expressing Ki67 and nuclear β -catenin, and the histology of regressed ADT-treated *Cttnb1*^{(ex3) Δ /+} prostate tissue, which expressed little Ki67 but retained some cells with nuclear β -catenin expression. The *Cttnb1*^{(ex3) Δ /+} panel to the right (Figure 4.3.4) shows the histology of more advanced HNPC and established CRPC driven by β -catenin activation alone, which was similar to *Nkx3.1*^{CreERT2} *Pten*^{fl/+} *Cttnb1*^{(ex3) Δ /+} prostate tissue. Ki67 immunohistochemical staining identified increased proliferation in epithelial cells within the CRPC tumours and high levels of nuclear β -catenin compared to controls (Figure 4.3.4). This illustrated that cells with β -catenin activation were actively proliferating following ADT.

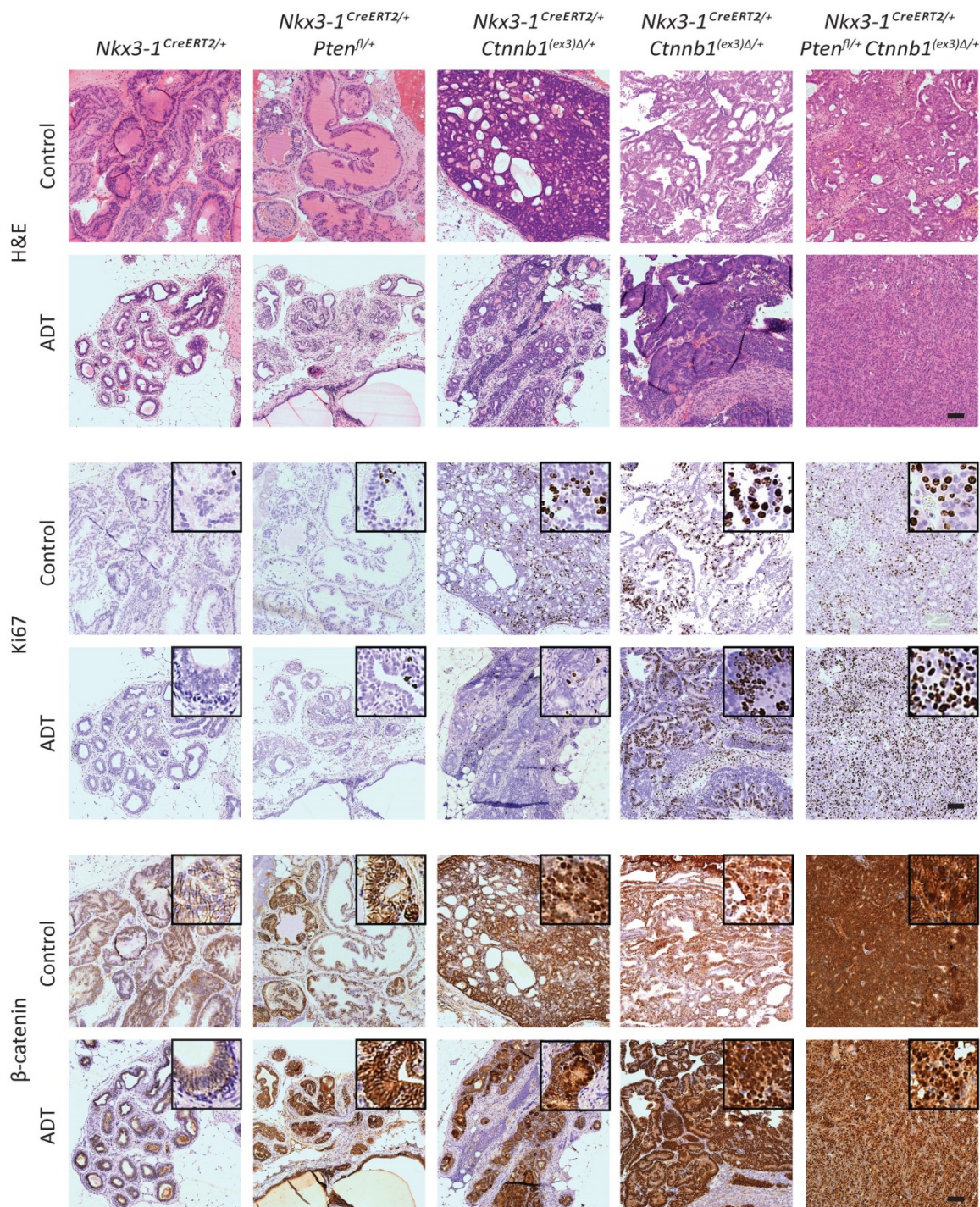


Figure 4.3.4 *Nkx3.1^{CreERT2} Pten^{fl/+} Ctnnb1^{(ex3)Δ/+}* mice develop aggressive adenocarcinoma and maintain high levels of proliferation following ADT

Representative haematoxylin and eosin staining, and ki67 and β-catenin immunohistochemical staining of FFPE sections of *Nkx3.1^{CreERT2} wildtype*, *Nkx3.1^{CreERT2} Pten^{fl/+}*, *Nkx3.1^{CreERT2} Ctnnb1^{(ex3)Δ/+}* and *Nkx3.1^{CreERT2} Pten^{fl/+} Ctnnb1^{(ex3)Δ/+}* comparing mouse prostate tissue from ADT treated mice to controls at clinical endpoint. To illustrate the variation observed in *Nkx3.1^{CreERT2} Ctnnb1^{(ex3)Δ/+}* control and ADT mice, two representative images are included. Left *Ctnnb1^{(ex3)Δ/+}* column represents 60% of control and 80% of ADT-treated *Ctnnb1^{(ex3)Δ/+}* prostate tissue; right *Ctnnb1^{(ex3)Δ/+}* column represents 40% of controls and 20% of cases with detectable CRPC. Scale bar: 100 μm. Insert box: 100 μm².

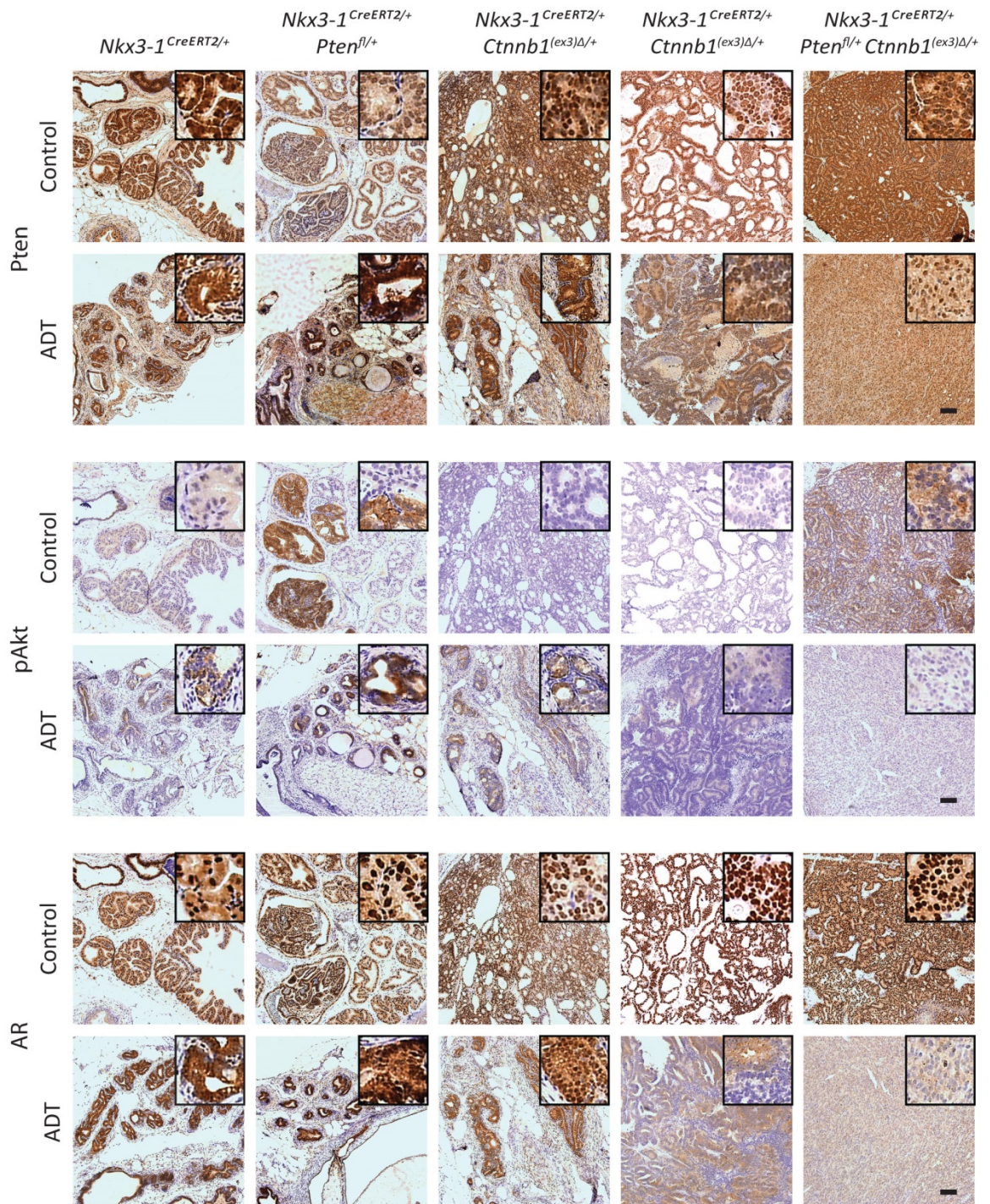


Figure 4.3.5 Growth of *Nkx3.1*^{CreERT2} *Pten*^{fl/+} *Ctnnb1*^{(ex3)Δ/+} castration-resistant tumours is not dependent on PI3K/Akt or classical androgen receptor signalling

Representative Pten, pAkt and AR immunohistochemical staining of FFPE sections of *Nkx3.1*^{CreERT2} wildtype, *Nkx3.1* *Cre*^{ERT2} *Pten*^{fl/+}, *Nkx3.1* *Cre*^{ERT2} *Ctnnb1*^{(ex3)Δ/+} and *Nkx3.1* *Cre*^{ERT2} *Pten*^{fl/+} *Ctnnb1*^{(ex3)Δ/+} mouse prostate tissue comparing ADT treated mice to controls at clinical endpoint. To illustrate the variation observed in *Nkx3.1*^{CreERT2} *Ctnnb1*^{(ex3)Δ/+} control and ADT mice, two representative images are included. Left *Ctnnb1*^{(ex3)Δ/+} column represents 60% of control and 80% of ADT-treated *Ctnnb1*^{(ex3)Δ/+} prostate tissue; right *Ctnnb1*^{(ex3)Δ/+} column represents 40% of controls and 20% of cases with detectable CRPC. Scale bar: 100 μm. Insert box: 100 μm².

Immunohistochemical staining of regressed prostate tissue from ADT-treated *Nkx3.1^{CreERT2} wildtype* mice, compared to controls, showed decreased Pten, increased phospho-Akt and loss of nuclear AR expression (Figure 4.3.5). In *Nkx3.1^{CreERT2} Pten^{fl/+}* prostate tissue, Pten haploinsufficiency led to increased phospho-Akt expression in intact mice, which was retained following castration (Figure 4.3.5). Corroborating data from the *Pb-Cre Ctnnb1^{(ex3)Δ/+}* mouse model (Chapter 3), high levels of nuclear Pten were present in *Nkx3.1^{CreERT2} Ctnnb1^{(ex3)Δ/+}* prostate tissue at earlier stages of tumour development (central panel, Figure 4.3.5) and decreased in advanced cancer (right panel, Figure 4.3.5), providing evidence for similar tumour evolution in this mouse model. *Ctnnb1^{(ex3)Δ/+}* prostates that regressed in response to ADT showed a modest increase in phospho-Akt expression and some nuclear AR expression, neither of which were present in CRPC (Figure 4.3.5).

Compared to intact controls, castration-resistant *Nkx3.1^{CreERT2} Pten^{fl/+} Ctnnb1^{(ex3)Δ/+}* tumours had lower Pten expression but no phospho-Akt activation (Figure 4.3.5). Furthermore, AR expression was completely lost (Figure 4.3.5). Therefore, β-catenin remains active and is able to sustain tumour proliferation in the absence of androgens, without reactivating classical androgen receptor signalling or requiring PI3K/Akt pathway activation.

4.3.2 The *Nkx3.1^{CreERT2} Pten^{fl/fl} Ctnnb1^{(ex3)Δ/+}* mouse model develops aggressive castration-resistant prostate cancer

In the *Pb-Cre* conditional transgenic mouse model, β-catenin exon3 mutation (*Ctnnb1^{(ex3)Δ/+}*) in combination with homozygous deletion of Pten (*Pten^{fl/fl}*) generated a very aggressive prostate cancer model (Chapter 3). I established *Nkx3.1^{CreERT2}* mice with the same mutations to investigate effects of ADT in a more aggressive model. Palpable tumour was detected at 5 months post-induction. One group of mice underwent castration at this time point, while the control group were untreated. Both groups were allowed to age to their respective clinical endpoints, determined by tumour burden, weight loss and haematuria.

ADT did provide a survival advantage for $Nkx3.1^{CreERT2} Pten^{fl/fl} Ctnnb1^{(ex3)\Delta/+}$ mice, which survived approximately 3 months longer than controls (Figure 4.3.6). However, at clinical endpoint, ADT-treated mice had developed CRPC and their tumour weight and body weight was comparable to control mice with HNPC (Figure 4.3.6).

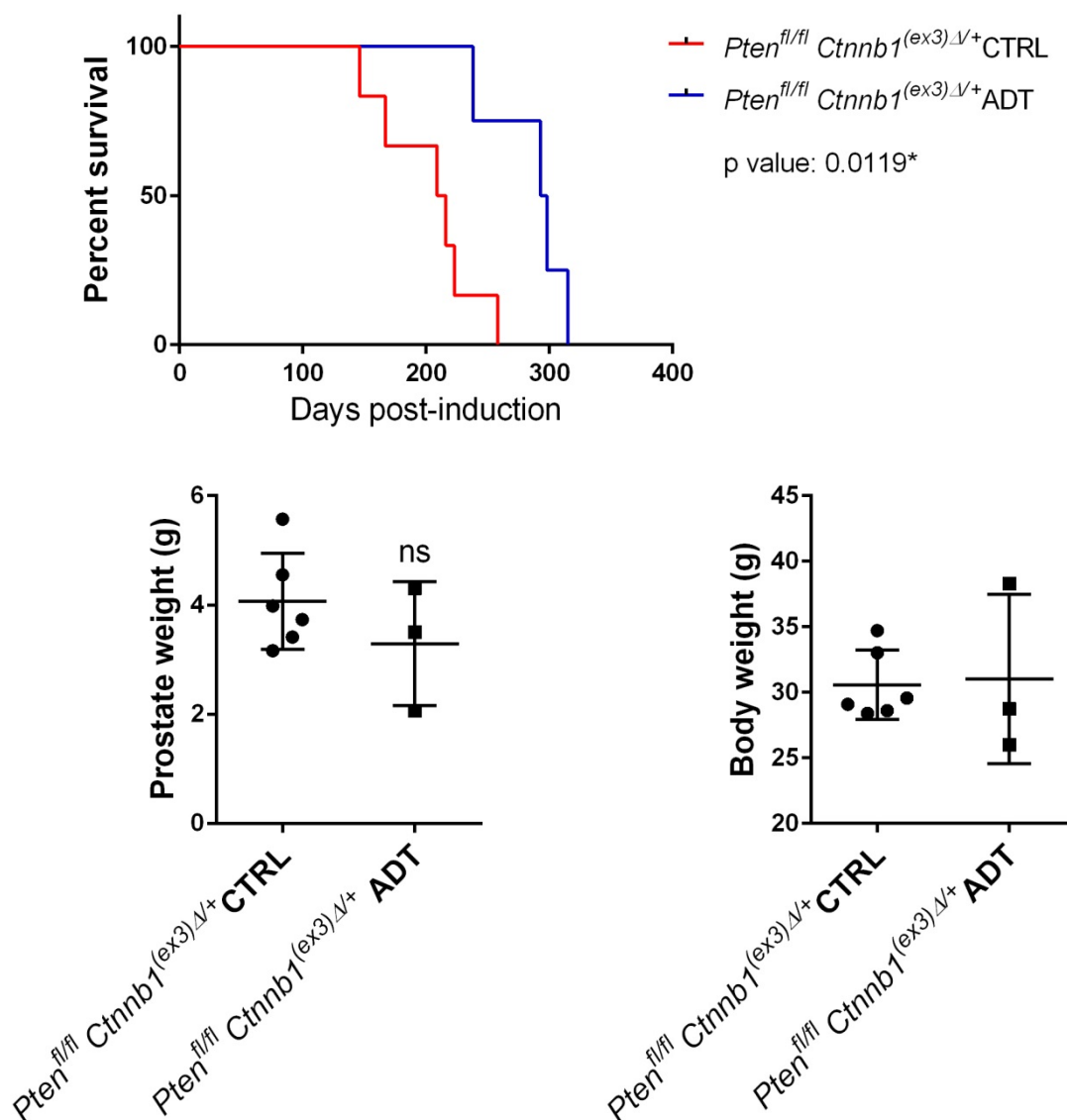


Figure 4.3.6 ADT increases survival in $Nkx3.1^{CreERT2} Pten^{fl/fl} Ctnnb1^{(ex3)\Delta/+}$ mice but tumour burden is comparable at endpoint

Kaplan-Meier survival plot for $Nkx3.1^{CreERT2} Pten^{fl/fl} Ctnnb1^{(ex3)\Delta/+}$ mice treated with ADT (n=4) compared to control (n=6) shows a significant increase in survival following ADT. (P = 0.0119; analysed by log-rank (Mantel-Cox) test). The graphs show prostate tumour weights (drained of any tumour infiltrate), and body weights of mice after prostate weight (including any tumour infiltrate) has been subtracted. Data are presented as mean \pm SD.

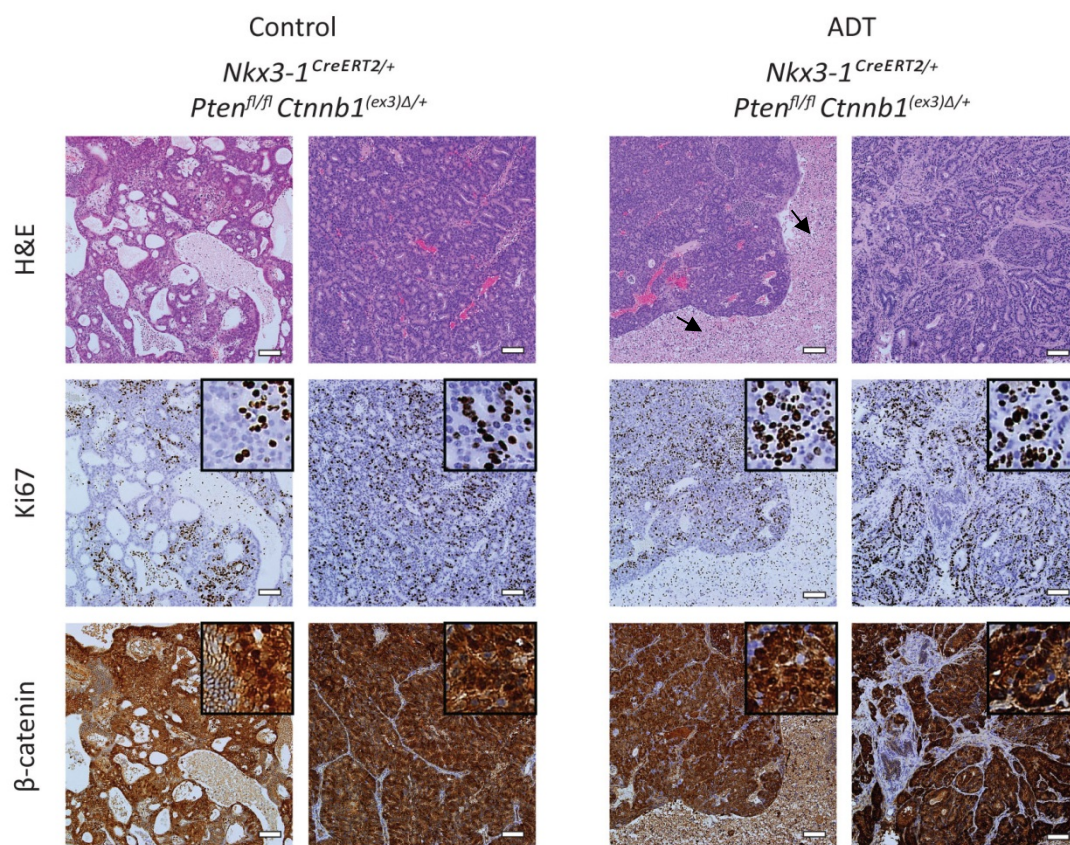


Figure 4.3.7 Castration-resistant *Nkx3.1^{CreERT2} Pten^{fl/fl} Ctnnb1^{(ex3)Δ/+}* tumours have increased stroma area, high levels of proliferation and maintain high levels of nuclear β -catenin. Haematoxylin and eosin staining, and ki67 and β -catenin immunohistochemical staining of FFPE sections of *Nkx3.1^{CreERT2} Pten^{fl/fl} Ctnnb1^{(ex3)Δ/+}* mouse prostate tissue, comparing ADT treated mice to controls at clinical endpoint. The two images for each set are representative of different areas observed in the tumours. Arrows indicate increased stromal area in *Pten^{fl/fl} Ctnnb1^{(ex3)Δ/+}* CRPC. Scale bar: 100 μ m. Insert box: 100 μ m².

Histopathological analysis of these tumours showed different tumour morphology following ADT. Control tumours had a greater number of regions with pockets of cystic fluid (left control H&E panel, Figure 4.3.7), while an expansion of stroma was observed in ADT-resistant tumours (left ADT H&E panel, Figure 4.3.7). Levels of proliferation (Ki67) were comparable between tumours and cells harbouring intense nuclear β -catenin were present throughout tumour epithelium of control and ADT-resistant tumours (Figure 4.3.7).

4.3.3 Transcriptomic analysis of gene expression changes associated with castration-resistant tumours highlighted increased expression of Wnts

To gain a better understanding of the differences between HNPC and CRPC driven by β -catenin activation and *Pten* loss, we performed RNA-sequencing (≥ 6 Gb, 90 nucleotide paired-end reads) and transcriptomic analysis on RNA from hormone-naïve and castration-resistant *Nkx3.1^{CreERT2} Pten^{fl/+} Ctnnb1^{(ex3) Δ /+}* tumours. Quality control analysis of RNA-sequencing data showed there was ~85% alignment to the mouse genome for all samples. Following data normalisation and differential gene expression analysis using R and DESeq2 software, we identified 422 genes that were at least twofold ($P < 0.05$) upregulated and 291 genes at least twofold ($P < 0.05$) downregulated in CRPC tumours compared to HNPC. MetaCore pathway analysis of these data indicated that one of the most significantly enriched pathways in CRPC was the Wnt signalling pathway (Pathway 5, Figure 4.3.8). This included increased expression of Wnt ligands, canonical Wnt pathway transcription factors, Tcf and Lef, and downstream target, Cyclin D1 (Figure 4.3.9).

Despite the primary difference between CRPC and HNPC mice being the ablation of androgens, androgen receptor nuclear signalling was number 16 in the list of most significantly altered pathways (Figure 4.3.8). Therefore, the downregulation of AR signalling was not as significant as the alteration of other pathways in this model of CRPC. Wnt expression and Cyclin D1 negatively regulate AR (Figure 4.3.10) and may prevent the reactivation of classical AR signalling in this model.

To confirm Wnt signalling was activated in prostate tissue with β -catenin *exon3* deletion, I quantified expression of Wnt target genes in *Nkx3.1^{CreERT2} Pten^{fl/+} Ctnnb1^{(ex3) Δ /+}* HNPC and *wildtype*, *Pten^{fl/+}* and *Ctnnb1^{(ex3) Δ /+}* controls. *Tcf3* and *Adcy8* expression was increased in *Pten^{fl/+} Ctnnb1^{(ex3) Δ /+}* compared to controls (Figure 4.3.11). *Adcy8* was also upregulated in *Ctnnb1^{(ex3) Δ /+}* compared to *wildtype*, while no difference in *Ccnd1* or *Myc* expression were observed (Figure 4.3.11).

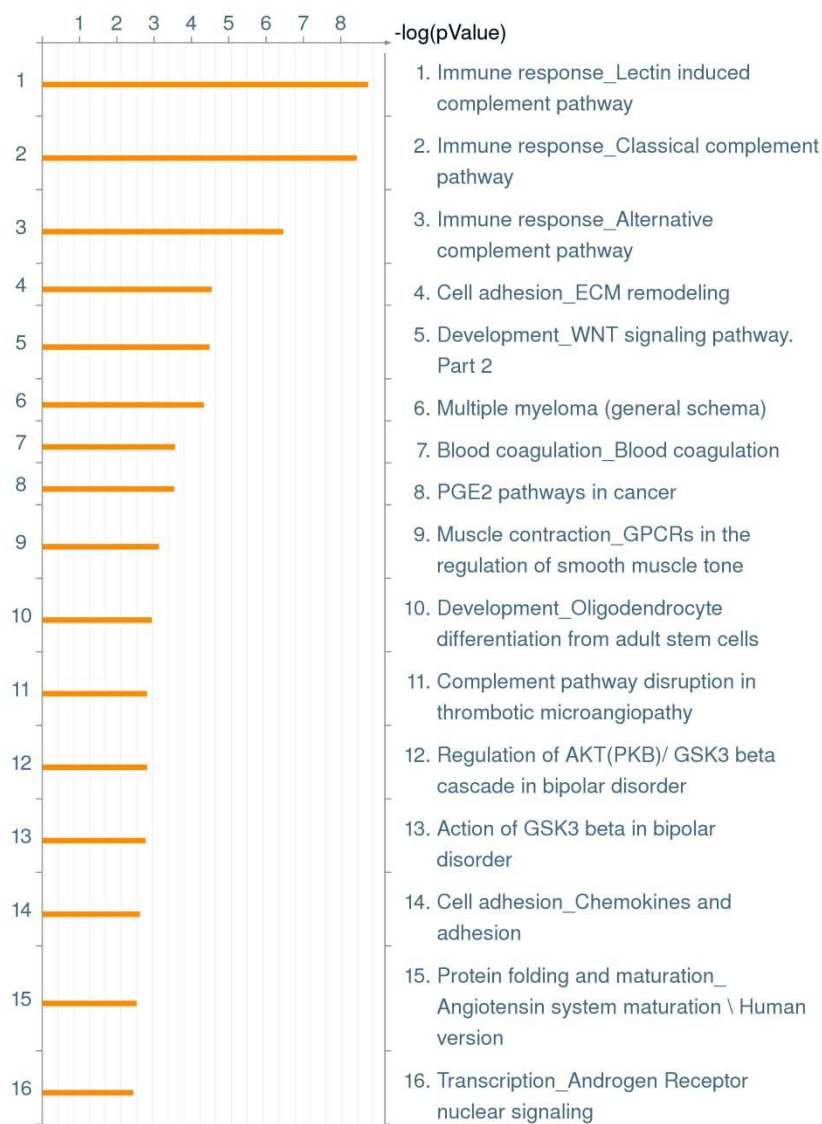


Figure 4.3.8 Pathways significantly altered in *Nkx3.1^{CreERT2} Pten^{fl/+} Ctnnb1^{(ex3)Δ/+}* castration-resistant tumours compared to hormone naïve controls

MetaCore pathway enrichment analysis was carried out on 655 genes identified as being at least twofold up- or downregulated ($P < 0.05$) in RNA sequencing gene expression data of *Nkx3.1^{CreERT2} Pten^{fl/+} Ctnnb1^{(ex3)Δ/+}* castration-resistant tumours ($n=3$) compared to hormone naïve controls ($n=2$). The top 16 significantly altered pathways are shown in this histogram. ($-\log(P \text{ value}) > 2 = P < 0.01$).

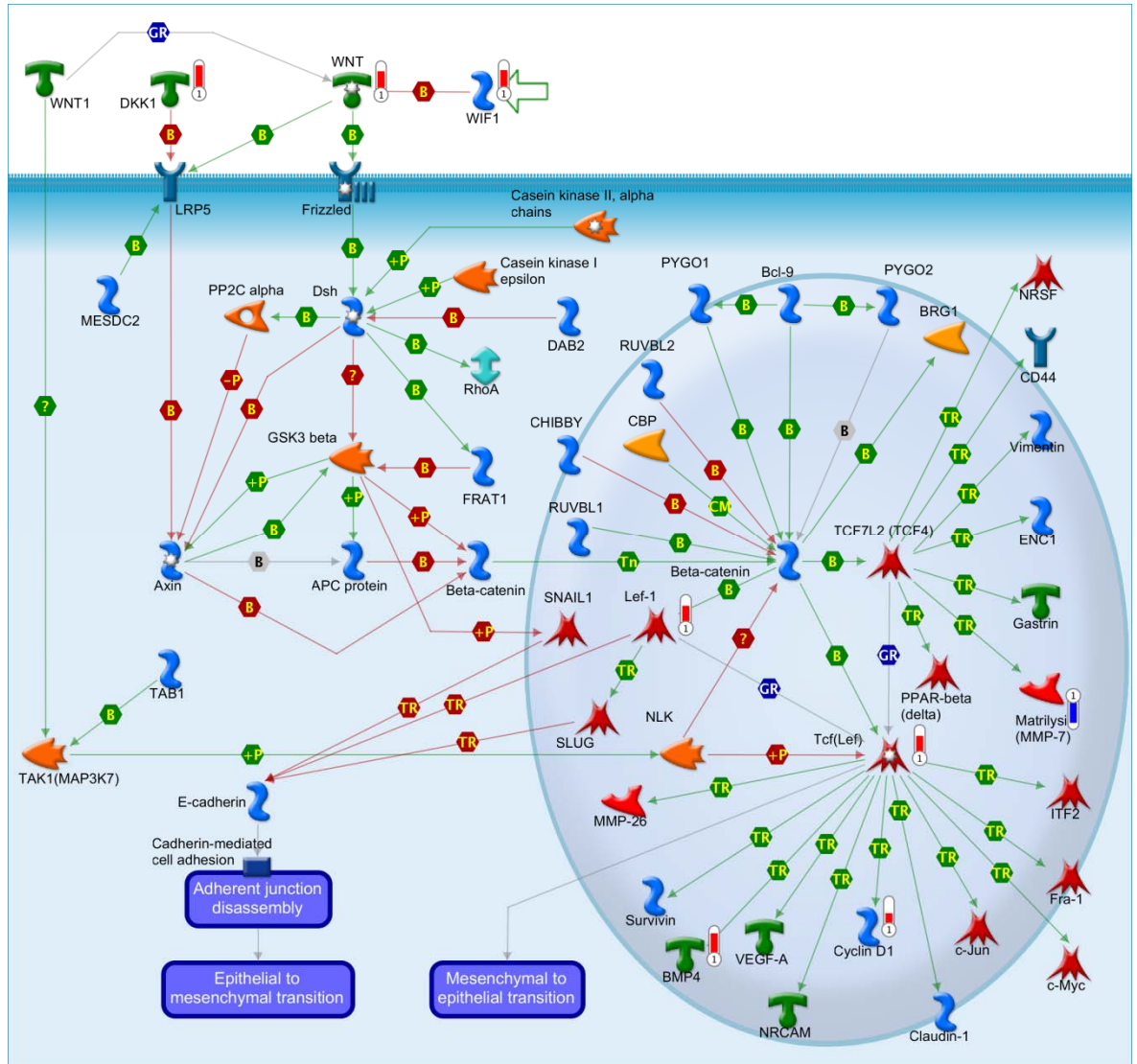


Figure 4.3.9 Increased Wnt signalling pathway activity in *Nkx3.1^{CreERT2} Pten^{fl/+} Ctnnb1^{(ex3)Δ/+}* castration-resistant tumours

Diagram of Wnt/ β -catenin signalling pathway. MetaCore pathway enrichment analysis carried out on RNA-sequencing data showed a significant change in Wnt signalling pathway components in *Nkx3.1^{CreERT2} Pten^{fl/+} Ctnnb1^{(ex3)Δ/+}* castration-resistant tumours compared to controls. The thermometer symbols indicate expression of Wnt signalling pathway components that are significantly upregulated (red) or downregulated (blue).

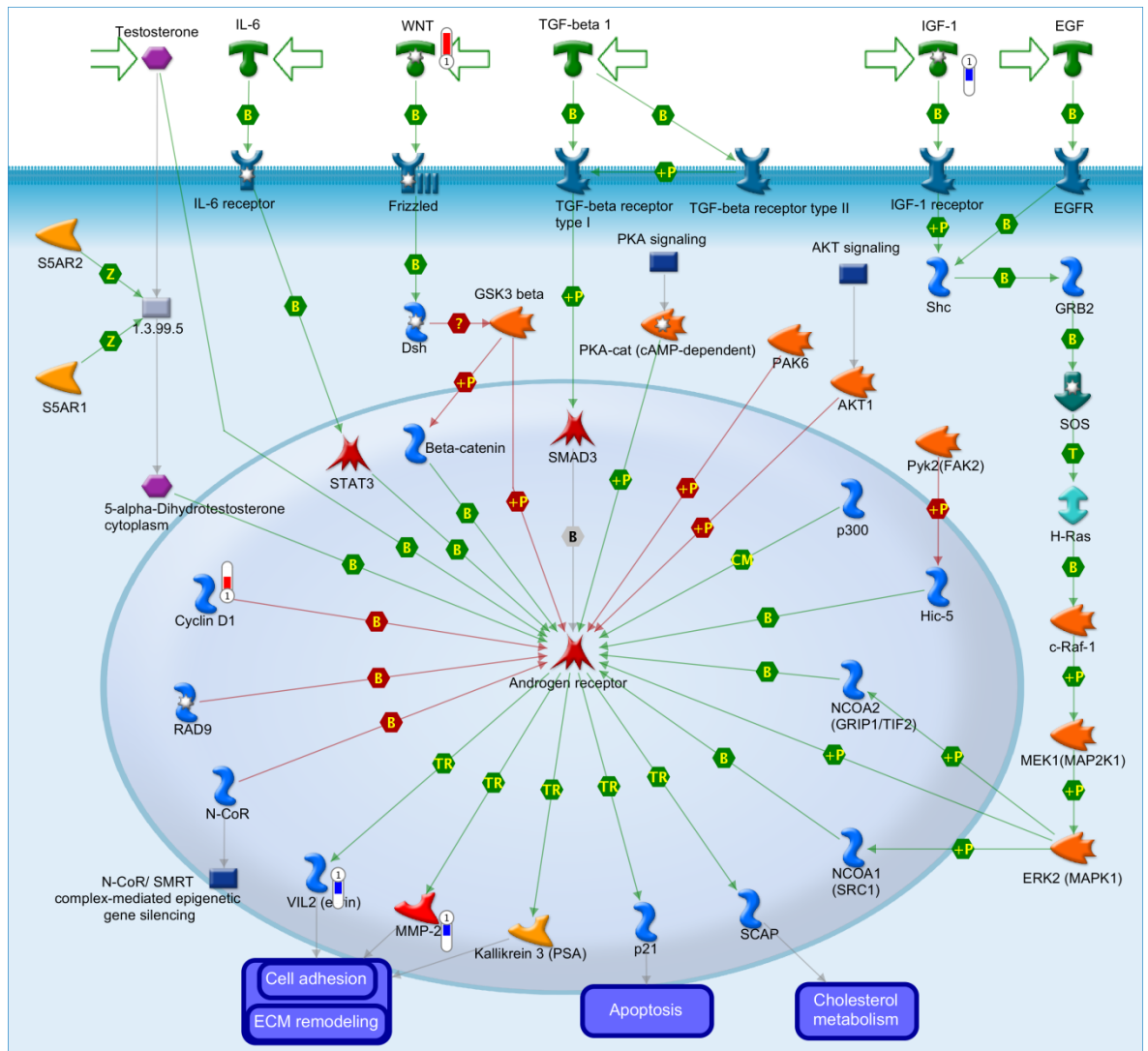


Figure 4.3.10 The classical androgen receptor signalling pathway is not reactivated in *Nkx3.1^{CreERT2} Pten^{fl/+} Ctnnb1^{(ex3)Δ/+}* castration-resistant tumours

Diagram of AR signalling pathway. MetaCore pathway analysis carried out on RNA-sequencing data showed a significant downregulation of positive regulators and downstream targets of the androgen receptor signalling pathway, and upregulation of a negative regulator, cyclin D1, in *Nkx3.1^{CreERT2} Pten^{fl/+} Ctnnb1^{(ex3)Δ/+}* castration-resistant tumours compared to controls. The thermometer symbols indicate expression of androgen receptor signalling pathway components that are significantly upregulated (red) or downregulated (blue).

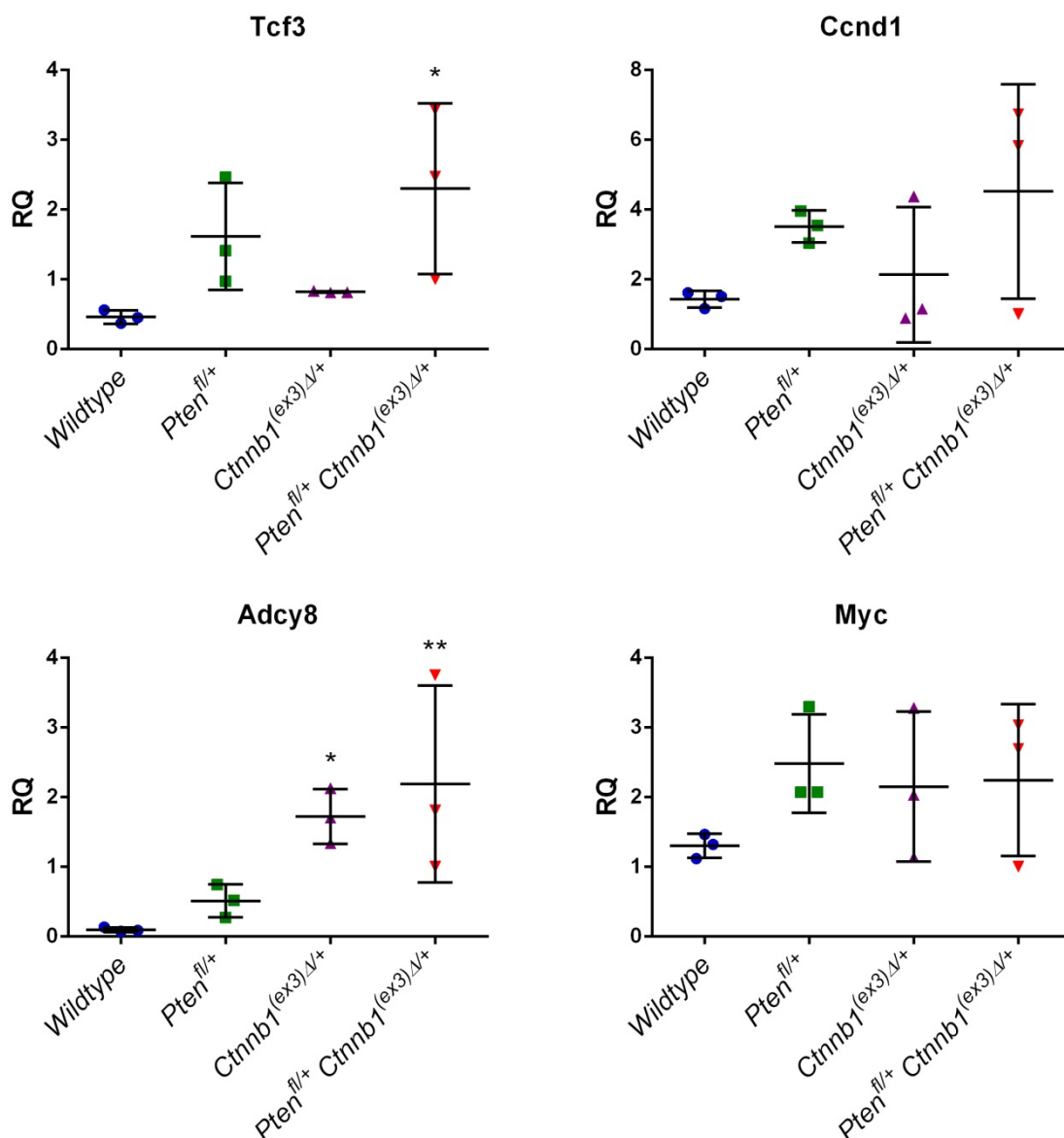


Figure 4.3.11 Expression of *Tcf3* and *Adcy8*, but not *Ccnd1* or *Myc*, is significantly upregulated in prostate tissue with β -catenin activation

The expression of Wnt target genes in hormone-naïve *Nkx3.1^{CreERT2} Pten^{fl/+} Ctnnb1^{(ex3)Δ/+}* prostate tumours at endpoint was compared to age-matched controls. TaqMan RT-qPCR analysis was carried out on RNA extracted from *Nkx3.1^{CreERT2} wildtype*, *Nkx3.1^{CreERT2} Pten^{fl/+}*, *Nkx3.1^{CreERT2} Ctnnb1^{(ex3)Δ/+}* and *Nkx3.1^{CreERT2} Pten^{fl/+} Ctnnb1^{(ex3)Δ/+}* prostate tissue. Normalised to 18S housekeeping gene and presented as relative quantity (RQ) of RNA expression. (** p value <0.01, * p value <0.05; analysed by one-way ANOVA with Fisher's LSD test, comparing each group to *wildtype*). Data are presented as mean \pm SD (n=3).

I proceeded to measure the expression of *Tcf3*, *Lef1*, *Ccnd1*, *Wnt4*, *Wnt5a*, *Wnt10b* and *Myc* in CRPC compared to HNPC. In the *Nkx3.1^{CreERT2} Pten^{fl/+} Ctnnb1^{(ex3)Δ/+}* model, there was a significant increase in the expression of *Lef1*, *Ccnd1*, *Wnt5a* and *Myc* in CRPC (Figure 4.3.12). There was a trend towards an increase in *Tcf3*, *Wnt4* and *Wnt10b* expression but the standard deviation between samples was high. In the *Pten^{fl/fl} Ctnnb1^{(ex3)Δ/+}* model, only *Tcf3*

expression was increased relative to untreated controls (Figure 4.3.12). There was a trend towards higher expression of *Lef1*, *Ccnd1*, *Wnt5a* and *Wnt10b* in CRPC compared to HNPC, but there was high standard deviation within the sample group.

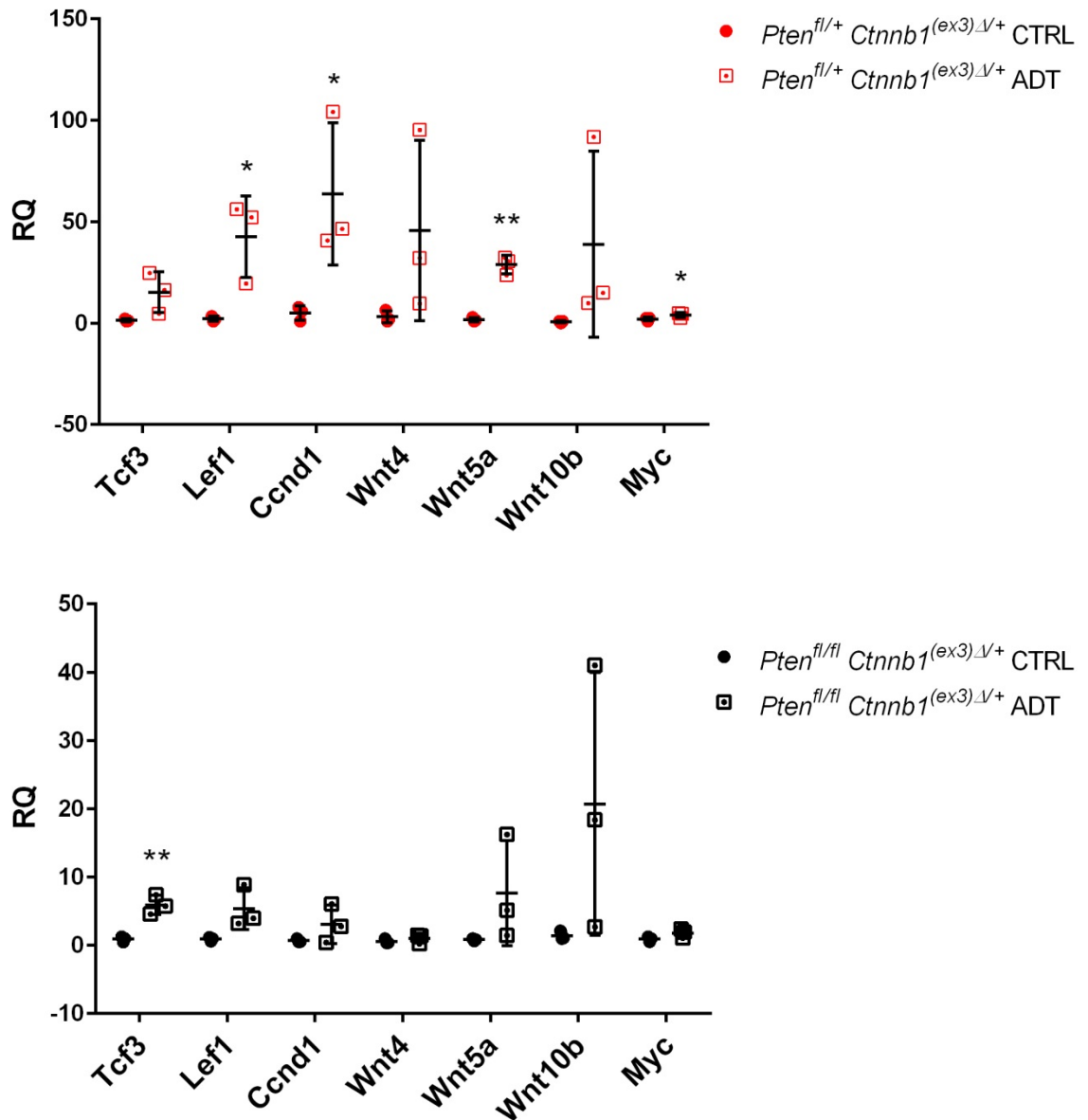


Figure 4.3.12 Upregulation of Wnt pathway genes in castration-resistant compared to hormone-naïve tumours

TaqMan RT-qPCR analysis was carried out on RNA extracted from castration-resistant (ADT) and hormone-naïve (CTRL) *Nkx3.1*^{CreERT2} *Pten*^{fl/+} *Ctnnb1*^{(ex3)Δ/+} (top graph) and *Nkx3.1*^{CreERT2} *Pten*^{fl/fl} *Ctnnb1*^{(ex3)Δ/+} (bottom graph) prostate tumours. Normalised to *18S* housekeeping gene and presented as relative quantity (RQ) RNA expression. (** p value <0.01, * p value <0.05; analysed by unpaired, one-tailed student t-test with Welch's correction). Data are presented as mean ± SD (n=3).

Further analysis was carried out on *Nkx3.1^{CreERT2} Pten^{fl/+} Ctnnb1^{(ex3) Δ /+}* tumours, as the greatest differences in Wnt pathway gene expression between HNPC and CRPC were observed in this model. Myc expression was analysed by immunohistochemical staining and confirmed that Myc protein levels were elevated in castration-resistant compared to hormone-naïve prostate tumours (Figure 4.3.13). Although staining was patchy, nuclear Myc was observed in CRPC in biological triplicate, while only low levels of Myc were observed in PIN lesions of control HNPC prostate and not in tumour.

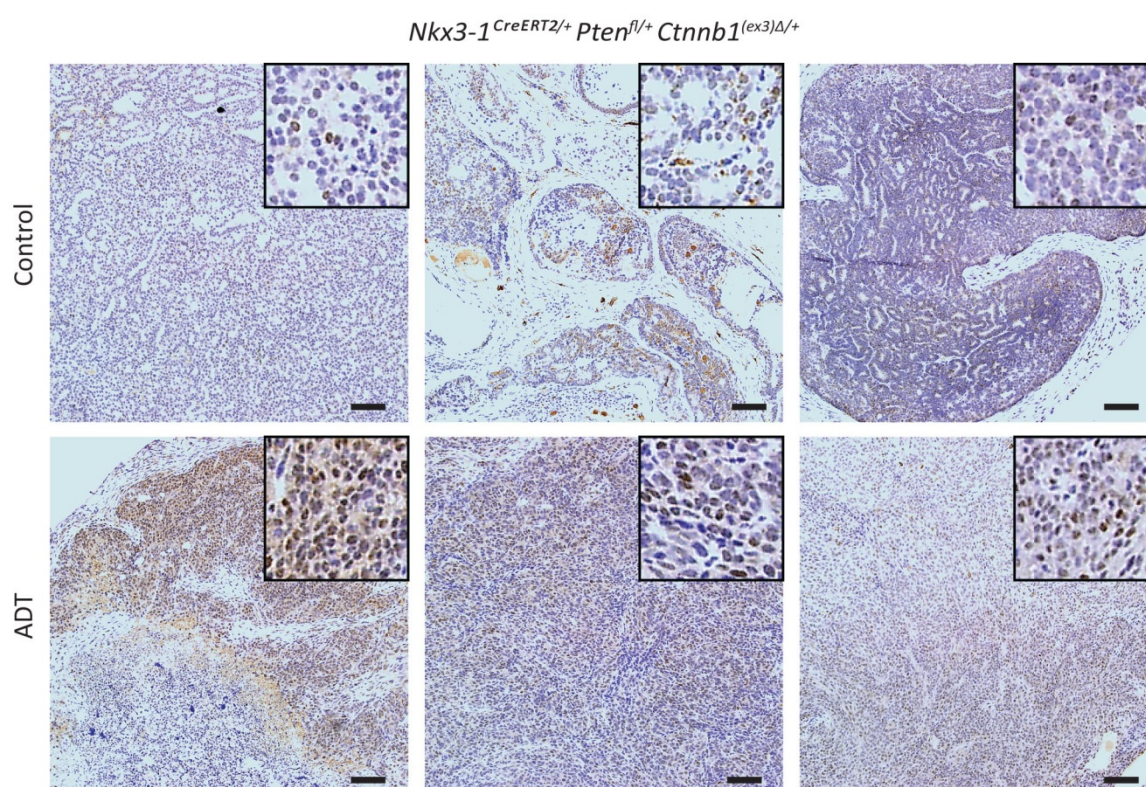


Figure 4.3.13 Myc expression is elevated in *Nkx3.1^{CreERT2} Pten^{fl/+} Ctnnb1^{(ex3) Δ /+}* castration-resistant tumours.

Representative images of Myc immunohistochemical staining of FFPE tissue sections, comparing mouse prostate tissue from ADT-treated *Nkx3.1^{CreERT2} Pten^{fl/+} Ctnnb1^{(ex3) Δ /+}* mice (n=3) to controls (n=3) at clinical endpoint. Scale bar: 100 μ m. Insert box: 100 μ m².

As immunohistochemical staining of Wnts can be challenging, RNAscope was used to detect the expression of *Wnt5a* in control and ADT-resistant *Nkx3.1^{CreERT2} Pten^{fl/+} Ctnnb1^{(ex3) Δ /+}* prostate tumour tissue. CRPC tumours had higher levels of *Wnt5a* than HNPC tumours (Figure 4.3.14), consistent with RT-PCR analysis of *Wnt5a* expression in these tumours (Figure 4.3.12). As Wnts are secreted, it is possible for epithelial and stroma cells to contribute to the levels of Wnt present in tumour tissue. However, *Wnt5a* is predominantly localised to the tumour

epithelial cells, indicating that these cells are responsible for the increased secretion of Wnt5a in CRPC.

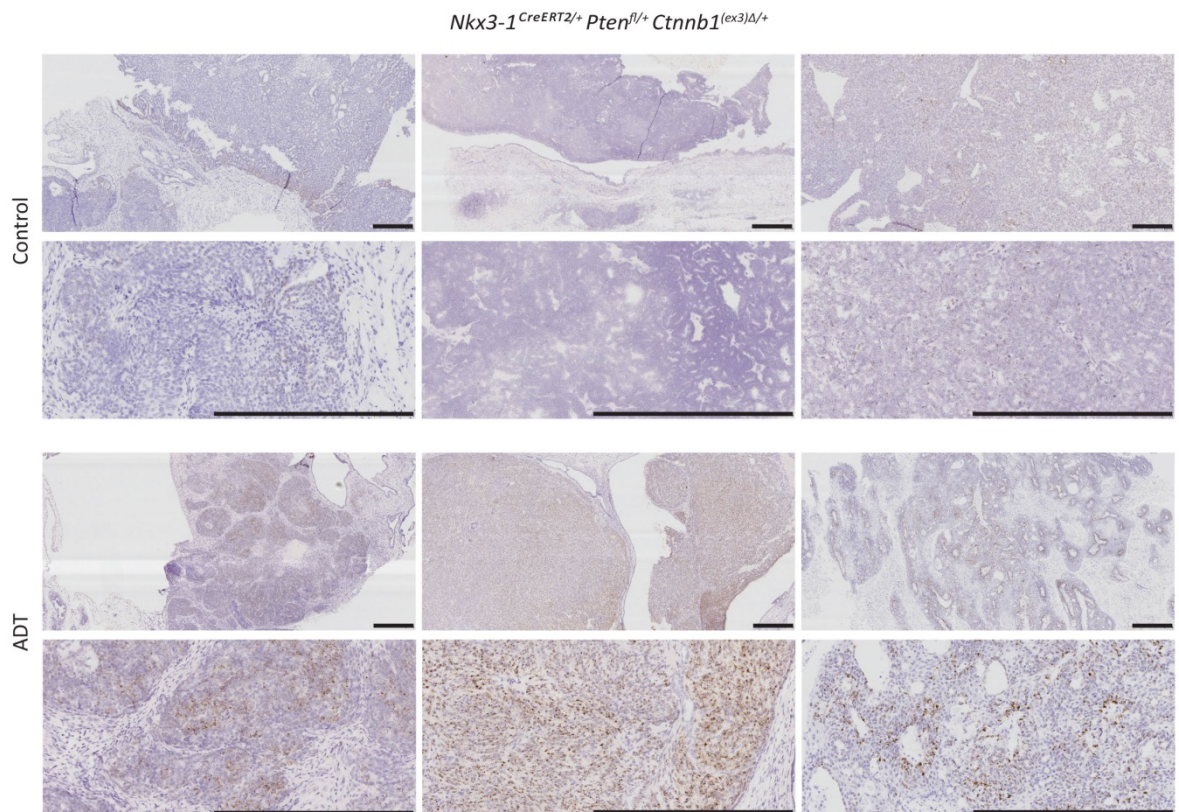


Figure 4.3.14 Wnt5a expression is elevated in castration-resistant prostate tumour tissue
 Representative images of Wnt5a RNAscope staining of FFPE tissue sections, comparing mouse prostate tissue from ADT-treated *Nkx3.1^{CreERT2} Pten^{fl/+} Ctnnb1^{(ex3)Δ/+}* mice (n=3) to controls (n=3) at clinical endpoint. Scale bar: 500 μ m.

Overall, I have confirmed there is significant Wnt pathway enrichment in *Nkx3.1^{CreERT2} Pten^{fl/+} Ctnnb1^{(ex3)Δ/+}* tumours which have become castration-resistant. This was demonstrated by a significant increase in *Lef1*, *Ccnd1*, *Wnt5a* and *Myc* expression in CRPC tissue compared to HNPC controls. The increase in *Wnt5a* mRNA was confirmed by RNAscope analysis. *Myc* protein expression was shown to be elevated in CRPC, corresponding with higher levels of *Myc* transcription, and likely to drive proliferation in castration-resistant prostate cells.

4.3.4 Investigating the effect of Wnt inhibition and androgen deprivation combination therapy in *Nkx3.1^{CreERT2} Pten^{fl/+} Ctnnb1^{Δ(ex3)/+}* mice

Having established that CRPC in mice with β -catenin activation and *Pten* loss had significant enrichment of Wnt ligand expression, we tested a Wnt inhibitor in combination with ADT *in vivo*. LGK-974 inhibits the N-palmitoyltransferase molecule Porcupine (PORCN), blocking Wnt post-translational acylation, which consequently blocks Wnt secretion [199].

On detection of palpable tumour, *Nkx3.1^{CreERT2} Pten^{fl/+} Ctnnb1^{(ex3)Δ/+}* mice were castrated. After 10 days recovery, mice were treated daily with 100 μ l of 1.25 mg/kg LGK-974 or vehicle control by gavage for one month. Doses of 1-3 mg/kg LGK-974 treatment have previously shown strong efficacy for inhibition of tumour growth in a Wnt tumour model [199]. Due to concerns of host toxicity, we selected a dose at the lower end of this range. A trend towards a decrease in prostate weight was observed following combined ADT and LGK treatment compared to ADT alone, but this did not reach statistical significance (Figure 4.3.15).

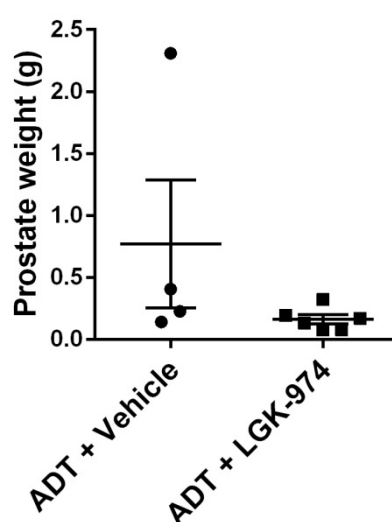


Figure 4.3.15 The effect of ADT and Wnt inhibition on regression of prostate tumours in *Nkx3.1^{CreERT2} Pten^{fl/+} Ctnnb1^{(ex3)Δ/+}* mice

The graph shows prostate weights of *Nkx3.1^{CreERT2} Pten^{fl/+} Ctnnb1^{(ex3)Δ/+}* mice after castration (ADT), and 1 months treatment with 1.25 mg/kg LGK-974 (PORCN inhibitor) or vehicle control. Mice were castrated 7-8 months post-induction when palpable tumour was detected. LGK-974 (or vehicle) treatment commenced 10 days post-castration and all mice were taken after 1 month of treatment. Data presented as mean \pm SEM.

Histopathological analysis of prostate tissue showed evidence of prostate regression and tumour following treatment with LGK or vehicle control (Figure 4.3.16). Overall observations suggest that Ki67 and β -catenin levels are lower in $Nkx3.1^{CreERT2} Pten^{fl/+} Ctnnb1^{(ex3)\Delta/+}$ prostate tissue following combined ADT and Wnt inhibitor treatment as compared to controls. It should be noted that Ki67 staining may reflect the proliferation of infiltrating immune cells rather than the continued proliferation of tumour epithelial cells. Further work is required to fully characterise the effects of Wnt inhibition in tissue in combination with ADT.

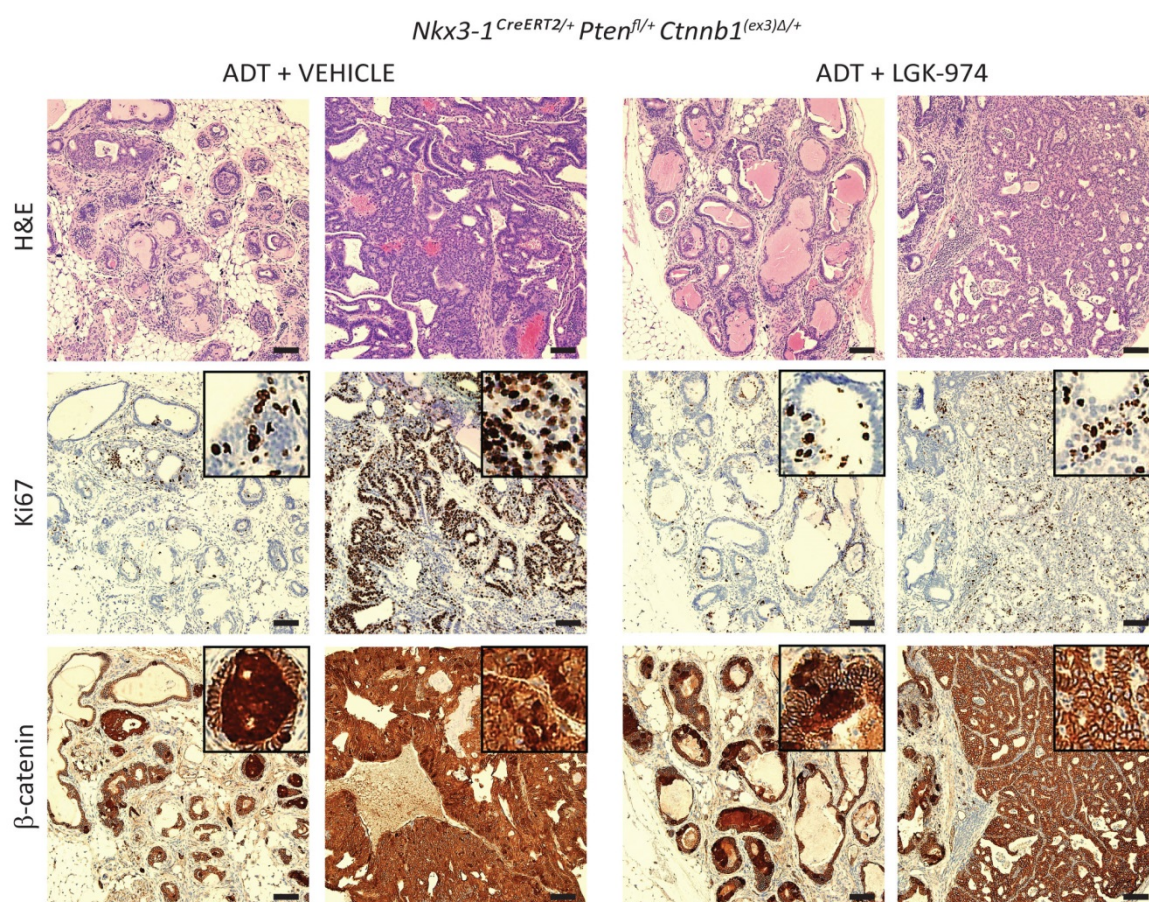


Figure 4.3.16 Histology of $Nkx3.1^{CreERT2} Pten^{fl/+} Ctnnb1^{(ex3)\Delta/+}$ tumours following treatment with ADT and Wnt inhibitor

Haematoxylin and eosin staining, and ki67 and β -catenin immunohistochemical staining of FFPE sections of $Nkx3.1^{CreERT2} Pten^{fl/+} Ctnnb1^{(ex3)\Delta/+}$ mouse prostate tissue, comparing ADT + LGK-974 treated mice to ADT treated controls. Mice were castrated 7-8 months post-induction when palpable tumour was detected. LGK-974 (or vehicle) treatment commenced 10 days post-castration and all mice were taken after 1 month of treatment. The two images for each treatment group are representative of the most regressed regions (left) and largest extent of tumour (right) observed in the prostates. Scale bar: 100 μ m. Insert box: 100 μ m².

4.4 Evidence for androgen receptor reprogramming in tumours with β -catenin activation

4.4.1 Identification of a pseudo-castrate gene expression signature in β -catenin-driven prostate cancer

β -catenin is a known AR cofactor [157] and can therefore influence the transcriptional regulation of AR target genes. Co-immunoprecipitation experiments were carried out in LNCaP and CWR-22 prostate cancer cell lines to confirm that AR and β -catenin interact in human prostate cancer (Figure 4.4.1).

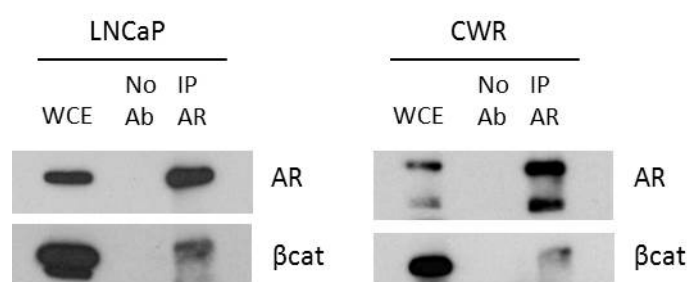


Figure 4.4.1 Co-immunoprecipitation experiments show AR and β -catenin interaction
Panels show western blot analysis of AR and β -catenin expression in protein from AR immunoprecipitation experiments in LNCaP and CWR-22 prostate cancer cell lines. WCE = whole cell extract, No Ab = negative IP beads control, IP AR = androgen receptor immunoprecipitation.

Immunohistochemical staining showed that AR is expressed in hormone-naïve *Nkx3.1^{CreERT2} Ctnnb1^{(ex3) Δ /+}* and *Nkx3.1^{CreERT2} Pten^{fl/+} Ctnnb1^{(ex3) Δ /+}* prostate tumours (Figure 4.3.5). AR is localised in the nucleus of tumour epithelial cells, indicating that it is actively functioning as a transcription factor in the presence of nuclear β -catenin.

To investigate the effects of β -catenin activation on AR activity, I initially studied the expression of AR-regulated genes in a microarray data set comparing *Pb-Cre Ctnnb1^{(ex3) Δ /+}* prostate tissue to *wildtype*. This data was generated in our laboratory by Meiling Gao, using a *Pb-Cre Ctnnb1^{(ex3) Δ /+}* mouse colony. The androgen responsive gene list was identified by Carver et al [119] from microarray analysis of intact and castrate *wildtype* mouse prostate. This gene set provided a castrate gene signature, clustering one set of genes that were upregulated post-ADT and another set downregulated post-ADT (Figure 4.4.2). Regulation of the murine androgen responsive gene data set in intact *Pb-Cre Ctnnb1^{(ex3) Δ /+}* prostate was similar to that observed in castrate *wildtype* prostate

(Fig. 4.4.2). Therefore, *Pb-Cre Ctnnb1^{(ex3)Δ/+}* tumours had a pseudo-castrate gene expression signature, providing evidence for AR reprogramming as a consequence of β-catenin activation.

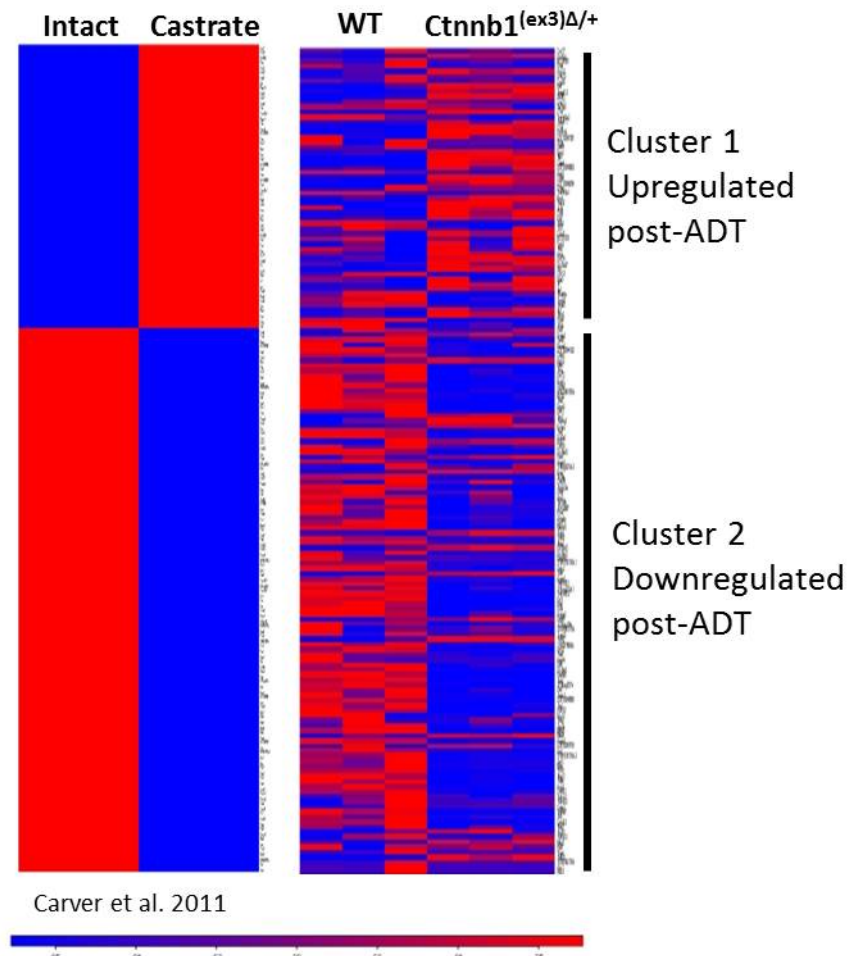


Figure 4.4.2 Prostate cancer driven by aberrant β-catenin activation has a pseudo-castrate gene expression signature

Heat maps represent expression changes in 133 androgen responsive genes identified in microarray data from *Pb-Cre Ctnnb1^{(ex3)Δ/+}* and *wildtype* (WT) prostate (data from Meiling Gao, produced using Illumina Mouse Ref-8 v2.0 BeadChip Array) and intact and castrate *wildtype* prostate [119]. The mouse androgen responsive gene set was identified by Carver et al [119] from gene expression differences observed between intact and castrate *wildtype* prostate tissue. This gene set was analysed in *Pb-Cre Ctnnb1^{(ex3)Δ/+}* and *wildtype* (WT) microarray data and genes are listed in the same order on both heat maps.

Having carried out RNA sequencing analysis of *Ctnnb1^{(ex3)Δ/+}* and *Pten^{fl/+}* *Ctnnb1^{(ex3)Δ/+}* tumours in both the *Pb-Cre* and *Nkx3.1^{CreERT2}* mouse colonies, I analysed the expression changes of the androgen responsive gene set in these data. I selected four genes from Cluster 2 (Figure 4.4.2), responsible for the expression of FK506 binding protein 5 (Fkbp5), apolipoprotein F (ApoF), tissue inhibitor of metalloproteinases 4 (Timp4) and transmembrane protein 97 (Tmem97). The same downregulation of *Fkbp5*, *ApoF*, *Timp4* and *Tmem97*

expression, as a result of β -catenin activation, was observed in one or both of *Pb-Cre Ctnnb1^{(ex3) Δ /+}* and *Pb-Cre Pten^{fl/+} Ctnnb1^{(ex3) Δ /+}* prostate tumours compared to *wildtype* (Table 4.4-1). These genes were selected because ChIP sequencing data from *wildtype* mouse epididymal [180] or prostate [181] tissue identified enrichment of AR binding in the promoter regions of these genes.

Table 4.4-1 Androgen responsive genes downregulated in HNPC with aberrant β -catenin activation

	Intact	Castrate	<i>Pb-Cre Ctnnb1^{(ex3)Δ/+}</i> vs <i>wildtype</i>	P value	<i>Pb-Cre Pten^{fl/+} Ctnnb1^{(ex3)Δ/+}</i> vs <i>wildtype</i>	P value
<i>Fkbp5</i>			-3.3	0.088	-4.1	0.022
<i>ApoF</i>			-4.4	0.047	-3.8	0.095
<i>Timp4</i>			-19.5	1.30E-03	-29.4	3.00E-05
<i>Tmem97</i>			-4.4	0.033	-6.4	0.003

Red indicates high expression and blue indicates low expression. Significant p values <0.05 in red.

Table 4.4-2 Androgen responsive genes downregulated in HNPC are not significantly altered in CRPC

	Intact	Castrate	<i>Nkx3.1^{CreERT2} Pten^{fl/+} Ctnnb1^{(ex3)Δ/+}</i> ADT vs CTRL	P value
<i>Fkbp5</i>			-3.11	0.110
<i>ApoF</i>			-3.36	0.334
<i>Timp4</i>			-7.15	0.210
<i>Tmem97</i>			1.18	1.000

Red indicates high expression and blue indicates low expression.

Analysis of RNA sequencing data from *Nkx3.1^{CreERT2} Pten^{fl/+} Ctnnb1^{(ex3) Δ /+}* CRPC compared to HNPC showed no statistically significant difference in the expression of *Fkbp5*, *ApoF*, *Timp4* or *Tmem97* (Table 4.4-2). Indeed, independent clustering analysis of the androgen responsive gene set in *Nkx3.1^{CreERT2} Pten^{fl/+} Ctnnb1^{(ex3) Δ /+}* HNPC and CRPC (compared to *wildtype*) demonstrated that significant AR reprogramming occurred in HNPC, but overall expression of these genes in CRPC was similar to HNPC (Figure 4.4.3). MetaCore pathway enrichment analysis showed that downregulation of the AR signalling pathway was not as significant as other pathway alterations in CRPC compared

to HNPC (Figure 4.3.8). This suggests that tumours had already developed a pseudo-castrate gene signature prior to castration, which was not significantly altered in CRPC.

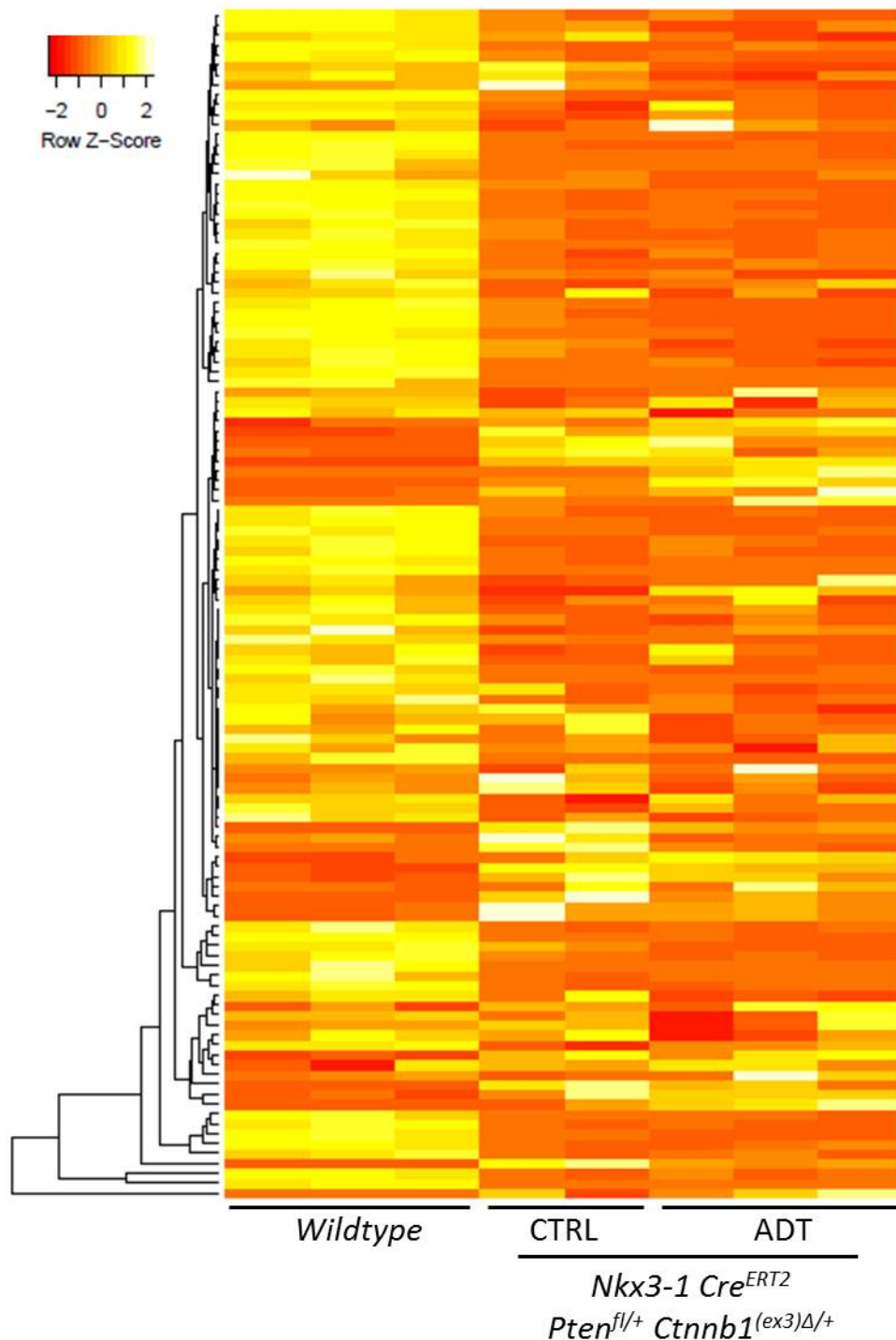


Figure 4.4.3 Expression of androgen responsive genes is reprogrammed in HNPC and maintained in CRPC

RNA was extracted from *wildtype* prostate tissue (12 months) and *Nkx3.1^{CreERT2} Pten^{fl/+} Ctnnb1^{(ex3)Δ/+}* hormone-naïve (CTRL) and castration-resistant (ADT) tumour tissue (endpoint). RNA was sent for sequencing and gene expression analysis. R and DESeq2 software was used to determine fold changes in gene expression of tumour RNA compared to *wildtype*. The heat map represents independent clustering analysis of expression changes in 133 androgen responsive genes, previously identified [119].

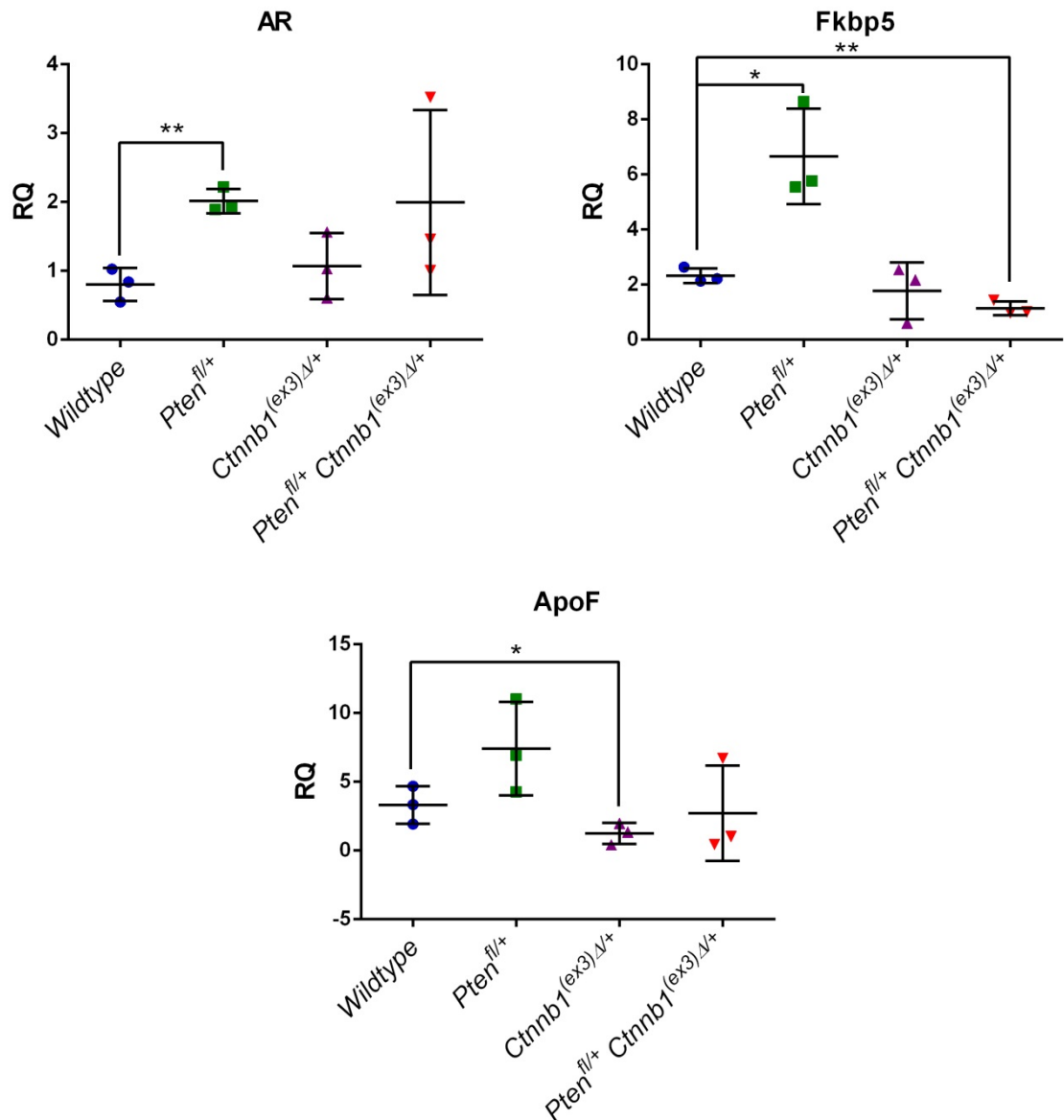


Figure 4.4.4 *Fkbp5* and *ApoF* transcript expression is downregulated in hormone-naïve prostate tissue with β -catenin activation

The expression of *AR*, *Fkbp5* and *ApoF* in hormone-naïve *Nkx3.1*^{CreERT2} *Pten*^{fl/+} *Ctnnb1*^{(ex3)Δ/+} prostate tumours at endpoint was compared to age-matched controls. TaqMan RT-qPCR analysis was carried out on RNA extracted from *Nkx3.1*^{CreERT2} *wildtype*, *Nkx3.1*^{CreERT2} *Pten*^{fl/+}, *Nkx3.1*^{CreERT2} *Ctnnb1*^{(ex3)Δ/+} and *Nkx3.1*^{CreERT2} *Pten*^{fl/+} *Ctnnb1*^{(ex3)Δ/+} prostate tissue. Normalised to 18S housekeeping gene and presented as relative quantity (RQ). (** p value <0.01, * p value <0.05; analysed by unpaired, one-tailed student t-test). Data are presented as mean \pm SD (n=3).

AR, *Fkbp5* and *ApoF* transcript expression was validated in end point, hormone-naïve *Nkx3.1*^{CreERT2} *Pten*^{fl/+} *Ctnnb1*^{(ex3)Δ/+} prostate tissue compared to *wildtype*, *Pten*^{fl/+} and *Ctnnb1*^{(ex3)Δ/+} age-matched controls. It was interesting to observe that *AR*, *Fkbp5* and *ApoF* expression was elevated in *Pten*^{fl/+} tissue compared to *wildtype* (Figure 4.4.4). In contrast, *Fkbp5* expression was significantly decreased in *Pten*^{fl/+} *Ctnnb1*^{(ex3)Δ/+} compared to *wildtype*, while *ApoF* was significantly decreased in *Ctnnb1*^{(ex3)Δ/+} compared to *wildtype* (Figure 4.4.4). *AR*

expression was not significantly different between genotypes, although there was high standard deviation in $Pten^{fl/+} Ctnnb1^{(ex3)\Delta/+}$ samples (Figure 4.4.4).

RT-PCR analysis of *AR*, *Fkbp5* and *ApoF* expression in ADT resistant and control tumours demonstrated that there was no significant difference in expression of these genes between CRPC and HNPC in both $Nkx3.1^{CreERT2} Pten^{fl/+} Ctnnb1^{(ex3)\Delta/+}$ and $Nkx3.1^{CreERT2} Pten^{fl/fl} Ctnnb1^{(ex3)\Delta/+}$ models (Figure 4.4.5). This corroborated observations from RNA sequencing analysis (Figure 4.4.3)

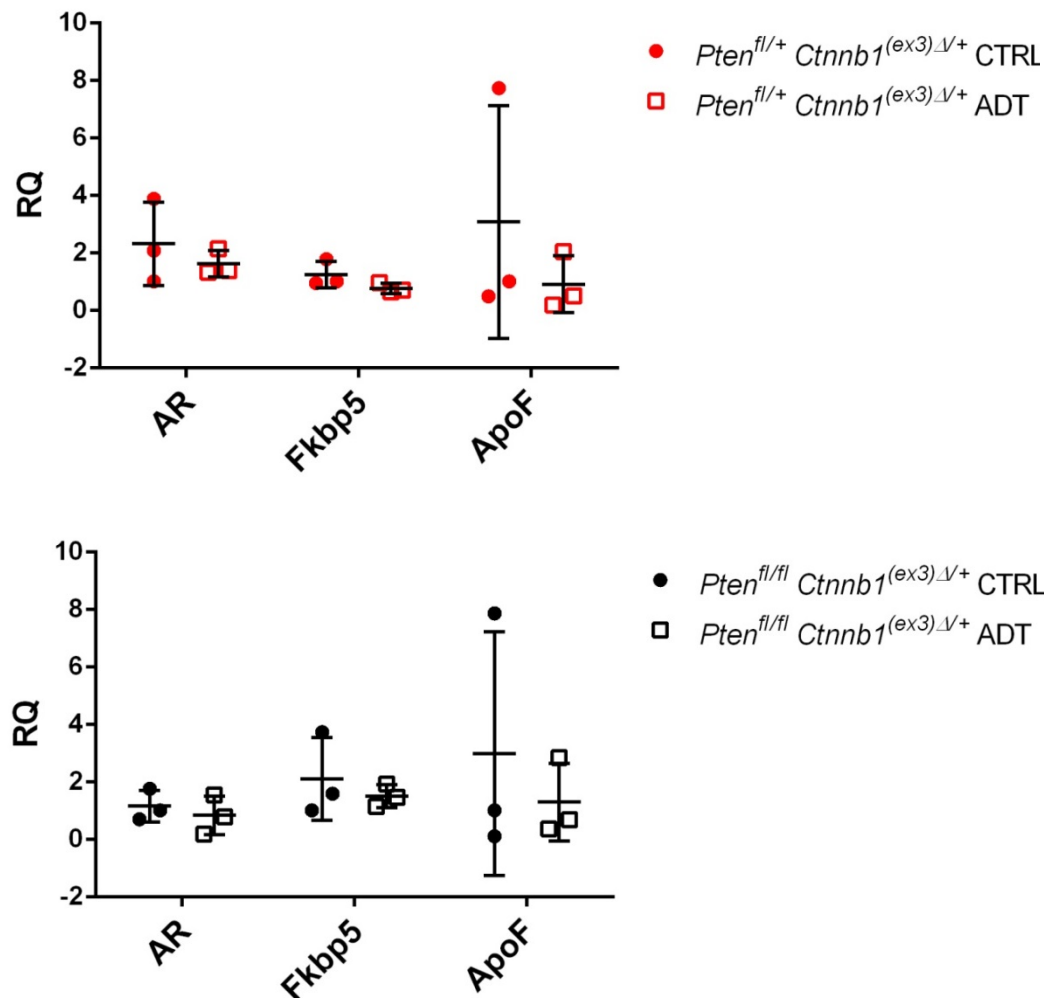


Figure 4.4.5 *AR*, *Fkbp5* and *ApoF* expression is similar in hormone-naïve and castration-resistant tumours with β -catenin activation and *Pten* loss

TaqMan RT-qPCR analysis was carried out on RNA extracted from castration-resistant (ADT) and hormone-naïve (CTRL) $Nkx3.1^{CreERT2} Pten^{fl/+} Ctnnb1^{(ex3)\Delta/+}$ (top graph) and $Nkx3.1^{CreERT2} Pten^{fl/fl} Ctnnb1^{(ex3)\Delta/+}$ (bottom graph) prostate tumours. Normalised to *18S* housekeeping gene and presented as relative quantity (RQ). Data are presented as mean \pm SD (n=3).

The down-regulation of androgen-responsive gene expression observed in RNA sequencing data relate to advanced tumours. However, upregulation of

androgen responsive gene expression has previously been observed in hyperplastic lesions of *Ctnnb1*^{(ex3)Δ/+} prostate tissue [149] and it was recently reported that castration of *Pb-Cre Ctnnb1*^{(ex3)Δ/+} mice at 16 weeks results in prostate regression [151], indicating that the presence of androgens and AR signalling are essential for cancer initiation in β-catenin-driven prostate cancer. Therefore, I hypothesised that expression of androgen responsive genes at early stages of β-catenin-driven tumour development will be similar or elevated in comparison to *wildtype* prostate tissue. RT-PCR analysis of prostate tissue sampled two months post-induction, showed similar levels of *AR* and *Fkbp5* expression between *wildtype*, *Pten*^{fl/+}, *Ctnnb1*^{(ex3)Δ/+} and *Pten*^{fl/+} *Ctnnb1*^{(ex3)Δ/+} (Figure 4.4.6). However, there was a trend towards elevated *ApoF* expression in *Pten*^{fl/+} *Ctnnb1*^{(ex3)Δ/+} prostate tissue compared to controls.

These data suggest that initiation of prostate cancer driven by aberrant β-catenin activation is dependent on AR signalling. However, at later stages of tumour development AR signalling is reprogrammed, generating a pseudo-castrate gene expression signature in androgen responsive genes and predisposing tumours to ADT-resistance.

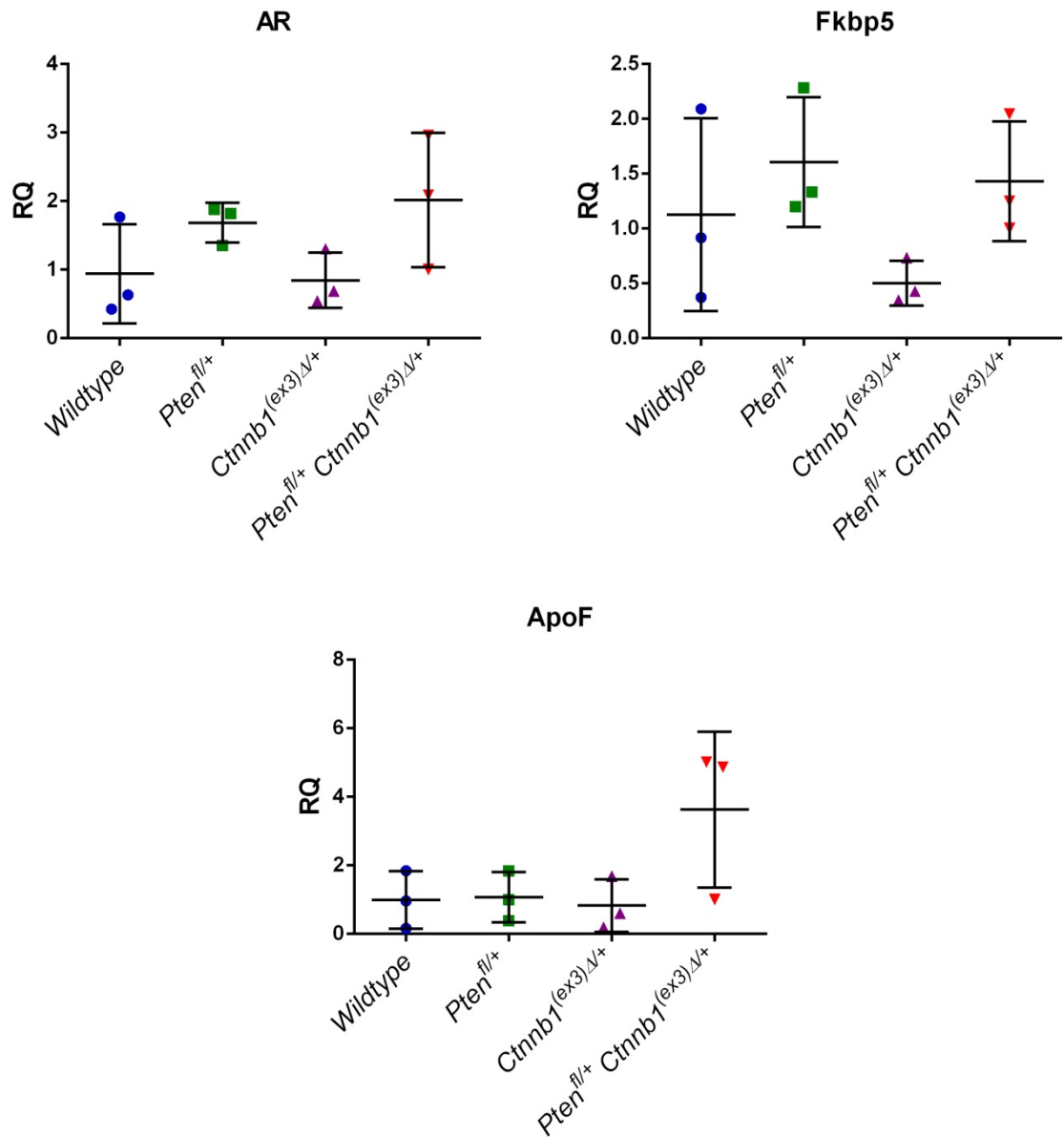


Figure 4.4.6 *Fkbp5* and *ApoF* are not downregulated at early stages of tumourigenesis

The expression of *AR*, *Fkbp5* and *ApoF* in hormone-naïve *Nkx3.1*^{CreERT2} *Pten*^{fl/+} *Ctnnb1*^{(ex3)Δ/+} prostate tissue 2-months post-induction was compared to age-matched controls. TaqMan RT-qPCR analysis was carried out on RNA extracted from *Nkx3.1*^{CreERT2} wildtype, *Nkx3.1*^{CreERT2} *Pten*^{fl/+}, *Nkx3.1*^{CreERT2} *Ctnnb1*^{(ex3)Δ/+} and *Nkx3.1*^{CreERT2} *Pten*^{fl/+} *Ctnnb1*^{(ex3)Δ/+} prostate tissue. Normalised to *18S* housekeeping gene and presented as relative quantity (RQ). Data are presented as mean ± SD (n=3).

4.4.2 Optimisation of ChIP protocol in tissue samples

To understand how AR binding at target genes is altered by aberrant β -catenin activation, a chromatin immunoprecipitation (ChIP) assay protocol was optimised to study the enrichment of AR at target genes in *wildtype* and tumour prostate tissue.

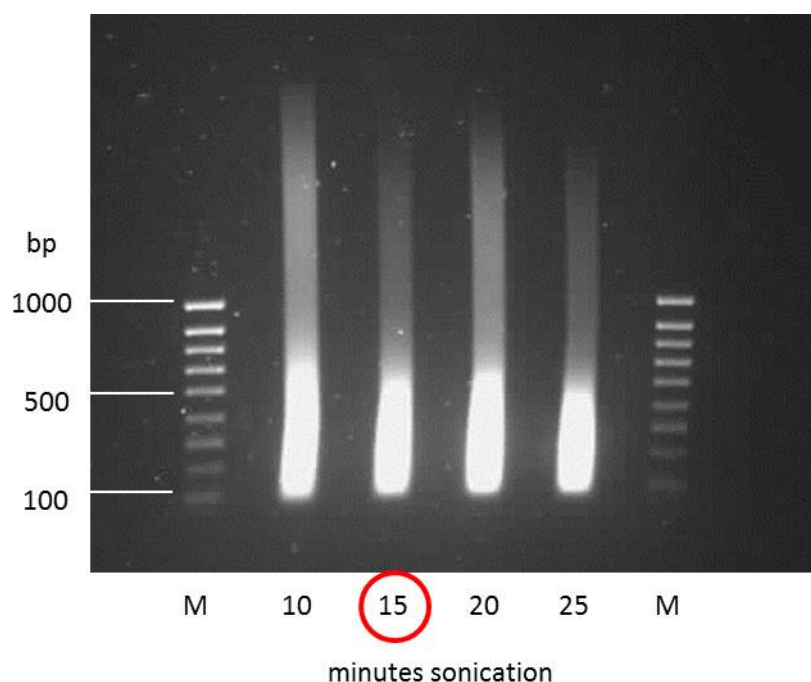


Figure 4.4.7 LNCaP chromatin sonication optimisation

Image of agarose DNA gel showing analysis of the sonication pattern of chromatin prepared from LNCaP cells. Cells were cross-linked with 1% formaldehyde for 10 minutes and, following lysis steps, were sonicated for 10, 15, 20 and 25 minutes with the Bioruptor sonicator; 24s on/24s off on high power setting. After 15 minutes sonication fragments were sheared to 150-500 bp in size. M = HyperLadder IV (100 bp).

Initially the basic ChIP protocol was tested in the LNCaP prostate cancer cell line. Cells were cross-linked with 1% formaldehyde solution for 10 minutes, prior to cell lysis to extract chromatin. The sonication of chromatin then had to be optimised to generate fragments 200-500 bp in size (Figure 4.4.7). This was achieved after 15 minutes of sonication in the Bioruptor sonicator. The ChIP assay was tested using an antibody for the transcriptional repressor CTCF to confirm good enrichment was achieved at known CTCF binding sites in LNCaP cells. Primers designed to amplify CTCF binding regions in *TMPRSS2*, *TAL1* and *KLK3* were used for qPCR analysis of CTCF ChIP DNA, and all three targets were

enriched as expected, while there was no enrichment at negative control regions (Figure 4.4.8)

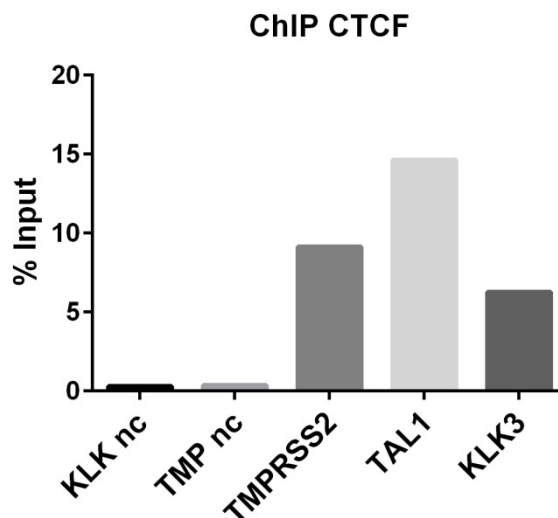


Figure 4.4.8 ChIP protocol validation using CTCF ChIP in LNCaPs

SYBR Green qPCR analysis of CTCF target gene enrichment following ChIP CTCF using chromatin from parental LNCaP cells. *TMPRSS2*, *TAL1* and *KLK3* primers correspond to known CTCF binding sites, while *KLK nc* (*KLK3* negative control) and *TMP nc* (*TMPRSS2* negative control) primers correspond to regions of *KLK3* and *TMPRSS2* where CTCF does not bind. Target gene enrichment presented as percentage input (n=1).

Satisfied that the basic ChIP protocol was working efficiently, I proceeded to optimise formaldehyde cross-linking and sonication steps in prostate tissue. Two batches of *wildtype* prostate tissue were cross-linked with 1% formaldehyde immediately after dissection; one for 10 minutes and the other for 15 minutes. Following cross-linking, samples were lysed to extract chromatin, and each batch was subjected to sonication for 10, 15, 20 or 25 minutes using the Bioruptor sonicator. DNA was fragmented to 100-300 bp in size following 25 minutes of sonication in samples cross-linked for 10 or 15 minutes (Figure 4.4.9). In future experiments prostate tissue was cross-linked for 15 minutes and chromatin was sonicated for 25 minutes before use in ChIP assays.

To select the best AR antibody for use in prostate tissue ChIP assays, ChIP was carried out in *wildtype* prostate tissue samples using the Santa Cruz sc-816X and sc-13062X antibodies. In two independent ChIP experiments, greater enrichment of *Fkbp5* and *Tmprss2* was observed in the eluted DNA after using the sc-13062 antibody to immunoprecipitate AR (4.4.10).

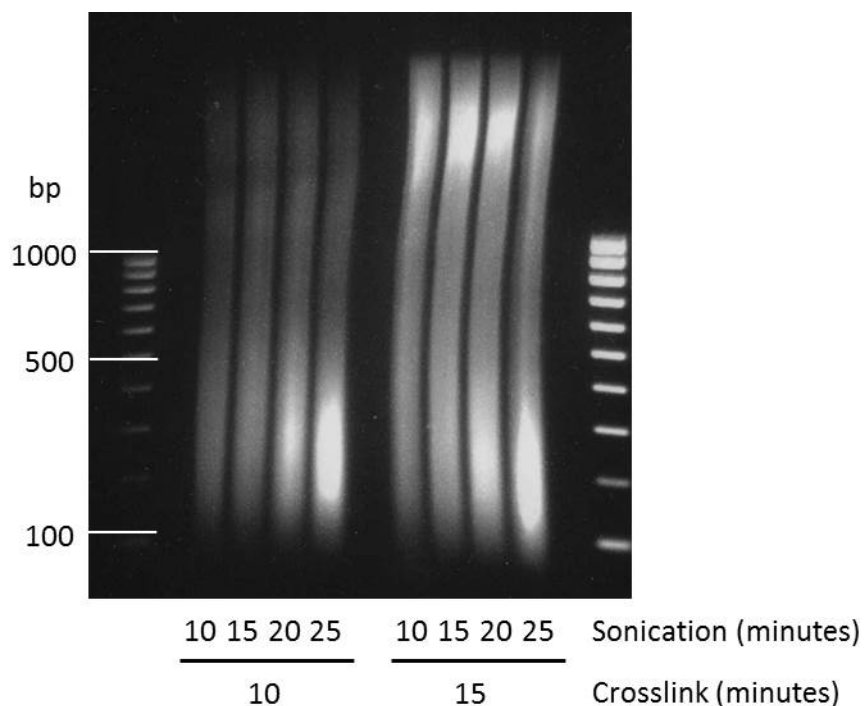


Figure 4.4.9 Optimisation of cross-linking and sonication in tissue chromatin

Image of agarose DNA gel showing analysis of the sonication pattern of chromatin prepared from *wildtype* mouse prostate tissue cross-linked with 1% formaldehyde for 10 or 15 minutes. Following lysis steps, chromatin was sonicated for 10, 15, 20 and 25 minutes with the Bioruptor sonicator; .30s on/30s off on high power setting. After 25 minutes sonication, fragments were sheared to 150-300 bp in size, regardless of cross-linking time. Marker = HyperLadder IV.

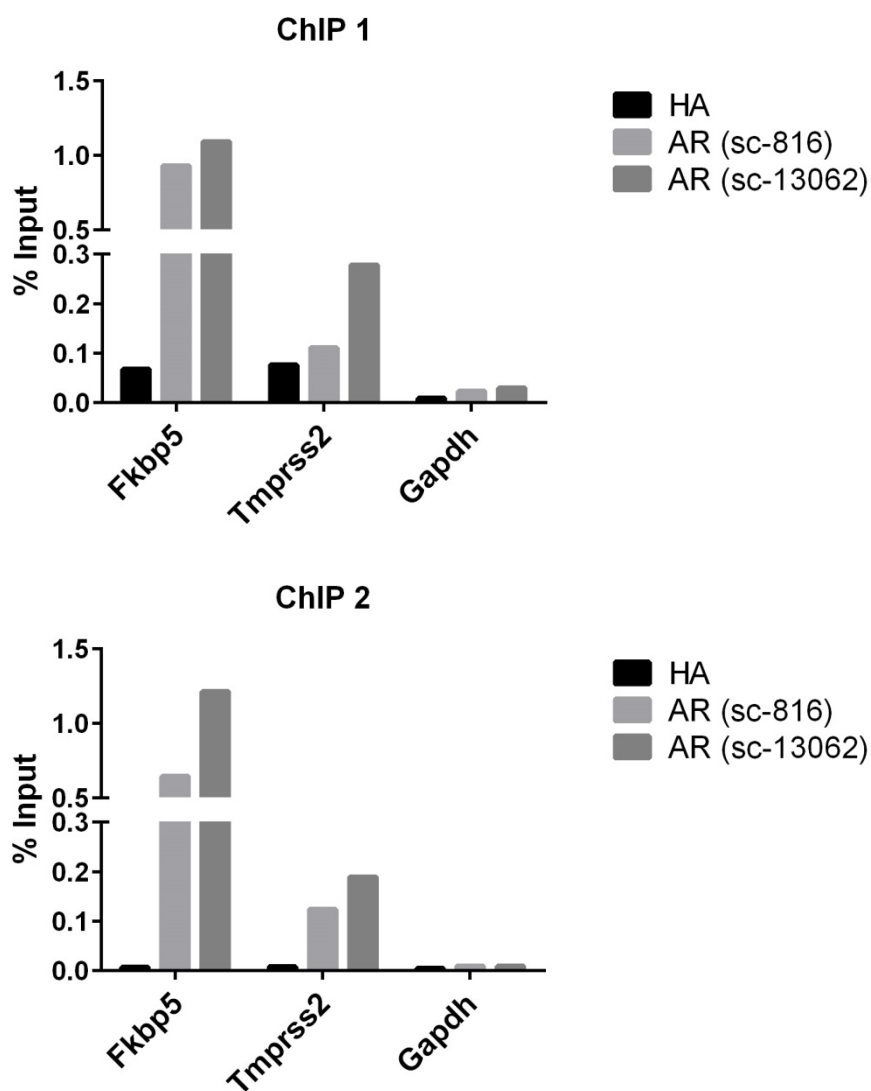


Figure 4.4.10 AR ChIP antibody selection

Graphs show SYBR Green qPCR analysis of replicate AR ChIP experiments to test the yield of AR target gene DNA using sc-816X or sc-13062X (Santa Cruz) AR antibodies. *Fkbp5* and *Tmprss2* primers correspond to known AR binding sites. *Gapdh* primers used as a negative control. Target gene enrichment presented as percentage input and compared to HA ChIP negative control.

Tumour samples to be analysed were snap frozen immediately following dissection and stored at -80°C . I wanted to compare AR enrichment in fresh and frozen tissue to make sure frozen tissue was suitable for AR ChIP analysis. AR ChIP was carried out on chromatin prepared from fresh and frozen *wildtype* prostate tissue. The enrichment of *Fkbp5* in fresh prostate tissue was greater than that in frozen tissue (Figure 4.4.11). However, *Fkbp5* enrichment was observed in DNA eluted from AR ChIP in frozen tissue, and was significantly higher than negative HA ChIP and non-target controls (Figure 4.4.11).

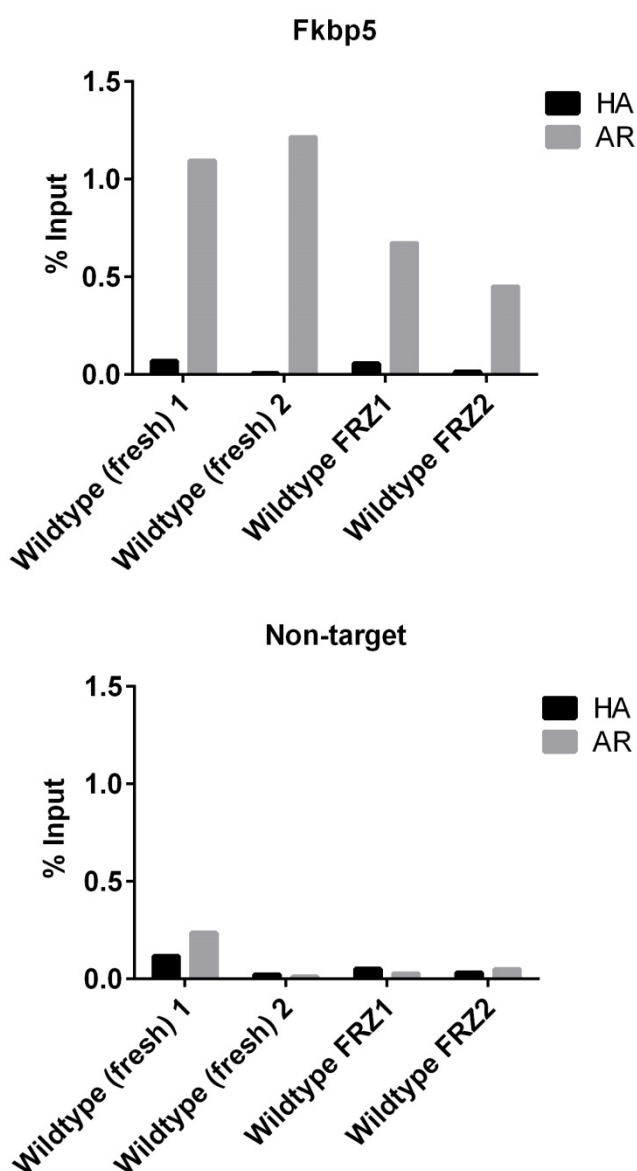


Figure 4.4.11 AR enrichment at *Fkbp5* in fresh and frozen tissue

Graphs show SYBR Green qPCR analysis of AR ChIP experiments to measure the enrichment of AR at *Fkbp5* enhancer region and non-target negative control in chromatin prepared from fresh and frozen *wildtype* prostate tissue. The intronic region of the ligand-dependent nuclear receptor corepressor-like (*Lcor*) gene was used for non-target control primers. Target gene enrichment is presented as percentage input and compared to HA ChIP negative control. (FRZ signifies frozen samples.)

4.4.3 Enrichment of AR binding at target genes is altered in β -catenin-driven prostate cancer

I proceeded to analysis AR enrichment at target genes in *wildtype* and hormone-naïve *Nkx3.1^{CreERT2} Pten^{fl/+} Ctnnb1^{(ex3) Δ /+}* prostate tissue that had been snap frozen immediately after dissection.

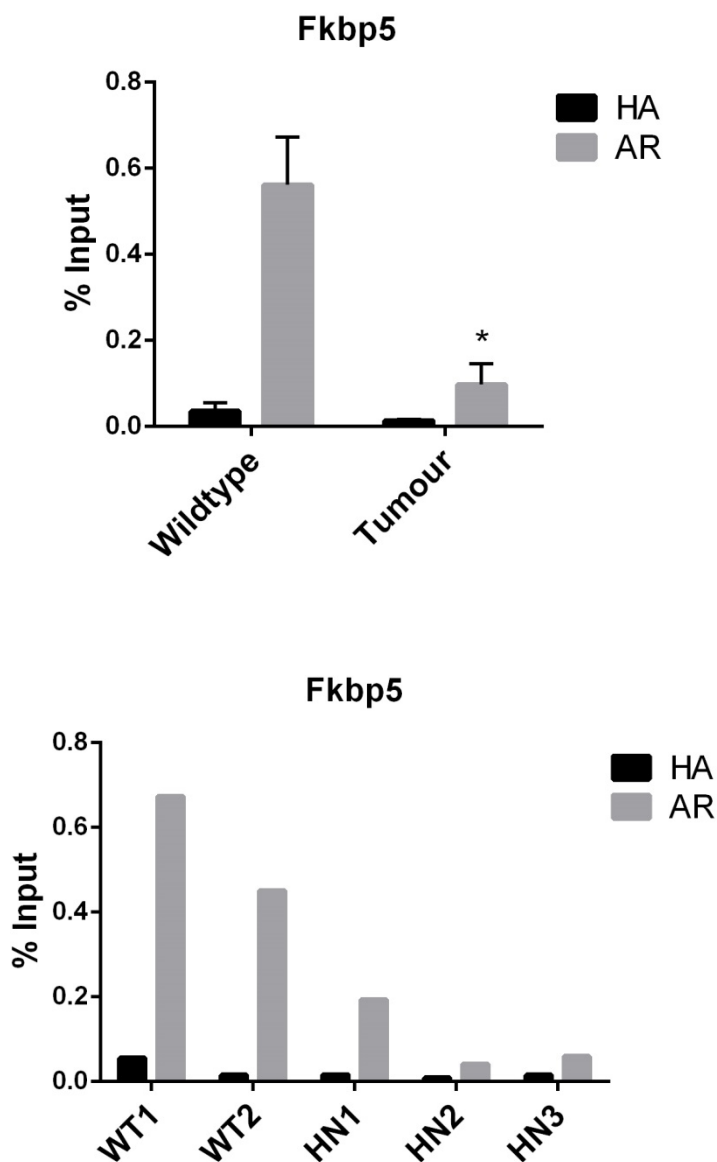


Figure 4.4.12 Hormone-naïve *Nkx3.1^{CreERT2} Pten^{fl/+} Ctnnb1^{(ex3) Δ /+}* tumours have decreased enrichment of AR binding at *Fkbp5* compared to *wildtype*

Graphs show SYBR Green qPCR analysis of AR enrichment at *Fkbp5* in *wildtype* (n=2) and *Nkx3.1^{CreERT2} Pten^{fl/+} Ctnnb1^{(ex3) Δ /+}* (n=3) prostate tissue. Upper graph shows combined analysis of *Fkbp5* enrichment in AR ChIP DNA samples for biological replicates; lower graph shows data for each sample. *Fkbp5* enrichment presented as percentage input and compared to HA ChIP negative control. (* p value <0.05; analysed by unpaired, two-tailed student t-test, compared to wildtype ChIP AR). Data are presented as mean \pm SD.

There was a significant decrease in AR enrichment at the *Fkbp5* enhancer binding site in tumour compared to *wildtype* prostate tissue (Figure 4.4.12). This correlated with decreased *Fkbp5* mRNA expression changes observed in *Nkx3.1^{CreERT2} Pten^{fl/+} Ctnnb1^{(ex3)Δ/+}* tumours (Figure 4.4.4). A similar decrease in AR enrichment at the *ApoF* promoter region was also observed (Figure 4.4.13), while there was no significant enrichment in non-target negative control (Figure 4.4.14).

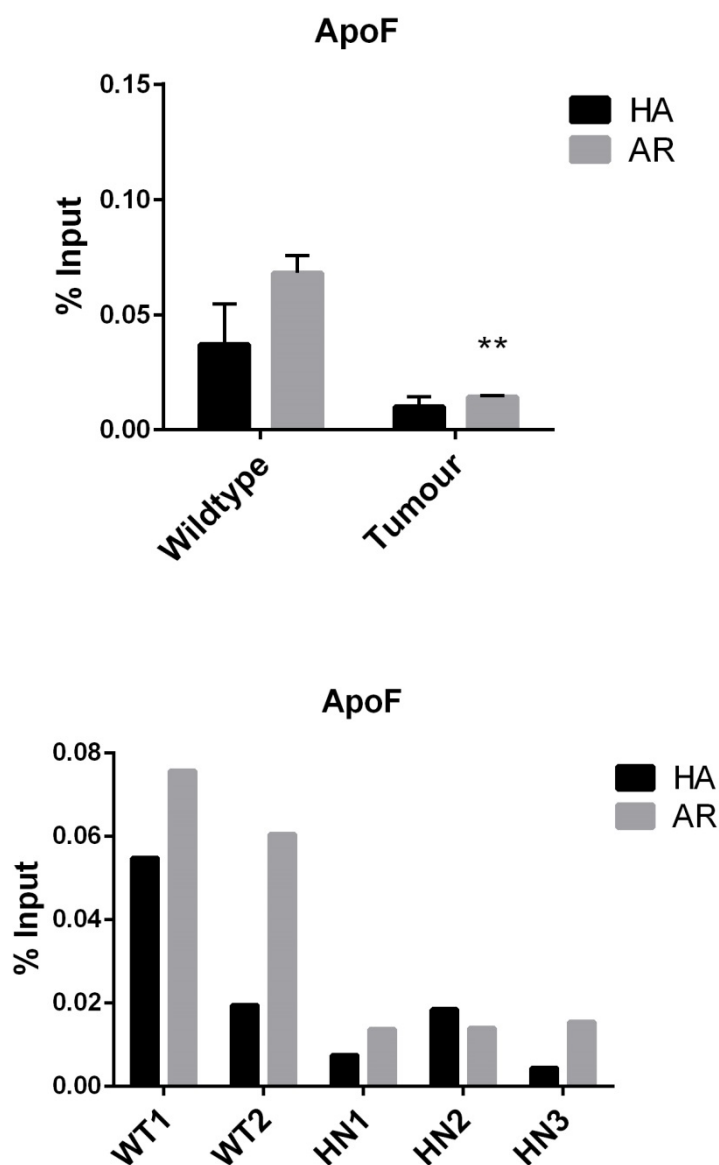


Figure 4.4.13 Hormone-naïve *Nkx3.1^{CreERT2} Pten^{fl/+} Ctnnb1^{(ex3)Δ/+}* tumours have decreased enrichment of AR binding at *ApoF* compared to *wildtype*

Graphs show SYBR Green qPCR analysis of AR enrichment at *ApoF* in *wildtype* (n=2) and *Nkx3.1^{CreERT2} Pten^{fl/+} Ctnnb1^{(ex3)Δ/+}* (n=3) prostate tissue. Upper graph shows combined analysis of *ApoF* enrichment in AR CHIP DNA samples for biological replicates; lower graph shows data for each sample. *ApoF* enrichment presented as percentage input and compared to HA CHIP negative control. (** p value <0.01; analysed by unpaired, two-tailed student t-test, compared to wildtype CHIP AR). Data are presented as mean ± SD.

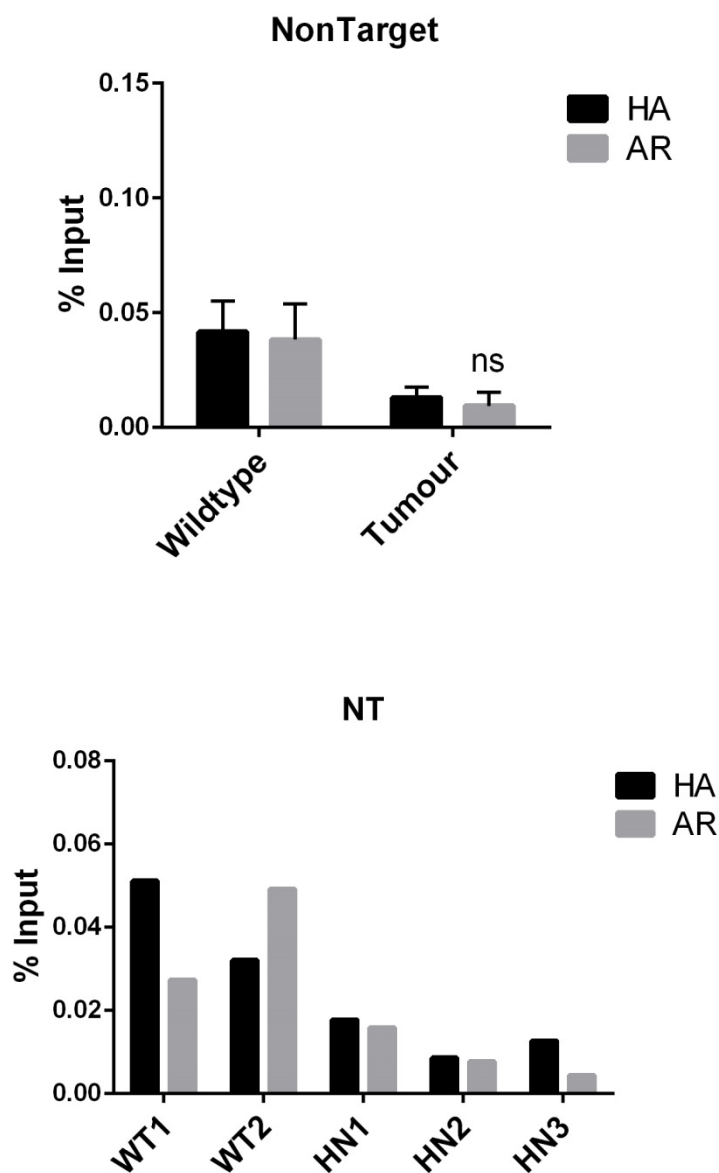


Figure 4.4.14 No enrichment of AR binding is observed at non-target negative control

Graphs show SYBR Green qPCR analysis of AR enrichment at non-target gene negative control in *wildtype* (n=2) and *Nkx3.1^{CreERT2} Pten^{fl/+} Ctnnb1^{(ex3) Δ /+}* (n=3) prostate tissue. The intronic region of the *Lcor* gene was used as a non-target control. Upper graph shows combined analysis of non-target gene enrichment in AR ChIP DNA samples for biological replicates; lower graph shows data for each sample. *Non-target* enrichment presented as percentage input and compared to HA ChIP negative control. (ns = not significant; analysed by unpaired, two-tailed student t-test, compared to wildtype ChIP AR). Data are presented as mean \pm SD.

ChIP-qPCR data indicated that the level of AR binding enrichment at target genes correlated with transcript expression. At least 3 ng DNA was acquired from each ChIP assay and samples have been sent for whole genome sequencing analysis to identify AR binding regions in *wildtype* prostate, and how this enrichment is altered in hormone-naïve tumours with β -catenin activation and Pten loss.

4.5 Discussion

Wnt/ β -catenin activation and PTEN loss are both associated with lethal metastatic CRPC in men [99]. Mice which develop advanced prostate tumours, as a consequence of genetic alterations that drive aberrant β -catenin activation and Pten loss, become resistant to ADT and progress to CRPC. Using the *Nkx3.1^{CreERT2}* system, I have generated novel pre-clinical *in vivo* models for CRPC with β -catenin activation (*Ctnnb1^{(ex3) Δ /+}*) alone and in combination with heterozygous (*Pten^{fl/+}*) or homozygous (*Pten^{fl/fl}*) Pten loss. Only one of five *Nkx3.1^{CreERT2} Ctnnb1^{(ex3) Δ /+}* mice developed detectable CRPC, following castration at 7 months post-*Cre* induction. Nonetheless, this confirms that β -catenin activation does promote tumour cell growth and proliferation post-castration, as previously described [149].

ADT provided no survival advantage to *Nkx3.1^{CreERT2} Pten^{fl/+} Ctnnb1^{(ex3) Δ /+}* mice when they were castrated 7 months post-induction. Although overall tumour burden was reduced at endpoint in comparison to intact controls, mice reached clinical endpoint due to weight loss and decreased activity, in the absence of obvious macroscopic evidence of widespread metastasis. This is relevant to clinical CRPC in that the prostate is often small, with low tumour load within the prostate, and patients develop paraneoplastic symptoms, such as weight loss and fatigue [200]. While *Nkx3.1^{CreERT2} Pten^{fl/fl} Ctnnb1^{(ex3) Δ /+}* ADT-treated mice lived ~3 months longer than controls, there was no significant difference in the endpoint tumour burden in this aggressive model of CRPC.

Castration resistant *Nkx3.1^{CreERT2} Pten^{fl/+} Ctnnb1^{(ex3) Δ /+}* prostate tumours are highly proliferative, correlating with nuclear β -catenin expression in a large proportion of tumour cells. Despite observing reduced levels of Pten expression, survival of tumour cells was not fuelled by PI3K/Akt signalling, as indicated by a lack of phospho-Akt expression. Critically, loss of nuclear AR expression indicates that classical AR signalling is not reactivated in this model of CRPC and growth and proliferation, therefore, occurs through alternative mechanisms. Similar observations were made in the *Nkx3.1^{CreERT2} Ctnnb1^{(ex3) Δ /+}* castration-resistant tumour, demonstrating the role of β -catenin activation in driving the transition from HNPC to CRPC.

Nkx3.1 loss of function in the mouse prostate is reported to cause cancer initiation [175], demonstrating the tumour suppressive role of *Nkx3.1*. *Cre* expression using the *Nkx3.1^{CreERT2}* system effectively results in heterozygous loss of *Nkx3.1*. While the histology of *Nkx3.1^{CreERT2} wildtype* mice, 12-months post-castration, showed little evidence of cancer initiation, castrated *Nkx3.1^{CreERT2} wildtype* mice have reduced *Pten*, increased Akt activation and loss of nuclear AR. This does not result in proliferation but may increase pro-survival signalling and stress in the prostatic epithelium. Co-operation between *Nkx3.1* and *Pten* haploinsufficiency in mouse prostate tissue has previously been shown to lead to invasive adenocarcinoma in aging mice [164] and androgen-independent growth following castration [201]. However, we did not find evidence of this in prostate tissue from *Nkx3.1^{CreERT2} Pten^{fl/+}* mice 12 months post-induction, indicating that the heterozygous loss of *Nkx3.1*, as result of induction, does not have a potent co-operative effect in this model.

The tumours that developed resistance to ADT were characterised by elevated expression of Wnt pathway components. Elevated *Myc* expression in *Nkx3.1^{CreERT2} Pten^{fl/+} Ctnnb1^{(ex3) Δ /+}* tumours indicated that there was increased canonical Wnt pathway activity, which drives cell cycle progression, protein synthesis and stem cell renewal, and is a known cancer oncogene [133]. High levels of the β -catenin-independent, non-canonical Wnt pathway ligand, *Wnt5a*, were also expressed in CRPC. Non-canonical Wnt signalling activates protein kinase C, Rho/ROCK and Rac/JAK pathways involved in cell polarity and migration [202]. *Wnt5a* is reported to play a role in the attenuation of canonical Wnt/ β -catenin signalling [203]. It is negatively regulated by testosterone during prostate development [204] and has been associated with aggressive prostate cancer and relapse following treatment intervention [205]. As our model forces the hyper-activation of Wnt/ β -catenin signalling in prostate epithelial cells, it is not clear whether the enrichment in *Wnt5a* is a specific consequence of aberrant β -catenin activation and/or *Pten* loss following ADT, or a more general response to ADT. However, we are further investigating the potential of *Wnt5a* as a biomarker or therapeutic target for CRPC.

Evidence of increased Wnt ligand expression in the CRPC tumours led us to test the efficacy of Wnt inhibition in combination with ADT. Treatment with PORCN inhibitor, LGK-974, showed modest effects with respect to controls, and

histopathological analysis suggested there was reduced cell proliferation and β -catenin levels following Wnt inhibition. However, due to the variation between samples in each group, it was difficult to conclude whether Wnt inhibitor treatment increased the rate of tumour regression in prostate cancer following ADT. Further work is required to assess the effects of Wnt inhibitor in prostate tissue, including measurement of Wnt expression in treated versus control tumours.

Variations between $Nkx3.1^{CreERT2} Ctnnb1^{(ex3)\Delta/+}$ and $Nkx3.1^{CreERT2} Pten^{fl/+} Ctnnb1^{(ex3)\Delta/+}$ mice are likely to be partly due to use of the tamoxifen-inducible system for *Cre* induction. Induction efficiency can be affected by tamoxifen batch variation and administration. In general, evidence of efficient recombination was observed in mice taken 2 months post-induction but tumour burden was not consistent at the time point established for castration. Additionally, the mixed background of mice may affect tumour-host interaction and contribute to this variation in rate of tumour development.

The ADT/Wnt inhibitor study may benefit from better stratification of mice prior to treatment intervention, using a method such as CT *in vivo* imaging to determine when tumour size has reached the required threshold to commence treatment. Unfortunately, this facility was not available during the course of this project. An increased dose of LGK-974, if tolerated by mice, could also be tested if the current dose has limited effect on Wnt inhibition. However, inhibiting Wnt secretion elicits some toxicity to other organs, such as skin, due to reliance on Wnt for homeostatic processes [206], and may result in side-effects. If Wnt5a is particularly important for sustaining growth and survival in CRPC, it may be possible to specifically target this ligand.

The upregulation of Wnt signalling in $Nkx3.1^{CreERT2} Pten^{fl/+} Ctnnb1^{(ex3)\Delta/+}$ CRPC does not lead to AR reactivation and proliferation occurs independently of classical AR signalling. A pseudo-castrate gene expression signature was associated with aberrant β -catenin activation in hormone-naïve prostate cancer and this pattern of androgen-responsive gene expression was not greatly altered in CRPC. In corroboration with published evidence that β -catenin activation downregulates AR signalling during progression to adenocarcinoma [150], this suggests that β -catenin is capable of reprogramming AR signalling, which may

promote resistance to ADT in invasive prostate tumours. AR reprogramming has previously been observed in *Pten* null prostate tumours, and was attributed to activation of PI3K/Akt bypassing the need for AR signalling [119]. I have shown in Chapter 3 that β -catenin activation drives progressive loss of Pten in advanced *Pb-Cre Cttnb1^{(ex3) Δ /+}* prostate tumours and also observe loss of Pten in advanced *Nkx3.1^{CreERT2} Cttnb1^{(ex3) Δ /+}* tumours. This may indicate co-operation between β -catenin and Pten loss is required to drive the pseudo-castrate gene signature. However, tumours harbouring β -catenin activation retain nuclear AR and do not have high levels of PI3K/Akt, indicating that two different mechanisms are at play in these and *Pten* null tumours. Each may predispose HNPC tumours to ADT-resistance but further work is required to understand the mechanisms of AR reprogramming and their co-operation in these models. Furthermore, there were a handful of genes that did not follow the castrate pattern of expression in hormone naïve tumours. These were not investigated in the scope of this project but their roles and regulation pre- and post-castration may be important in the development of CRPC.

Fkbp5, *ApoF*, *Timp4* and *Tmem97* expression was down-regulated in *wildtype* prostate tissue following castration [119] and in β -catenin-driven HNPC. However, their expression was not further downregulated in CRPC with β -catenin activation. *Fkbp5* is known to play a major role in the activity of steroid receptors, including androgen receptor, through complexes formed with heat-shock protein 90 (Hsp-90) [207]. The downregulation of *Fkbp5* expression itself is indicative of AR reprogramming. *ApoF*, also known as lipid transfer inhibitor protein (LTIP), has reported roles in HDL metabolism and reverse cholesterol transport, and has been found to reduce HDL cholesterol metabolism when overexpressed in mice [208]. However, another study on the effects of *ApoF* deficiency did not show any significant change in HDL cholesterol metabolism [209] and there are no reports of its role in prostate cancer. *Timp4* is an endogenous inhibitor of matrix metalloproteinases (MMPs) and the decline in TIMP-4 expression has been associated with invasive prostate cancer [210]. MMPs, also known as matrixins, are key regulators of cell-cell and cell-extracellular matrix interactions and are associated with the tumour microenvironment in cancer, promoting tumour progression, invasion and immune escape [211]. Therefore, *Timp4* loss may correlate with increased MMPs

activity in tissue, contributing to aggressive tumourigenesis. *Tmem97*, also known as MAC30, plays a role in cholesterol metabolism [212] and its downregulation has been associated with the inhibition of proliferation and migration in gastric cancer cells [213], while its overexpression has been correlated with poor prognosis in breast cancer [214]. The mechanisms by which the downregulation of *Fkbp5*, *ApoF*, *Timp4* and *Tmem97* expression elicits effects in HNPC driven by β -catenin activation are unclear. Further work is required to ascertain the clinical significance of expression changes in these genes.

AR ChIP experiments in hormone-naïve *Nkx3.1^{CreERT2} Pten^{fl/+} Ctnnb1^{(ex3) Δ /+}* prostate tissue confirmed that lower expression of *Fkbp5* and *ApoF* correlated with lower AR binding enrichment at these genes. This indicates that β -catenin activation alters AR binding at target genes, perhaps by sequestering AR or due to competition for binding with other transcription factors regulated by β -catenin, and, in this way, AR signalling is reprogrammed. Whole genome sequencing of AR ChIP DNA samples from *wildtype* and *Nkx3.1^{CreERT2} Pten^{fl/+} Ctnnb1^{(ex3) Δ /+}* tumour tissue will help to identify changes in AR binding enrichment at target genes. ChIP sequencing data can be overlaid with RNA sequencing gene expression data to identify the functional effects of changes in AR enrichment at target genes, which are associated with β -catenin activation in tumours.

Work so far has investigated the effects of ADT in advanced stages of prostate cancer, but experiments have been set up to investigate resistance at early stages of tumourigenesis in mice castrated 1 month post-induction. Published data suggests that, at early stages of tumourigenesis, prostate tissue will regress in response to ADT regardless of β -catenin activation [151] or *Pten* loss [118]. Indeed, our data show that AR signalling in *Ctnnb1^{(ex3) Δ /+}* and *Pten^{fl/+} Ctnnb1^{(ex3) Δ /+}* tissue is comparable to *wildtype* 2 months-post induction, with a trend towards upregulation of *AR* and *ApoF* expression in *Pten^{fl/+} Ctnnb1^{(ex3) Δ /+}* prostates. It is interesting to note that *Pten^{fl/+}* prostate tissue develops PIN at 12 months post-induction and increased expression of *AR* and *Fkbp5* was observed at this time point, correlating with early tumourigenesis in this model.

While it appears that ablation of androgens at early stages of prostate tumourigenesis effectively attenuates tumour progression [151], further work is required to establish the stage at which ADT-resistant cells emerge in tumours driven by β -catenin activation. Having confirmed that CARNs remain in regressed prostate tissue following castration and are regenerated after AR reactivation, as previously described [23], we can also use the *Nkx3.1^{CreERT2}* system to study whether genetic alterations such as β -catenin mutation and *Pten* loss can drive regeneration and tumourigenesis in these cells following ADT and without androgen replacement. Work is ongoing to study the effects of tamoxifen-induction of *Cre* at 1 month post-castration in *Nkx3.1^{CreERT2} Pten^{fl/fl} Ctnnb1^{(ex3) Δ /+}* mice in comparison to *Nkx3.1^{CreERT2} Pten^{fl/fl}* controls. Initial experiments have been initiated using this aggressive prostate cancer model which is likely to drive more pronounced tumourigenic effects. In the future, RFP can be used as a marker in our *Nkx3.1^{CreERT2}* prostate cancer models to monitor the role of CARNs in CRPC.

In summary, ADT is having an incomplete effect on the treatment of advanced, invasive prostate cancer driven by aberrant β -catenin activation, leading to CRPC. Higher grade tumours have hyper-activation of multiple pro-growth, pro-survival pathways, making them less reliant on AR signalling. Therefore, tumour cells can quickly overcome AR loss as a consequence of ADT, particularly if a proportion of tumour epithelial cells have adapted to actively proliferate in a pseudo-castrate environment. This highlights the value of using a combinatorial therapeutic approach from the outset to eradicate tumour cells that may be pre-disposed to ADT-resistance, while also targeting ADT-responsive cells.

Chapter 5 – Final Summary and Concluding Remarks

5.1 Final Summary

Prostate cancer is a highly heterogeneous disease, with varying risk of cancer progression following diagnosis. Current methods of diagnosis by serum PSA testing and histopathological Gleason score of needle biopsies have limited prognostic capability. To effectively manage prostate cancer treatment, better diagnostic biomarkers require to be developed in order to distinguish between cancers with high-risk of progression to locally advanced and metastatic disease, and those that will remain indolent. At least 20% of patients develop locally advanced and metastatic prostate cancer and ADT is generally the first line therapy for these men. Prostate cancers invariably develop resistance to ADT, leading to lethal metastatic CRPC. Earlier detection and therapeutic intervention may avoid progression to locally advanced disease and the requirement for ADT. However, this does not benefit patients with locally advanced disease at the time of diagnosis. Therefore, it is essential that mechanisms driving aggressive prostate cancers and castration-resistance are understood in order to improve treatment options for these patients.

Over the past 5 years, researchers have made a concerted effort to understand prostate cancer evolution and molecular aberrations associated with poor prognosis, through phylogenetic mapping and molecular profiling of clinical prostate cancer samples. In one study, Markert et al. [100] identified five molecular subtypes that could be used to stratify prostate cancer patients, in a watchful-waiting cohort, according to risk of cancer progression and survival outcome. This demonstrated that a number of patients initially diagnosed with low Gleason score prostate cancer progress to aggressive disease. Prostate cancers harbouring an ESC-like signature, *MYC* activation, *PTEN* loss, and increased proliferation were the most aggressive and correlated with the poorest prognosis [100]. *MYC* activation is indicative of Wnt/ β -catenin pathway activation and *PTEN* loss with PI3K/Akt pathway activation. Both pathways are frequently deregulated in aggressive, metastatic prostate cancer [41] and enriched in lethal metastatic CRPC [99], illustrating the significant role they play in aggressive and treatment-resistant disease. Furthermore, data from our laboratory confirms that co-occurrence of nuclear β -catenin and *PTEN* loss in Gleason score 3-5 prostate cancers positively correlates with poor survival outcome.

Clinically, molecular profiling offers a means of earlier diagnosis and better prediction of patient prognosis. From a research perspective, it has highlighted the genetic aberrations associated with aggressive prostate cancers that currently have limited treatment options. Investigation into the biological co-operation between aberrations that drives aggressive prostate cancer, and elucidation of alterations that may confer resistance to treatment, is required to inform novel strategies for therapy and prostate cancer management.

Therefore, this project was initiated to investigate the role of canonical Wnt pathway activation and its co-operation with PTEN loss during prostate cancer initiation and progression, and in the emergence of castration-resistant disease.

Using pre-clinical transgenic mouse models with prostate-targeted, heterozygous deletion of *Ctnnb1 exon3*, I have shown that constitutive activation of β -catenin drives prostate cancer initiation and ultimately leads to advanced adenocarcinoma, with a clinical endpoint of ~12 months in the *Pb-Cre* model, evidence of which has only recently been reported [151]. Consistent with clinical data [99, 156] and a previous mouse study [149], β -catenin-driven tumours develop castration-resistance, with cells continuing to proliferate following ADT.

Concurrent heterozygous deletion of *Pten exon5* increases the rate of cancer progression, and *Pten* null tumours with β -catenin activation have the shortest latency and poorest survival outcome. This dose-dependent effect of *Pten* loss demonstrates the co-operation between β -catenin and *Pten* loss in aggressive prostate cancer, corroborated by recently published data from a similar mouse model [138]. *Pten* loss increases cell survival signals through PI3K/Akt pathway activation and increased expression of survivin, while β -catenin activation drives increased levels of Cyclin D1 and Myc, driving cell cycle progression and proliferation. In this way, PI3K/Akt and Wnt/ β -catenin signalling pathways co-operate to drive aggressive prostate cancer.

There is evidence to suggest that PTEN loss is able to activate Wnt/ β -catenin signalling, via Akt phosphorylation of GSK3 β and inactivation of the β -catenin destruction complex, independently of Wnt signalling [153, 154]. However, β -catenin was not required for tumourigenesis in a *Pten* null prostate cancer mouse model [138], suggesting little impact of this mechanism in prostate

tumorigenesis, while mechanisms for PTEN modulation by β -catenin have not been reported.

I have provided evidence that β -catenin-driven prostate tumorigenesis is limited by Pten and overcomes Pten-mediated tumour suppression to facilitate cancer progression (Figure 5.1.1). Consistent with previous observations in intestinal stem cells [182], the proliferation of prostate cells with nuclear β -catenin is ROS-dependent. During β -catenin-driven cancer initiation, increased ROS correlates with elevated expression of Rac-GEFs, *Tiam1* and *Vav3*, and higher levels of active Rac1-GTP, which mediates ROS production through interaction with the NOX signalling complex [182]. Elevated ROS, in turn, drives the phosphorylation, stabilisation and nuclear accumulation of Pten observed in *Cttnb1*^{(ex3) Δ /+} PIN lesions. Although this contributes to phosphatase-independent Pten/p53-mediated growth arrest in the nucleus [110, 112], it simultaneously reduces levels of cytoplasmic Pten and relieves phosphatase-dependent Pten tumour suppression at the cell membrane. This results in low levels of Akt activation, which is sufficient for cell survival. While Pten/p53-mediated growth arrest contributes to the increased latency of prostate tumours with β -catenin activation alone, it is not sufficient to stop progression to adenocarcinoma. Thus, β -catenin modulates Pten by a ROS-mediated mechanism to overcome endogenous tumour suppression, and activates downstream targets, including Myc and Cyclin D1, which drive tumour growth and proliferation.

The quenching of ROS by NAC treatment in *Pb-Cre Cttnb1*^{(ex3) Δ /+} mice reduces nuclear Pten, increases cytoplasmic Pten and abrogates Akt activation and cell proliferation, demonstrating the validity of this mechanism. The same experiment in *Pten*^{fl/+} *Cttnb1*^{(ex3) Δ /+} mice did not show a significant effect, due to co-operation with Pten haploinsufficiency, which conversely promotes cell survival and proliferation in the absence of ROS, as demonstrated in previous work from our laboratory [110]. The capacity for molecular aberrations, such as β -catenin activation and Pten loss, to determine the role of ROS in tumour initiation and progression has implications for the use of antioxidants for prostate cancer prevention. Although oxidative stress and DNA damage are considered to be prostate cancer risk factors [65, 66], there has been mixed success in prevention trials investigating the potential of antioxidant supplements to reduce prostate cancer risk [68-70]. Indeed, our data suggest a

context-dependent role for ROS with respect to the genetic alterations responsible for driving prostate cancer initiation and progression and help to explain the variations in efficacy of antioxidant supplements for prostate cancer prevention.

In addition to driving ROS-mediated modulation of Pten localisation, I have shown that β -catenin activation leads to downregulation of *Pten* expression and genomic loss of *Pten* in advanced prostate cancer (Figure 5.1.1). Tumours initiated from activation of β -catenin alone, progressively lose *Pten* mRNA expression, correlating with increased expression of *miRNAs 17, 18a, 19b* and *21*, which negatively regulate *Pten*. Moreover, I observe a reduction in *Pten* copy number in tumour epithelial cells relative to stroma, suggesting these tumours become *Pten* haploinsufficient. As *Pten*^{fl/+} *Ctnnb1*^{(ex3) Δ /+} prostate cancer progresses to advanced adenocarcinoma there is LOH in *Pten*, which accounts for the decrease in *Pten* mRNA expression beyond levels associated with heterozygous *Pten* loss. Thus, loss of *Pten* occurs when there is activation of β -catenin in tumours, placing Pten loss as a later event in prostate cancer evolution with respect to β -catenin activation, and is consistent with reports that *Pten* copy number loss occurs during the development of localised adenocarcinoma [39-41]. Elevated levels of ROS, driven by β -catenin activation, will increase DNA damage and are likely to contribute to genomic loss of *Pten*. This provides an explanation for the incidence of *PTEN* haploinsufficiency in human prostate cancers with canonical Wnt pathway activation, and furthermore, explains the frequent co-occurrence of high levels of nuclear β -catenin and *PTEN* loss in aggressive prostate cancers.

AR signalling remains the central target for treatment of locally advanced and metastatic prostate cancer [76], due to its pivotal role in the survival and proliferation of prostate cancer cells [2]. It is apparent from the literature that malignant prostate cells harbouring mutant *β -catenin* [151] or homozygous *Pten* loss [118] are ablated in response to castration at early stages of tumourigenesis. However, castration of *Nkx3.1*^{CreERT2} *Pten*^{fl/+} *Ctnnb1*^{(ex3) Δ /+} mice at later stages of tumour development leads to the emergence of CRPC. Although a reduction in tumour size indicates a proportion of tumour cells are responsive to androgen deprivation, the remaining castration-resistant cells are highly proliferative. Various mechanisms have been proposed for the invariable emergence of

castration-resistant disease following treatment with ADT, including the reactivation of AR signalling due to alterations in cofactors [84]. While β -catenin is a known AR cofactor [157], its aberrant activity does not result in classical AR reactivation in CRPC, demonstrated by the absence of nuclear AR in these tumours. Therefore, CRPC in this model must be driven by an alternative mechanism, independently of classical AR signalling.

I have identified a pseudo-castrate expression signature of androgen-responsive genes in hormone-naïve *Cttnb1*^{(ex3) Δ /+} prostate cancer and propose that this is likely to confer resistance to ADT (Figure 5.1.1). A similar pseudo-castrate gene expression signature has been identified in hormone-naïve *Pten* null prostate tumours that progress to CRPC following ADT [119]. This indicates that both β -catenin activation and *Pten* loss reprogram AR signalling during tumour progression, promoting (classical) AR-independent mechanisms for cell survival and proliferation. Hence, β -catenin activation and PTEN loss are not only prognostic markers for poor survival outcome but also molecular biomarkers for high risk of developing resistance to ADT. These data highlight the significant requirement for alternative methods to treat patients with aggressive prostate cancer, either alone or in combination with ADT, to avoid progression to lethal castration-resistant disease.

By driving *Pten* loss, β -catenin activation facilitates the co-operation between pathways mediated by these two aberrations. It is this pathway co-operation that drives aggressive prostate cancer by tumour intrinsic and extrinsic mechanisms. I have shown that β -catenin driven tumours are characterised by activation of AMPK and PKA signalling pathways, which further coincides with the upregulation of genes involved in lipid and cholesterol uptake and transport, and cyclic-AMP biosynthesis. This illustrates the enhanced nutrient uptake and high energy requirements of cells for survival and proliferation, and offers a potential axis on which to therapeutically target these tumours. High systemic levels of lipid and cholesterol, associated with obesity, hypertension and Western lifestyle, may be etiological factors that contribute to the progression of highly catabolic prostate tumours. Therefore, some patients may benefit from dietary intervention to lower lipid and cholesterol availability.

β -catenin-driven tumours are further characterised by increased mTOR signalling, which is enhanced through co-operation with Pten loss, via Akt activation. mTOR pathway activation is indicative of increased amino acid uptake and energy metabolism required to fuel protein synthesis and cell growth [185]. However, tumours driven by canonical Wnt and PI3K/Akt pathway activation have been shown to be insensitive to mTOR inhibitors [193]. A recent study reported that mTOR pathway activation inhibits the utilisation of extracellular nutrients, which suppresses proliferation of highly catabolic cells [194]. Thus, mTOR inhibitors relieve this suppression, leading to uptake of extracellular amino acids as an alternative nutrient supply for highly catabolic cells, such as β -catenin-driven prostate tumour cells. This may have implications for the use of mTOR inhibitors for patients with prostate cancers harbouring Wnt/ β -catenin and PI3K/Akt pathway activation. It may be advisable to seek alternative therapies, despite the upregulation of mTOR signalling in these tumours.

Alternative therapeutic targets may be elucidated through better understanding of the co-operation between tumour extrinsic events associated with aggressive prostate tumourigenesis. I have identified changes in cytokine expression within tumours that may promote cancer progression, including the upregulation of cytokine IL-1ra when Pten is lost. IL-1ra dampens the effects of pro-inflammatory cytokines [197], released following the infiltration of macrophages and neutrophils, during cancer initiation and tumourigenesis. This is likely to be pro-tumourigenic by helping to evade anti-tumourigenic effects of innate immune response. In contrast, β -catenin activation, both independently and concurrently with Pten loss, appears to prevent upregulation of BLC/CXCL13 in tumours, indicating that these tumours evade recruitment of B lymphocytes to tissue. Additional work is required to link these findings to the significant enrichment of differential gene expression in classical, alternative and lectin-induced complement pathways in advanced *Pten*^{fl/+} *Cttnb1*^{(ex3) Δ /+} prostate tumours. However, it is apparent that underlying genetic aberrations within prostate tumours differentially modulate pro- and anti-tumourigenic effects of the host immune response to facilitate cancer progression.

Finally, the emergence of CRPC in *Nkx3.1*^{CreERT2} *Pten*^{fl/+} *Cttnb1*^{(ex3) Δ /+} mice is associated with significant enrichment of the Wnt signalling pathway, including

upregulation of *Myc* and *Wnt5a* (Figure 5.1.1). This suggests a role for both canonical and non-canonical Wnt signalling in AR-independent CRPC. *Myc* activation drives cell cycle progression and proliferation [133], contributing to the continuous growth of these castration-resistant cells. *Wnt5a* is negatively regulated by testosterone [204] and may be a useful biomarker for androgen-independent disease progression. Its association with aggressive prostate cancer and relapse following treatment [205] may also implicate *Wnt5a* as a therapeutic target for CRPC. There is certainly potential for the use of Wnt inhibitors, to target both canonical and non-canonical pathways, in combination with ADT. By simultaneously targeting AR-dependent and AR-independent mechanisms for cell survival and proliferation, aggressive prostate cancers may be effectively treated, avoiding the emergence of CRPC.

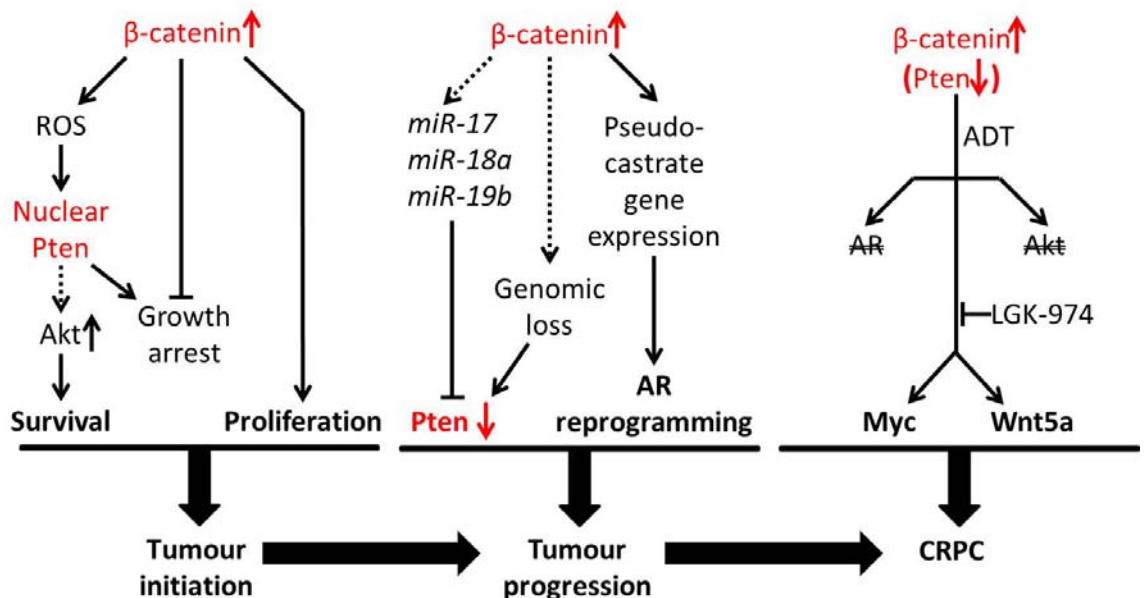


Figure 5.1.1 Summary of the role of β -catenin in prostate cancer tumourigenesis and treatment resistance

β -catenin activation must overcome Pten-mediated tumour suppression to drive prostate tumourigenesis. β -catenin activation drives ROS-mediated modulation of Pten localisation, resulting in nuclear accumulation of Pten and activation of Akt at the membrane, which promotes cell survival. β -catenin activation overcomes Pten-mediated growth arrest and drives proliferation, resulting in tumour initiation. During the progression of β -catenin-driven prostate cancer, Pten expression is downregulated, coinciding with increased expression of microRNAs that negatively regulate *Pten*, and genomic loss of *Pten*. A pseudo-castrate androgen-responsive gene expression signature occurs in β -catenin-driven tumours and may facilitate the emergence of CRPC that occurred following ADT. β -catenin-driven CRPC progresses independently of classical AR signalling and Akt activation. Instead tumour progression is associated with upregulation of canonical and non-canonical Wnt signalling. Thus, Wnt inhibition (LGK-974) in combination with ADT may be efficacious in preventing the emergence of CRPC.

The mouse models used in this project reliably mimic stages of human cancer progression and provide novel models for CRPC. These provide useful tools for the continued study of β -catenin-driven prostate cancer to identify efficacious therapeutic targets, and further elucidate mechanisms of treatment-resistance which lead to lethal CRPC. The *Nkx3.1^{CreERT2}* system can now be further manipulated to study the contribution of CARNs to the emergence of β -catenin-driven CRPC.

5.2 Concluding Remarks

Despite a plethora of evidence associating the upregulation of Wnt/ β -catenin signalling and PTEN loss with aggressive and castration-resistant prostate cancer, the role of β -catenin in prostate cancer tumourigenesis and treatment resistance is unclear. I have presented work which characterises the role of β -catenin as an oncogenic driver in prostate cancer, from cancer initiation to the emergence of castration-resistance, and confirm that concurrent deregulation of Wnt/ β -catenin and PTEN/PI3K signalling pathways drives aggressive prostate cancer with poor prognosis. I have shown what I believe to be a novel mechanism for the evolution of prostate tumours harbouring β -catenin activation, through the modulation and progressive loss of *Pten*, explaining the significant co-occurrence of β -catenin activation and *PTEN* loss observed in the most aggressive subset of human prostate cancers.

Within these tumours, pathway co-operation occurs through the activation of a number of intrinsic downstream signalling events that increase tumour cell survival, growth and proliferation, and may confer resistance to ADT by AR-reprogramming. Further pathway co-operation occurs through tumour extrinsic events, manipulating tumour-host interaction, via regulation of cytokines and immune response, to facilitate cancer progression. Together these mechanisms, resulting from concurrent β -catenin activation and *Pten* loss, drive aggressive prostate cancer and contribute to the progression of castration-resistant disease. These data identify biomarkers and molecular targets that can potentially be exploited to inform management strategies and provide new treatment options for the most aggressive prostate cancers, leading to improved clinical outcome for these patients, and ultimately overcoming mechanisms of castration-resistance.

References

1. CancerResearchUK, *Prostate Cancer Statistics*. <http://www.cancerresearchuk.org/health-professional/cancer-statistics/statistics-by-cancer-type/prostate-cancer#heading-Five>, 2015(Accessed August 2015).
2. Huggins, C. and C.V. Hodges, *Studies on prostatic cancer. I. The effect of castration, of estrogen, and of androgen injection on serum phosphatases on metastatic carcinoma of the prostate*. *Cancer Research*, 1941(1): p. 293-297.
3. Saad, F. and K.S. Fizazi, *Androgen Deprivation Therapy and Secondary Hormone Therapy in the Management of Hormone-Sensitive and Castration Resistant Prostate Cancer*. *Urology*, 2015.
4. Cunha, G.R., et al., *The endocrinology and developmental biology of the prostate*. *Endocrine reviews*, 1987. **8**(3): p. 338-62.
5. Cunha, G.R., *Growth factors as mediators of androgen action during male urogenital development*. *The Prostate. Supplement*, 1996. **6**: p. 22-5.
6. Hayward, S.W., M.A. Rosen, and G.R. Cunha, *Stromal-epithelial interactions in the normal and neoplastic prostate*. *British journal of urology*, 1997. **79 Suppl 2**: p. 18-26.
7. Abate-Shen, C. and M.M. Shen, *Molecular genetics of prostate cancer*. *Genes & development*, 2000. **14**(19): p. 2410-34.
8. Litvinov, I.V., A.M. De Marzo, and J.T. Isaacs, *Is the Achilles' heel for prostate cancer therapy a gain of function in androgen receptor signaling?* *The Journal of clinical endocrinology and metabolism*, 2003. **88**(7): p. 2972-82.
9. Bonkhoff, H., U. Stein, and K. Remberger, *The proliferative function of basal cells in the normal and hyperplastic human prostate*. *The Prostate*, 1994. **24**(3): p. 114-8.
10. Bonkhoff, H., T. Fixemer, and K. Remberger, *Relation between Bcl-2, cell proliferation, and the androgen receptor status in prostate tissue and precursors of prostate cancer*. *The Prostate*, 1998. **34**(4): p. 251-8.
11. Robinson, E.J., D.E. Neal, and A.T. Collins, *Basal cells are progenitors of luminal cells in primary cultures of differentiating human prostatic epithelium*. *The Prostate*, 1998. **37**(3): p. 149-60.
12. van Leenders, G., et al., *Demonstration of intermediate cells during human prostate epithelial differentiation in situ and in vitro using triple-staining confocal scanning microscopy*. *Laboratory investigation; a journal of technical methods and pathology*, 2000. **80**(8): p. 1251-8.
13. Bonkhoff, H., et al., *Differential expression of 5 alpha-reductase isoenzymes in the human prostate and prostatic carcinomas*. *The Prostate*, 1996. **29**(4): p. 261-7.
14. Abrahamsson, P.A., *Neuroendocrine differentiation in prostatic carcinoma*. *The Prostate*, 1999. **39**(2): p. 135-48.
15. Yuan, T.C., S. Veeramani, and M.F. Lin, *Neuroendocrine-like prostate cancer cells: neuroendocrine transdifferentiation of prostate adenocarcinoma cells*. *Endocrine-related cancer*, 2007. **14**(3): p. 531-47.
16. Komiya, A., et al., *Neuroendocrine differentiation in the progression of prostate cancer*. *International journal of urology : official journal of the Japanese Urological Association*, 2009. **16**(1): p. 37-44.
17. Li, Z., et al., *Neuroendocrine differentiation of prostate cancer*. *Asian journal of andrology*, 2013. **15**(3): p. 328-32.

18. Wang, Z.A. and M.M. Shen, *Revisiting the concept of cancer stem cells in prostate cancer*. *Oncogene*, 2011. **30**(11): p. 1261-71.
19. Lawson, D.A. and O.N. Witte, *Stem cells in prostate cancer initiation and progression*. *The Journal of clinical investigation*, 2007. **117**(8): p. 2044-50.
20. Goldstein, A.S. and O.N. Witte, *Does the microenvironment influence the cell types of origin for prostate cancer?* *Genes & development*, 2013. **27**(14): p. 1539-44.
21. Xin, L., *Cells of origin for cancer: an updated view from prostate cancer*. *Oncogene*, 2013. **32**(32): p. 3655-63.
22. Goldstein, A.S., et al., *Identification of a cell of origin for human prostate cancer*. *Science*, 2010. **329**(5991): p. 568-71.
23. Wang, X., et al., *A luminal epithelial stem cell that is a cell of origin for prostate cancer*. *Nature*, 2009. **461**(7263): p. 495-500.
24. Wang, Z.A., et al., *Luminal cells are favored as the cell of origin for prostate cancer*. *Cell reports*, 2014. **8**(5): p. 1339-46.
25. De Marzo, A.M., et al., *Prostate cancer: New answers prompt new questions regarding cell of origin*. *Nature reviews. Urology*, 2010. **7**(12): p. 650-2.
26. Koh, C.M., et al., *MYC and Prostate Cancer*. *Genes & cancer*, 2010. **1**(6): p. 617-28.
27. De Marzo, A.M., et al., *Human prostate cancer precursors and pathobiology*. *Urology*, 2003. **62**(5 Suppl 1): p. 55-62.
28. De Marzo, A.M., et al., *Proliferative inflammatory atrophy of the prostate: implications for prostatic carcinogenesis*. *The American journal of pathology*, 1999. **155**(6): p. 1985-92.
29. Shappell, S.B., et al., *Prostate pathology of genetically engineered mice: definitions and classification. The consensus report from the Bar Harbor meeting of the Mouse Models of Human Cancer Consortium Prostate Pathology Committee*. *Cancer research*, 2004. **64**(6): p. 2270-305.
30. Bostwick, D.G., et al., *Antioxidant enzyme expression and reactive oxygen species damage in prostatic intraepithelial neoplasia and cancer*. *Cancer*, 2000. **89**(1): p. 123-34.
31. Meeker, A.K., et al., *Telomere shortening is an early somatic DNA alteration in human prostate tumorigenesis*. *Cancer research*, 2002. **62**(22): p. 6405-9.
32. Meeker, A.K., et al., *Telomere length abnormalities occur early in the initiation of epithelial carcinogenesis*. *Clinical cancer research : an official journal of the American Association for Cancer Research*, 2004. **10**(10): p. 3317-26.
33. Abate-Shen, C., M.M. Shen, and E. Gelmann, *Integrating differentiation and cancer: the Nkx3.1 homeobox gene in prostate organogenesis and carcinogenesis*. *Differentiation; research in biological diversity*, 2008. **76**(6): p. 717-27.
34. Asatiani, E., et al., *Deletion, methylation, and expression of the NKX3.1 suppressor gene in primary human prostate cancer*. *Cancer research*, 2005. **65**(4): p. 1164-73.
35. Gurel, B., et al., *Nuclear MYC protein overexpression is an early alteration in human prostate carcinogenesis*. *Modern pathology : an official journal of the United States and Canadian Academy of Pathology, Inc*, 2008. **21**(9): p. 1156-67.

36. Clark, J., et al., *Complex patterns of ETS gene alteration arise during cancer development in the human prostate*. *Oncogene*, 2008. **27**(14): p. 1993-2003.
37. Mosquera, J.M., et al., *Characterization of TMPRSS2-ERG fusion high-grade prostatic intraepithelial neoplasia and potential clinical implications*. *Clinical cancer research : an official journal of the American Association for Cancer Research*, 2008. **14**(11): p. 3380-5.
38. Albadine, R., et al., *TMPRSS2-ERG gene fusion status in minute (minimal) prostatic adenocarcinoma*. *Modern pathology : an official journal of the United States and Canadian Academy of Pathology, Inc*, 2009. **22**(11): p. 1415-22.
39. Verhagen, P.C., et al., *The PTEN gene in locally progressive prostate cancer is preferentially inactivated by bi-allelic gene deletion*. *The Journal of pathology*, 2006. **208**(5): p. 699-707.
40. Schmitz, M., et al., *Complete loss of PTEN expression as a possible early prognostic marker for prostate cancer metastasis*. *International journal of cancer. Journal international du cancer*, 2007. **120**(6): p. 1284-92.
41. Taylor, B.S., et al., *Integrative genomic profiling of human prostate cancer*. *Cancer cell*, 2010. **18**(1): p. 11-22.
42. Zhang, Z., et al., *Expression of p14ARF, p15INK4b, p16INK4a, and DCR2 increases during prostate cancer progression*. *Modern pathology : an official journal of the United States and Canadian Academy of Pathology, Inc*, 2006. **19**(10): p. 1339-43.
43. Humphrey, P.A., *Diagnosis of adenocarcinoma in prostate needle biopsy tissue*. *Journal of clinical pathology*, 2007. **60**(1): p. 35-42.
44. de la Taille, A., et al., *Beta-catenin-related anomalies in apoptosis-resistant and hormone-refractory prostate cancer cells*. *Clinical cancer research : an official journal of the American Association for Cancer Research*, 2003. **9**(5): p. 1801-7.
45. Chen, G., et al., *Up-regulation of Wnt-1 and beta-catenin production in patients with advanced metastatic prostate carcinoma: potential pathogenetic and prognostic implications*. *Cancer*, 2004. **101**(6): p. 1345-56.
46. Shen, M.M. and C. Abate-Shen, *Molecular genetics of prostate cancer: new prospects for old challenges*. *Genes & development*, 2010. **24**(18): p. 1967-2000.
47. Gelmann, E.P., *Molecular biology of the androgen receptor*. *Journal of clinical oncology : official journal of the American Society of Clinical Oncology*, 2002. **20**(13): p. 3001-15.
48. Nieto, M., et al., *Prostate cancer: Re-focusing on androgen receptor signaling*. *The international journal of biochemistry & cell biology*, 2007. **39**(9): p. 1562-8.
49. Bolton, E.C., et al., *Cell- and gene-specific regulation of primary target genes by the androgen receptor*. *Genes & development*, 2007. **21**(16): p. 2005-17.
50. Barbieri, C.E., et al., *Exome sequencing identifies recurrent SPOP, FOXA1 and MED12 mutations in prostate cancer*. *Nature genetics*, 2012. **44**(6): p. 685-9.
51. Gao, J., J.T. Arnold, and J.T. Isaacs, *Conversion from a paracrine to an autocrine mechanism of androgen-stimulated growth during malignant transformation of prostatic epithelial cells*. *Cancer research*, 2001. **61**(13): p. 5038-44.

52. Begley, L., et al., *CXCL12 overexpression and secretion by aging fibroblasts enhance human prostate epithelial proliferation in vitro*. *Aging cell*, 2005. **4**(6): p. 291-8.
53. Bavik, C., et al., *The gene expression program of prostate fibroblast senescence modulates neoplastic epithelial cell proliferation through paracrine mechanisms*. *Cancer research*, 2006. **66**(2): p. 794-802.
54. Bethel, C.R., et al., *Gene expression changes are age-dependent and lobe-specific in the brown Norway rat model of prostatic hyperplasia*. *The Prostate*, 2009. **69**(8): p. 838-50.
55. Dhom, G., *Epidemiologic aspects of latent and clinically manifest carcinoma of the prostate*. *Journal of cancer research and clinical oncology*, 1983. **106**(3): p. 210-8.
56. Dunn, J.E., *Cancer epidemiology in populations of the United States--with emphasis on Hawaii and California--and Japan*. *Cancer research*, 1975. **35**(11 Pt. 2): p. 3240-5.
57. Haverkamp, J., B. Charbonneau, and T.L. Ratliff, *Prostate inflammation and its potential impact on prostate cancer: a current review*. *Journal of cellular biochemistry*, 2008. **103**(5): p. 1344-53.
58. Klein, E.A. and R. Silverman, *Inflammation, infection, and prostate cancer*. *Current opinion in urology*, 2008. **18**(3): p. 315-9.
59. Bardia, A., et al., *Anti-inflammatory drugs, antioxidants, and prostate cancer prevention*. *Current opinion in pharmacology*, 2009. **9**(4): p. 419-26.
60. Borowsky, A.D., et al., *Inflammation and atrophy precede prostatic neoplasia in a PhIP-induced rat model*. *Neoplasia*, 2006. **8**(9): p. 708-15.
61. Nakai, Y., W.G. Nelson, and A.M. De Marzo, *The dietary charred meat carcinogen 2-amino-1-methyl-6-phenylimidazo[4,5-b]pyridine acts as both a tumor initiator and promoter in the rat ventral prostate*. *Cancer research*, 2007. **67**(3): p. 1378-84.
62. Elkahwaji, J.E., R.J. Hauke, and C.M. Brawner, *Chronic bacterial inflammation induces prostatic intraepithelial neoplasia in mouse prostate*. *British journal of cancer*, 2009. **101**(10): p. 1740-8.
63. Blum, D.L., et al., *Chemokine markers predict biochemical recurrence of prostate cancer following prostatectomy*. *Clinical cancer research : an official journal of the American Association for Cancer Research*, 2008. **14**(23): p. 7790-7.
64. De Marzo, A.M., et al., *Inflammation in prostate carcinogenesis*. *Nature reviews. Cancer*, 2007. **7**(4): p. 256-69.
65. Khandrika, L., et al., *Oxidative stress in prostate cancer*. *Cancer letters*, 2009. **282**(2): p. 125-36.
66. Minelli, A., et al., *Oxidative stress-related aging: A role for prostate cancer?* *Biochimica et biophysica acta*, 2009. **1795**(2): p. 83-91.
67. Nakayama, M., et al., *GSTP1 CpG island hypermethylation as a molecular biomarker for prostate cancer*. *Journal of cellular biochemistry*, 2004. **91**(3): p. 540-52.
68. Chen, L., et al., *Oxidative DNA damage in prostate cancer patients consuming tomato sauce-based entrees as a whole-food intervention*. *Journal of the National Cancer Institute*, 2001. **93**(24): p. 1872-9.
69. Lippman, S.M., et al., *Effect of selenium and vitamin E on risk of prostate cancer and other cancers: the Selenium and Vitamin E Cancer Prevention Trial (SELECT)*. *JAMA*, 2009. **301**(1): p. 39-51.

70. Kirsh, V.A., et al., *Supplemental and dietary vitamin E, beta-carotene, and vitamin C intakes and prostate cancer risk*. Journal of the National Cancer Institute, 2006. **98**(4): p. 245-54.
71. Wolf, D.A., P. Schulz, and F. Fittler, *Transcriptional regulation of prostate kallikrein-like genes by androgen*. Molecular endocrinology, 1992. **6**(5): p. 753-62.
72. Stamey, T.A., et al., *Prostate-specific antigen as a serum marker for adenocarcinoma of the prostate*. The New England journal of medicine, 1987. **317**(15): p. 909-16.
73. Gleason, D.F., *Histologic grading of prostate cancer: a perspective*. Human pathology, 1992. **23**(3): p. 273-9.
74. Bok, R.A. and E.J. Small, *Bloodborne biomolecular markers in prostate cancer development and progression*. Nature reviews. Cancer, 2002. **2**(12): p. 918-26.
75. Payne, H.K., M., *Improving the awareness and understanding of modern prostate cancer management*. Trends in Urology and Men's Health, 2013(September/October 2013).
76. NICE, *Prostate cancer: diagnosis and treatment*. Clinical guideline 175, January 2014.
<http://www.nice.org.uk/guidance/cg175/resources/guidance-prostate-cancer-diagnosis-and-treatment-pdf>, 2014.
77. Holzbeierlein, J., et al., *Gene expression analysis of human prostate carcinoma during hormonal therapy identifies androgen-responsive genes and mechanisms of therapy resistance*. The American journal of pathology, 2004. **164**(1): p. 217-27.
78. Rick, F.G., N.L. Block, and A.V. Schally, *Agonists of luteinizing hormone-releasing hormone in prostate cancer*. Expert opinion on pharmacotherapy, 2013. **14**(16): p. 2237-47.
79. Nadiminty, N. and A.C. Gao, *Mechanisms of persistent activation of the androgen receptor in CRPC: recent advances and future perspectives*. World journal of urology, 2012. **30**(3): p. 287-95.
80. Sharma, N.L., et al., *The androgen receptor induces a distinct transcriptional program in castration-resistant prostate cancer in man*. Cancer cell, 2013. **23**(1): p. 35-47.
81. Locke, J.A., et al., *Androgen levels increase by intratumoral de novo steroidogenesis during progression of castration-resistant prostate cancer*. Cancer research, 2008. **68**(15): p. 6407-15.
82. Ferraldeschi, R., et al., *Abiraterone and novel antiandrogens: overcoming castration resistance in prostate cancer*. Annual review of medicine, 2013. **64**: p. 1-13.
83. Gregory, C.W., et al., *Androgen receptor stabilization in recurrent prostate cancer is associated with hypersensitivity to low androgen*. Cancer research, 2001. **61**(7): p. 2892-8.
84. Scher, H.I. and C.L. Sawyers, *Biology of progressive, castration-resistant prostate cancer: directed therapies targeting the androgen-receptor signaling axis*. Journal of clinical oncology : official journal of the American Society of Clinical Oncology, 2005. **23**(32): p. 8253-61.
85. Bernard, D., et al., *Myc confers androgen-independent prostate cancer cell growth*. The Journal of clinical investigation, 2003. **112**(11): p. 1724-31.
86. Ellwood-Yen, K., et al., *Myc-driven murine prostate cancer shares molecular features with human prostate tumors*. Cancer cell, 2003. **4**(3): p. 223-38.

87. Hedvat, M., et al., *The JAK2 inhibitor AZD1480 potently blocks Stat3 signaling and oncogenesis in solid tumors*. *Cancer cell*, 2009. **16**(6): p. 487-97.
88. Sharma, A., et al., *The retinoblastoma tumor suppressor controls androgen signaling and human prostate cancer progression*. *The Journal of clinical investigation*, 2010. **120**(12): p. 4478-92.
89. Nelson, P.S., *Molecular states underlying androgen receptor activation: a framework for therapeutics targeting androgen signaling in prostate cancer*. *Journal of clinical oncology : official journal of the American Society of Clinical Oncology*, 2012. **30**(6): p. 644-6.
90. English, H.F., R.J. Santen, and J.T. Isaacs, *Response of glandular versus basal rat ventral prostatic epithelial cells to androgen withdrawal and replacement*. *The Prostate*, 1987. **11**(3): p. 229-42.
91. Grasso, C.S., et al., *The mutational landscape of lethal castration-resistant prostate cancer*. *Nature*, 2012. **487**(7406): p. 239-43.
92. Signoretti, S., et al., *Her-2-neu expression and progression toward androgen independence in human prostate cancer*. *Journal of the National Cancer Institute*, 2000. **92**(23): p. 1918-25.
93. Osman, I., et al., *HER-2/neu (p185neu) protein expression in the natural or treated history of prostate cancer*. *Clinical cancer research : an official journal of the American Association for Cancer Research*, 2001. **7**(9): p. 2643-7.
94. Dehm, S.M., et al., *Splicing of a novel androgen receptor exon generates a constitutively active androgen receptor that mediates prostate cancer therapy resistance*. *Cancer research*, 2008. **68**(13): p. 5469-77.
95. Cooper, C.S., et al., *Corrigendum: analysis of the genetic phylogeny of multifocal prostate cancer identifies multiple independent clonal expansions in neoplastic and morphologically normal prostate tissue*. *Nature genetics*, 2015. **47**(6): p. 689.
96. Gundem, G., et al., *The evolutionary history of lethal metastatic prostate cancer*. *Nature*, 2015. **520**(7547): p. 353-7.
97. Hong, M.K., et al., *Tracking the origins and drivers of subclonal metastatic expansion in prostate cancer*. *Nature communications*, 2015. **6**: p. 6605.
98. Talmadge, J.E. and I.J. Fidler, *AACR centennial series: the biology of cancer metastasis: historical perspective*. *Cancer research*, 2010. **70**(14): p. 5649-69.
99. Robinson, D., et al., *Integrative clinical genomics of advanced prostate cancer*. *Cell*, 2015. **161**(5): p. 1215-28.
100. Markert, E.K., et al., *Molecular classification of prostate cancer using curated expression signatures*. *Proceedings of the National Academy of Sciences of the United States of America*, 2011. **108**(52): p. 21276-81.
101. Sboner, A., et al., *Molecular sampling of prostate cancer: a dilemma for predicting disease progression*. *BMC medical genomics*, 2010. **3**: p. 8.
102. Ben-Porath, I., et al., *An embryonic stem cell-like gene expression signature in poorly differentiated aggressive human tumors*. *Nature genetics*, 2008. **40**(5): p. 499-507.
103. Mizuno, H., et al., *Inactivation of p53 in breast cancers correlates with stem cell transcriptional signatures*. *Proceedings of the National Academy of Sciences of the United States of America*, 2010. **107**(52): p. 22745-50.
104. Hieronymus, H., et al., *Copy number alteration burden predicts prostate cancer relapse*. *Proceedings of the National Academy of Sciences of the United States of America*, 2014. **111**(30): p. 11139-44.

105. Li, D.M. and H. Sun, *TEP1, encoded by a candidate tumor suppressor locus, is a novel protein tyrosine phosphatase regulated by transforming growth factor beta*. *Cancer research*, 1997. **57**(11): p. 2124-9.
106. Li, J., et al., *PTEN, a putative protein tyrosine phosphatase gene mutated in human brain, breast, and prostate cancer*. *Science*, 1997. **275**(5308): p. 1943-7.
107. Steck, P.A., et al., *Identification of a candidate tumour suppressor gene, MMAC1, at chromosome 10q23.3 that is mutated in multiple advanced cancers*. *Nature genetics*, 1997. **15**(4): p. 356-62.
108. Cantley, L.C. and B.G. Neel, *New insights into tumor suppression: PTEN suppresses tumor formation by restraining the phosphoinositide 3-kinase/AKT pathway*. *Proceedings of the National Academy of Sciences of the United States of America*, 1999. **96**(8): p. 4240-5.
109. Engelman, J.A., *Targeting PI3K signalling in cancer: opportunities, challenges and limitations*. *Nature reviews. Cancer*, 2009. **9**(8): p. 550-62.
110. Patel, R., et al., *Sprouty2, PTEN, and PP2A interact to regulate prostate cancer progression*. *The Journal of clinical investigation*, 2013. **123**(3): p. 1157-75.
111. Bermudez Brito, M., E. Goulielmaki, and E.A. Papakonstanti, *Focus on PTEN Regulation*. *Frontiers in oncology*, 2015. **5**: p. 166.
112. Chang, C.J., et al., *PTEN nuclear localization is regulated by oxidative stress and mediates p53-dependent tumor suppression*. *Molecular and cellular biology*, 2008. **28**(10): p. 3281-9.
113. Shen, W.H., et al., *Essential role for nuclear PTEN in maintaining chromosomal integrity*. *Cell*, 2007. **128**(1): p. 157-70.
114. Di Cristofano, A., et al., *Pten is essential for embryonic development and tumour suppression*. *Nature genetics*, 1998. **19**(4): p. 348-55.
115. Di Cristofano, A. and P.P. Pandolfi, *The multiple roles of PTEN in tumor suppression*. *Cell*, 2000. **100**(4): p. 387-90.
116. Jerde, T.J., *Phosphatase and Tensin Homologue: Novel Regulation by Developmental Signaling*. *Journal of signal transduction*, 2015. **2015**: p. 282567.
117. De Velasco, M.A. and H. Uemura, *Preclinical Remodeling of Human Prostate Cancer through the PTEN/AKT Pathway*. *Advances in urology*, 2012. **2012**: p. 419348.
118. Wang, S., et al., *Prostate-specific deletion of the murine Pten tumor suppressor gene leads to metastatic prostate cancer*. *Cancer cell*, 2003. **4**(3): p. 209-21.
119. Carver, B.S., et al., *Reciprocal feedback regulation of PI3K and androgen receptor signaling in PTEN-deficient prostate cancer*. *Cancer cell*, 2011. **19**(5): p. 575-86.
120. Lin, H.K., et al., *Regulation of androgen receptor signaling by PTEN (phosphatase and tensin homolog deleted on chromosome 10) tumor suppressor through distinct mechanisms in prostate cancer cells*. *Molecular endocrinology*, 2004. **18**(10): p. 2409-23.
121. Wu, Z., et al., *Upregulation of miR-153 promotes cell proliferation via downregulation of the PTEN tumor suppressor gene in human prostate cancer*. *The Prostate*, 2013. **73**(6): p. 596-604.
122. Tian, L., et al., *Four microRNAs promote prostate cell proliferation with regulation of PTEN and its downstream signals in vitro*. *PloS one*, 2013. **8**(9): p. e75885.
123. Shan, S.W., et al., *Mature miR-17-5p and passenger miR-17-3p induce hepatocellular carcinoma by targeting PTEN, GalNT7 and vimentin in*

- different signal pathways*. Journal of cell science, 2013. **126**(Pt 6): p. 1517-30.
124. Mouw, J.K., et al., *Tissue mechanics modulate microRNA-dependent PTEN expression to regulate malignant progression*. Nature medicine, 2014. **20**(4): p. 360-7.
 125. Liu, C., et al., *MicroRNA-21 acts as an oncomir through multiple targets in human hepatocellular carcinoma*. Journal of hepatology, 2010. **53**(1): p. 98-107.
 126. Klaus, A. and W. Birchmeier, *Wnt signalling and its impact on development and cancer*. Nature reviews. Cancer, 2008. **8**(5): p. 387-98.
 127. Grigoryan, T., et al., *Deciphering the function of canonical Wnt signals in development and disease: conditional loss- and gain-of-function mutations of beta-catenin in mice*. Genes & development, 2008. **22**(17): p. 2308-41.
 128. Rosenbluh, J., X. Wang, and W.C. Hahn, *Genomic insights into WNT/beta-catenin signaling*. Trends in pharmacological sciences, 2014. **35**(2): p. 103-9.
 129. Li, V.S., et al., *Wnt signaling through inhibition of beta-catenin degradation in an intact Axin1 complex*. Cell, 2012. **149**(6): p. 1245-56.
 130. He, T.C., et al., *Identification of c-MYC as a target of the APC pathway*. Science, 1998. **281**(5382): p. 1509-12.
 131. Crawford, H.C., et al., *The metalloproteinase matrilysin is a target of beta-catenin transactivation in intestinal tumors*. Oncogene, 1999. **18**(18): p. 2883-91.
 132. Tetsu, O. and F. McCormick, *Beta-catenin regulates expression of cyclin D1 in colon carcinoma cells*. Nature, 1999. **398**(6726): p. 422-6.
 133. Dang, C.V., et al., *The c-Myc target gene network*. Seminars in cancer biology, 2006. **16**(4): p. 253-64.
 134. Fanjul-Fernandez, M., et al., *Matrix metalloproteinases: evolution, gene regulation and functional analysis in mouse models*. Biochimica et biophysica acta, 2010. **1803**(1): p. 3-19.
 135. Choi, Y.J., et al., *The requirement for cyclin D function in tumor maintenance*. Cancer cell, 2012. **22**(4): p. 438-51.
 136. Heuberger, J. and W. Birchmeier, *Interplay of cadherin-mediated cell adhesion and canonical Wnt signaling*. Cold Spring Harbor perspectives in biology, 2010. **2**(2): p. a002915.
 137. Xu, W. and D. Kimelman, *Mechanistic insights from structural studies of beta-catenin and its binding partners*. Journal of cell science, 2007. **120**(Pt 19): p. 3337-44.
 138. Francis, J.C., et al., *beta-catenin is required for prostate development and cooperates with Pten loss to drive invasive carcinoma*. PLoS genetics, 2013. **9**(1): p. e1003180.
 139. Voeller, H.J., C.I. Truica, and E.P. Gelmann, *Beta-catenin mutations in human prostate cancer*. Cancer research, 1998. **58**(12): p. 2520-3.
 140. Chesire, D.R., et al., *Detection and analysis of beta-catenin mutations in prostate cancer*. The Prostate, 2000. **45**(4): p. 323-34.
 141. Chesire, D.R., et al., *In vitro evidence for complex modes of nuclear beta-catenin signaling during prostate growth and tumorigenesis*. Oncogene, 2002. **21**(17): p. 2679-94.
 142. Gerstein, A.V., et al., *APC/CTNNB1 (beta-catenin) pathway alterations in human prostate cancers*. Genes, chromosomes & cancer, 2002. **34**(1): p. 9-16.

143. Kumar, A., et al., *Exome sequencing identifies a spectrum of mutation frequencies in advanced and lethal prostate cancers*. Proceedings of the National Academy of Sciences of the United States of America, 2011. **108**(41): p. 17087-92.
144. Whitaker, H.C., et al., *Alterations in beta-catenin expression and localization in prostate cancer*. The Prostate, 2008. **68**(11): p. 1196-205.
145. Kypta, R.M. and J. Waxman, *Wnt/beta-catenin signalling in prostate cancer*. Nature reviews. Urology, 2012.
146. Sun, Y., et al., *Treatment-induced damage to the tumor microenvironment promotes prostate cancer therapy resistance through WNT16B*. Nature medicine, 2012. **18**(9): p. 1359-68.
147. Jatko, T.A., et al., *A urine-based methylation signature for risk stratification within low-risk prostate cancer*. British journal of cancer, 2015. **112**(5): p. 802-8.
148. Gounari, F., et al., *Stabilization of beta-catenin induces lesions reminiscent of prostatic intraepithelial neoplasia, but terminal squamous transdifferentiation of other secretory epithelia*. Oncogene, 2002. **21**(26): p. 4099-107.
149. Yu, X., et al., *Activation of beta-Catenin in mouse prostate causes HGPIN and continuous prostate growth after castration*. The Prostate, 2009. **69**(3): p. 249-62.
150. Yu, X., et al., *Wnt/beta-catenin activation promotes prostate tumor progression in a mouse model*. Oncogene, 2011. **30**(16): p. 1868-79.
151. Lee, S.H., et al., *Androgen signaling is a confounding factor for beta-catenin-mediated prostate tumorigenesis*. Oncogene, 2015.
152. Ahmad, I., et al., *beta-Catenin activation synergizes with PTEN loss to cause bladder cancer formation*. Oncogene, 2011. **30**(2): p. 178-89.
153. Sharma, M., W.W. Chuang, and Z. Sun, *Phosphatidylinositol 3-kinase/Akt stimulates androgen pathway through GSK3beta inhibition and nuclear beta-catenin accumulation*. The Journal of biological chemistry, 2002. **277**(34): p. 30935-41.
154. Fang, D., et al., *Phosphorylation of beta-catenin by AKT promotes beta-catenin transcriptional activity*. The Journal of biological chemistry, 2007. **282**(15): p. 11221-9.
155. Weischenfeldt, J., et al., *Integrative genomic analyses reveal an androgen-driven somatic alteration landscape in early-onset prostate cancer*. Cancer cell, 2013. **23**(2): p. 159-70.
156. Rajan, P., et al., *Next-generation sequencing of advanced prostate cancer treated with androgen-deprivation therapy*. European urology, 2014. **66**(1): p. 32-9.
157. Yang, F., et al., *Linking beta-catenin to androgen-signaling pathway*. The Journal of biological chemistry, 2002. **277**(13): p. 11336-44.
158. Truica, C.I., S. Byers, and E.P. Gelmann, *Beta-catenin affects androgen receptor transcriptional activity and ligand specificity*. Cancer research, 2000. **60**(17): p. 4709-13.
159. Wan, X., et al., *Activation of beta-catenin signaling in androgen receptor-negative prostate cancer cells*. Clinical cancer research : an official journal of the American Association for Cancer Research, 2012. **18**(3): p. 726-36.
160. Wang, G., J. Wang, and M.D. Sadar, *Crosstalk between the androgen receptor and beta-catenin in castrate-resistant prostate cancer*. Cancer research, 2008. **68**(23): p. 9918-27.

161. Lee, E., et al., *Inhibition of androgen receptor and beta-catenin activity in prostate cancer*. Proceedings of the National Academy of Sciences of the United States of America, 2013. **110**(39): p. 15710-5.
162. Brzezinska, E.A., et al., *Genetically engineered mouse models to study prostate cancer*. Methods in molecular biology, 2015. **1267**: p. 73-91.
163. Di Cristofano, A., et al., *Pten and p27KIP1 cooperate in prostate cancer tumor suppression in the mouse*. Nature genetics, 2001. **27**(2): p. 222-4.
164. Abate-Shen, C., et al., *Nkx3.1; Pten mutant mice develop invasive prostate adenocarcinoma and lymph node metastases*. Cancer research, 2003. **63**(14): p. 3886-90.
165. Couto, S.S., et al., *Simultaneous haploinsufficiency of Pten and Trp53 tumor suppressor genes accelerates tumorigenesis in a mouse model of prostate cancer*. Differentiation; research in biological diversity, 2009. **77**(1): p. 103-11.
166. Sauer, B. and N. Henderson, *Cre-stimulated recombination at loxP-containing DNA sequences placed into the mammalian genome*. Nucleic acids research, 1989. **17**(1): p. 147-61.
167. Cleutjens, K.B., et al., *A 6-kb promoter fragment mimics in transgenic mice the prostate-specific and androgen-regulated expression of the endogenous prostate-specific antigen gene in humans*. Molecular endocrinology, 1997. **11**(9): p. 1256-65.
168. Maddison, L.A., et al., *Prostate specific expression of Cre recombinase in transgenic mice*. Genesis, 2000. **26**(2): p. 154-6.
169. Wu, X., et al., *Generation of a prostate epithelial cell-specific Cre transgenic mouse model for tissue-specific gene ablation*. Mechanisms of development, 2001. **101**(1-2): p. 61-9.
170. Sciavolino, P.J., et al., *Tissue-specific expression of murine Nkx3.1 in the male urogenital system*. Developmental dynamics : an official publication of the American Association of Anatomists, 1997. **209**(1): p. 127-38.
171. Greenberg, N.M., et al., *The rat probasin gene promoter directs hormonally and developmentally regulated expression of a heterologous gene specifically to the prostate in transgenic mice*. Molecular endocrinology, 1994. **8**(2): p. 230-9.
172. Zhang, J., et al., *A small composite probasin promoter confers high levels of prostate-specific gene expression through regulation by androgens and glucocorticoids in vitro and in vivo*. Endocrinology, 2000. **141**(12): p. 4698-710.
173. Metzger, D. and P. Chambon, *Site- and time-specific gene targeting in the mouse*. Methods, 2001. **24**(1): p. 71-80.
174. Birbach, A., *Use of PB-Cre4 mice for mosaic gene deletion*. PloS one, 2013. **8**(1): p. e53501.
175. Kim, M.J., et al., *Nkx3.1 mutant mice recapitulate early stages of prostate carcinogenesis*. Cancer research, 2002. **62**(11): p. 2999-3004.
176. Lesche, R., et al., *Cre/loxP-mediated inactivation of the murine Pten tumor suppressor gene*. Genesis, 2002. **32**(2): p. 148-9.
177. Harada, N., et al., *Intestinal polyposis in mice with a dominant stable mutation of the beta-catenin gene*. The EMBO journal, 1999. **18**(21): p. 5931-42.
178. Luche, H., et al., *Faithful activation of an extra-bright red fluorescent protein in "knock-in" Cre-reporter mice ideally suited for lineage tracing studies*. European journal of immunology, 2007. **37**(1): p. 43-53.

179. Friedrich, G. and P. Soriano, *Promoter traps in embryonic stem cells: a genetic screen to identify and mutate developmental genes in mice*. *Genes & development*, 1991. **5**(9): p. 1513-23.
180. Hu, S., et al., *Research resource: Genome-wide mapping of in vivo androgen receptor binding sites in mouse epididymis*. *Molecular endocrinology*, 2010. **24**(12): p. 2392-405.
181. Chen, Y., et al., *ETS factors reprogram the androgen receptor cistrome and prime prostate tumorigenesis in response to PTEN loss*. *Nature medicine*, 2013. **19**(8): p. 1023-9.
182. Myant, K.B., et al., *ROS production and NF-kappaB activation triggered by RAC1 facilitate WNT-driven intestinal stem cell proliferation and colorectal cancer initiation*. *Cell stem cell*, 2013. **12**(6): p. 761-73.
183. Pawlak, M., et al., *Zeptosens' protein microarrays: a novel high performance microarray platform for low abundance protein analysis*. *Proteomics*, 2002. **2**(4): p. 383-93.
184. Lukacs, R.U., et al., *Isolation, cultivation and characterization of adult murine prostate stem cells*. *Nature protocols*, 2010. **5**(4): p. 702-13.
185. Laplante, M. and D.M. Sabatini, *mTOR signaling in growth control and disease*. *Cell*, 2012. **149**(2): p. 274-93.
186. Ganz, T., *Defensins: antimicrobial peptides of innate immunity*. *Nature reviews. Immunology*, 2003. **3**(9): p. 710-20.
187. Sassone-Corsi, P., *The cyclic AMP pathway*. Cold Spring Harbor perspectives in biology, 2012. **4**(12).
188. Allan, C.M. and J.M. Taylor, *Expression of a novel human apolipoprotein (apoC-IV) causes hypertriglyceridemia in transgenic mice*. *Journal of lipid research*, 1996. **37**(7): p. 1510-8.
189. Xiao, X., et al., *Pancreatic lipase-related protein-2 (PLRP2) can contribute to dietary fat digestion in human newborns*. *The Journal of biological chemistry*, 2011. **286**(30): p. 26353-63.
190. Zhao, P., et al., *Regulation of survivin by PI3K/Akt/p70S6K1 pathway*. *Biochemical and biophysical research communications*, 2010. **395**(2): p. 219-24.
191. Han, L., et al., *MicroRNA-21 expression is regulated by beta-catenin/STAT3 pathway and promotes glioma cell invasion by direct targeting RECK*. *CNS neuroscience & therapeutics*, 2012. **18**(7): p. 573-83.
192. Inoki, K., et al., *TSC2 integrates Wnt and energy signals via a coordinated phosphorylation by AMPK and GSK3 to regulate cell growth*. *Cell*, 2006. **126**(5): p. 955-68.
193. Clegg, N.J., et al., *MYC cooperates with AKT in prostate tumorigenesis and alters sensitivity to mTOR inhibitors*. *PloS one*, 2011. **6**(3): p. e17449.
194. Palm, W., et al., *The Utilization of Extracellular Proteins as Nutrients Is Suppressed by mTORC1*. *Cell*, 2015. **162**(2): p. 259-70.
195. O'Neill, H.M., G.P. Holloway, and G.R. Steinberg, *AMPK regulation of fatty acid metabolism and mitochondrial biogenesis: implications for obesity*. *Molecular and cellular endocrinology*, 2013. **366**(2): p. 135-51.
196. Sarma, J.V. and P.A. Ward, *The complement system*. *Cell and tissue research*, 2011. **343**(1): p. 227-35.
197. Arend, W.P., *The balance between IL-1 and IL-1Ra in disease*. *Cytokine & growth factor reviews*, 2002. **13**(4-5): p. 323-40.
198. Ammirante, M., et al., *Tissue injury and hypoxia promote malignant progression of prostate cancer by inducing CXCL13 expression in tumor myofibroblasts*. *Proceedings of the National Academy of Sciences of the United States of America*, 2014. **111**(41): p. 14776-81.

199. Liu, J., et al., *Targeting Wnt-driven cancer through the inhibition of Porcupine by LGK974*. Proceedings of the National Academy of Sciences of the United States of America, 2013. **110**(50): p. 20224-9.
200. Hotte, S.J. and F. Saad, *Current management of castrate-resistant prostate cancer*. Current oncology, 2010. **17 Suppl 2**: p. S72-9.
201. Gao, H., et al., *Emergence of androgen independence at early stages of prostate cancer progression in Nkx3.1; Pten mice*. Cancer research, 2006. **66**(16): p. 7929-33.
202. Anastas, J.N. and R.T. Moon, *WNT signalling pathways as therapeutic targets in cancer*. Nature reviews. Cancer, 2013. **13**(1): p. 11-26.
203. Bisson, J.A., et al., *Wnt5a and Wnt11 inhibit the canonical Wnt pathway and promote cardiac progenitor development via the Caspase-dependent degradation of AKT*. Developmental biology, 2015. **398**(1): p. 80-96.
204. Pu, Y., et al., *Androgen regulation of prostate morphoregulatory gene expression: Fgf10-dependent and -independent pathways*. Endocrinology, 2007. **148**(4): p. 1697-706.
205. Yamamoto, H., et al., *Wnt5a signaling is involved in the aggressiveness of prostate cancer and expression of metalloproteinase*. Oncogene, 2010. **29**(14): p. 2036-46.
206. Huelsken, J., et al., *beta-Catenin controls hair follicle morphogenesis and stem cell differentiation in the skin*. Cell, 2001. **105**(4): p. 533-45.
207. Li, L., Z. Lou, and L. Wang, *The role of FKBP5 in cancer aetiology and chemoresistance*. British journal of cancer, 2011. **104**(1): p. 19-23.
208. Lagor, W.R., et al., *Overexpression of apolipoprotein F reduces HDL cholesterol levels in vivo*. Arteriosclerosis, thrombosis, and vascular biology, 2009. **29**(1): p. 40-6.
209. Lagor, W.R., et al., *The effects of apolipoprotein F deficiency on high density lipoprotein cholesterol metabolism in mice*. PloS one, 2012. **7**(2): p. e31616.
210. Lee, S., et al., *Coordinated peak expression of MMP-26 and TIMP-4 in preinvasive human prostate tumor*. Cell research, 2006. **16**(9): p. 750-8.
211. Murphy, G. and H. Nagase, *Progress in matrix metalloproteinase research*. Molecular aspects of medicine, 2008. **29**(5): p. 290-308.
212. Bartz, F., et al., *Identification of cholesterol-regulating genes by targeted RNAi screening*. Cell metabolism, 2009. **10**(1): p. 63-75.
213. Xu, X.Y., et al., *Down-regulated MAC30 expression inhibits proliferation and mobility of human gastric cancer cells*. Cellular physiology and biochemistry : international journal of experimental cellular physiology, biochemistry, and pharmacology, 2014. **33**(5): p. 1359-68.
214. Xiao, M., et al., *Expression of MAC30 protein is related to survival and clinicopathological variables in breast cancer*. Journal of surgical oncology, 2013. **107**(5): p. 456-62.

Appendix I - Publication